Optimization Methods for Multiphase Systems in the Subsurface

- Application to Methane Migration in Coal Mining Areas -

Von der Fakultät Bau- und Umweltingenieurwissenschaften der Universität Stuttgart
zur Erlangung der Würde eines Doktors der
Ingenieurwissenschaften (Dr.-Ing.) genehmigte Abhandlung

Vorgelegt von

Kenichiro KOBAYASHI

aus Japan

Hauptberichter:	Prof. Dr.-Ing. R.HELMIG
Mitberichter:	Prof. Dr.-Ing. T.KOIKE
Mitberichter:	Prof. Dr.-Ing. R.HINKELMANN
Tag der mündlichen Prüfung:	09.Juli 2004

Institut für Wasserbau der Universität Stuttgart

2004

D93 Optimization Methods for Multiphase Systems in the Subsuface
- Application to Methane Migration in Coal Mining Areas -

Kobayashi, Kenichiro:
Optimization Methods for Multiphase Systems in the Subsuface
- Application to Methane Migration in Coal Mining Areas - / von Kenichiro Kobayashi. Institut für Wasserbau, Universität Stuttgart. - Stuttgart: Inst. für Wasserbau, 2005

(Mitteilungen / Institut für Wasserbau, Universität Stuttgart ; H. 139)
Zugl.: Stuttgart, Univ., Diss., 2005
ISBN 3-933761-42-5

Herausgegeben 2005 vom Eigenverlag des Instituts für Wasserbau
Druck: Sprint-Druck, Stuttgart

Acknowledgement

Four years have already passed since I came to Germany, intending to carry out my Ph.D work here at the Institute of Hydraulic Engineering, University of Stuttgart. I can say that these four years were really long and yet very short as well. Of course, I experienced not only pleasures, but also annoyances during this time. However, I must say quite clearly that these four years were and will be one of the most valuable periods of my life and I will never forget them. There are too many people to whom I owe thanks for their support during my stay in Germany and I cannot mention all of them here. I thank only some of them chronologically in this acknowledgment, but it does not mean that I do not appreciate the other people whose names do not appear.

My stay in Germany was made possible through the cooperation agreement between the University of Stuttgart and the University of Tokyo, Japan. The cooperation at that time was managed by both Prof. Tamai and Prof. Kobus. Prof. Tamai proposed that I study in Germany when I started my master's thesis at the University of Tokyo. Together, we sent several letters to Prof. Kobus several times and Prof. Kobus decided to include me as a Ph.D. student at the Institute. Jochen Appt, my former colleague and friend, supported me in all the procedures necessary to get here and to start my life in Germany. First of all, I would like to thank all of them from the bottom of my heart.

Around one year later, at the Technical University of Braunschweig I met Prof. Helmig who was supposed to move to Stuttgart as a full professor. The first impression of him was rather shocking: "Oh!, Is he a professor?" But he was. Then I decided to work in his group, later named Hydromechanics and Modelling of Hydrosystems. Prof. (Dr. at that time!) Hinkelmann was also in the group and I decided to work with these two in a project. I do not know whether or not it was because of the cultural differences between us, but I often had discussions with them and, sometimes, I could even say fought, especially with Prof. Hinkelmann. One aspect which I find very good in German culture is that people are allowed to discuss even with an older person in a very critical manner, although it was quite hard for me until I had adjusted to that. Of course, I feel in some aspects it would be wonderful if the people here could learn from my culture. Anyway, my research life went on. In this time, both Prof. Helmig and Prof. Hinkelmann always gave me their heartwarming support, not only in my research but also in my private life. I really would like to thank both of them for giving me the chance to live in this wonderful environment.

Prof. Koike, the current professor at the University of Tokyo, kindly accepted to be on the examination board of my Ph.D. exam. I have known him for around five years. I still remember vividly when he told me that it was better to be optimistic if I wanted to be a good researcher. I do not know how optimistic I was in the course of my Ph.D. research because this topic was really difficult for me to carry out well. However, at least I always try to remember his words. The

international cooperation is still carried on by Prof. Helmig and Prof. Koike, which is my great pleasure. I would like to thank Prof. Koike also, from the bottom of heart, for often having visited me, sending e-mails and encouraging me.

In the reaseach context, I would also like to thank Dr. Finsterle at LBNL and Dr. Cirpka, my colleague, who gave me a lot of useful information especially concerning inverse modelling.

As mentioned, although really (repeat 100 times!) all my colleagues supported me a lot, I would especially like to mention among them all: Ms. Lawday, who always helped me since my command of German is sometimes not well enough to carry out all the administrative procedures by myself. She also helped me with English corrections for my papers as well as my dissertation; Ulrich Oelmann, who supported me not only physically but also mentally as my office roommate. He was also in charge of the parallel computer. My research life has been spent together with the parallel computer and, without it, I would never have been able to finish my enormous simulations; Maren Paul, who was always a good conversation partner as well as a teacher of German culture and who gave me two sentences, ”Man muss Ken nicht unterdrücken. Drücken reicht vollkommen”; Dorothee Schweizer and David Werner, wonderful computer professionals who arranged and sometimes fixed my crazy computers; Anongnart Assteerawatt, who inspired me a lot by showing a different way of adjusting as an Asian to this society; and Wolfgang Rempp, who always jogged together with me for four years and helped in many senses; then I noticed, after all, that I must mention all the names in my group. I would like to thank Andreas Bielinski, Thomas Breiting, Holger Class, Hartmut Eichel, Sandra Hölzemann, Jennifer Niessner, Steffen Ochs, Sabine Manthey, Insa Neuweiler, Hussam Sheta, Mia Suß, Annette Silberhorn, and Hartmut Jakobs.

I would also like to thank Japanese friends, Mr. Kato and Dr. Ishikawa, who reduced my loneliness in this strange society (so is Japan for many non-Japanese people).

Finally and naturally, I would like to thank my parents, brothers, relatives and, of course, my wife Shiho, who always helped me whether I was in a good mood or not.

Thanks, Danke and Arigato !

Contents

List of Figures

List of Tables

Notation

The following table shows the significant symbols used in this work. Local notations are explained in the text.

Symbol	Definition	Dimension
Greek Letters:		
Chapter 2:		
$O(\mathbf{x})$	Objective function	
$\mathbf{C}_1(\mathbf{x})$	Constraint of objective function	
$\mathbf{C}_2(\mathbf{x})$	Constraint of objective function	
i	Index i for accepted steps	
j	Index j for rejected steps	
k	Index k for cooling schedule	
$x^c_{j,i}$	Current decision vector for greedy search	
$x^n_{j,i}$	New decision vector for greedy search	
$x^{best}_{j,i}$	Best decision vector for greedy search	
$\mathbf{x}^{i,j,k}_c$	Current decision vector for simulated annealing	
$\mathbf{x}^{i,j,k}_n$	New decision vector for simulated annealing	
$x^{best}_{i,j,k}$	Best decision vector for the acception of deteriorated solution	
$\mathscr{R}_j$	Random variables	
$Obj(x)$	Objective function	
$Obj^{best}_{j,i}$	Best value of objective function so far	
σ^k	Standard deviation for simulated annealing	
P_{Bol}	Boltzmann probability for simulated annealing	
K_B	Boltzmann constant for simulated annealing	[-]
T_k	Temperature for simulated annealing	
α	Coefficient for cooling schedule	
δ_j	Random variable for the next decision vector	
$xMax$	Maximal value of decision vector	
$xMin$	Minimal value of decision vector	
$jMax$	Maximal values for j	
$f(\sigma^k, \mu)$	Gaussian distribution for simulated annealing	

σ^k	Standard deviation for Gaussian distribution	
Chapter 3:		
ϕ	Porosity	[-]
ϕ_e	Effective porosity	[-]
S_α	Saturation of phase α	[-]
S_{we}	Effective water saturation	[-]
S_{wr}	Residual water saturation	[-]
ϕ_α	Phase α occupancy	[-]
X_α^κ	Mass fraction of component κ in phase α	[-]
m_α^κ	Mass of component κ in phase α	$[kg]$
m_α	Mass of phase α	$[kg]$
x_α^κ	Mole fraction of component κ in phase α	[-]
n_α^κ	Mole number of component κ in phase α	$[mol]$
n_α	Mole number of phase α	$[mol]$
p_g	Gas phase pressure	$[Pa]$
V	Volume of gas	$[m^3]$
T	Temperature	$[K]$
n_g	Mole number of gas phase	$[mol]$
R	Universal gas constant (= 8.31451)	$[\frac{Pa \cdot m^3}{K \cdot mol}]$
ρ_g^{mol}	Molar density of gas phase	$[mol/m^3]$
H_w^a	Henry constant of air dissolved into water phase	$[Pa^{-1}]$
ρ_w	Water density	$[kg/m^3]$
ρ_0	Reference water density	$[kg/m^3]$
M^κ	Molecular weight	$[kg/kmol]$
μ_g	Dynamic viscosity of gas phase	$[Pa \cdot s]$
M^j	Molecular weight of component j	$[kg/mol]$
$\mathbf{J}_C$	Diffusion flux of component C	$[mol/m^2 s]$
$\mathbf{D}_{dif}$	Diffusion tensor	
D_{dif}	Component of diffusion tensor	$[m^2/s]$
$\mathbf{I}$	Unit tensor	[-]
$\mathbf{D}_{dis}$	Dispersion tensor	
D_{xx}	Component of dispersion tensor	$[m^2/s]$
D_{xy}	Component of dispersion tensor	$[m^2/s]$
D_{yx}	Component of dispersion tensor	$[m^2/s]$
D_{yy}	Component of dispersion tensor	$[m^2/s]$
α_L	Longitudinal dispersivity	$[m]$
α_T	Transverse dispersivity	$[m]$
v_x	Velocity in the x-direction	$[m/s]$
v_y	Velocity in the y-direction	$[m/s]$
$D_g^{a,w}$	Binary diffusion for air-water system	$[m^2/s]$
$D_g^{m,w}$	Binary diffusion for methane-water system	$[m^2/s]$
$D_g^{a,m}$	Binary diffusion for air-methane system	$[m^2/s]$
D_g^w	Diffusion coefficient for water in gas phase	$[m^2/s]$
D_g^m	Diffusion coefficient for methane in gas phase	$[m^2/s]$
$p_{g,R}$	Reference pressure (=1 bar)	$[bar]$

T_R	Reference temperature (=273.15 K)	$[K]$
$D_g^{i,j}$	Binary diffusion coefficient for a mixture gas of the component i and j	$[m^2/s]$
$\sigma^{i,j}$	Characteristic length	$[A]$
Ω	Diffusion collision integral	[-]
p_c	Capillary pressure	$[Pa]$
p_n	Pressure of non-wetting phase	$[Pa]$
p_w	Pressure of wetting phase	$[Pa]$
p_d	Entry pressure	$[Pa]$
λ	Form parameter	[-]
m	Form parameter	[-]
τ_0	Shear stress	$[N/m^2]$
γ	Specific weight of a fluid	$[N/m^3]$
S_f	Friction slope	[-]
R	Hydraulic radius	$[m]$
D	Diameter	[m]
K_h	Hydraulic conductivity	$[m/s]$
Re	Reynolds number	[-]
$\mathbf{K}_i$	Absolute permeability	$[m^2]$
$\mathbf{g} = (0,0,-g)$	Gravity	$[m/s^2]$
$k_{r\alpha}$	Relative permeabilty	[-]
μ_α	Phase α dynamic viscosity	$[Pa \cdot s]$
$\mathbf{v}_{por}$	Pore velocity	$[m/s]$
$\mathbf{v}_{\alpha,por}$	Pore velocity of phase α	$[m/s]$
k_{rw}	Residual wetting phase saturation	[-]
k_{rn}	Residual non-wetting phase saturation	[-]
$k_{r\alpha}$	Phase α relative permeability	[-]
B	Extensive property	
β	Intensive property	
dV	Volume of a control volume	$[m^3]$
$\mathbf{J_C}$	Convective flux	$[mol/m^2s]$
$\mathbf{J_D}$	Diffusive flux	$[mol/m^2s]$
$\mathbf{dS}$	Control surface	$[m^2]$
Q	Source/sink	
S_0	Specific storage coefficient	
ρ_{w0}	Reference water density	$[kg/m^3]$
p_w^{sat}	Water vapor saturation pressure	$[Pa]$
Chapter 5:		
i	Well number i	[-]
num	Total number of well	[-]
$Q_{g,i}$	Gas amount containing methane extracted at well i	[-] or $[m^3/s]$, [mol/s]
Q^{top}	Gas amount containing methane reaching to the top	[-] or $[m^3/s]$, [mol/s]
p_i	Extraction pressure at the i-th extraction well	[Pa]
$\mathbf{x}_i = (x_i, y_i, z_i)$	Coordinate of the i-th extraction well	[m]
$f_1(p_i)$	Operational cost required for active extraction	e.g. [$]

$f_2(\mathbf{x}_i)$	Well installation cost (i.e. changes according to the location $\mathbf{x}_i$ of the well)	e.g. [$]
$f_3(Q_{g,i})$	Profit from energy production by extracted gas containing methane	e.g. [$]
$f_k(Q^{top})$	Cost (or risk) due to gas containing methane which reaches to the surface.	e.g. [$]

Abstract

This thesis has two foci.

The first focus is the development of a so-called simulation-optimization model. An optimization algorithm, Simulated Annealing (SA), is coupled with a Multiphase/ Multicomponent simulator, MUFTE-UG, to solve a real-world simulation-optimization problem (henceforth MUFTE-SA). In this thesis, the simulation-optimization model is tailored to the study of better (optimal) methane-extraction strategies from an abandoned coal mine in the Ruhrgebiet, Germany. The question of how to deal with the methane from abandoned coal mines is always of great concern for the administrators. Thus, I try to provide one numerical tool to support this decision making in the context of extraction-well operations. The skills required for modelling, for example using computational fluid dynamic theories, have been making progress for the past couple of decades. So nowadays, additionally, the importance of developing a so-called decision-support system integrating these skills is starting to be noticed. This simlation-optimization model is designed to answer these new requirements. Although, the use of the simulation-optimization model in this thesis is limited to the investigation of better methane-extraction strategies, the model itself can be utilized anologously for many processes whose abstracted aspects can be modelled by the multiphase/ multicomponent model. In the past, this sort of simulation-optimization model could only be applied to an artificially designed example since the computational time needed to make real-world simulations is generally enormous, although optimization procedures require dozens, hundreds, thousands of iterations. Thus, a pseudo parallelization design of the optimization procedure is proposed in order to use a parallel computer, having succeeded in reducing the total computational time by a factor of 23.

The second focus is to make comparative studies using different model concepts (i.e. a two-phase and a two-phase/ three-component model) for the simulation of methane-migration and methane-water interaction processes in saturated coal mines. This work includes the new development of a two-phase (liquid, gas) / three-component (water, air and methane) model in order to incorporate mass-transfer processes between the phases. Considering the mass transfer processes between the phases sometimes becomes very important, especially when the coal mine is modelled after groundwater rebound. This is because the dissolution of the methane in the liquid phase is relatively high under some conditions.

Kurzfassung

Diese Dissertation behandelt zwei Kernpunkte: erstens die Entwicklung eines Simulations-Optimierungsmodells für Mehrphasenströmungen im Untergrund und zweitens Vergleichsuntersuchungen von verschiedenen Modellierungskonzepten.

Zur Entwicklung des Simulations-Optimierungsmodells wurde ein Optimierungsalgorithmus, Simulated Annealing, programmiert und mit einem Mehrphasen-Mehrkomponenten-Simulationsprogramm (MUFTE-UG) gekoppelt. Dieses Simulations-Optimierungsmodell wird auf die Untersuchung von optimalen Methan-Extraktionsstrategien für ein stillgelegtes Kohlebergwerk im Ruhrgebiet zugeschnitten.

Die Frage, wie mit dem Methan aus stillgelegten Kohlebergwerken umgegangen werden soll, ist von großzer Bedeutung. Einerseits ist einer möglichen Explosionsgefahr durch unkontrollierte Methanmigration vorzubeugen, anderseits wird die wirtschaftliche Nutzung des Methans zur Energieerzeugung untersucht. Deshalb versuche ich, ein numerisches Werkzeug zur Verfügung zu stellen, das diese Entscheidungen in Bezug auf den Betrieb von Extraktionsbrunnen unterstützt.

Die Möglichkeiten der Modellierung von realen Lagerstätten haben innerhalb der letzten Jahrzehnte stark zugenommen, da leistungsfähige numerische Methoden und Rechner entwickelt worden sind. Deshalb wird heutzutage die Bedeutung der Entwicklung sogenannter decision-support Systeme, die diese Kenntnisse integrieren, mehr und mehr geschätzt. Dieses Simulations-Optimierungsmodell stellt eine Antwort auf diese neuen Anforderungen dar. Obwohl das Simulations-Optimierungsmodell in dieser Dissertation auf die Untersuchung besserer Methan-Extraktionsstrategien beschränkt ist, kann das Modell analog für viele andere Anwendungen verwendet werden, die durch ein Mehrphasen-Mehrkomponentenmodell modelliert werden können. In der Vergangenheit konnte diese Art von Simulations-Optimierungsmodell nur auf künstliche Beispiele angewandt werden, da die Rechenzeit für praktische Simulationen im Allgemeinen enorm ist. Da Optimierungsprozeduren Hunderte von Iterationen benötigen, wird eine pseudo-parallele Ausführung der Optimierungsprozedur durchgeführt, um Parallelrechner verwenden zu können. Damit kann die Rechenzeit dieser Prozedur um einen Faktor 23 verringert werden.

Der zweite Punkt dieser Arbeit sind Vergleichsuntersuchungen unter Verwendung verschiedener Modellkonzepte (d.h., eines Zweiphasen- und eines Zweiphasen - Dreikomponentenmodells) für die Simulation von Methanmigration und Methan-Wasser-Interaktionsprozessen in den gefluteten Kohlebergwerken. Diese Arbeit schließt die Neuentwicklung eines Zweiphasen (Flüssigkeit, Gas) / Dreikomponenten (Wasser, Luft und Methan) - Modells ein, um den Massentransfer zwischen den Phasen beschreiben zu können. Die Betrachtung des Massentransfers zwischen den Phasen

wird besonders dann sehr wichtig, wenn das Kohlebergwerk nach dem Grundwasseranstieg modelliert wird. Das liegt daran, dass die Löslichkeit des Methans in der Flüssigphase unter bestimmten Bedingungen relativ hoch ist.

Chapter 1

Introduction

1.1 Motivation

For the past decades, the mining sector has played a major role in energy production all over the world. The importance of coal-mining activities can be seen in the fact that in 1951 European Coal and Steel Community (ECSC) was estabilished; this was an origin of the current European Union. The mining sector has, however, been forced to change its role due to the replacement of coal by petroleum as the main energy source. This kind of change has led to the closure of coal mines in industrialized countries.

These closures have had both negative and positive results. For example, dewatering is often terminated after coal mines are abandoned. As a result, the mines are flooded by groundwater whose level rises up near to the surface water level (Figure 1.1). This process is called groundwater rebound. Mined strata, however, generally contain soluble minerals which are often toxic for creatures. In the course of the groundwater rebound process, the groundwater dissolves these ecotoxic metals which induce the deterioration of the groundwater quality (Adams and Younger (2001)[1]).

In addition, the degassing facilities are terminated as well after these abandonements. In these coal mines, methane gas is normally absorbed by coal seams. The methane emission causes fewer problems while mines are in operation since it is carefully controlled by the ventilation. However, the termination of the gas-control facilities has led to uncontrolable methane-gas migrations to the surface of the earth via old mine workings, shafts, permeable strata, faults and mining-induced fractures. Methane-gas emission close to residential areas is dangerous because methane is a fire and explosion risk, and the accumulation of gases in houses normally causes human health problems. Methane is a greenhouse gas and its effect is considered to be dozens of times more potent than that of carbon dioxide. On the other hand, methane gas is expected to be utilized as an energy source if the flow is large enough and controlled suction is possible (e.g. Abandoned Mine Methane (AMM), Methane hydrate, etc.).

Thus, as a matter of course, some of the primary concerns of administrators of coal-mine operations are always how to prevent the deterioration of the groundwater quality and/or how to control and extract the methane from the subsurface, whether the workings are still in operation or have already been abandoned. The latter is the primary concern of this thesis. At this stage, numerical

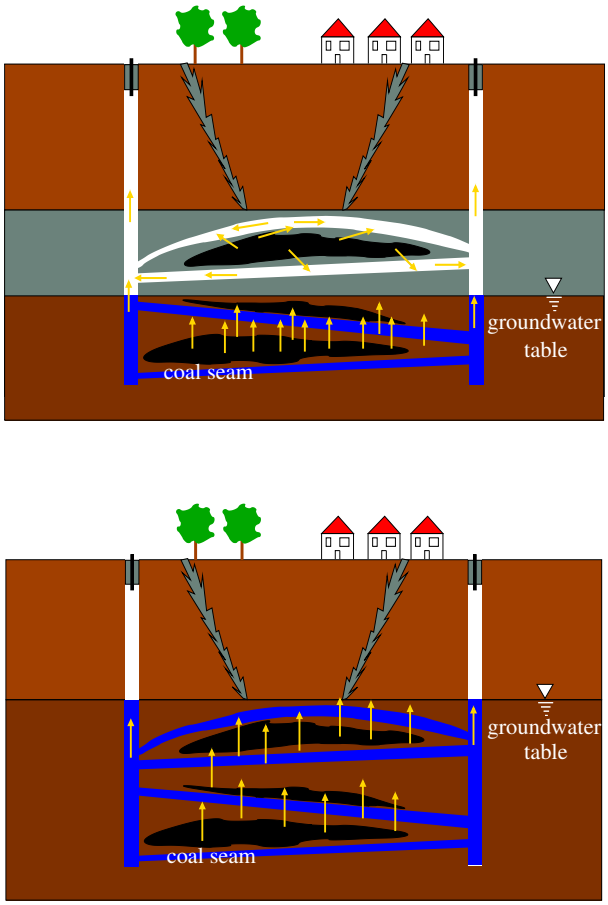

Figure 1.1: Groundwater rebound in a former coal mine, which causes the dissolution of soluble minerals and/or uncontrollable gas (methane) migration.

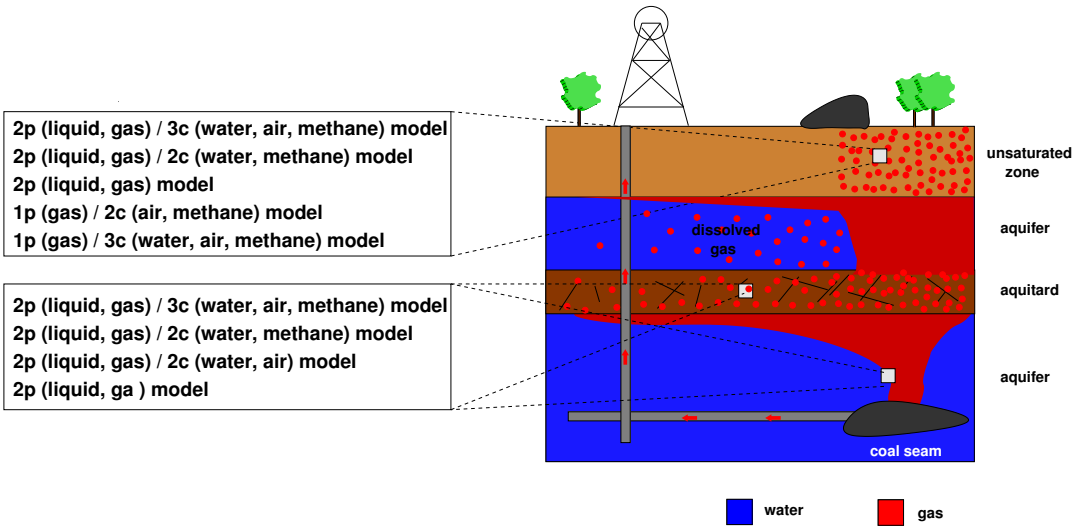

Figure 1.2: Multiphase/ multicomponent model concepts for a coal-mine site

tools can be a great help, for example, to investigate better methane-extraction strategies from these abandoned coal mines, and/or to improve process understanding of methane-migration in the subsurface. In the first case, so-called simulation-optimization models can be utilized in order to decide on the operational strategies for methane extraction (e.g. the decision on the location of the passive extraction wells, of the extracting schedules by the active extraction wells etc.), which is the main purpose of this thesis. This aspect will be addressd in more detail in Section 1.3, since some a-priori knowledge is necessary to explain these simulation-optimization models. Generally speaking, the first considerations among the utilizations of numerical tools for these coal mine problems would be simply to make simulations of the methane migration processes. Let me discusse this aspect in more depth in the next section, first by asking how we can use numerical simulators for these coal-mine problems. The consideration here is restricted to multiphase/ multicomponent models for porous media.

1.2 Model Concepts for Methane Migration in Coal Mines

Numerical simulations can be carried out on various scales both quantitatively and qualitatively. A schematic diagram for the explanation of multiphase/ multicomponent model concepts which can be utlized for these coal-mine problems is seen in Figure 1.2. There are different types of conceptual models which are to be used corresponding to the problem. The choice of the model concept depends very much on the aspects which we want to capture most accurately. First of all, let me distingish the saturated and unsaturated zone. I begin by considering the saturated zone. *The focus of the consideration here is always on how to simulate methane (gas) migration, so that we always have to keep the methane (gas) element in the model concepts. Thus, the view may be completely opposite to the one geneally seen on the basis of the distinctions between groundwater systems.*

In the saturated zone, be it an aquifer or aquitard, we are required to consider two phases, a liquid and a gas phase because, besides the gas (methane), groundwater in a liquid state always has to be considered. Thus, two-phase type models should normally be applied. Now, if the gas phase is composed of mostly methane and only slightly water vapor, using the simplest two-phase model (e.g. Helmig (1993)[40], Bastian et al. (1997)[7], Helmig et al. (1997)[42], Helmig et al. (1998)[46], Sheta et al. (1998)[82], Huber et al. (1998)[53], Huber et al. (1999)[54], Paul et al. (2000) [72], Paul (2003)[71], Breiting et al. (2000) [13], Kobayashi et al. (2002)[59]) is appropriate to describe the relevant process. The problem in this case is that mass transfers of the components between phases cannot be dealt with. In order to deal with mass transfers, a two-phase (gas, liquid)/ two-component (water, methane) model should be used instead. For example, if we want to estimate the mass transfer caused by the dissolution of methane into the liquid phase, we need the two-phase/ two-component model (Helmig et al. (1996)[44], Helmig et al. (2000)[47], Jakobs et al. (2002)[56]). However, this model is not appropriate enough when the gas phase consists not only of methane and water vapor but also of some amount of air (e.g. 60% methane, 35% air and 5% water vapor). In this case, a two-phase (gas, liquid)/ three-component (water, methane, air) model (Huber et al. (1997)[52], Class et al. (2002) [18][17], Hinkelmann et al. (2002) [49], Kobayashi et al. (2002)[59]) should be used instead. Even such a complex model has to be applied occasionally in saturated coal mines.

On the other hand, the first question in modelling of the unsaturated zone would be whether we want to consider the contributions of liquid water or not. If so, we always need to consider using two-phase-type models again. The choice of a two-phase model among various alternatives (e.g. two-phase, two-phase/ two-component, two-phase/ three-component) should mostly be based on the same considerations as those for the saturated zone. However, for example, when water in a liquid state is in a residual-water saturation state, it would not be a great problem to neglect the liquid phase. In this case, using one-phase type models should be valid. Two types of one-phase model are described in the figure, i.e. the one-phase (gas)/ two-component (air, methane) model and the one-phase (gas)/ three-component (air, methane, water vapor) model. The choice between these two depends mostly on whether or not the methane component should be distiguished from the air component.

After all, many alternatives exist even if we want to simulate methane-migration processes alone. Although the two-phase/ three-component model contains the maximum numbers of abstracted aspects of the physical processes among the models, it does not simultaneously mean that this choice is always the best, especially considering that handling the model is difficult and it is generally the most expensive in terms of computational times. Thus, there are always trade-offs in times of model selection and we always need to ask ourselves, ”Which aspect should be really answered in the problem ?”.

1.3 State of the Art

In this section, I carry out a review of the state-of-the-art simulation-optimization models and multiphase/ multicomponent simulators. Simulation-optimzation models are the key issue of this thesis, so the review of them is conducted first, followd by the review of multiphase/ multicomponent simulators. In Chapter 5, I will show an application of a multiphase/ multicomponent simulation-optimization model to a field site in the Ruhrgebiet, Germany as one of the concrete example. Thus, the final purpose of this review is, paradoxcally speaking, to conclude that the number of applications using this type of multiphase/ multicomponent simulation-optimization models is rather low, and those generally use artificial examples.

1.3.1 Simulation - Optimization Model

Very simply speaking, a so-called simulation-optimization model is a model which combines a simulation model with an optimization model. This simulation-optimization model can be applied in many contexts of scientific and engineering tasks in order to solve combined simulation-optimization problems. I carry out the review of these applications by dividing the use into two types, i.e. estimating required parameters in mathematical models or choosing the best strategy among alternatives in terms of, for instance, subsurface management. Since the simulation-optimization model developed within the framework of this thesis is applied for the latter purpose (i.e. as a decision-support tool), the focus of the review here is on the latter.

Let us start with the review of the first use. Applying the simulation-optimization model to estimate parameters is often referred to as inverse modelling. Inverse modelling stands for a procedure for estimating certain parameters inversely using laboratory/field data and the corresponding

results of numerical simulations. Generally, the objective function takes the form of the square or absolute value of the weighted residual. The task of the optimization model is to minimize these objective functions by means of adjusting the input parameters required for the simulation (for further details, see e.g. Finsterle (1993) [28]).

Literature surveys of inverse modelling in the hydrogeological field, especially focusing on the flow and transport processes in the *saturated* zone, are shown e.g. in Neumann (1973) [68], Yeh (1986) [94], Ewing and Lin (1991) [25], Zimmerman et al. (1998) [99] (referred to Finsterle (2004) [30]). The application of inverse modelling to the *unsaturated* zone seems to be less extensive. Relatively small number of data inversion studies have been reported in the literatures. The difficulty lies in the fact that, in the unsaturated zone, the gas phase has to be distinguished from the liquid phase; this requires the application of at least a so-called Richard's equation, or more general multiphase flow equations (Richard's equation is a simplified form of the two-phase (gas, liquid) model). In this case, we often meet problems such as: lack of experimental data tailored to multiphase inverse-modelling studies; a lack of skill in solving multiphase flow forward simulations; nonlinear behavior of the objective functions obtained from the multiphase flow simulations, which requires efficient and stable multiphase inverse modeling codes etc. These reviews are shown, for example, in Kool et al. (1987) [61], Hopmans and Simunek (1997) [50], Durner et al. (1997) [23], and especially Finsterle (2004) [30].

More specifically, inverse-modeling studies with (non-) isothermal two-phase model can be seen, for isothermal two-phase systems, in Finsterle and Pruess (1995) [33], Schultze et al. (1997) [80], Vasco and Datta-Gupta (1997) [85], Wu et al. (1999) [93], Tran et al. (1999) [83], Datta-Gupta and Yoon (2002) [93], Vega et al.(2003) [86], Senger et al.(2003) [81] and, for nonisothermal two-phase systems, Finsterle et al. (1998) [31], Finsterle et al. (2000) [32], Engelhardt et al. (2003) [24], White et al. (2003) [92], Bjoernsson et al. (2003) [12]. Thus, the number of inverse-modelling applications with multiphase flow models as the forward process simulators is not yet large, although it is increasing steadily.

On the other hand, literature introducing the second use, i.e. deciding on the best strategy among alternatives in terms of subsurface management, can be found relatively frequently in case when the combined simulators are groundwater flow and transport models, while only little exists for multiphase/ multicomponent models. In the former case, the objective function can be, for example, to optimize physical processes, or the financial costs associated with drilling boreholes and well installations, and/or the operational costs with regard to pumping groundwater, and/or remediations of contaminated groundwater. The parameters to be optimized (design variables) in these cases are, for example, hydraulic gradients, pumping capacities, head and concentration limits, and the minimum number of active wells needed at any time from the total candidate wells.

For instance, C. Zheng developed ModGA (1996-2000, see [95] [96] [97] both for ModGA and the subsequent MGO), a simulation-optimization model which can be applied for the optimal design of groundwater hydraulic control and remediation systems in general field conditions. The simulation in this model is carried out with MODFLOW (McDonald and Harbaugh (1988) [65]) and MT3D (C.Zheng (1990) [98]), while the incorporated optimization algorithm is a global search method Genetic Algorithms (GA). Moreover, C. Zheng developed MGO (Modular Groundwater Optimizer) combined with the MODFLOW and MT3D. MGO contains three global optimization methods, i.e. Genetic Algorithm, Simulated Annealing and Tabu Search, which are linked by a common input/output structure and integrated with a gradient-based optimization

module to reduce the comuputational burden.

The models of C. Zheng were especially tailored for use in groundwater and tranport problems reproduced by, for example, MODFLOW. On the other hand, optimization models are often developed independently of the type of the simulation model. In other words, many of this type of optimization package (at least) states that these optimization models can be combined with any kind of simulator. For exmaple, ASAP (Adaptive Simulated Annealing Package) by A.H. ALY (1999) [2] [3] states that it can provide rigorously optimized water-resource and environmental-management designs by combining well-accepted simulation packages (e.g. MODFLOW and MT3D) with an artificial neural network (ANN) and adaptive simulated annealing (ASA) techniques incorporated in ASAP. PEST by J. Doherty (2001) [21][22] using Gauss-Marquardt-Levenberg method, UCODE by E. Poeter and M. Hill (1997,1998) [73][48] using a modified Gauss-Newton method belongs to this type of optimization package.

As far as the application of multiphase/ multicomponent simulation-optimization models is concerned, we can find far fewer references in the literature. As far as I could see, the sole researcher who used a multiphase/ multicomponent simulation-optimization model in the decision-support context systematically seems to be Finsterle et al. (1995)[33] and Finsterle (2000)[29].

Finsterle et al. utilized the iTOUGH2 code in order to optimize the pumping schedule for an aquifer cleanup operation. They considered an artificially confined aquifer whose permeability field is geostatistically generated. TCE is released from an area of the aquifer where the groundwater flows in one direction due to the natural hydraulic gradient. Thus, this artificial aquifer is contaminated by TCE. For the remediation of this contaminated site, wells are installed in or near the TCE plume. The model used is a nonisothemal three-phase (gas, water, non-aqueous phase liquid (NAPL))/ three-component (air, water, TCE) model T2VOC, an extension of a multiphase code TOUGH2 (for the details of the TOUGH family, see the next section). The optimization code iTOUGH2 was coupled with T2VOC. iTOUGH2 encompasses five different optimization algorithms, i.e. the Gauss-Newton method, the Levenberg-Marquardt method, the Downhill Simplex method, the Simulated Annealing, and the Grid Search. A comparison of the optimized pumping schedule obtained from these five algorithms reveals the advantages and disadvantages of each method.

As another example of iTOUGH2, a generic cost function is formulated for thermally enhanced soil-vapor extraction. Finsterle first reproduce the air/steam-injection experiment carried out at the University of Stuttgart in Germany (Betz et al., 1998 [11]), then formulate the generic cost function accounting for the costs caused by the residual TCE contamination in the system, the penalty term by the recondensed TCE reaching the bottom, and the costs required for the injection of steam and air. The model domain represents a vertical test cell filled with coarse sand and a lens of finer sand embedded around the center of the domain. TCE at residual NAPL saturation is placed around the center of the domain, partially penetrating the finer sand lense. Steam and air are injected at certain areas on the left-hand boundary. The generic cost function has a characteristic in that the penalty term is added. Finally, the set of parameters (steam enthalpy and air-injection rate) which minimize the generic cost function is obtained.

Though significant theoretical progress has been made for simulation-optimization models, either the groundwater flow and tranport model or the multiphase/ multicomponent model is used as the simulator, the application of these models to real-world problems has remained very limited. This

is mainly because the optimization algorithms, especially global search methods, require quite a number of iteration steps, i.e. huge CPU times equal to CPU time of each simulation multiplied by the number of iterations. Thus, most of the examples shown in the literature still use artficially assumed domains. While this limitation will be mitigated to a large extent by rapid advances in computers, we should always weigh the pro and cons, i.e. can we accept near-optimal solutions generally requiring a much lower number of forward simulations than that necessary to identify the global optimum ?

1.3.2 Multiphase/ Multicomponent Model

There are relatively few numerical codes for multiphase/ multicomponent flow in subsurface systems. Historically speaking, engineers and scientists from the petroleum engineering field have taken the initiative in the developments. Nevertheless, I will not mention all the works from this field, mainly because it is simply not easy to do this comprehensively. Instead, I limit my attention to well-known general-purpose simulators.

TOUGH2, the successor of TOUGH, is one of the best-known codes for the modelling of multiphase/ multicomponent systems and was released to the public in 1991 (K. Pruess et al. [75]). The code employs the integral finite difference method. At the time of release, the number of grid blocks which TOUGH2 was able to use in a practical sense was around 2000 for 2D problems and a few hundred for 3D problems. To overcome these limitations, a set of three preconditioned conjugated gradient solvers was added to TOUGH2 (T2CG1, Moridis and Pruess 1995 [67]). Around the same time, a module T2VOC was added, primarily designed for environmental-contamination problems involving volatile organic chemicals (Falta et al., 1995 [26]). T2VOC retains the full two-phase coupled fluid and heat-flow capabilities of the geothermal modules of TOUGH2, so that it is applicable to the migration of a volatile tracer in two-phase geothermal reservoirs. Since then, several new fluid-property modules have been added in order to handle multi-component fluids. For instance, EOS7 deals with variable-salinity fluids as mixtures of water and NaCl brine, while EOS7R includes an additional capability for tracers with parent-daughter chain decay (Oldenburg et al., 1995 [70], Oldenburg and Pruess, 1997 [69]). EWASG fluid-property modules (Battistelli et al., 1997 [9]) describe three-phase (aqueous, solid, gas) mixtures of three-components (water, sodium chloride, non-condensible gas). In this module, several choices are possible for the non-condensible gas (CO_2, air, CH_4, H_2, N_2), and changes in gas solubility with salinity are included. These all belong to the so-called TOUGH family.

STOMP (Subsuface Transport Over Multiple Phases, 1996), developed by Mark White and Mart Oostrom [91] at the Pacific Northwest National Laboratory's Hydrology Groups, is also a widely distributed simulator. The STOMP simulator solves the partial differential equations that describe the conservation of mass or enegry quantities by employing an integrated volume finite difference method for the spatial discretization and a backward Euler scheme for the temporal discretization. The solver for the resulting nonlinear coupled algebraic equations is based on Newton-Raphson method. This simulator is arranged in such a way that the user can choose the solved governing equatins (e.g. water mass, air mass, dissolved oil mass, oil mass, salt mass, thermal energy). Depending on the chosen operational mode, the governing tranport equations are be written over one to four phases (e.g. aqueous phase, gas phase, NAPL phase, ice phase, solid phase). Solute tranport, radioactive decay, and first-order chemical reactions are solved using a direct solution

technique (e.g. Patankar's power law formulation, TVD scheme) following the solution of the coupled flow equations.

UTCHEM (University of Texas Chemical Flood Simulator) is a three-dimentional nonisothermal multiphase/ multicomponent finite difference type simulator [20]. It was originally developed by Pope and Nelson (1978) at the Center for Petroleum and Geosystems Engineering, University of Texas at Austin, to simulate enhanced recovery of oil using surfactant and polymer processes. Then, it was generalized by Bhuyan et al. (1990), who extended the model to include other chemical processes and a variety of geochemical reactions between the aqueous and solid phases. Since then, appropriate physical, chemical and biological process models capable of simulating the fate and tranport of NAPLs in the saturated and unsaturated zones of aquifers (i.e. multiphase/ multicomponent systems in the subsurface) have been added gradually. UTCHEM applies a third-order finite difference method with a flux limiter and an Implicit Pressure Explicit Saturation (IMPES) type formulation, where the pressure is solved implicity but concentrations instead of saturations are solved explicitly.

CompFlow, developed by Forsyth et al. (1991) [34], is designed to simulate multiphase flow and tranport in discretely fractured porous media. The model uses a compositional approach which allows the simulation of multicomponent NAPLs. The model was originally based on a block-centered finite differences method and now uses a control-volume finite element method which allows elements with high aspect ratios adjacent to fracture elements. The resulting sparse matrix is solved by incomplete LU factorization and CGSTAB acceleration.

The group at the Institute for Computational Engineering and Sciences at the University of Texas at Austin has been eager to develop a so-called simulator framework IPARS (Integrated Parallel Accurate Reservoir Simulator [62]. This framework can provide interfaces into which new algorithms can be plugged and combined with existing algorithms to form a new application simulator. At present, IPARS can deal with system up to three-phases. An important property of IPARS is that it allows the coupling of different models in different subdomains and supports message-passing parallel computations including dynamic load balancing.

Since 1990, the University of Heidelberg has been active in developing a so-called unstructured grid (UG) framework. It supports hierarchical unstructured meshes in two and three dimensions, adaptive local mesh refinement and message-passing parallel computation including dynamic load balancing. The framework has shown the capabilities very well for a large variety of problems. As a library based on UG, MUFTE (Multi-Phase Flow, Transport and Energy Model for porous and fractured porous media) has been developed jointly by the groups at the University of Stuttgart and the Univerity of Heidelberg [14][45] (henceforth, MUFTE-UG). MUFTE-UG incorporates several different types of spatial discretization method (e.g. BOX, CVFE method) and a Newton-Raphson type solver. Several time-discretization schemes are selectable (see in the following brackets). MUFTE-UG currently supports the following schemes: single-phase stationary, solute transport (implicit/explicit/characteristic), nonlinear transport-reaction system (implicit), two-phase (implicit, sequential and IMPES), two-phase in fractured porous media (implicit), two-phase/ three-component nonisothermal (implicit), three-phase/ three-component nonisothermal (implicit).

Thus, compared with groundwater and transport models relatively little work on developing multiphase/ multicomponent simulators has been conducted. Recently, the development seems to

be shifting toward making so-called comprehensive software frameworks rather than to make fragmental code for each individual problem found in nature. This is mainly because practical application problems require advanced models incorporating many physical processes, accurate discretization schemes, fast solvers and efficient pre- and postprocessing techniques. One difficulty in developing these software frameworks is predicting exactly what will be required in future developments.

1.4 Aim of the Work

This thesis focuses mainly on two aspects:

The first focus is the development of a simulation-optimization model. I have developed an optimization model coupled with a multiphase/ multicomponent model, applicable to simulation-optimization problems. In this thesis, the model is tailored to the study of better (optimal) methane-extraction schemes from coal mines in the unsaturated zone. The question of how to extract the methane from unsaturated coal mines is always of great concern to the administrators. Thus, I try to provide one numerical tool to support this decision making. The skills required to model fields, for example using the theories of computational fluid dynamics, have made progress in the past couple of decades. So nowadays additionally, the development of a so-called decision support system integrating these skills are starting to be quite important. In this thesis, the optimization model coupled with the multiphase/ multicomponent model is designed to answer these new requirements. Although, the use of the simulation-optimization model in this thesis is limited to the investigation of better methane-extraction schemes, the model itself can be utilized anologously for many processes whose abstracted aspects can be modelled by the multiphase/ multicomponent model.

The second focus is on making comparative studies using different model concept (i.e. a two-phase model and a two-phase/ three-component model) for the simulation of methane-migration and methane-water interaction processes in saturated coal mines. This work includes the new development of a two-phase (liquid, gas) / three-component (water, air and methane) model in order to incorporate mass-transfer processes between the phases. The mass-transfer processes between the phases sometimes becomes very important, especially when the coal mines is modelled after the groundwater rebound, in that the dissolution of the methane into the liquid phase seems to be relatively great under some conditions.

The structure of this thesis is as follows:

Chapter 1: A brief description of the problems dealt with in this thesis is presented. The motivation behind the series of research work within the framework of a project, problems often observed in coal mines after closure due to methane emission, some methane characteristics, the significance of numerical-model utilization in the context of this thesis, and the goal of all the research work are briefly explained. Moreover, the-state-of-the-art for simulation-optimization models as well as multiphase/ multicomponent simulators is described in this chapter in order to show where we now stand.

Chapter 2: Items necessary for the development of optimization models are explained. This starts with the formulation of a so-called objective function, then the optimization algorithms for find-

ing the global extremum of the objective function are described. Lator in this thesis, the optimization algorithms are classified into several types, depending on whether the calculation of the first/second derivative of the objective function is required or not. For the purpose of this thesis, a so-called Simulated Annealing (SA) algorithm is chosen due to its flexibility, irrespective of the shape of the objective functions. The coupling procedure of the Simulated Annealing algorithm with the multiphase/ multicomponent model (MUFTE-UG) is also introduced (MUFTE-SA). Moreover, a parallerization strategy by means of a domain decomposition for MUFTE-SA is explained. I often refer to Finsterle (1993) [28] often for the contents of this section, although this thesis is characterised by the fact that the multiphase/ multicomponent-simulation model is applied to a real-world problem. The use of a parallel computer is also one of the challenges of this thesis.

Chapter 3: The conceptual, mathematical and numerical model concepts required for the development of a so-called multiphase/ multicomponent model are described. The focus of this chapter is, especially on the elements necessary for the development of a two-phase (liquid, gas) model and a two-phase (liquid, gas)/ three-component (water, air and methane) model to be used ultimately in the subsequent applications (Chapter 4 and Chapter 5). Priority is given to descriptions of the parameters, the constitutive relations etc. especially needed for gas-liquid systems. For the conceptual model, the theories of continum mechanics and thermodynamics are first of all introduced. Then, the paramters and constitutive relationships introduced from the theories are explained in detail. Naturally these paramters are ultimately calculated. Then, the conceptual model is tranferred to the mathematcal model. With Reynolds transport theorem, mass conservation equations are derived. An extended Darcy's law is applied as the momentum equation. In this thesis, the solver is explained only briefly since it was in priciple developed by my forerunners. For the further details in this regard, I recommend readers refer to the work carried out by my present and former colleagues (see the publications in Section 1.2).

Chapter 4: Comparative studies are made, focusing on methane-migration and methane-water interaction processes in artificially designed saturated subsurfaces using the two-phase model and the two-phase/ three-component model. This process is necessary for the appropriate choice of the model concept. The essence of this comparative study is nothing less than to quantify the methane mass dissolution process from the gas phase to the liquid phase. This study indicates that the use of the two-phase model is questionable in some conditions if we only regard the accuracy of the model as the decision factor in the model selection.

Chapter 5: The simulation-optimization model MUFTE-SA is applied to a site in Dortmund, a part of the Ruhr, Germany, where a coal mine used to be, and at present a furniture company is opening its store on the surface. A series of simulation-optimization procedures are taken in order to mitigate the risks resulting from the on-going methane production from the mine. The main purpose of this application is to find out better methane-extraction starategies by using passive extraction wells. MUFTE-SA is applied in this context to detect better locations for the wells. The details are explained in this chapter.

Chapter 6: The contents of this thesis are summarized and outlook for the future is given.

Chapter 2

Optimization Model

2.1 General Description

The procedure called optimization is nothing less than finding a solution to optimize a so-called objective function which is defined over the solution space. Very simply speaking, we have an objective function $O(\mathbf{x})$, where $\mathbf{x}$ is a parameter set defined either in a discrete solution space R_d or in a continuous space R_c, thus $\mathbf{x} \in R_s(s = d, c)$. Generally, there are constraints within the parameters such that $\mathbf{C}_1(\mathbf{x}) \leq 0$ and/or $\mathbf{C}_2(\mathbf{x}) = 0$. Here, in most cases, optimizing means finding a solution $\mathbf{x}^{opt}$ which maximizes or minimizes the objective function under the constraints, i.e. achieving $O(\mathbf{x}^{opt}) > O(\mathbf{x})$ or $O(\mathbf{x}^{opt}) < O(\mathbf{x})$ for all $\mathbf{x}$ is the goal of the optimization. The difference between the minimization and maximization is only a matter of changing the sign of the objective function. In this context, the first classification I could probably make is based on the difference of the solution space of the objective function, i.e. either the optimization problem is defined in a discrete solution space or in a continuous space. These two ”branches” of the optimization often require slightly different optimization algorithms to yield the solutions.

Optimization with the discrete parameter space is often called combinatorial optimization. The word combinatorial is derived from the word combinatorics, which is a branch of mathematics concerned with the study of the arrangement and selection of discrete objects (M.Sait et al. [77]). In combinatorics, we are usually concerned with finding answers to questions such as: ”Does a particular arrangement exist?” or ”How many arrangements of some set of discrete objects exist?”. The travelling salesman problem or the design of complex integrated circuits are concrete examples. The former is a problem of finding a cheapest way of visiting all cities and returning to the starting point, provided a finite number of cities exist and the travelling cost between each pair of cities can be defined. The latter concerns optmizing the arrangement of several hundred thousand circuit elements on a tiny silicon substrate in order to minimize interference among the connecting wires.

Optimization problems which I deal with in the following are those with the continuous solution space. One typical shape of the objective function for a two dimensional continuous parameter space is shown in Figure 2.1. This is the case when the objective function is nonlinear; thus it exhibits a global minimum and some local minima.

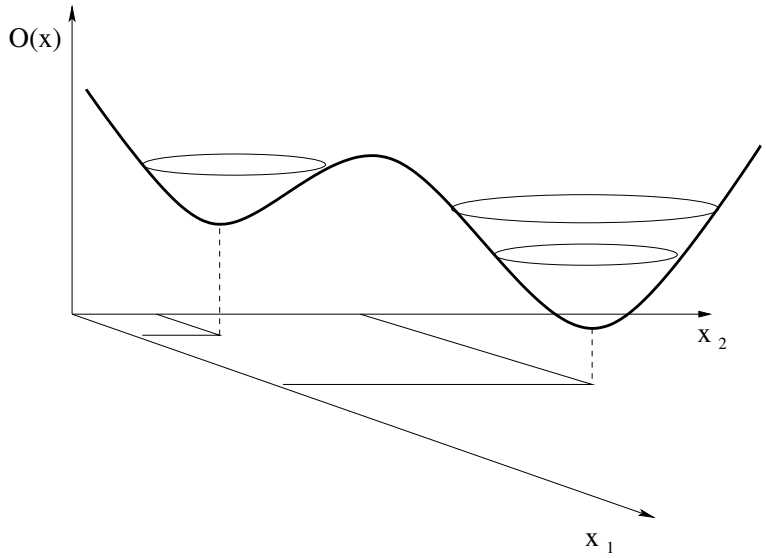

Figure 2.1: An objective function in two-parameter space

Irrespective of its type (whether the solution space is discrete or continuous), what we always have to do is, first, to define the objective function with its constraints, and secondly to minimize (maximize) it using one of the optimization algorithms. At this stage, some optimization algorithms have to be introduced. There are several ways of categorizing the optimization algorithms. For example, we could classify the type of algorithms into (see again M.Sait et al. [77]):

- exact algorithms, and
- approximation algorithms, or heuristic algorithms.

The best known in the first category are linear programing, dynamic programing and so forth. The problem of optimizing a linear function subject to linear inequality and equality constraints is called Linear Programing (LP). Dynamic programing is a stage-wise search method suitable for optimisation problems whose solutions may be viewed as the result of a sequence of decisions.

However, in practice, depending on exact enumerative algorithms is hardly possible because the total search space is huge; instead, we must depend on approximation algorithms. Approximation algorithms are also known as heuristic methods. A heuristic algorithm will only search inside a subspace of the total search space for a good, rather than for the best solution which satisfies the design constraints. Therefore, the time requirement of heuristic algorithm is small compared to that of full enumerative algorithms. Examples of approximation algorithms are the constructive greedy method, local search, genetic algorithms, tabu search, simulated evolution, and stochastic evolution.

On the other hand, as another example, we can classify the algorithms as follows: either the algorithm needs no derivatives, or needs the first derivatives, or the second derivatives of the objective function (this classification is based on Finsterle (1993) [28]):

- Non-Derivative Type Algorithms
  In these methods, the model is evaluated for different parameter combinations, mapping

out the objective function in the n-dimensional parameter space. They are also referred to as Function Comparison Methods. Because no derivatives of the objective function with respect to the parameters must be calculated, these methods are not restricted to smooth models. However, they usually require many trial simulations and are therefore inefficient. Examples of such direct methods include:

  - Trial and error
  - Grid search
  - Downhill Simplex
  - Greedy search
  - Simulated Annealing
  - Genetic Algorithms

- First Derivative Type Algorithms
  These methods require calculating the gradient of the objective function with regard to the parameter vector. Updating the parameter vector in small steps along the search direction determined by the gradient is a robust, albeit inefficient, procedure. Various modifications of this basic scheme have been proposed. Their main difference lies in the choice of an appropriate step length. Efficient ways of calculating the gradient have been described in the literature. Examples of gradient based methods include:

  - Steepest descent
  - Quasi-Newton methods
  - Conjugated gradient methods

- Second Derivative Type Algorithms
  These methods are based on the Hessian matrix or various approximations (quasi-linearization). They perform well for nearly linear least-squares problems. The computational cost for calculating the second derivatives is usually compensated by an efficient stepping in the parameter space. Examples of second-order methods include:

  - Newton Method
  - Gauss-Newton method
  - Levenberg-Marquardt

Each of these methods has its advantages and disadvantages. The choice of an appropriate method largely depends on the presumed properties of the objective function.

The presumed property of my objective function formulated in the following application is:

- The exact shape of the objective funtion is not known, but it is certain that there are multiple local extrema. It is not certain whether or not the objective function is smooth enough to allow the calculation of its derivatives.

Thus, in this thesis, at least as a first step, I decided to the use non-derivative type method since it does not require the calculation of the derivatives and is relatively robust irrespective of the shape of the objective function. The Simulated Annealing (SA) algorithm is especially chosen in this thesis because of its flexibility and robustness.

2.2 Simulated Annealing

The description of this section is based on M.Sait et al. (1999)[77] and Press et al. (1995)[74].

The term *annealing* refers to heating a metal in a solid state to a very high temperature until it is melted (whereby the atoms gain enough energy to break the chemical bonds and become free to move) and then slowly cooling the molten metal in a controled manner until it crystallizes again. By cooling the molten metal at the proper speed, atoms gain an increased chance of obtaining the proper crystal structure of perfect lattices. During this annealing procedure, the free energy of the metal in the solid state is minimized.

In 1953, Metropolis and his colleagues [66] introduced an algorithm to simulate this annealing process, using the transition process of a solid in a heat bath. In their algorithm, they assume that the current state of the solid is S_i with the free energy E_i, while the subsequent state is S_{i+1} with E_{i+1}. The transition from the current state to a new state is expressed by applying a random perturbation rule (henceforth *New State Generation*). If the energy of the subsequent state is lower than the energy of the current state, i.e. $\Delta E = E_{i+1} - E_i \leq 0$, then the new state is accepted. However, if the energy of the new state is higher, then the new state is rejected unless the state can overcome the so-called *Boltzmann probability* $P = e^{(-\frac{\Delta E}{K_B T})}$, where K_B is the Boltzman constant and T the temperature. These procedures are known as the *Metropolis procedure*. This algorithm is then repeated a large number of times until it reaches the thermal equlibrium (henceforth *termination criteria*).

Around 30 years later, Kirkpatrick et al. (1983) [58] pointed out the similarity between this annealing process and combinatorial optimization. In concrete terms, attaining the global minimum is analogous attaining the perfect crystal structure whose energy state is minimum, while the attainment of imperfect structures corresponds to being trapped by local optima. Since then, the so-called Simulated Annealing algorithm based on the annealing process has become one of the most well-developed and widely used iterative techniques for solving optimization problems.

This method is a general adaptive heuristic method and belongs to the class of nondeterministic algorithms. There are already many examples of Simulated Annealing applications. It has been applied not only to combinatorial optimization problems but also to problems with continuous parameter space. One typical feature of Simulated Annealing is that, besides accepting solutions with an improved objective function, it also, to a limited extent, accepts solution with a deteriorated objective function. Initally, the probability of accepting inferior solutions is large but, as the search progresses, only smaller deteriorations are accepted and, finally, only good solutions are accepted. The Simulated Annealing algorithm is effective and robust. Regardless of the choice of the initial configuration, it has the potential to produce high-quality solutions because of the ability to escape from local minima, although it may, of course, take a larger number of iterations until it reaches there. It is also relatively easy to implement.

The cores of the Simulated Anneling algorithm are the Metropolis procedure (namely, New State Generation, Bolzmann probability), the cooling schedule and the termination criteria. There are many varieties in these procedures, although one drawback of the Simulated Annealing is that none of these procedures is general enough yet to be applied to every kind of problem. I use the following form of the Simulated Annealing (Finsterle (1993)[28]). Note that the following proce-

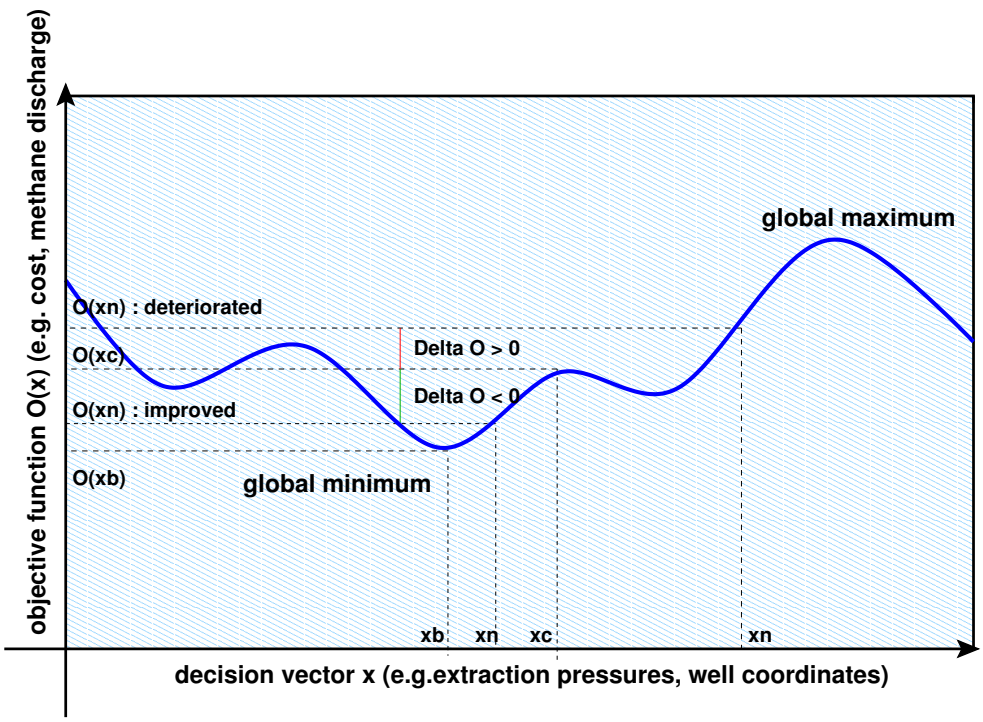

Figure 2.2: A schematic diagram for the Simulated Annealing algorithm.

dure is described in terms of minimization problems and a schematic diagram for the explanation of the following procedures is shown in Figure 2.2.

- **Metropolis Procedure**

  - **New State Generation**
    First of all, the new state has to be generated using a random perturbation rule. In this thesis, the new state is determined using a pseudo-random number generator following the normal distribution:

    $$f(\sigma^k, \mu) \tag{2.1}$$

    where σ^k is the standard deviation in the k-th iteration and μ the mean. As the cooling step proceeds, the standard deviation σ^k is decreased as:

    $$\sigma^k = \left(\frac{k_{max}+10}{k_{max}+11}\right)^k \sigma^0 \tag{2.2}$$

    where σ^0 is the standard deviation at the initial temperature, k_{max} the total number of cooling steps. The standard deviation at the k-th cooling step ($k = 0$ to 10, $k_{max} = 10$, $\sigma^0 = 1/3$) is shown in Figure 2.3. This decrease of the standard deviation is necessary to limit the search space as the temperature decreases. This is analogous to the fact that the mobilities of the atoms of the solid decrease as the temperature of the metal

decreases. Thus, the next decision vector $\mathbf{x}$, is determined such that:

$$\Delta\mathbf{x} = A(\mathbf{x}_{bnd}^{up} - \mathbf{x}_{bnd}^{low}) \tag{2.3}$$

$$\mathbf{x}_{i+1} = \mathbf{x}_i + f(\sigma^k, \mu) \cdot \Delta\mathbf{x} \tag{2.4}$$

where A is the coefficient determined by trial and error, $\mathbf{x}_{bnd}$ the boundary value of the decison vector. The superscripts up and low denote the upper (maximum) and lower (minimum) boundaries. For the exact values and coefficients used in the following application, see Chapter 5.

– **Boltzmann Probability Distribution**
We then have to give the acceptance criterion, the Boltzmann probability. This probability is expressed by:

$$P_{Bol} = e^{\left(\frac{-(O(\mathbf{x}_{i+1}) - O(\mathbf{x}_i))}{K_B T_k}\right)} = e^{\left(\frac{-\Delta O}{K_B T_k}\right)} \tag{2.5}$$

where $O(\mathbf{x})$ is the objective function, $\Delta O = O(\mathbf{x}_{i+1}) - O(\mathbf{x}_i)$, T_k the temperature at the k-th cooling stage. The Boltzmann Probabilty is shown in Figure 2.4. This probabilty is plotted against $\Delta O (= -1$ to $1)$ for the temperature T_0. The Boltzmann constant K_B is 1.0. As shown, the probability is always 1 when $\Delta O \leq 0$, i.e. $O(\mathbf{x}_{i+1}) \leq O(\mathbf{x}_i)$. This means that the new solution is always accepted because the new solution is always improved (minimized) in these cases. On the other hand, if $\Delta O \geq 0$, then the deteriorated solution is accepted only when a randomly generated number exceeds the Boltzmann probability.

- **Cooling Schedule**
Apparently, the essence of the success of this algorithm is how to lower the temperature which allow atoms to be redistributed properly. This schedule is called the cooling schedule and is, in this thesis, expressed:

$$T_k = \alpha^k T_0 \tag{2.6}$$

where T_0 is the initial temperature, and α the coefficient detemined heuristically (however the value generally lies in between 0.8 and 1). The k-th ($k = 0$ to 10) temperature when $T_0 = 0.25$ and $\alpha = 0.8$ is shown in Figure 2.5.

- **Termination Criteria**
There are several criteria considered to be reasonable in order to terminate the simulation. I stop my simulation after taking k_{max} number of cooling steps.

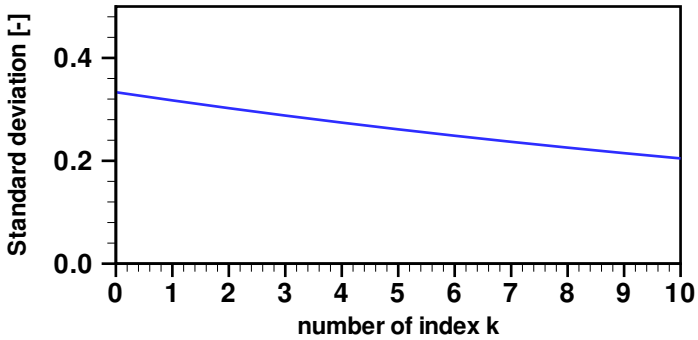

Figure 2.3: A standard deviation for the Simulated Annealing algorithm.

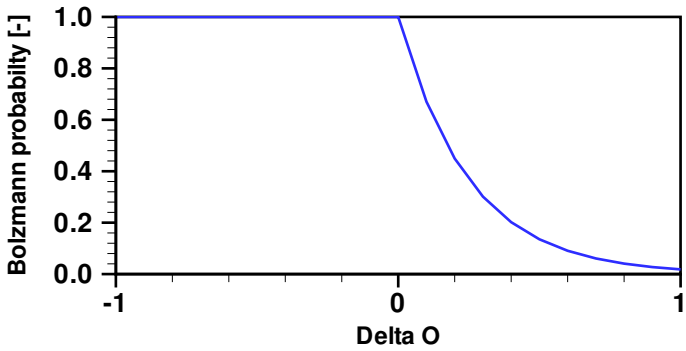

Figure 2.4: A Boltzmann probability for the Simulated Annealing algorithm.

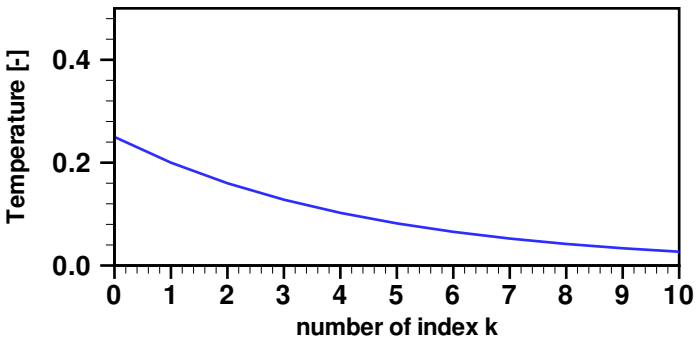

Figure 2.5: A cooling schedule for the Simulated Annealing algorithm.

The chart of the overall procedure is as follows:

Simulated Annealing Algorithm
variables
i , index for accepted steps ;
j , index for rejected steps ;
k , index for cooling schedule ;
$\mathbf{x}_c^{i,j,k}$, current decision vector ;
$\mathbf{x}_n^{i,j,k}$, new decision vector ;
$x_{i,j,k}^{best}$, best decision vector ;
$Obj(x), Obj_{j,i}^{best}$, objective function and the best value ;
$\delta_j, \mathscr{R}_j$, random variables ;
$x_{max}, x_{min}, iMax, jMax$, boundary values for x, i, j;

Choose $\mathbf{x}_c^{0,0,0}$;
Compute $F(\mathbf{x}_c^{0,0,0})$ by MUFTE-UG;
set $i = 1, j = 0, k = 0$;
  Repeat
    {
    - New State Generation (henceforce, NSG) -;
    Generate $f(\sigma^k, \mu)$, a random number;
    Compute $\mathbf{x}_n^{i,j,k} = x_c^{i,j,k} + f(\sigma^k, \mu) \cdot \Delta x_c^{i,j,k}$;
    If $\{\mathbf{x}_n^{i,j,k} > \mathbf{x}_{max}$ or $< \mathbf{x}_{min}\}$, **goto NSG** ;
    Compute $F(\mathbf{x}_n^{i,j,k})$ by MUFTE-UG ;
      If $\{F(\mathbf{x}_n^{i,j,k}) - F(\mathbf{x}_c^{i,j,k}) = \Delta F > 0\}$,
        then $\mathbf{x}_c^{i+1,j,k} = \mathbf{x}_n^{i,j,k}$, $F(\mathbf{x}_c^{i+1,j,k}) = F(\mathbf{x}_n^{i,j,k})$;
        set $i = i+1, j = j, k = k$;
      else
        Generate $\mathscr{R}_j$, a psuedo-random number $(0 < \mathscr{R}_j < 1)$;
        if $\{\mathscr{R}_j > P_{Met}\}$
          then $\mathbf{x}_c^{i+1,j,k} = \mathbf{x}_n^{i,j,k}$, $F(\mathbf{x}_c^{i+1,j,k}) = F(\mathbf{x}_n^{i,j,k})$;
          set $i = i+1, j = j, k = k$;
          else $\mathbf{x}_c^{i,j+1,k} = \mathbf{x}_c^{i,j,k}$, $F(\mathbf{x}_c^{i,j+1,k}) = F(\mathbf{x}_c^{i,j,k})$;
          set $i = i, j = j+1, k = k$;
        if $\{i > i_{max}, j > j_{max} = i_{max}/5\}$;
        then $i = 0, j = 0, k = k+1$;
  }
  until $\{k > k_{max}\}$;
end

A coupling procedure of the Simulated Annealing algorithm with a multiphase/ multicomponent model (see Chapter 3) is described in the next section. Additionally, a parallerization strategy of the simulation-optimization model by a pseudo-parallel SA design is discussed in Section 2.4.

2.3 Coupling Procedure for MUFTE-SA

To solve simulation-optimization problems, an optimization model has to be coupled with a simulation model. A coupling procedure of the Simulated Annealing algorithm (SA) with a MUltiphase/ multicomponent, Flow, Transport and Energy model (MUFTE) is outlined in Figure 2.6

(see Chapter 3 for the multiphase model). This coupled model is henceforth called MUFTE-SA. For this model, I first have to give the initial input parameters necessary for MUFTE-SA. These

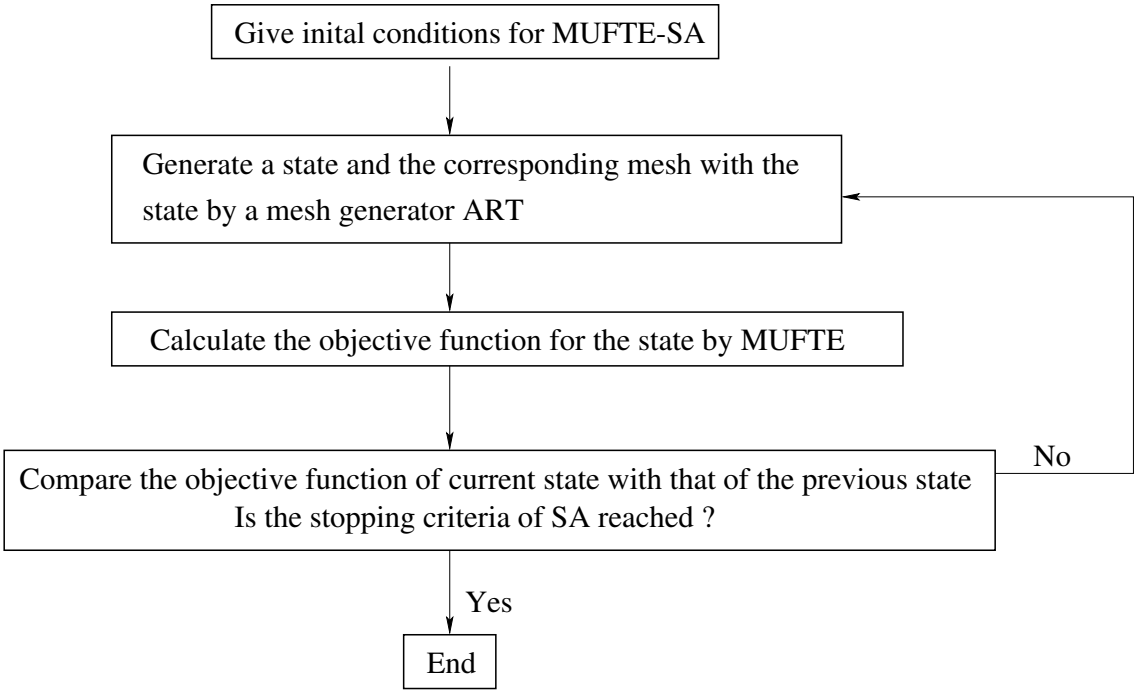

Figure 2.6: A coupling strategy of SA with MUFTE (MUFTE-SA) including the coupling of a mesh generator ART.

input parameters are, for example, the initial decision vector (e.g. coordinates of extraction wells), the α value, the temperature for the cooling schedule of SA, the initial and boundary conditions for MUFTE. Then, the initial mesh is generated by a mesh generator ART (Fuchs (1999)[35]) based on the system set-up (if the decision vector contains the system coordinates, then the generated mesh is different each time). Initial and boundary conditions are then assigned to the mesh according to the rules of the simulator MUFTE, and the initial simulation starts. The objective function is nothing less than the response of this simulation. Thus, we obtain the objective function calculated with the initial decision vector. Then, the SA yields the next decision vector as explained (New State Generation), ART generates the mesh again, and MUFTE computes the objective function for the next vector. After that, the current objective function is always compared with the previous objective function, and the acceptance of the new solution is determined by the Boltzmann probability. After repeating the same procedures, the optimization is terminated when it reaches the termination criteria. The coupling between two models is realized via a shell script which contains a sequence of commands in a batch form. The updated parameter passing is also done by the command in the shell script.

2.4 Parallelization Strategy for MUFTE-SA

The reason why the parallelization strategy had to be considered in this thesis is that, in the application (Chapter 5), one loop of the SA procedure (i.e. from the new state generation to the

evaluation in Figure 2.6) took around 7-8 hours (even some simplifications and compromises in the simulations are made), while SA generally requires dozens, hundreds, thousands of iterations. For example, I was able to approximate the total time in a case of the application by a simple calculation.

$$\frac{7\,hrs \times 1000\,iterations}{24\,hrs/day} \approx 292\,days, \tag{2.7}$$

which is, as a matter of course, not acceptable. This fact forced me to use a parallel computer.

According to Sanchez et al. (2002) [79], a parallel design of SA algorithms can be classified in two categories (for further details of the methods described in the following, see, for example, Sanchez et al. (2000) [78], Greening (1990) [37], Azencott (1992) [5]):

- Pseudo-parallel SA algorithms: sequential SA algorithms run on different processors at the same time or the data domain is assigned to different processors where a sequential SA is running. The principal methods are Data Configuration Partition (DCP), Parallel Independent Annealing (PIA) and Parallel Markov Chains (PMC).
- Parallel SA algorithms: an SA algorithm is divided into tasks which are distributed among several processors. Parallel Markov Chains (PMC), Parallel Markov Trials (PMT), Adaptive Parallel Simulated Annealing (APSA), Speculative Trees and Systolic are parallel SA algorithms.

The parallelization strategy used in this thesis is from the first category, i.e. pseudo-parallel algorithm. The schematic diagram of the parallelization strategy is shown in Figure 2.7. We first select k combinations from a total of n possible combinations for different system set ups of our simulation-optimzation problem. Then, MUFTE-SA procedures for one combination among the k-combinations are carried out on one processor of a parallel computer. The MUFTE-SA procedures on each processor produce an optimum solution (at least locally!). These optimum solutions from each processor are collected on the processor 1, carrying out a main program and looking for a global optimum solution among the candidates. If this main program regards a solution among the solutions as (at least quasi-globally) optimum, then the entire process ends, otherwise the main program selects different k-combinations among the remaining system set-ups, assigns these k to the k-processors again until the main program recognizes that it has found the global optimum solution.

This is a relatively easy way of parallelizing, although the application range is limited. The concrete description of this parallelization for the application is explained in Chapter 5.

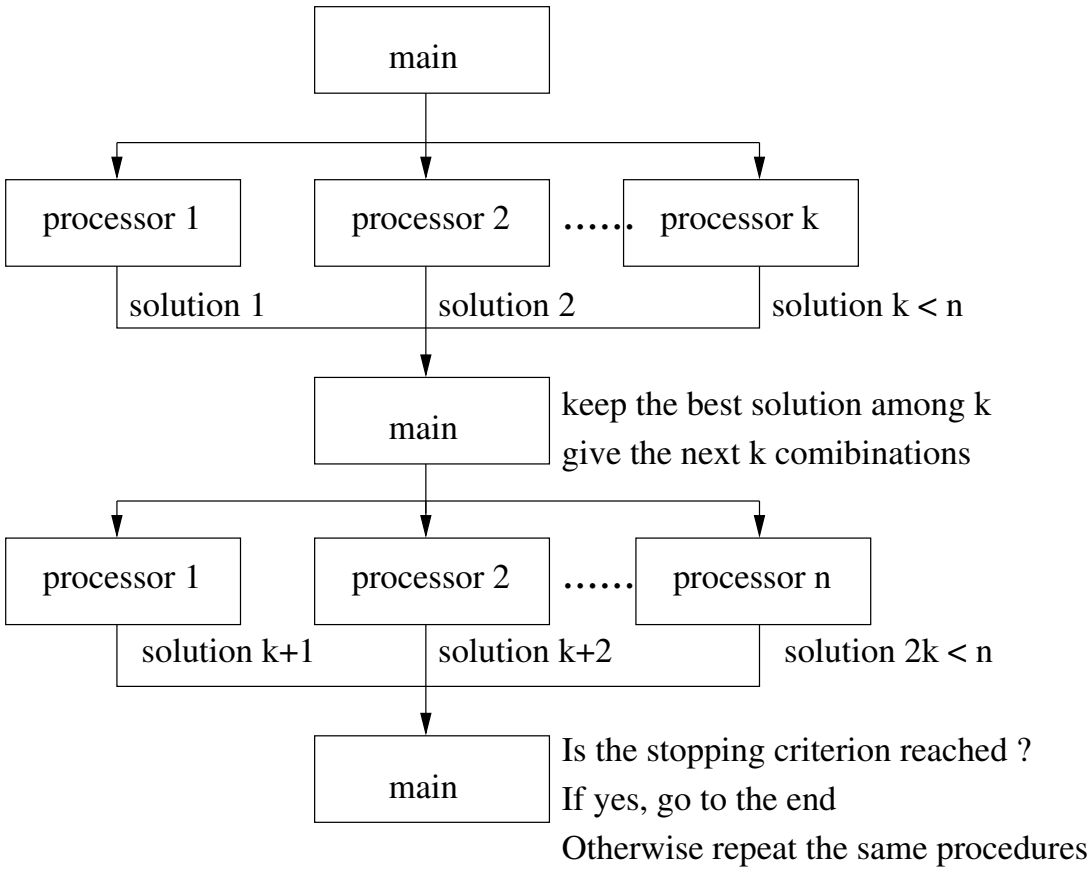

Figure 2.7: A parallelization design

Chapter 3

Multiphase/ Multicomponent Model

The basic theories required for the development of multiphase/ multicomponent models are introduced in this chapter. These explanations are carried out in order from the conceptual model, the mathematical model to the numerical model. The basic idea for the selection of a conceptual model among alternatives, especially for the simulation of methane migration in the subsurface, has already been discussed in Section 1.2. Among the alternatives, a two-phase (water-gas) model and a two-phase (water-gas)/ three-component (water, air and methane) model are selected for the following applications (Chapter 4 and Chapter 5). Thus, the foci in this chapter are, especially on the items necessary for the development of the two-phase and the two-phase/ three-component models.

First of all, natural phenomena have to be abstracted, using the conceptual model by extracting some essential processes in nature. The theories and laws required for setting up the conceptual model, the parameters introduced by the conceptual model and constitutive relationships among the parameters are described item by item in Section 3.1. The basics of continuum mechanics and thermodynamics are first explained in the former half. Then, in the latter half, the parameters required for the two-phase and the two-phase/ three-component models are calculated concretely.

As a next step, this conceptual model is transferred to a mathematical model. We are generally required to give mathematical expressions to the conceptual model in order to reproduce natural processes by numbers. Here, mass conservation, momentum equations are introduced as mathematical models. Since mathematical models can be derived on the basis of a so-called Reynolds tranport theorem, I first introduce this theory briefly in Section 3.2. Then, the mass conservation equations for the two-phase and the two-phase/ three-component models are derived. Generally, the number of unknowns in the mass conservation equations is more than that of the mass conservation equations. Thus, we need to use constraints which come from the constitutive relationships in the conceptual model. How to close the system of equations using these constraints is explained in detail.

Generally, only few analytical solutions exist for these mathematical models. Furthermore, these analytical solutions can be found only for very simple systems. Thus, at this stage, we need to solve these mathematical models using computers. For this requirement, the mathematical model derived in the continuous solution space has to be converted into the numerical model for the digital world. The procedures (i.e. discretization, numerical schemes and solvers) used in this thesis are explained briefly in Section 3.3.

3.1 Conceptual Model

3.1.1 Basics for Continum Mechanics and Thermodynamics

3.1.1.1 Porous Media

We know intuitively that materials such as soil, porous or fissured rocks, ceramics, fibrous aggregates, filter paper, sand filter, a loaf of bread etc. are called porous media. However, in order to consider the physical processes in porous media (here, for instance, flow and transport processes of fluids in the subsurfaces) it is, as a matter of course, better to define the term porous media more rigorously. Here, I quote the definition by Bear et al. (1968) [10] since it is considered one of the most elaborate and reliable. Some of the terms in the definition, not yet mentioned in this thesis, are to be explained in the following sections:

- A portion of space is occupied by heterogeneous or multiphase matter. At least one of the phases comprising this matter is not solid. They may be gaseous and/or liquid phases. The solid phase is called the solid matrix. That space within the porous medium domain that is not part of the solid matrix is referred as void space.
- The solid phase should be distributed throughout the porous medium within the domain occupied by a porous medium; solid must be present inside each representative elementary volume. An essential characteristic of a porous medium is that the specific surface of the solid matrix is relatively high. In many respects, this characteristic dictates the behavior of fluids in porous media. Another basic feature of a porous medium is that the various openings comprising the void space are relatively narrow.
- At least some of the pores comprising the void space should be interconnected. The interconnected pore space is sometimes termed the effective pore space. As far as flow through the porous media is concerned, unconnected pores may be considered as part of the solid matrix. Certain portions of the interconnected pore space may, in fact, also be ineffective as far as flow through the medium is concerned. For example, pores may be dead-end pores (or blind pores), i.e., pores or channels with only a narrow single connection to the interconnected pore space, so that almost no flow occurs through them. Another way to define this porous medium characteristic is by requiring that any two points within the effective pore space may be connected by a curve that lies completely within it. Moreover, except for special cases, any two such points may be connected by many curves within an arbitrary maximal distance between any two of them. For a finite porous medium domain, this maximal distance is dictated by the domain's dimensions.

An enlarged view of a porous medium taken by a tomograph is shown in Figure 3.1 (for the details of this photo, see Vogel (1998) [88]), while two types of aquifer composed of porous media and fractured porous media are shown in Figure 3.2 as references.

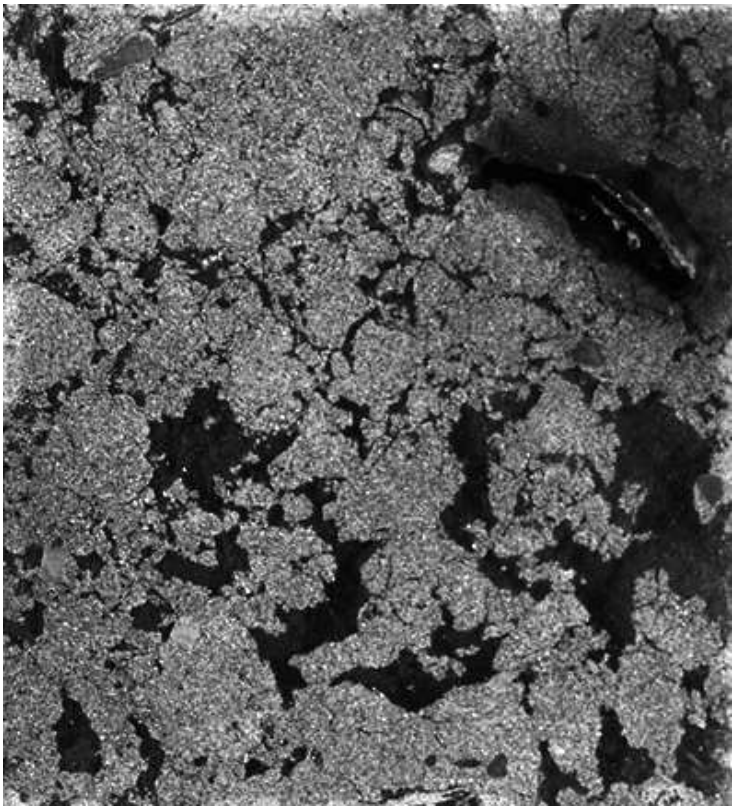

Figure 3.1: Porous medium in a soil sample of $15 \times 15mm$ (VOGEL (1998)[88])

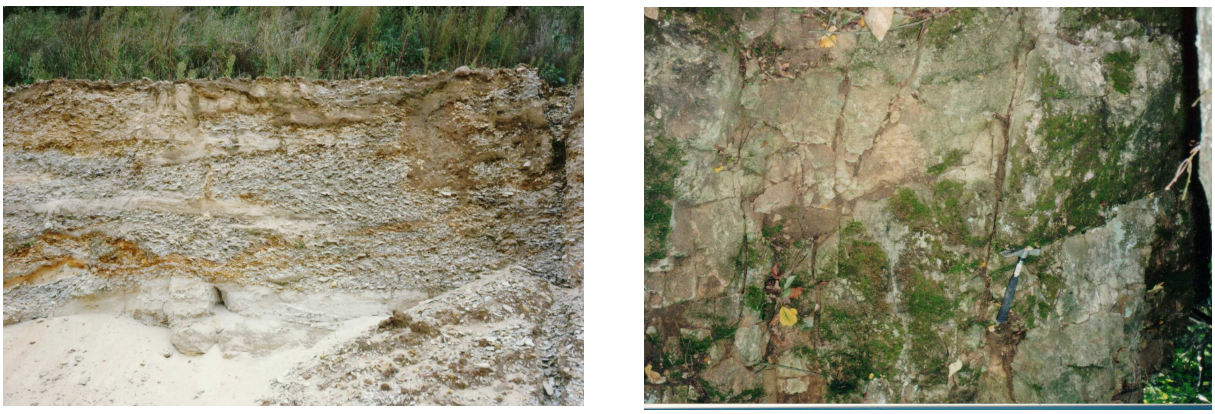

Figure 3.2: Porous medium (left) and fractured porous medium (right)

3.1.1.2 Representative Elementary Volume

There are two main approaches for handling the physical processes in porous media. The first is called the Lagrangian approach, and the second the Eulerian approach. Although both approaches were, in an actual sense, developed by Euler, Lagrange preferred to use the first approach more often and improved it; thus, it is called Lagrange approach.

The Lagrange approach tries to capture the movements of the indivual molecules which consist of, here, the fluid in the porous media. This approach is based on solid mechanics. For exmaple, if we want to trace the movement of a molecule in a fluid in the subsurface based on solid mechanics, we need at least to know the mass of the molecule, all the forces acting on the molecule and its initial position; nevertheless, it is almost impossible to obtain complete information of this kind. In addition, if we want to capture the behavior of a total amount of $1mol$ fluid (the number of molecules contained is ca. 10^{23}), we have additionally to consider the interactions of the 10^{23} molecules, such as the collisions among molecules, between the pore wall and the molecules etc. Furthermore, as we all know, obtaining a complete description of the pore size, the grain size, the geometry etc. of porous media is generally a desperate job. So it is not realistic.

Thus, we should generally take the second, the Eulerian, approach. In the Eulerian approach, we take a certain volume whose center is fixed at a point. In this case, attention is not turned to each individual molecule, but the system properties averaged over the volume. This appoach is well established in the field of so-called continuum mechanics. For the continuum approach, the appearance of the natural processes looks differently according to the spatial scale which emcompasses it, although the natural processes taking place in a certain area are always the same. A schematic diagram of these scale considerations is shown in Figure 3.3. This figure shows the scales which range from the reservoir scale to the boundary layers. As is apparent, the processes which should be taken into consideration at the time of modelling change according to the scale considered (e.g. it is not wise to consider molecular-scale phenomena accurately in the reservoir-scale model!). Thus, the first step for the application of the continuum approaches is how to choose the scale and the appropriate volume in order to divide the entire domain for the reproduction of the processes. This appropriate volume is called the Representative Elementary Volume (REV).

So the next question is how big the volume should be. A schematic diagram intended to answer this question is shown in Figure 3.4. Here, let us consider the porosity of the porous media (see Section 3.1.1.5 for the definition). As shown in the figure, if the volume is very small, the porosity fluctuates strongly due to the microscale heterogeneities: for example, either the small volume contains microcracks or not. On the other hand, if the volume is very large, the porosity fluctuates as well because of the macroscale heterogeneities (e.g. faults, fractures) of the porous media. The ideal volume at which these fluctuations vanish is called REV. The schematic diagram of this REV concept is shown in Figure 3.5. As shown, new sets of parameters are created by the averaging process over the REV, although some system properties are smeared out. This approach is advantageous especially in that we can quantify some averaged values (parameters) which are not possible by the aforementioned Lagrangian approach. Thus, in the following we construct our conceptual models using this REV concept. Speaking frankly, the existence of the REVs with regard to some systems is not yet proved. Nevertheless, we maintain in the following that the REVs always exist in our systems and the detailed discussions in this respect are not addressed anymore. For further details on this aspect, see Jakobs (2003) [55].

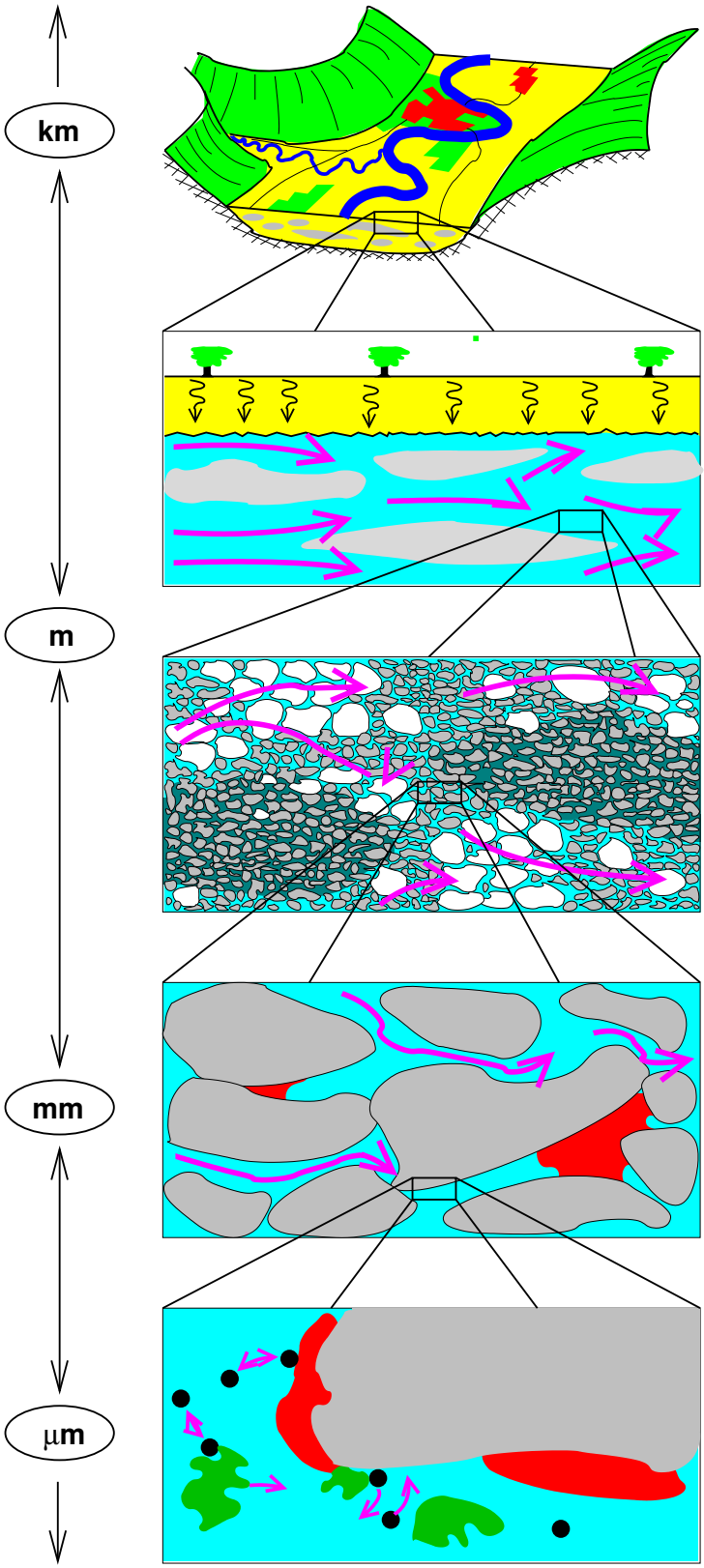

Figure 3.3: Spatial scale considerations in subsurface systems by KOBUS, DE HAAR (1995)[60]

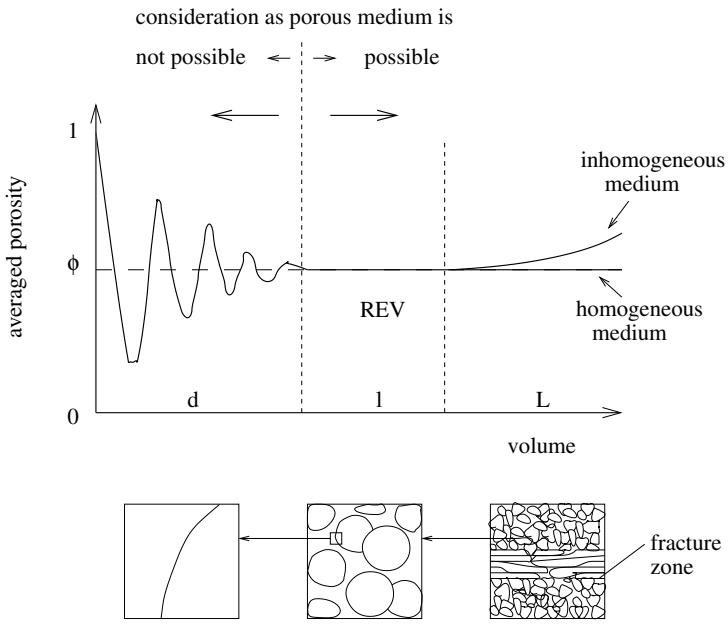

Figure 3.4: Schematic diagram for the explanation of the Representative Elmentary Volume (REV) (Bear (1972) [10], Helmig (1997) [41])

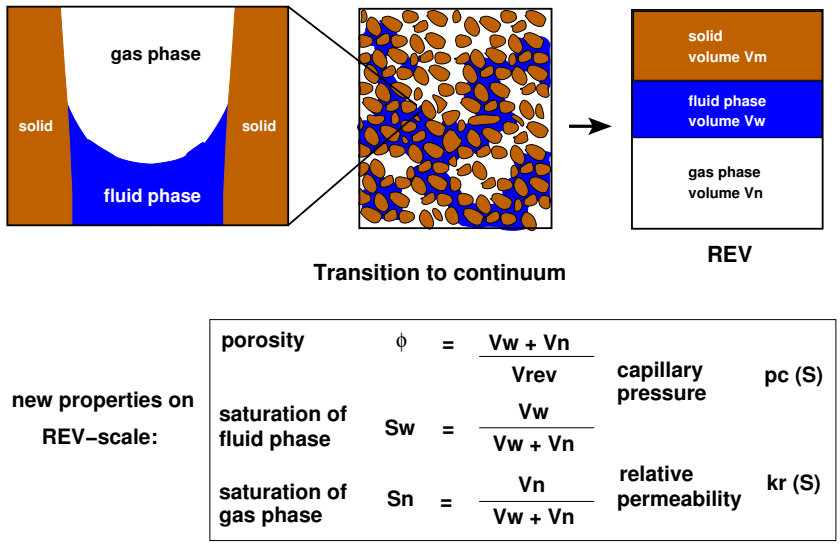

Figure 3.5: Transition to REV (Paul (2003) [71])

3.1.1.3 Thermodynamic System

In thermodynamic systems, the mass and energy are exchanged via the boundaries of the systems by means of actions due to heat and/or work. These systems can be classified according to the type of interaction with the surroundings. I classify here three type of thermodynamic system (refer to Helmig et al. (2000) [43], modified by Kobayashi):

- Completely closed system:
  The boundaries of the system do not allow any interaction with the environment, i.e. there is no exchanage of mass and energy between the inside and outside of the system.
- Closed system:
  There is no mass flux across the system boundaries.
- Open system:
  The boundaries of the system are open for any interaction with the environment.

The systems which I deal with from now on are always assumed to be open systems.

In addition, I have to assume so-called thermodynamic equilibrium. This is based on the following considerations (H.K.VERSTEEG et al. (1995)[87]):

- The fluid velocities may be large, but they are usually small enough that, even though the properties of a fluid particle change rapidly from place to place, the fluid can thermodynamically adjust itself to new conditions so quickly that the changes are effectively instantaneous. Thus, the fluid always remains in thermodynamic equilibrium. The only exceptions are certain flows with strong shockwaves, but even some of those are often well enough approximated by equilibrium assumptions.

By this assumption, we can obtain some of the equations of state which relate the thermodynamic variables (e.g. the pressure, the density and the temperature) to each other. For example, the perfect gas law is one of those equations of state. If the fluids are compressible, the perfect gas law provides the link between the energy equation on the one hand and the mass conservation, momentum equations on the other hand. This link arises through the density variations as a result of the pressure and temperature variations in the flow field. Without these variations, the flow field can often be solved by considering the mass conservation and momentum equations only. The energy equation only needs to be solved alongside the others if the problem involves heat transfer.

For the following model constructions, I further sub-divide this thermodynamic equilibrium condition into three:

- Local thermal equilibrium
  The local thermal equilibrium states that the temperature within the system is locally equal in all phases.

- Chemical equilibrium
  Chemical equilibrium states that the exchange of the componnents between the phases is equal. This means, the chemical potential of the components is equal between the phases. The chemical potential of the components is expressed as the change of the internal energy per change of the moles of the component. We neglect the chemical reactions and the biological decompositions hereafter.

- Mechanical equilibrium
  Mechanical equilibrium states that the pressures on both sides of a phase boundary must be equal. For porous media, we have to always consider the pressure jump between fluid-fluid interfaces due to capillary pressure.

3.1.1.4 Phase and Component

For the multiphase/ multicomponent system, the terms ”Phase” and ”Component” have to be defined earlier than anything else. Throughout this thesis, they are defined as follows (refer to Class et al. (2002) [18], modified by Kobayashi):

- Phase
  Matter which has a homogeneous chemical composition and a physical state is termed phase. We distinguish three phases here, a solid, a liquid, and a gas phase. The solid phase is the matrix of the porous medium and considered only implicitly in the following formulations, i.e. mass and momentum equations for the solid phase do not exist. Several liquid phases can exist in a porous medium, while only one gas phase can be present. The phases are separate from each other.

- Component
  The term component stands for constituents of the phases which can be associated with a unique chemical species. The number of the components in a system is the minimum number of independent chemical species necessary to define the composition of all the phases present in the system. Air is treated here as a single pseudocomponent and its composition (N_2, O_2 and CO_2) is neglected. On the other hand, methane itself is treated as a single component in a soil gas because the primary concern in this thesis is methane behavior. Thus, which element should be defined as the component always depends on the aspect to be examined.

3.1.1.5 Porosity

As shown, for example in Figure 3.5, there is void space in porous media. The amount of void space in the porous media needs to be quantified using the so-called porosity ϕ which is defined as:

$$\text{porosity}\,\phi = \frac{\text{volume of the pore space within the REV}}{\text{volume of the REV}} \tag{3.1}$$

Additionally speaking, the fluids can pass through only when the pore spaces are connected i.e. it produces the flow paths. In other word, a portion of the void space is not utilized as a flow field. The pores in which flow cannot exist are often called dead-end pores. This characteristic is accounted for by the concept of so-called effective porosity:

$$\text{effective porosity}\,\phi_e = \frac{\text{volume of the flow paths}}{\text{volume of the REV}} \tag{3.2}$$

3.1.1.6 Saturation

In multiphase systems, each phase occupies a portion of the void space, although the exact distribution of each phase is not identified any more because of averaging procedures (see again Figure 3.5). We quantify this amount by the so-called saturation of the phase α, or S_α:

$$S_\alpha = \frac{\text{volume of the phase } \alpha \text{ within the REV}}{\text{volume of the pore space within the REV}}, \tag{3.3}$$

$$\Sigma_\alpha S_\alpha = 1 \tag{3.4}$$

The second equation is a constraint which precribes that the sum of the saturations of all phases becomes one. This is apparent from the definition itself.

Additionally, especially for water, the concept of so-called effective water saturation exists and is defined by:

$$S_{we} = \frac{S_w - S_{wr}}{1 - S_{wr}} \tag{3.5}$$

where S_{wr} is the residual saturation of the water. This concept tries to account for the mobile portion of the water only in the pore space; thus the residual saturation is subtracted from the saturation.

The air-water system is often examined in hydrology. In this case, the parameter called moisture content θ is often utilized instead of the saturation:

$$\theta = S_w\phi = \frac{\text{volume of the phase water within the REV}}{\text{volume of the REV}}, \tag{3.6}$$

In addition, the parameter ϕ_α is often defined, using the saturation of the phase and the porosity:

$$\phi_\alpha = S_\alpha\phi = \frac{\text{volume of the phase } \alpha \text{ within the REV}}{\text{volume of the REV}}, \tag{3.7}$$

3.1.1.7 Mass and Mole Fraction

In multiphase/ multicomponent systems, not only phases but also the composition of the phases has to be taken into consideration. These compositions are quantified using the parameters called the mass and mole fractions of the components:

$$X_\alpha^\kappa = \frac{m_\alpha^\kappa}{m_\alpha} \tag{3.8}$$

$$x_\alpha^\kappa = \frac{n_\alpha^\kappa}{n_\alpha} \tag{3.9}$$

where X_α^κ and x_α^κ are the mass and mole fractions, m_α and n_α the total mass and mole of the phase α, m_α^κ and n_α^κ the mass and mole of the component κ in the phase α. This definition indicates that the mass (mole) fraction is the mass (mole) of the component κ in the phase α to the total mass (mole) of the phase α. These mass and mole fractions are apparently constrained by:

$$\sum_\kappa X_\alpha^\kappa = 1 \tag{3.10}$$

$$\sum_\kappa x_\alpha^\kappa = 1 \tag{3.11}$$

3.1.1.8 Perfect Gas Law

Although I do not use the energy equation for a multiphase system in the following application, mainly due to lack of data related to the thermal property of methane, some equations of state are introduced here in order to close the systems of equations (refer to Helmig et al. (2000) [43], modified by Kobayashi; see Section 3.2.5 as well):

Boyle found experimentally that the pressure p_g of a gas at a constant temperature is inversely proportional to its volume V:

$$p_g \propto \frac{const.}{V} \tag{3.12}$$

Similary, Charle found by experiment that the volume V of a gas at a constant pressure is proportional to its temperature T:

$$V \propto const. \cdot T \tag{3.13}$$

The principle found by Avogadro describes that any gas of the same volume at a constant temperature contains the same number of molecules n_g:

$$V \propto const. \cdot n_g \tag{3.14}$$

Manipulating the above three equations yields:

$$p_g \cdot V \propto n_g \cdot const \cdot T \tag{3.15}$$

The constant can be determined experimentally and is called the universal gas constant, i.e. $const. = R = 8.31451\ [\frac{Pa \cdot m^3}{K \cdot mol}]$. Using this universal gas constant, we obtain the following perfect gas law:

$$p_g V = n_g RT \tag{3.16}$$

The molar denstiy of the gas phase can be calculated by transforming Equation (3.16):

$$p_g = \frac{n_g}{V} RT = \rho_g^{mol} RT, \quad i.e. \quad \rho_g^{mol} = \frac{p_g}{RT} \tag{3.17}$$

3.1.1.9 Dalton's Law

Dalton's Law states that the total pressure of mixture of the perfect gases is the sum of the partial pressures of the gases. The partial pressure of the individual gas corresponds to the pressure which is obtained if the system is occupied by the gas only. Thus, we obtain the following relationship:

$$p_g = \sum_{\kappa} p_g^{\kappa} = \sum \frac{n_g^{\kappa} RT}{V} = \sum_{\kappa} x_g^{\kappa} p_g \tag{3.18}$$

where κ indicates components in the gas phase and the following relations are used in the course:

$$\frac{p_g^{\kappa}}{p_g} = \frac{n_g^{\kappa}}{n_g} = x_g^{\kappa} \tag{3.19}$$

3.1.1.10 Henry's Law

Henry's Law is expressed in the form:

$$x_w^{\kappa} = \frac{p_g^{\kappa}}{H_w^{\kappa}} \tag{3.20}$$

where H_w^{κ} is the Henry coefficient. This law can be applied only when the concentration of the component κ in the water is very low. It states that the amount of the component κ dissolved in the water is proportional to the partial pressure of the component in the gas phase. The proportional factor is called the Henry coefficient.

3.1.1.11 Transport Processes

There are three different types of transport process which have to be clearly distinguished for transport in the porous media, i,e. transport due to convection, diffusion and dispersion. A schematic diagram of transport processes is shown in Figure 3.6. A key here is that transport due to convection and diffusion are the result of the real physical processes, while dipersion is caused by the averaging process over the REV, i.e. not the result of the physical process. Each transport is explained in detail one by one in the following.

Convection

Convection transport is the transport of a substance (or mass, momentum, energy, etc.) caused by the mass motion of a fluid and generally expressed in the form:

$$\mathbf{J}_C = Cv \tag{3.21}$$

where J_C is the flux vector due to the convection, v the fluid velocity and C could be the concentration (or mass, momentum, energy, etc.) of the substance. Convection transport occurs through the mass movement of the fluid with different velocities, rather than through the movement of individual molecules (molecular diffusion). Convection transport is, in general, much greater than diffusion transport described later.

Diffusion

Diffusion transport is the transport of a substance (or mass, momentum, energy etc.) caused by the gradient of its concentration. The flux vector due to diffusion is generally expressed using Fickian's Law:

$$\mathbf{J}_D = -\mathbf{D}_{dif}\nabla C \tag{3.22}$$

where $\mathbf{J}_D$ stands for the flux vector due to the diffusion, $\mathbf{D}_{dif}$ the diffusion tensor and C the

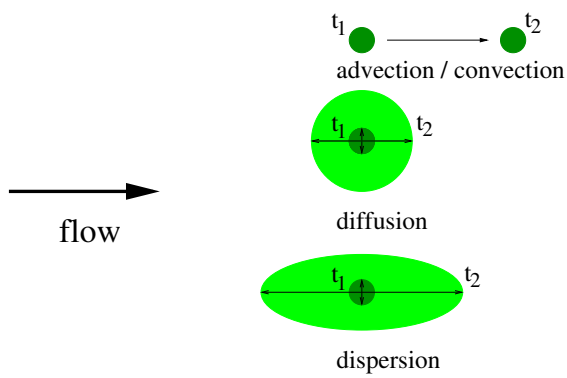

Figure 3.6: A schematic diagram for the explanation of transport processes due to convection, diffusion and dispersion (Barlag (1997)[6])

concentration (or mass, momentum, energy etc.). The diffusion tensor is expressed using the unit tensor $\mathbf{I}$:

$$\mathbf{D}_{dif} = D_{dif}\mathbf{I} = \begin{bmatrix} D_{dif} & 0 \\ 0 & D_{dif} \end{bmatrix}, \tag{3.23}$$

where D_{dif} is the diffusion coefficient. This tensor is isotropic and independent of the flow direction. The diffusion effects are generally classified into two types, i.e. molecular diffusion and turbulent diffusion. Molecular diffusion is caused by the motion of individual molecules. This

motion of individual molecules is often called Brownian movement and tries to compensate for concentration differences by producing fluxes in the direction of the lower concentration. On the other hand, turbulent diffusion is caused literally by the turbulence of the flow fields and expressed in the same form as Equation (3.22), although the coeffcient tensor has to be replaced with one for turbulent diffusion. This turbulent diffusion is generally much larger than moleculer diffusion. Nevertheless, turbulent diffusion is not considered here because, in most cases, flow in porous media is laminar and the turbulent effects are negligible. Thus, in the following, diffusion means molecular diffusion and the coefficient is expressed as $D_{dif} = D_{mol}$.

The magnitudes of the molecular diffusion coefficient are different depending on whether the substance is in the gas phase or in the water phase. Generally speaking, the diffusion coefficient is several orders of magnitude larger in the gas phase ($\approx 10^{-5} m^2/s$) than in the water phase ($\approx 10^{-9} m^2/s$).

Dispersion

Dispersion is, unlike diffusion, not a real physical process. In other words, it is the results of handling the real flow field by continuum mechanics, i.e. averaging the flow field over the REV. In the subsurface, we have to distinguish between two types of dispersion according to the spatial scale, microdispersion and macrodispersion. A schematic diagram, intended to explain these differences, is shown in Figure 3.7.

Microdispersion, shown in the left columm of Figure 3.7, is caused by small-scale velocity distribution, such as the parabolic velocity profile within a pore (top of the columm), or the velocity differences due to the bifurcation processes of the flow around the soil grain (center and bottom of the columm). These velocity deviations are smeared out by the averaging process over the REV

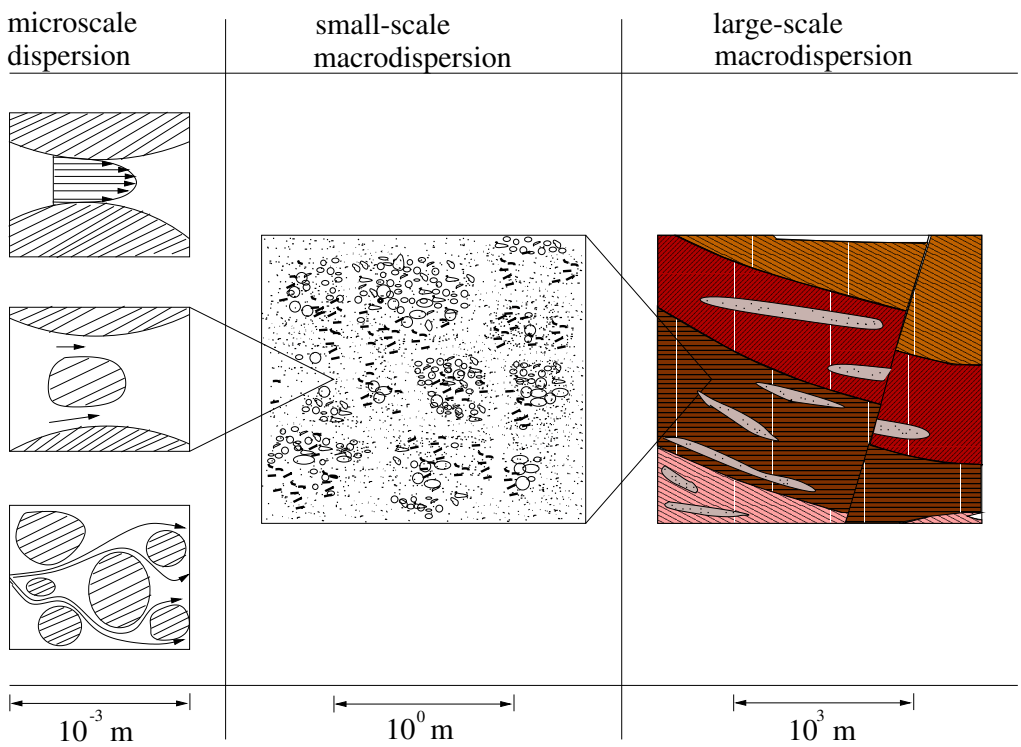

Figure 3.7: Schematic diagram for dispersion (Kinzelbach (1992)[57])

and this smearing causes the dispersion. On the other hand, the macrodispersion is caused by the large scale heterogeneities (e.g. fracture, fault etc.) of the aquifer in large REVs (in the middle and right columm of the Figure 3.7).

As is apparent, these dispersions are direction-dependent phenomena and the mathematical expression has to take this characteristic into account. The most general expression of the dispersion tensor $\mathbf{D}_{dis}$ is given by Scheidegger as follows:

$$\mathbf{D}_{dis} = \begin{bmatrix} D_{xx} & D_{xy} \\ D_{yx} & D_{yy} \end{bmatrix} \tag{3.24}$$

$$D_{xx} = \alpha_L \frac{v_x^2}{|\mathbf{v}|} + \alpha_T \frac{v_y^2}{|\mathbf{v}|} \tag{3.25}$$

$$D_{xy} = D_{yx} = (\alpha_L - \alpha_T) \frac{v_x v_y}{|\mathbf{v}|} \tag{3.26}$$

$$D_{yy} = \alpha_T \frac{v_x^2}{|\mathbf{v}|} + \alpha_L \frac{v_y^2}{|\mathbf{v}|} \tag{3.27}$$

where $\mathbf{v}$ is the Darcy velocity vector and α_L and α_T are the longitudinal and transversal dispersivities (in m). In most cases, α_T is smaller than α_L by one order of maginitude. As shown, the dispersion tensor is anisotropic, although it can be diagonal if the x-coordinate is taken in the flow direction as:

$$\mathbf{D}_{dis} = \begin{bmatrix} D_L & 0 \\ 0 & D_T \end{bmatrix} = \begin{bmatrix} \alpha_L |\mathbf{v}| & 0 \\ 0 & \alpha_T |\mathbf{v}| \end{bmatrix} \tag{3.28}$$

This dispersion is often called mechanical dispersion to distinguish it from so-called hydrodynamic dispersion which expresses the sum of the aforementioned molecular diffusion and mechanical dispersion. We denote the mechanical and the hydrodynamic dispersion coefficient as $\mathbf{D}_{mec}(= \mathbf{D}_{dis})$ and $\mathbf{D}_{hyd}$; thus, we obtain the following relation:

$$\mathbf{D}_{hyd} = \mathbf{D}_{mol} + \mathbf{D}_{mec} = \begin{bmatrix} D_{xx} + D_{mol} & D_{xy} \\ D_{yx} & D_{yy} + D_{mol} \end{bmatrix}, \tag{3.29}$$

where D_{xx}, D_{xy}, D_{yx}, D_{yy} are the same as in Equation (3.24).

3.1.1.12 Capillary Pressure

Let us consider an air-water system in porous media. An enlarged schematic view of the interface between the phases is shown in Figure 3.8. The area at the bottom with the slanted lines represents a solid phase (e.g. the soil grain of the porous medium). As shown in the figure, angles θ_i $(i =$

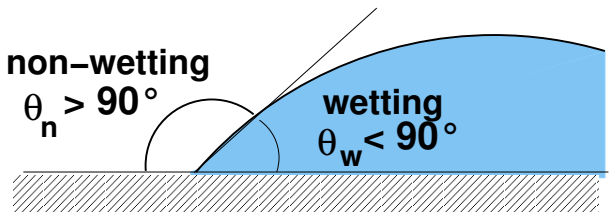

Figure 3.8: Contact angle formed by a wetting, a non-wetting and a solid phase.

w,n) are always formulated from the tangent of each phase toward the solid surface. These are called the contact angles which contribute to distinguish the types of the phases. The phase whose contanct angle is bigger than 90° is called the non-wetting phase (i.e. air), while the phase smaller than 90° is called the wetting phase (i.e. water).

As is apparent, this means that the pressure of the non-wetting phase is always greater than that of the wetting phase, and this pressure difference is called capillary pressure, expressed as:

$$p_c = p_n - p_w \ , \tag{3.30}$$

where p_c is the capillary pressure, p_n and p_w are the non-wetting phase and the wetting phase pressure respectively.

Several approaches are proposed to express the capillary pressure as a function of one of the phase saturations. I introduce here the two most well-known approaches developed by Brooks and Corey (1964) [15] and van Genuchten (1980) [84]. Brooks-Corey model for a two-phase system is expressed as:

$$p_c = p_d S_{we}^{\frac{-1}{\lambda}} . \tag{3.31}$$

where p_d is the entry pressure, λ the form parameter determined experimentally, and S_{we} the effective water saturation. The Brooks-Corey curve is shown in Figure 3.9 when the entry pressure $p_d = 3000Pa$ and the form parameter $\lambda = 2.0$. This Brooks-Corey function is used in one of the following applications. As imagined from the curve around $(S_w = 1.0)$ in the figure, the physical interpretation of the entry pressure is that it is the pressure necessary for the non-wetting phase to displace the saturated wetting phase from the largest pores.

On the other hand, the Van Genuchten model is expressed as:

$$p_c = \frac{1}{\alpha}(S_{we}^{\frac{-1}{m}} - 1)^{\frac{1}{n}} . \tag{3.32}$$

where α and m are the form parameters which can be related with the parameters p_d and λ of the Brooks-Corey model (Lenhard et al. (1989) [64]):

$$m = 1 - \frac{1}{m} \tag{3.33}$$

$$\lambda = \frac{m}{1-m}(1 - S_{we}^{\frac{1}{m}}) \tag{3.34}$$

$$S_x = 0.72 - 0.35e^{-n^4} \tag{3.35}$$

$$\alpha = \frac{S_x^{\frac{1}{\lambda}}}{p_d}(S_x^{-\frac{1}{m}} - 1)^{1-m} \tag{3.36}$$

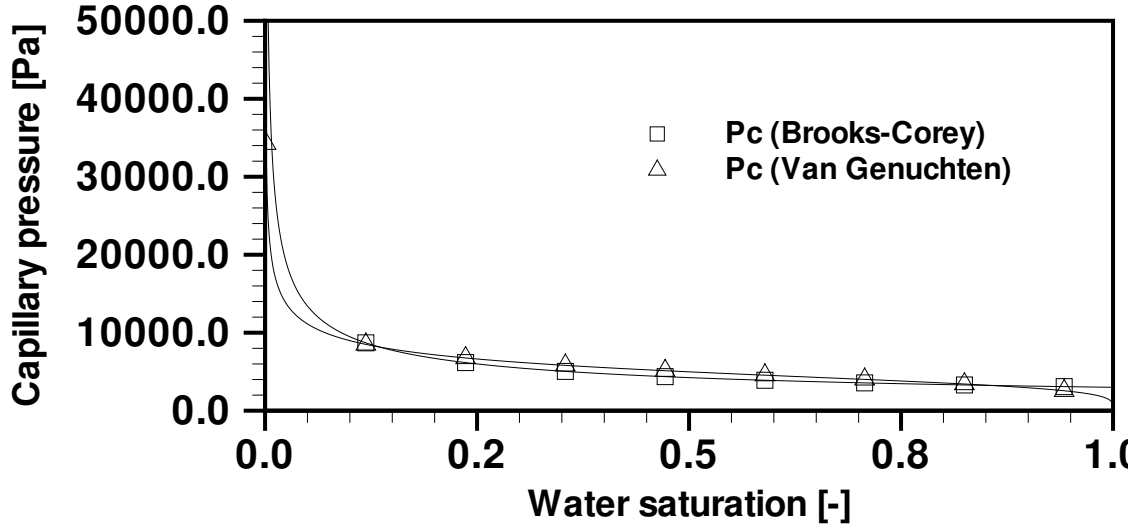

Figure 3.9: Capillary-pressure curves as functions of the water-phase saturation by the Brooks-Corey model) and the Van Genuchten model ($\lambda = 2.0$, $P_d = 3000\ Pa$, $n = 4.35$, $m = 0.77$). This function is used in one of the following applications.

Using these relationships (although the averaged values are used for both λ and α), the Van Genuchten curve which is equivalent to the Brooks-Corey curve is also plotted in Figure 3.9. One big difference between the two is the capillary pressure of the Van Genuchten model, unlike the Brooks-Corey curve, becomes zero when the water saturation is one.

3.1.1.13 Darcy's Law

The explanation of the former half of this section is mostly based on Chow (1998) [16]. Provided that the porous medium is composed of interconnected conduits of various shapes and sizes, and a conduit can be represented as a circular pipe with the diameter D, then, for steady uniform flow, we can approximate the shear stress acting on the wall of the pipe as:

$$\tau_0 = \gamma R S_f, \tag{3.37}$$

where τ_0 is the shear stress, γ the specific weight of the fluid flowing through the pipe, S_f the friction slope, and R the hydraulic radius ($R = D/4$). Similarly, the shear stress on the wall in a circular pipe is approximated, for laminar flow, by:

$$\tau_0 = \frac{8\mu v}{D} \tag{3.38}$$

where τ_0 is the shear stress, μ the dynamic viscosity of the fluid and v the fluid velocity.

Manipulating Equations (3.37) and (3.38) yields:

$$v = \frac{\gamma D^2}{32\mu} S_f \tag{3.39}$$

which is the Hagen-Poiseulle Equation for laminar flow in a circular conduit.

In 1D, we define Darcy flux as a volumetric flux $v = \frac{Q}{A}$, where A is the cross-sectional area and Q the discharge of the flow. This Darcy flux is estimated by :

$$v = K_h S_f \tag{3.40}$$

where K_f is the hydraulic conductivitiy of the medium in m/s. From Equation (3.39), we know $K_f = \frac{\gamma D^2}{32\mu}$. Darcy's law is valid as long as the flow is laminar. In order to distinguish whether or not the flow is laminar, we can define the Reynolds number as:

$$Re = \frac{vD}{\nu} \tag{3.41}$$

The flow in a circular conduit is laminar when its Reynolds number is less than 2000. This condition is generally satisfied with almost all naturally occuring flows in porous media.

Similarly in 3D, Darcy's law is written as:

$$\mathbf{v} = -\mathbf{K}_h \nabla h \tag{3.42}$$

where $\mathbf{v}$ is the velocity vector, $\mathbf{K}_h$ the hydraulic conductivitiy tensor. We approximate the friction head by $S_f = -\nabla h$, where ∇ is nabla and h the hydraulic head which is equal to the sum of the pressure head and the potential head, i.e.:

$$h = \frac{p}{\rho g} + z. \tag{3.43}$$

Thus, we get:

$$\mathbf{v} = -\mathbf{K}_h \nabla h = -\mathbf{K}_h \nabla(\frac{p}{\rho g} + z) = -\mathbf{K}_i \frac{\rho g}{\mu} \nabla(\frac{p}{\rho g} + z) = -\mathbf{K}_i \frac{1}{\mu}(\nabla p - \rho \mathbf{g}) \tag{3.44}$$

where $\mathbf{K}_h = \mathbf{K}_i \frac{\rho g}{\mu}$ and $\mathbf{g} = (0, 0, -g)$. $\mathbf{K}_i$ is called the intrinsic permeability with the dimension of m^2. If the fluid is water, then $\frac{\rho g}{\mu} \approx \frac{10^3 \cdot 9.81 Pa/m^3}{10^{-3} Pa\,s} \approx 10^7 m^{-3} s^{-1}$, while if air, then $\frac{\rho g}{\mu} \approx \frac{0.7 \cdot 9.81 Pa/m^3}{1.72 \cdot 10^{-6} Pa\,s} \approx 10^7 m^{-3} s^{-1}$. Thus, we can approximate the intrinsic permeabilty from the hydraulic conductivity as: $\mathbf{K}_i \approx 10^{-7} \mathbf{K}_h$. This relationship is applied to estimate the permeability from the hydraulic conductivity in the following real-site application.

Analogously, Darcy's law can be extended for multiphase flow:

$$\mathbf{v}_\alpha = -\mathbf{K}_{i,\alpha} \frac{1}{\mu_\alpha}(\nabla p_\alpha - \rho \mathbf{g}) = -\mathbf{K}_i \frac{k_{r\alpha}}{\mu_\alpha}(\nabla p_\alpha - \rho \mathbf{g}) = -\mathbf{K}_i \lambda_\alpha (\nabla p_\alpha - \rho \mathbf{g}) \tag{3.45}$$

where $\mathbf{v}_\alpha$ is the phase velocity vector, $\mathbf{K}_i$, $k_{r\alpha}$ and λ_α are the intrinsic permeability, the so called relative permeability and the mobility for the phase α.

Additionally, for actual flow in porous media, part of the cross-sectional area A is occupied by the solid phase (e.g. soil, rock strata, etc.). Thus, the actual flow velocity, often called the pore velocity, for the single-phase flow must be:

$$\mathbf{v}_{por} = \frac{\mathbf{v}}{\phi_e} \tag{3.46}$$

where $\mathbf{v}_{por}$ is the pore velocity and ϕ_e the effective porosity. For the multiphase flow, it becomes

$$\mathbf{v}_{\alpha,por} = \frac{\mathbf{v}_\alpha}{\phi_{\alpha e}} = \frac{\mathbf{v}_\alpha}{S_\alpha \phi_e}. \tag{3.47}$$

3.1.1.14 Relative Permeability

When we deal with multiphase flow processes, we have to take the interactions among the phases into account in some ways. For example, when we consider the flow velocity of a phase α, we need to introduce a parameter called the relative permeability as shown in Equation (3.45); this accounts for the disturbances by the other phases to the flow of the phase α.

Brooks and Corey, and Van Genuchten developed also models for this relative permeability of the phases as functions of those saturations. The Brooks-Corey model for relative permeability is:

$$\begin{aligned} k_{rw} &= S_{we}^{\frac{2+3\lambda}{\lambda}}, \\ k_{rn} &= (1-S_{we})^2 \left(1 - S_{we}^{\frac{2+\lambda}{\lambda}}\right), \end{aligned} \tag{3.48}$$

where $k_{r\alpha}$ stands for the relative permeability of the phase α. The paramters of the relative permeabilty can be related to those of the capillary pressure, so the form parameter λ is the same.

On the other hand, the Van Genuchten model is expressed as :

$$\begin{aligned} k_{rw} &= \sqrt{S_{we}} \left[1 - \left(1 - S_{we}^{\frac{1}{m}}\right)^m\right]^2, \\ k_{rn} &= (1-S_{we})^{\frac{1}{3}} \left[1 - S_{we}^{\frac{1}{m}}\right]^{2m}, \end{aligned} \tag{3.49}$$

Again, the parameters are the same as those of the capillary pressure. These curves are shown in Figure 3.10. The Brooks-Corey function is applied in the following applications. applications.

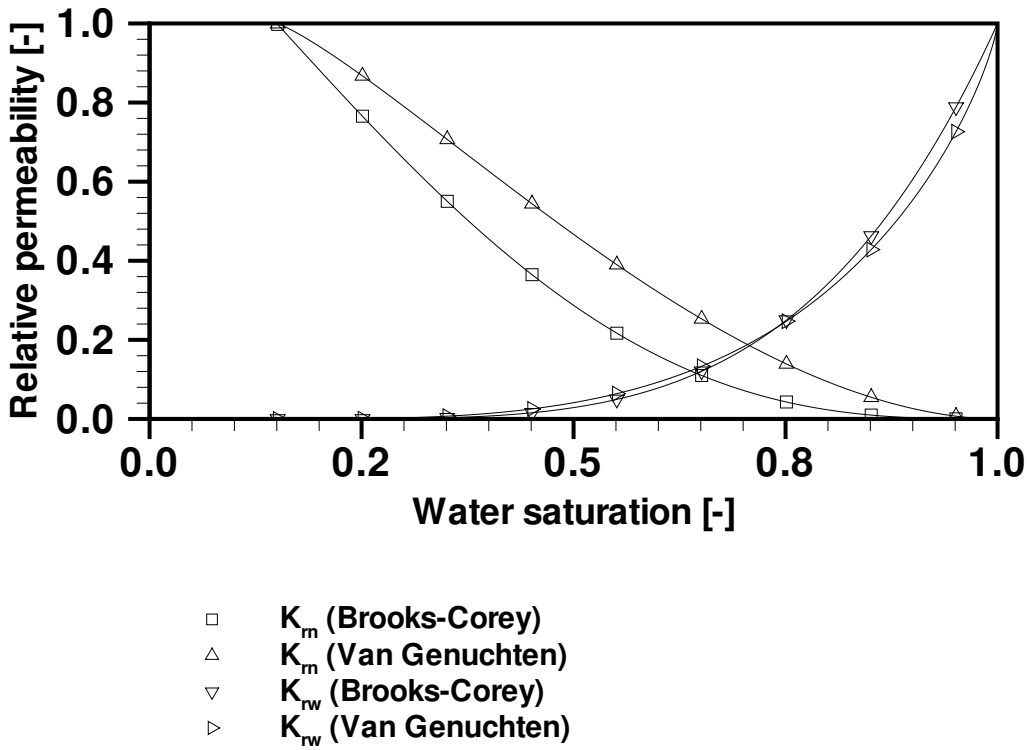

Figure 3.10: Relative permeability curves as function of a saturation by the Brook-Corey model and by the Van Genuchten model ($\lambda = 2.0$, $S_{wr} = 0.15$, $m = 0.77$).

3.1.2 Parameter Calculations

Sections 3.1.2.1 to 3.1.2.5 present the calculations of the parameters especially for the two-phase and two-phase/ three-component models. For both models, I assume there are two immiscible phases, a liquid (water: w) phase and a gas phase (g), and for the two-phase/ three-component model, three components, water (w), air (a) and methane (m).

3.1.2.1 Mole Fractions of the Components in the Gas Phase

The mole fractions of the components in the gas phase are always calculated by Equation (3.19):

$$x_g^\kappa = \frac{p_g^\kappa}{p_g}, \quad \kappa = a, m, w \tag{3.50}$$

where p_g^κ is the partial pressure of the component κ in the gas phase, and p_g the total pressure of the gas phase. I assume the validity of the perfect gas law (Equation (3.16)) for the partial pressures of the air and the methane component in the gas phase as:

$$p_g^\kappa = \frac{n_g^\kappa RT}{V}, \quad \kappa = m, a. \tag{3.51}$$

where n_g^κ is the mole number (in mol) of the component κ, R the universal gas constant, T the temperature in Kelvin and V the volume of the gas phase in m^3.

When gas and water phases coexist in the system, the partial pressure of the component water is assumed to be equal to the water-vapor pressure, i.e. $p_g^w = p_{sat}^w$.

The total pressure of a mixture of ideal gases is the sum of the partial pressures of the components according to the Equation (3.18). Thus, we obtain the following relation for this three-component system:

$$p_g = \sum_\kappa p_g^\kappa = \frac{n_g^a RT}{V} + \frac{n_g^m RT}{V} + p_{sat}^w \tag{3.52}$$

3.1.2.2 Mole Fractions of the Components in the Water Phase

Henry's law (Equation (3.20)) is used in order to compute the mole fractions of the components air and methane in the water phase:

$$x_w^\kappa = \frac{p_g^\kappa}{H_w^\kappa}, \quad \kappa = a, m \tag{3.53}$$

where H_w^κ is the Henry coefficient. When the component is air, the Henry coefficient is

$$H_w^a = (0.8942 + 1.47e^{-0.04394 \cdot T}) \times 10^{-10} \tag{3.54}$$

where the units of the temperature and of the Henry coefficient are ^0C and Pa^{-1} respectively.

The Henry coefficient for the methane as a function of the system temperature could not unfortunately be found so that the constant value $2.08 \times 10^{-10} Pa^{-1}$ is used in the following applications.

The mole fraction of the component water in the water phase is thus calculated by $x_w^w = 1 - x_w^a - x_w^m$.

3.1.2.3 Molar Density of the Gas Phase

The molar density of the gas phase can be calculated by Equation (3.17) :

$$\rho_g^{mol} = \frac{n}{V} = \frac{p_g}{RT}\,. \tag{3.55}$$

3.1.2.4 Mass Density of the Liquid Phase

The mass density of water is used to represent mass density of the liquid phase. This assumption means that I neglect the change of the mass density due to the component air and methane dissolving in the liquid phase; the volume of the liquid phase also remains constant. The information for the water density can be obtained from, for example, Lang (1990) [63] as a function of the temperature:

$$\rho_w = \rho_0[1-(7(T-T_0)^2)\cdot 10^{-6}]\,, \tag{3.56}$$

where ρ_0 $(= 999.972 kg/m^3)$ is the mass density of pure water at the temperature of $T_0 (= 4^o C)$

3.1.2.5 Relationship between Mass and Molar Density

I have already described how to calculate the molar densities of the gas and the mass density of water phase (Sections 3.1.2.3 and 3.1.2.4). The mass densities of the gas and water phase are then calculated by the following relationships:

$$\rho_\alpha^{\kappa,mass} = \rho_\alpha^{\kappa,mol} M^\kappa, \quad \kappa = a,m,w \tag{3.57}$$

$$\rho_\alpha^{mass} = \rho_\alpha^{mol} \sum_\kappa x_\alpha^\kappa M^\kappa, \quad \kappa = a,m,w \tag{3.58}$$

where M^κ is the molecular weight of the component κ in $kg/kmol$.

3.1.2.6 Dynamic Viscosity of the Gas Phase

There are several methods for calculating the dynamic viscosity of the gas phase consisting of multicomponents. I introduce here the method of Wilke [76]. In this method, the dynamic viscosity of the gas phase composed of, for example, three components is approximated by:

$$\mu_g = \sum_{i=1}^{3} \frac{x_g^i \mu_g^i}{\sum_{j=1}^{3} x_g^j \phi^{i,j}}, \tag{3.59}$$

$$\phi^{i,j} = \frac{\left(1+\sqrt{\frac{\mu_g^i}{\mu_g^j}}\cdot\left(\frac{M^j}{M^i}\right)^{1/4}\right)^2}{\sqrt{8\cdot\left(1+\frac{M^i}{M^j}\right)}}, \tag{3.60}$$

$$\phi^{j,i} = \frac{\mu_g^j}{\mu_g^i}\frac{M^i}{M^j}\phi^{i,j}, \tag{3.61}$$

where μ_g^i is the dynamic viscosity of the component i, x_g^i the mole fraction and M^i the molecular weight. However, for most of the components, we can obtain generally only a single μ_g^i value at either a constant temperature or a constant pressure. In addition, these temperatures and pressures at which those values are obtained are not always the same. Thus, it is considered that to make the calculation of viscosity complex in vain without enough data set is useless. For this reason, the viscosity of the component methane $10.2 \times 10^{-6} Pa \cdot s$ is used as a representative value for the gas phase. The function above itself is already incorporated in the numerical simulator.

3.1.2.7 Dynamic Viscosity of the Water Phase

The viscosity of the water phase is set to $1.002 \cdot 10^{-3} Pa \cdot s$, which is equivalent to the value of pure water at $4^o C$. This is based on the assumption that the dissolution of the components air and methane in the water phase are negligible. In addition, the volume of the liquid phase is also kept constant.

3.1.2.8 Diffusion Coefficients in the Gas Phase

For the diffusion coeffcient in the two-phase/ three-component system, I calculate the diffusion coefficients of the water vapor and methane in the gas phase using the following formulae (Falta et al. (1992) [27]) as a modification of the work Class et al. (2002) [18] :

$$\begin{aligned} D_g^w &= \frac{1 - x_g^w}{\frac{x_g^a}{D_g^{a,w}} + \frac{x_g^m}{D_g^{m,w}}}, \\ D_g^m &= \frac{1 - x_g^m}{\frac{x_g^w}{D_g^{m,w}} + \frac{x_g^a}{D_g^{a,m}}}, \end{aligned} \tag{3.62}$$

where $D_g^{a,w}$, $D_g^{m,w}$ and $D_g^{a,m}$ are the binary diffusion coefficients of the air–water vapor, methane–water vapor and air–methane system, respectively. The binary diffusion coefficient $D_g^{a,w}$ is calculated by the method of Vargaftik (1975) [76] and Walker et al.(1981) [76]:

$$D_g^{a,w} = D_{g,R}^{a,w} \frac{p_{g,R}}{p_g} \left(\frac{T}{T_R} \right)^{\theta} \tag{3.63}$$

At a temerature of $T_R = 273.15$ K and pressure of $p_{g,R} = 1$ bar, $D_{g,R}^{aw}$ is $2.13 \cdot 10^{-5} m^2/s$. For the air–water vapor mixture, θ is 1.8. Thus, $D_g^{a,w}$ can be calculated as a function of the pressure and temperature of the gas phase.

The binary coefficients $D_g^{m,w}$ and $D_g^{a,m}$ are calculated by the method of Neufield et al. (1972)[76]:

$$
\begin{aligned}
D_g^{i,j} &= \frac{0.00266\,T^{3/2}\sqrt{M^r}}{p_g\,(\sigma^{i,j})^2\,\Omega} \\
M^r &= (M^i + M^j)/(M^i M^j) \\
\sigma^{i,j} &= (\sigma^i + \sigma^j)/2 \\
\Omega &= \frac{1.06036}{(T^*)^{0.15610}} + \frac{0.19300}{exp[T^* \cdot 0.47635]} + \frac{1.03587}{exp[T^* \cdot 1.52966]} + \frac{1.76474}{exp[T^* \cdot 3.89411]} \\
T^* &= \frac{T}{[(\varepsilon^i/k)\cdot(\varepsilon^j/k)]^{1/2}}
\end{aligned}
\tag{3.64}
$$

where $D_g^{i,j}$ is the binary diffusion coefficient for a gas mixture of the components i and j, p_g the total pressure of the gas phase in bar, T the temperature in K, M^i the molecular weight of the component i, $\sigma^{i,j}$ the characteristic length in A, Ω the diffusion collision integral, a dimensionless number, ε^i the characteristic energy of the component i, and k the Boltzmann constant. σ^i and $\frac{\varepsilon^i}{k}$ are obtained from Reid et al: σ^w = 2.641, σ^m = 3.758, σ^a = 3.711, $\frac{\varepsilon^w}{k}$ = 809.1, $\frac{\varepsilon^m}{k}$ = 148.6, $\frac{\varepsilon^a}{k}$ = 78.6.

This method yields a constraint with regard to the diffusion fluxes:

$$J_g^a + J_g^w + J_g^m = 0. \tag{3.65}$$

Two fluxes of Equation (3.65), for example J_g^w and J_g^m, are always calculated using Equation (3.62) and then the rest, for example, J_g^a by the constraint $J_g^a = -(J_g^w + J_g^m)$.

3.1.2.9 Diffusion Coefficients in the Water Phase

For the diffusion coeffcients of the dissolved methane and air in the water phase, $D_w^m = 0.85 \times 10^{-9} m^2/s$, $D_w^a = 3.55 \times 10^{-9} m^2/s$ are applied (Atkins (1996) [4]).

3.2 Mathematical Model

3.2.1 Reynolds Transport Theorem

The so called Reynolds transport theorem is often applied when we derive the mathematical equations (the mass conservation equations, the momentum equations, the energy equation etc.) for continuous fluids. The theorem is generally expressed in the integral form (see Chow (1998)[16] but modified for multiphase systems in the subsurface):

$$\begin{aligned} \frac{dB}{dt} &= \frac{\partial}{\partial t}\int_{c.v.} \beta\hat{\rho}dV + \int_{c.s.} (\mathbf{J_C}+\mathbf{J_D})\cdot \mathbf{dS} - Q \\ &= \underbrace{\frac{\partial}{\partial t}\int_{c.v.} \beta\hat{\rho}dV}_{(I)} + \underbrace{\int_{c.s.} \nabla\cdot(\mathbf{J_C}+\mathbf{J_D})\,dV}_{(II)} - Q. \end{aligned} \tag{3.66}$$

$$\text{where} \quad \mathbf{J_C} = \beta\hat{\rho}\mathbf{v}_{por} \quad and \quad \mathbf{J_D} = -D\nabla\cdot(\beta\hat{\rho}) \tag{3.67}$$

where B is called the extensive property and is the value related to the mass of the fluid in the control volume, while β is the intensive property independent of the mass. $c.v.$ indicates the volume of a control volume, and $c.s.$ the area of the control surface. The Gauss integral theorem, $\int_{c.s.} \mathbf{A}\cdot\mathbf{dS} = \int_{c.v.} \nabla\cdot\mathbf{A}\,dV$ where A is a vector, is applied to the term (II) in the middle of the transformation. For a extensive property B, an corresponding intensive propery β can be always defined as the quantity of B per unit mass of fluid, i.e. $\beta = \frac{dB}{dm}$, where m is the mass of the fluid. B and β can be scalar or vector quantities depending on the property considered. $\hat{\rho}$ is a value which accounts for amount of the mass per unit volume of the fluid considered. For example, it becomes $\hat{\rho} = S_\alpha\phi_e\rho_\alpha$ if we consider a multiphase system in porous media. The Reynolds transport theorem states that the total rate of temporal change of an extensive property of the fluid is equal to the rate of temporal change of the extensive property stored in the control volume (I), plus the net outflux of the extensive property through the control surface (II). $\mathbf{J_C}$ and $\mathbf{J_D}$ stand for the flux vectors due to convection and diffusion/dispersion effects respectively (Section 3.1.1.11). Here, the influxes have always a negative sign, the outfluxes a positive one. Q is the source/sink of the fluids (e.g. phases, components etc.) in the control volume. In analogy to the fluxes, the source always has a negative sign and the a sink positive one. If this theorem is applied to the flow in the subsurface, the source is caused by processes such as desorptions, chemical reactions, biological decompositions etc. If the mean of the convective flux is much larger than the deviation, the diffusion/dispersion fluxes are often neglected.

3.2.2 Mass Conservation Equation for Phases

In this section, I introduce the mass conservation equation with regard to a phase α in a porous medium using the aformentioned Reynolds transport theorem. Let me look again at the control volume shown in Figure 3.11. The control volume is a cube, whose edge lengths are dx, dy, and dz. The volume is thus $dxdydz$. If the control volume is a porous medium and the void is partially filled with phase α, the mass of phase α within the volume can be expressed as $dxdydz\rho_\alpha\phi_e S_\alpha$. If we think of a component κ of the phase, the mass of the component becomes $dxdydz\rho_\alpha\phi_e S_\alpha X_\alpha^\kappa$.

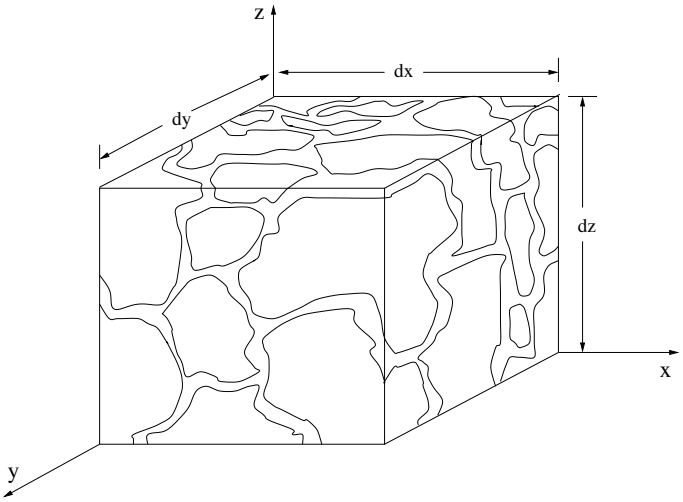

Figure 3.11: A control volume

Let $\Omega \in R^d, d = 2,3$ be an open domain and $I = (0,T)$ the time interval. Suppose the extensive property B is the mass of the phase, then we obtain $\beta = dB/dm = 1$. In addition, if the temporal change of the extensive property in the control volume does not take place (i.e. phase changes do not occur), then we get $dB/dt = 0$. Thus, the Reynolds transport theorem is transformed into:

$$0 = \underbrace{\frac{\partial}{\partial t}\int_{c.v.} \hat{\rho} dV}_{(I)} + \underbrace{\int_{c.s.} \nabla \cdot (\hat{\rho}\mathbf{v}_{\alpha,por})\, dV}_{(II)} - Q, \quad in \quad \Omega \times I, \tag{3.68}$$

where $\mathbf{v}_{\alpha,por}$ is the pore velocity of the phase α at the coordinate (x,y,z) which can be calculated using the extended Darcy's law as $\mathbf{v}_{\alpha,por} = \frac{\mathbf{v}_\alpha}{\phi_\alpha} = \frac{\mathbf{v}_\alpha}{S_\alpha \phi_e}$. $\mathbf{v}_\alpha$ is the Darcy velocity (Section 3.1.1.13). Diffusion/ dispersion effects are not taken into account, because the phase itself does not have such effects. Thus (I) can be approximated as:

$$\frac{\partial}{\partial t}\int_{c.v.} \hat{\rho} dV = \frac{\partial}{\partial t}(\rho_\alpha \phi_e S_\alpha dxdydz) = dxdydz \frac{\partial}{\partial t}(\rho_\alpha \phi_e S_\alpha) \tag{3.69}$$

Here, we assign $\hat{\rho} = \phi_e \rho_\alpha S_\alpha$ and assume that the spatial dimensions of the control volume are fixed. Similarly, (II) can be replaced by:

$$\int_{c.v.} \nabla \cdot (\mathbf{v}_{\alpha,por}\hat{\rho}) dV = dxdydz \nabla \cdot (\mathbf{v}_{\alpha,\mathbf{por}} \rho_\alpha \phi_e S_\alpha) \tag{3.70}$$

where ∇ is nabla. As a consequence, we get the following mass conservation equation with regard to phase α:

$$\frac{\partial(\rho_\alpha \phi_e S_\alpha)}{\partial t} + \nabla \cdot (\mathbf{v}_{\alpha,por}\rho_\alpha \phi_e S_\alpha) - Q = \frac{\partial(\rho_\alpha \phi_e S_\alpha)}{\partial t} + \nabla \cdot (\mathbf{v}_\alpha \rho_\alpha) - Q = 0. \tag{3.71}$$

Here, we applied the relation $\mathbf{v}_\alpha = \phi_e S_\alpha \mathbf{v}_{\alpha,por}$. This equation is also often called the continuity equation.

3.2.3 Momentum Equations

Momentum equations can also be derived on the basis of the Reynolds transport theorem. In this case, we set the parameters $\mathbf{B}$ and β to $\mathbf{B} = m\mathbf{v}_{por}$ and $\beta = d\mathbf{B}/dm = \mathbf{v}_{por}$. In addition, since Newton's second law states that the rate of temporal change of momentum is equal to the net force on the system, we obtain $d\mathbf{B}/dt = d(m\mathbf{v}_{por})/dt = \sum \mathbf{F}$. Thus, from equation (3.66), we get:

$$\sum \mathbf{F} = \frac{\partial}{\partial t} \int_{c.v.} \mathbf{v}_{por} \hat{\rho} \, dV + \int_{c.s.} \nabla \cdot (\hat{\rho} \mathbf{v}_{por} \cdot \mathbf{v}_{por}) dV. \tag{3.72}$$

This is an original form of the different varieties of the momentum equations for an unsteady, nonuniform flow in the integral form. Equation (3.72) can be transformed into, for example, the Navier-Stokes equation by defining the forces acting on the system. It is also possible to transform Equation (3.72) into the Darcy equation, which is conventionally used as a macroscale momentum equation for flow in porous media. There are many controversies on how to transform Equation (3.72) into the Darcy equation. According to Helmig (1997) [41], Whitaker derived the Darcy equation for a single-phase (1986) [89] and a two-phase system (1986)[90] by averaging the incompressible Navier-Stokes equation over a volume. As one of the most general ways of deriviation, Hassanizadeh and Gray (1980) [38] derived the Darcy equation for a single-phase system without having made any assumptions on the incompressivity and the constitutive relationship between the stress and the shear. This is extended for multiphase flow by Gray (1983) [36] and for multicomponent flow by Hassanizadeh (1986) [39]. These deriviations are not described here, and we use the Darcy equation as the momentum equation in the following.

3.2.4 Two-Phase Model

Mass conservation equations for a two-phase system are derived in this section. Two mass conservation equations are required for the two phases. Two phases can be any combination of two-immiscible-fluids, like gas and water, water and NAPL etc. For the deriviation here, a system of a water (liquid) phase and a gas phase is assumed. A schematic diagram of the two-phase model concept is shown in Figure 3.12. In this model concept, mass transfers between the phases are not taken into account.

Let $\Omega \in R^d, d = 2,3$ be an open domain and $I = (0,T)$ the time interval. As already discussed in Section 3.2.2, $\hat{\rho} = \rho_\alpha \phi_e S_\alpha$. From the Reynolds tranport theorem (3.66), two mass conservation equations for the two phases in porous media can be described as follows:

$$\frac{\partial(\rho_\alpha \phi_e S_\alpha)}{\partial t} + \nabla \cdot (\mathbf{v}_{\alpha,por} \rho_\alpha \phi_e S_\alpha) = \rho_\alpha q_\alpha, \quad in \quad \Omega \times I, \quad \alpha = w, g, \tag{3.73}$$

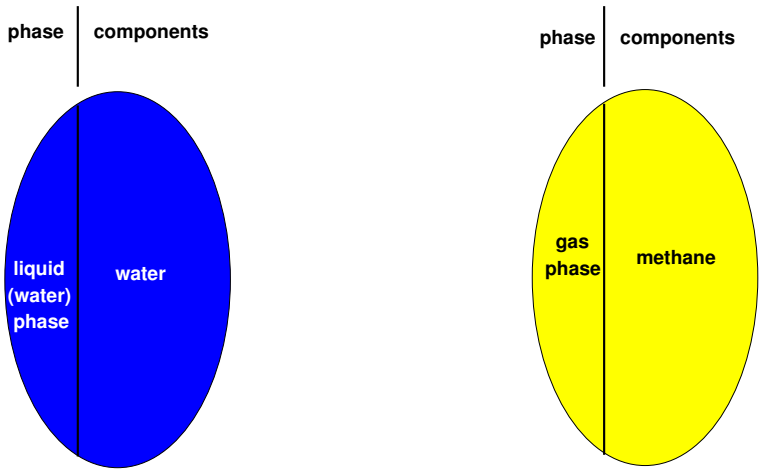

Figure 3.12: Conceptual diagram for a two-phase model (refer to Class et al. (2002) [18] modified by Kobayashi)

where α represents the water (liquid) phase (w) and the gas phase (g). The source is expressed as $Q = \rho_\alpha q_\alpha$. The velocity vector $\mathbf{v}_\alpha$ $(= S_\alpha \phi_e \mathbf{v}_{\alpha,por})$ is given by the extended Darcy's law (see Section 3.1.1.13):

$$\mathbf{v}_\alpha = -\frac{k_{r\alpha}}{\mu_\alpha}\mathbf{K}_i(\nabla p_\alpha - \rho_\alpha \mathbf{g}) = -\lambda_\alpha \mathbf{K}_i(\nabla p_\alpha - \rho_\alpha \mathbf{g}), \quad where \quad \lambda_\alpha = \frac{k_{r\alpha}}{\mu_\alpha} \tag{3.74}$$

where $\mathbf{K}_i$ is the intrinsic permeability tensor, $k_{r\alpha}$ the scalar relative permeability, μ_α the dynamic viscosity, p_α the pressure, $\mathbf{g}$ the vector due to gravity, and λ_α the mobility. Thus, we get:

$$\frac{\partial(\rho_\alpha \phi_e S_\alpha)}{\partial t} + \nabla \cdot \mathbf{v}_\alpha = \rho_\alpha q_\alpha, \quad in \quad \Omega \times I, \quad \alpha = w, g. \tag{3.75}$$

with the constraint:

$$S_w + S_g = 1, \qquad p_c = p_g - p_w. \tag{3.76}$$

The number of unknowns in this system of equations is four $(i.e. p_w, p_g, S_w, S_g)$, and we have two mass conservation equations and two constraints, i.e. four equations in all; thus, the system of the equations is closed. Normally, in order to solve the system of equations, we first eliminate two unknowns using the constraints and then formulate the two mass conservation equations with the remaining two unknowns. There are a couple of possible formulations according to the choice of the primary variables from unknowns. In the following, three formulations, the pressure formulation, the pressure-saturation formulation and the saturation formulation, are introduced. Although the pressure-saturation formulation is chosen in the following application, I briefly introduce three types of formulation here (refer to Helmig (1997) [41]).

Pressure Formulation

As discussed in Section 3.1.1.12, the capillary pressure is the function of the water-phase saturation (and accordingly of the gas-phase saturation):

$$p_c = f_\alpha(S_\alpha). \tag{3.77}$$

If the capillary pressure function behaves monotonically, i.e. $\frac{dpc}{dS_\alpha} \neq 0$, then the inverse function exists

$$S_\alpha = f_\alpha^{-1}(p_c) = f_\alpha^{-1}(p_g - p_w). \tag{3.78}$$

Using these relations, we elminate two unknowns S_w, S_g and formulate the two mass conservation equations (3.75) with the primary variables p_w, p_g to:

$$\begin{aligned} L_w(p_w, p_g) &= \frac{\partial(\rho_w \phi_e f_w^{-1}(p_g - p_w))}{\partial t} - \nabla \cdot (\rho_w \lambda_w \mathbf{K}_i(\nabla p_w - \rho_w \mathbf{g})) \\ &- \rho_w q_w = 0, \end{aligned} \tag{3.79}$$

$$\begin{aligned} L_g(p_w, p_g) &= \frac{\partial(\rho_g \phi_e f_g^{-1}(p_g - p_w))}{\partial t} - \nabla \cdot (\rho_g \lambda_g \mathbf{K}_i(\nabla p_g - \rho_g \mathbf{g})) \\ &- \rho_g q_g = 0. \end{aligned} \tag{3.80}$$

These equations are strongly coupled via the relative permeability-saturation and the capillary pressure-saturation relationship. There is a great disadvantage in this formulation, which is that the gradient of the capillary pressure with regard to the saturations always has to be non-zero for the existence of the inverse function; nevertheless, the gradient can be nearly zero in the subsurface where fractures, shears, permeability transitions etc. exist. This restriction critically limits the use of this formulation, especially for multiphase flows in heterogeneous media.

Pressure - Saturation Formulation

For the pressure-saturation formulation, there are four combinations of the two primary variables, i.e. $p_w - S_g$, $p_g - S_w$, $p_w - S_w$ and $p_g - S_g$. I select $p_w - S_g$ here for the example. This formulation is also applied in lator applications (Chapter 4). From the constraints (3.76), we get the following relations:

$$\frac{\partial S_w}{\partial t} = \frac{\partial(1 - S_g)}{\partial t} = -\frac{\partial S_g}{\partial t}, \tag{3.81}$$

$$\nabla p_g = \nabla(p_w + p_c). \tag{3.82}$$

Thus, we obtain:

$$L_w(p_w, S_g) = -\frac{\partial(\rho_w \phi_e S_g)}{\partial t} - \nabla \cdot (\rho_w \lambda_w \mathbf{K}(\nabla p_w - \rho_w \mathbf{g})) - \rho_w q_w = 0, \tag{3.83}$$

$$L_g(p_w, S_g) = \frac{\partial(\rho_g \phi_e S_g))}{\partial t} - \nabla \cdot (\rho_g \lambda_g \mathbf{K}(\nabla(p_w + p_c) - \rho_g \mathbf{g})) - \rho_g q_g = 0. \tag{3.84}$$

This formulation has the advantage that it can be applied to the systems in which a $\frac{dpc}{dS_\alpha} \neq 0$ zone exists because the capillary pressure is explicitly included in the system of equations.

Saturation Formulation

Only the resultant equations are shown for this saturation formulation. This is valid only when

both phases are imcompressible. The saturation formulation for two-phase flow is:

$$L(S_w) = -\underbrace{\frac{\partial(\phi_e S_w)}{\partial t}}_{(I)} - \underbrace{\nabla S_w \cdot \{\mathbf{v}_t \frac{df_w}{dS_w} - \mathbf{K}_i(\rho_w \mathbf{g} - \rho_g \mathbf{g})\frac{d\overline{\lambda}}{dS_w}\}}_{(II)}$$

$$\underbrace{-\nabla \cdot \{\overline{\lambda}\mathbf{K}_i \frac{dp_c}{dS_w}\nabla S_w\}}_{(III)} + \underbrace{q_w - f_w q_t}_{(IV)} = 0. \tag{3.85}$$

The terms (I), (II), (III), (IV) stand for accumulation, advective, diffusion and source/sink effects respectively. When the water saturation is low, the derivative of the capillary pressure with regard to the saturation, or $\frac{dp_c}{dS_w}$, is quite large; thus, the term (III) is dominant and Equation (3.85) becomes parabolic. On the other hand, when the water saturation is very high, $\frac{dp_c}{dS_w}$ becomes nearly zero; thus, the term (II) is dominant and the equation is hyperbolic type. This formulation is characteristic in that a so called total velocity is introduced in mid course, although this is not appllicable for the following applications. For further details, see Huber (1999) [51].

3.2.5 Two-Phase/ Three-Component Model

In this section, mass conservation equations for a two-phase/ three-component system are derived. They are derived with regard to each component, instead of each phase. Thus, the number of equations is three. To derive the mass conservation equations with regard to each component is advantageous in that transport equations are not required to represent mass (component) transfers between phases; this would be necessary if I derived them with regard to each phase. This two-phase/ three-component model is applied in the applications in Chapters 4 and 5; thus, the description hereafter follows the context. A schematic diagram of the two-phase/ three-component model concept is shown in Figure 3.13. Suppose there are two immiscible phases, a liquid phase and a gas phase, both of which consist of three components, water, air and methane.

Let $\Omega \in R^d, d = 2,3$ be an open domain and $I = (0,T)$ the time interval. From the Reynolds transport theorem (3.66), three mass conservation equations for the three components are derived as follows:

$$\frac{\partial \sum_\alpha(\rho_\alpha^{mol}\phi_e x_\alpha^\kappa S_\alpha)}{\partial t} + \sum_\alpha \nabla \cdot \left(\mathbf{v}_\alpha \rho_\alpha^{mol} x_\alpha^\kappa - \rho_\alpha^{mol}\mathbf{D}_\alpha^\kappa \nabla x_\alpha^\kappa\right) = q^\kappa, \quad in \quad \Omega \times I, \tag{3.86}$$

$$\alpha = w, g \quad \kappa = w, m, a.$$

where the subscript α denotes the water (liquid) phase (w) and the gas phase (g), while the superscript κ represents the three components, water (w), air (a) and methane (m). ρ_α^{mol} represents the molar density, x_α^κ the mole fraction, $\mathbf{D}_\alpha^\kappa$ the diffusion coefficient, and q^κ the source/sink. The velocity vector $\mathbf{v}_\alpha$ is given by the extended Darcy's law:

$$\mathbf{v}_\alpha = -\frac{k_{r\alpha}}{\mu_\alpha}\mathbf{K}(\nabla p_\alpha - \rho_\alpha^{mass}\mathbf{g}). \tag{3.87}$$

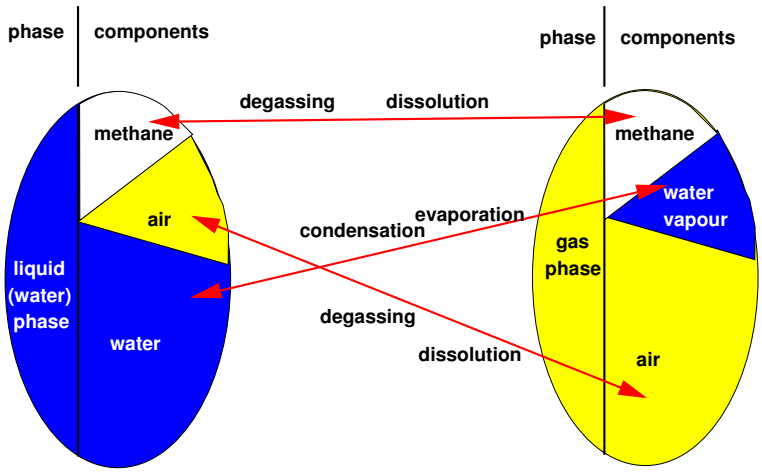

Figure 3.13: Conceptual diagram for two-phase/ three-component model (refer to Class et al. (2002) [18] modified by Kobayashi).

In addition, there are four constraints among the parameters.

$$S_g + S_w = 1, \quad p_c = p_g - p_w, \quad x_g^a + x_g^w + x_g^m = 1, \quad x_w^a + x_w^w + x_w^m = 1. \tag{3.88}$$

This system of equations has ten unknowns $(p_g, p_w, S_g, S_w, x_g^a, x_g^w, x_g^m, x_w^a, x_w^w, x_w^m)$, and the total number of the equations is now seven (three mass conservation equations plus four constraints). Thus, the system of equations is not yet closed. In order to solve this, I need to obtain three additional equations, or to reduce the number of the unknowns by three. For this, I have to distinguish three different phase states, i.e. the gas-water state, the water only state and the gas only state. When the phase state is the gas-water state and provided that the system is thermodynamically in equilibrium, the pressure of the component water in the gas phase is assumed to correspond to the saturated water-vapor pressure (Section 3.1.2.1):

$$x_g^w = \frac{p_w^{sat}}{p_g} \tag{3.89}$$

In addition, the mole fractions of the air and the methane in the water phase are calculated by the Henry's law (Section 3.1.1.10):

$$x_w^a = H_w^a p_g^a, \quad x_w^m = H_w^m p_g^m. \tag{3.90}$$

With this approach, I obtain three more equations for the gas-water phase state, and the system of equations is then closed.

On the other hand, when the phase state is either only gas or only water, the mole fractions of the components in either the gas or the water phase become zero. Thus, the number of unknowns is reduced by three and the system of the equations can be closed.

As a next step, I have to choose three primary variables for the three mass conservation equations. The three primary variables listed in Table 3.1 are selected for each phase state.

phase state	primary variables	phase transition conditions
w, g	S_w, x_g^m, p_g	**if** $(S_w = 0)$, **then** $w, g \rightsquigarrow g$: **if** $(S_g = 0)$, **then** $w, g \rightsquigarrow w$
w	x_w^m, x_w^a, p_g	**if** $(p_{sat}^w + H_w^m x_w^m + H_w^a x_w^a > p_g)$, **then** $w \rightsquigarrow w, g$
g	x_g^w, x_g^a, p_g	**if** $(x_g^w p_g > p_{sat}^w)$, **then** $g \rightsquigarrow w, g$

Table 3.1: Phase states, corresponding primary variables, and phase transition conditions (refer to Class et al. (2002) [18] modified by Kobayashi)

The following describes how the remaining seven (four) unknowns are calculated from these three primary variables. The parameter with ˆ indicates that the parameter is the primary variable.

- Gas-Water State

$$\begin{aligned} S_w &= \hat{S_w}, \quad S_g = 1 - \hat{S_w}, \quad p_g = \hat{p_g}, \quad p_w = \hat{p_g} - p_c, \quad x_g^m = \hat{x_g^m}, \quad x_g^w = \frac{p_w^{sat}}{\hat{p_g}}, \\ x_g^a &= 1 - x_g^w - \hat{x_g^m}, \quad x_w^a = H_w^a p_g^a = H_w^a x_g^a p_g, \quad x_w^m = H_w^m x_g^m p_g, \quad x_w^w = 1 - x_w^a - x_w^m. \end{aligned} \tag{3.91}$$

- Water Only State

$$\begin{aligned} S_w &= 1, \quad S_g = 0, \quad p_g = \hat{p_g}, \quad p_w = \hat{p_g} - p_c, \quad x_g^a = 0, \quad x_g^m = 0, \\ x_g^w &= 0, \quad x_w^a = \hat{x_w^a}, \quad x_w^m = \hat{x_w^m}, \quad x_w^w = 1 - \hat{x_w^a} - \hat{x_w^m}. \end{aligned} \tag{3.92}$$

- Gas Only State

$$\begin{aligned} S_w &= 0. \quad S_g = 1, \quad p_g = \hat{p_g}, \quad p_w = \hat{p_g} - p_c, \quad x_g^a = \hat{x_g^a}, \quad x_g^w = \hat{x_g^w}, \\ x_g^m &= 1 - \hat{x_g^w} - \hat{x_g^a}, \quad x_w^a = 0, \quad x_w^m = 0, \quad x_w^w = 0. \end{aligned} \tag{3.93}$$

Additionally, as shown in Table 3.1, phase-transition conditions are implemented.

- When the phase state changes from the gas-water phase state to the gas only or water only state, the transition conditions are determined by whether or not the gas or water saturation becomes zero:
  If $S_w = 0$ then $w, g \rightsquigarrow g$ or If $S_g = 0$ then $w, g \rightsquigarrow w$.

- When the phase state changes from the water only state to the gas-water state, the transition conditions are determined by whether or not the total gas pressure calculated is less than $p_{sat}^w + H_w^m x_w^m + H_w^a x_w^a$:
  If $(p_{sat}^w + H_w^m x_w^m + H_w^a x_w^a) > p_g$, then $w \rightsquigarrow w, g$

- If the gas pressure become greater than the saturated water-vapor pressure, then there is a phase transition from the gas only state to the gas-water state:
  If $x_g^w p_g > p_{sat}^w$, then $g \rightsquigarrow w, g$

3.3 Numerical Model

This section contains a brief explanation of numerical algorithms. These numerical algorithms are implemented in the numerical simulator MUFTE-UG (see Section 1.3.2).

Steps for solving Equation (3.73) and Equation (3.86) by numerical methods are as follow:

- Equations (3.73) and (3.86) are transformed into the weak formulations using a Subdomain Collocation (BOX) method. The weighting function for the residuals is a piecewise constant:

$$W = \begin{cases} 1 & if \quad x \in cv_i \\ 0 & else \end{cases} \tag{3.94}$$

  where cv_i is a control volume.

- In the evaluation of all integrals in the weak formulation, the midpoint rule is applied. This evaluation is called a lumped mass approach. Mass lumping is effective for avoiding non-physical oscillations of the solution.

- A fully-upwind weighting of the convective flux-term is also applied. This results in a stable discretization of the first order for the hyperbolic part.

- A fully implicit Euler scheme is applied for the temporal discretization.

- The nonlinearities in the resultant equations are handled with a Newton-Raphson method (a damped inexact Newton method). The Jacobian matrix is computed by numerical differentiation.

The performance of this approach can be seen in Helmig (1997) [41], Bastian (1999) [8], or Class (2000) [19].

Chapter 4

Comparative Studies

A series of comparative studies is conducted in this chapter. Two different model concepts, the two-phase model from Section 3.2.4 and two-phase/ three-component model from Section 3.2.5, are used to simulate methane-migration processes and methane-water interaction processes in artificially designed subsurfaces. The purpose of these comparative studies is to investigate the different responses resulting from the differences in the model concept. This contributes ultimately to supporting the selection of the model concept in general and especially for the simulation-optimization in the next chapter. The significant difference between these two models is that the two-phase/ three-component model can simulate the composition (water, methane and air) of the phases (water (liquid) and gas). Thus, in the two-phase/ three-component model, the dissolution and degassing of air and methane in and out of the water phase, the evaporation of water to the gas phase and the condensation of water vapor to the water phase, in short the mass transfers between the phases, can be dealt with. These studies make it clear that the reliability of the two-phase model is questionable in some conditions since the mass of the methane dissolved in the water is not negligible.

4.1 Gas-Water Processes in Two-Dimensional Porous Media

4.1.1 Example 1

System Set-Up

Before I start these comparative studies, one thing we have to recognize cleary is that the parameters required for the two models are partially different. This means that it is actually difficult to make an example completely the same unless transformations are possible between the corresponding parameters. This is mainly due to the fact that the composition of the phases is also taken into account for the two-phase/ three-component model. As a result, the two-phase/ three-component model requires the introduction of some new parameters (e.g. the mole fraction of each component). Moreover, mass conservation equations for the two-phase model are derived with regard to each phase (thus, the total number of equations is 2), while the mass conservation equations for the two-phase/ three-component model are derived with regard to each component (thus, the number is 3). As a result, for instance, the source terms of the two-phase model are the

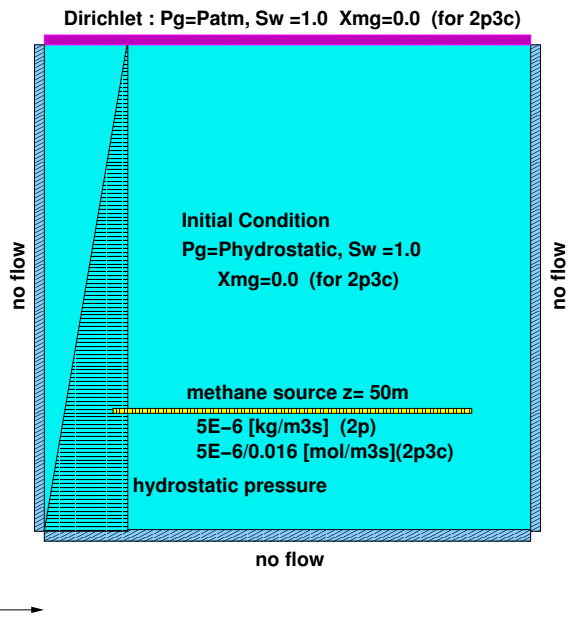

Figure 4.1: Schematic diagram of the system for Example 1

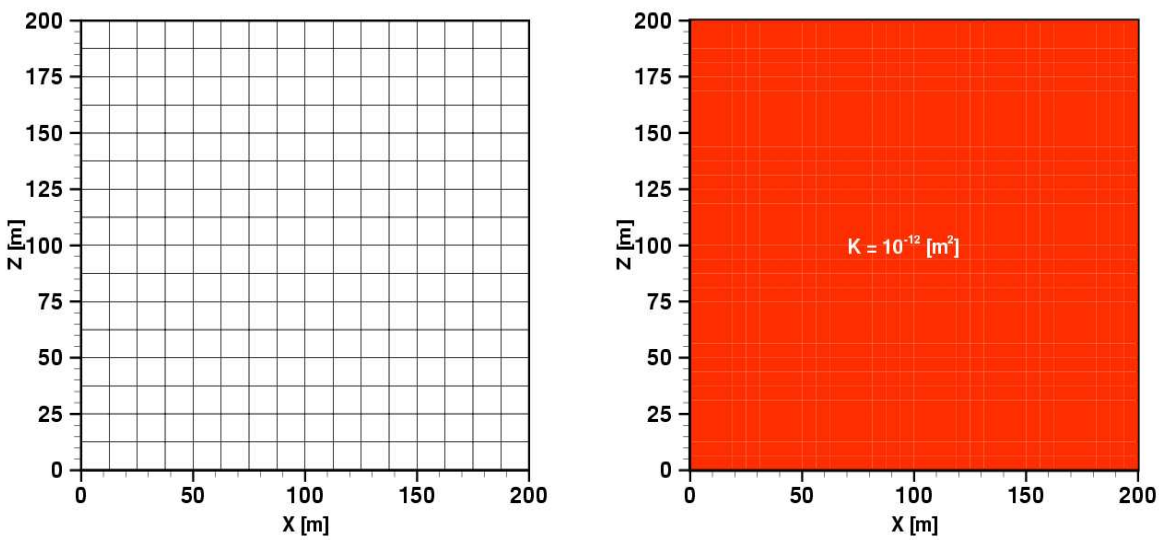

Figure 4.2: Computational mesh (left) and the absolute permeability field $[m^2]$ (right)

sources for each phase, while those of the two-phase/ three-component model are the sources for each component.

Nevertheless, the examples are designed to be as similar to each other as possible. For simplicity's sake, I consider a system consisting of a homogeneous layer where a line methane source is introduced, as shown in Figure 4.1. The computational grid and the absolute permeability field are shown on the left- and right-hand side of Figure 4.2 respectively. This system is intended to represent a saturated coal mine after the groundwater rebound has taken place. The system is $200m$ long, $200m$ high and the domain is discretized spatially by 256 rectangular elements and 289 nodes. The number of elements is rather low, although I have arranged it so intentionally in order to incorporate the three-dimensional effects later in this chapter which more elements are required. Scaling effects are ignored here since, first of all, the system is homogeneous and, in addition, the element size may, for example, change the time required for the methane to reach the top of the system; however, the exact time is not our primary concern in this comparative study. The methane line source is located at $30m \leq x \leq 170m$, $z = 50m$ ($150m$ down from the surface). The absolute permeability is set to $1.0 \times 10^{-12} m^2$.

The initial and boundary conditions are given as follows:

Initial and Boundary Conditions
For two-phase model:

no flow (Neumann):	$q_g = 0.0,$	$q_w = 0.0$
Dirichlet:	$p_g = 100000\,[Pa],$	$S_w = 1.0$
initial condition:	$p_g = 100000 + \rho g(200 - z)\,[Pa],$	$S_w = 1.0$

For two-phase/ three-component model:

no flow (Neumann):	$q^m = 0.0,$	$q^a = 0.0,$	$q^w = 0.0$
Dirichlet:	$p_g = 100000\,[Pa],$	$S_w = 1.0,$	$x_g^m = 0.0$
initial condition:	$p_g = 100000 + \rho g(200 - z)\,[Pa],$	$S_w = 1.0,$	$x_g^m = 0.0$

The right, left and lower boundaries of the system are closed, so the gas and water flux perpendicular to the boundaries is set to zero for the two-phase model, while the air, methane and water flux is zero for the two phase/ three-component model (i.e. Neumann BC). On the upper boundary, the water saturation is set to 1, and the gas pressure is atomospheric pressure ($1bar$) (Dirichlet BC) for both models. Additionally, the mole fraction of the methane in the gas phase has to be given for the two phase/ three-component model: it is zero. Since the system is fully saturated, a hydrostatic pressure field is assigned initially to the pressure of the gas phase. In the entire simulation, the mole fraction of the water in the gas phase is always calculated by setting $x_g^w = p_{sat}^w / p_g$ on the assumption that the system is thermodynamically in equilibrium. For the parameters for the simulation, see *Simulation Parameters* on the next page.

Moreover, special attention has to be paid to the source terms. The unit of the gas source for the two-phase model is kg/m^3s, a mass source, while the unit of the methane source for the two-phase/ three-component model is mol/m^3s, a molar source. Therefore, we are required to convert

Simulation Parameters

For both models

dynamic viscosity (gas) :	$\mu = 1.02 \times 10^{-5} [Pa\,s]$
dynamic viscosity (liquid) :	$\mu = 1.0 \times 10^{-3} [Pa\,s]$
residual gas saturation :	$S_{gr} = 0.01$ [-]
residual water saturation :	$S_{wr} = 0.1$ [-]
porosity :	$\phi = 0.57$ [-]
absolute permeability :	$K = 1.0 \times 10^{-12} [m^2]$
relative permeability :	Brooks-Corey
capillary pressure :	Brooks-Corey
entry pressure :	$p_d = 3000\,[Pa]$
form parameter :	$\lambda = 2$

For two-phase/ three-component model

Henry coeff (air) :	$H_w^a = 1.34 \times 10^{-10} [Pa^{-1}]$
Henry coeff (methane) :	$H_w^m = 2.08 \times 10^{-10} [Pa^{-1}]$
diffusion coeff (air in water) :	$D_w^a = 0.85 \times 10^{-9} [m^2/s]$
diffusion coeff (methane in water) :	$D_w^m = 3.55 \times 10^{-9} [m^2/s]$

the mass source into the molar source by means of dividing the mass source by the molecular weight of methane ($0.016 kg/mol$). The nodal value of the gas source is set to $5.0 \times 10^{-6}\ kg/m^3 s$, so the value of the methane source accordingly becomes $\frac{5.0 \times 10^{-6}}{0.016}\ mol/m^3 s$.

Simulation Results

On the basis of these conditions, the methane upward-migration processes are simulated by these two models. The results are shown in Figure 4.3. The distributions of the methane saturation after ca. 10.0 days are shown in the upper left for the two-phase/ three-component model and the upper right for the two-phase model. We can clearly observe that the methane gas migrates upwards faster in the case of the two-phase model than in the case of the two-phase/ three-component model. In order to investigate the factors which cause the difference in the migration speeds, the mass of the methane in each phase at each node and time step, i.e. $\rho_\alpha^{mass} S_\alpha X_\alpha^m \phi\ (\alpha = w, g)\ kg/m^3 s$ is calculated. The distributions are shown for the gas phase (lower left) and for the water phase (lower right) in Figure 4.3. Furthermore, to explain how the values $\rho_\alpha^{mass} S_\alpha X_\alpha^m \phi\ (\alpha = w, g)$ in Figure 4.3 change, Figure 4.4 presents the mass fraction of the methane in the gas phase (upper left), in the water phase (upper right), and the mass density of the gas phase (lower left), and of the water phase (lower right) As is apparent from the distributions of the mass fractions, most of the gas phase is occupied by the methane, while the mass fraction of the methane dissolved in the water phase is rather small. The difference between these mass fractions reaches three orders of magnitude. On the other hand, the mass density of the water phase is 990 to 1100 kg/m^3 (lower right), while the density of the gas phase is around 1 to 30 kg/m^3 (lower left). Thus, the difference between these densities attains two orders of maginitude. The mass of the methane in either the water or the gas phase is nothing less than the multiplication of these values, the phase saturation and the porosity of the subsurface. Then the total mass of the methane based on the nodal values is estimated, and the ratio of the methane mass in each phase to the total mass is calculated until

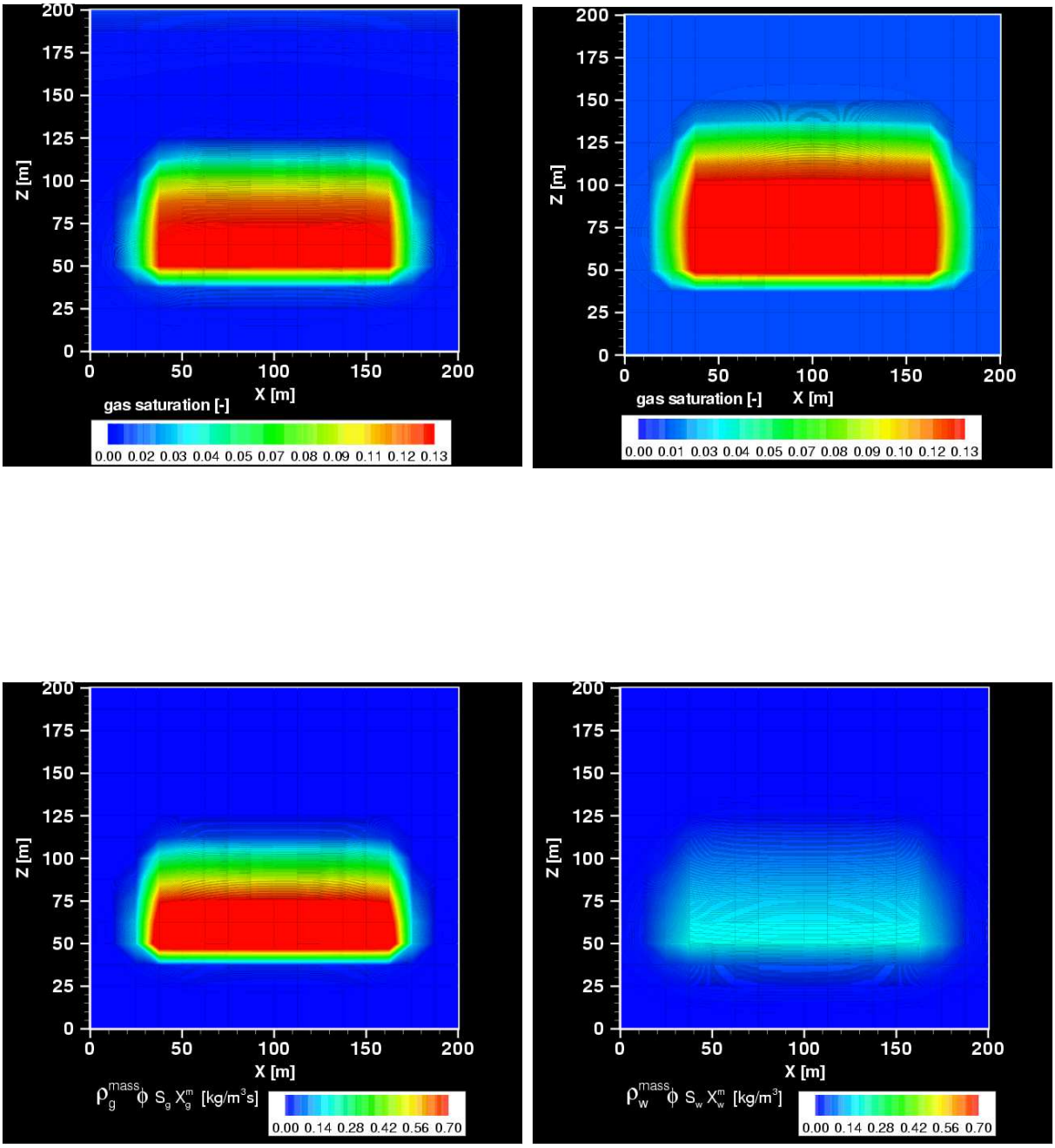

Figure 4.3: Gas saturation distribution after ca. 10.0 days, using the two-phase/ three-component model (upper left) and the two-phase model (upper right). Distribution of methane mass at each node and time step in the gas phase (lower left) and in the water phase (lower right)

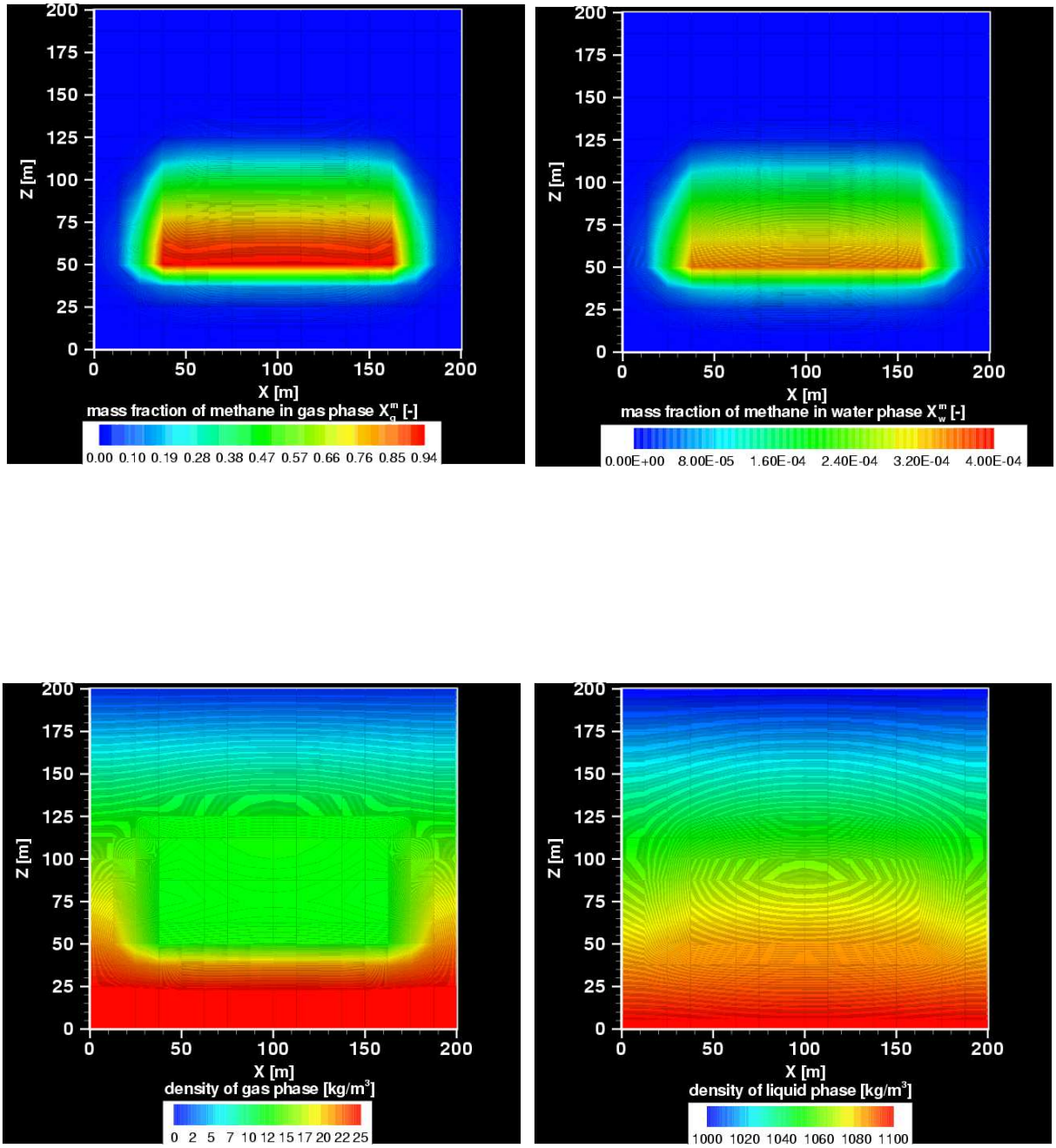

Figure 4.4: Distribution of the mass fractions of methane after ca. 10.0 days in the gas phase (upper left) and in the water phase (upper right). Distribution of the mass densities for the gas phase (lower left) and for the water phase (lower right)

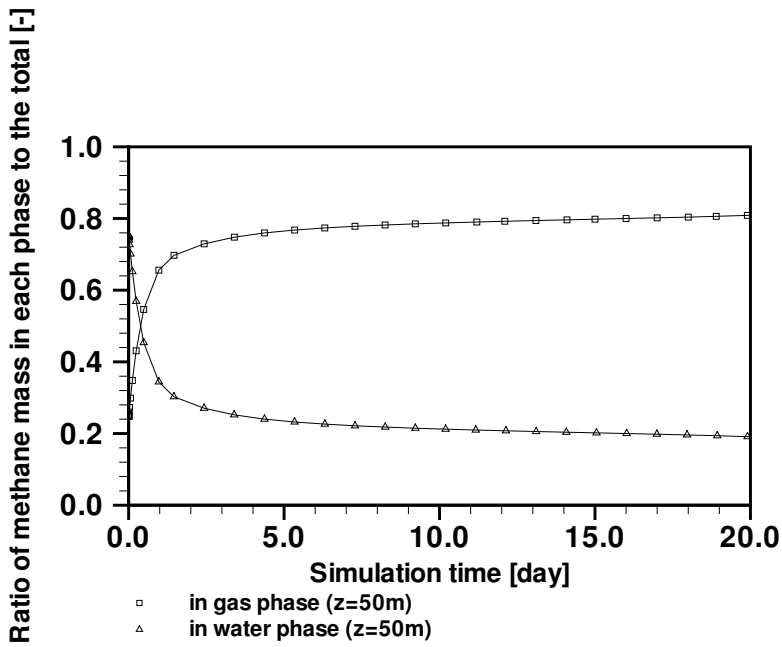

Figure 4.5: The ratio of the methane mass in each phase to the total mass for Example 1

for 20 days. This is shown in Figure 4.5.

The methane injected into the system is first dissolved in the water phase until the amount of dissolution is beyond the capacity expressed by Henry's law, and then the gas saturation, (i.e. the mass of the methane in the gas phase) starts to increase. The ratio in the gas phase increases in the middle of the simulation. Then, the ultimate ratio of the methane mass in the water phase, in this case, becomes around 20%, although this value itself changes widely according to the simulation conditions (this aspect will be discussed later). Thus, we could draw the inference that the reason the upward migration of the methane becomes slower when the two-phase/ three-component model is applied is the dissolution of the methane in the water phase.

4.1.2 Example 2

System Set-Up

What Henry's law clearly states is that the methane dissolves more in the water phase as the pressure of the gas phase containing methane increases. Therefore, as a next step, a series of simulations is carried out in which the depth of the methane source is changed. Generally speaking, the pressure of the gas phase generated by mass injection increases as the location of the methane source becomes deeper because of the weight of the water above. Exactly the same system as well as the same simulation conditions as in Example 1 are used in Example 2, except that the location of methane sources varies from $z = 50m$ to $z = 150m$ in $50m$ stages (i.e. $z = 50, 100, 150m$).

Simulation Results

The ratio of the methane mass in each phase to the total mass is calculated with regard to each depth of the source in the same manner as in Example 1. The results are shown on the left of Figure 4.6, while the cumulative masses of the methane in each phase as functions of the simulation time are shown on the right. The time at which each curve in the figure terminates almost corresponds to the time at which the upward methane front reaches the top of the system, where the gas can no longer escape out because of the boundary constraint $S_w = 1$.

The following is observed:

- The amount of methane dissolved in the water phase increases with the depth of the source because of the higher gas pressure.
- On the other hand, the methane in the gas phase decreases with the depth, because the amount of methane injected is always the same.
- The time at which the ratio in the gas phase exceeds the ratio in the water phase is delayed as the methane source becomes deeper, and the ultimate ratio in the gas phase is lowest when the methane source is deepest because most methane can be dissolved in the water phase most in this case.

These observations correspond to the inferences from Henry's law.

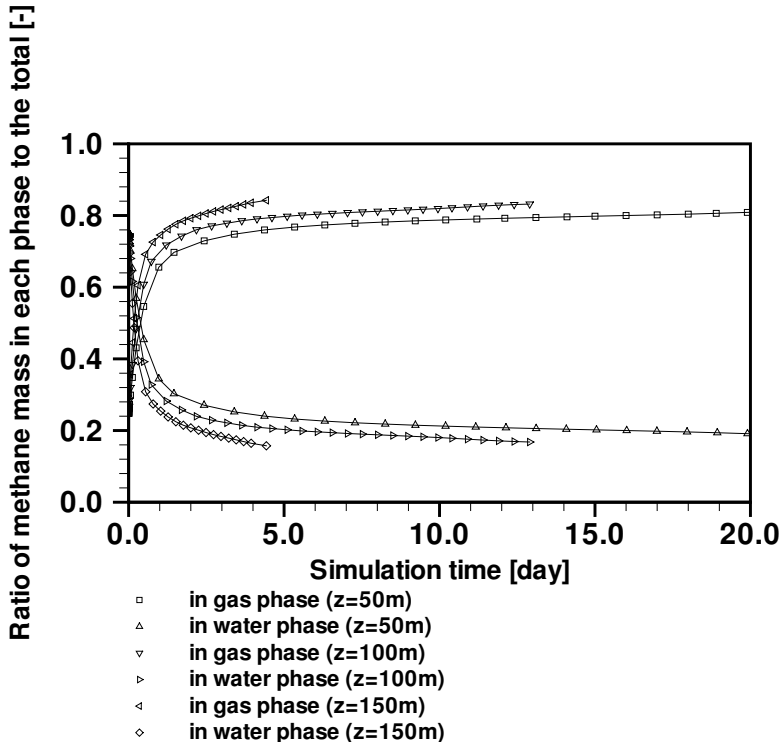

Figure 4.6: The ratios of the methane mass in each phase to the total mass at different depths of the source

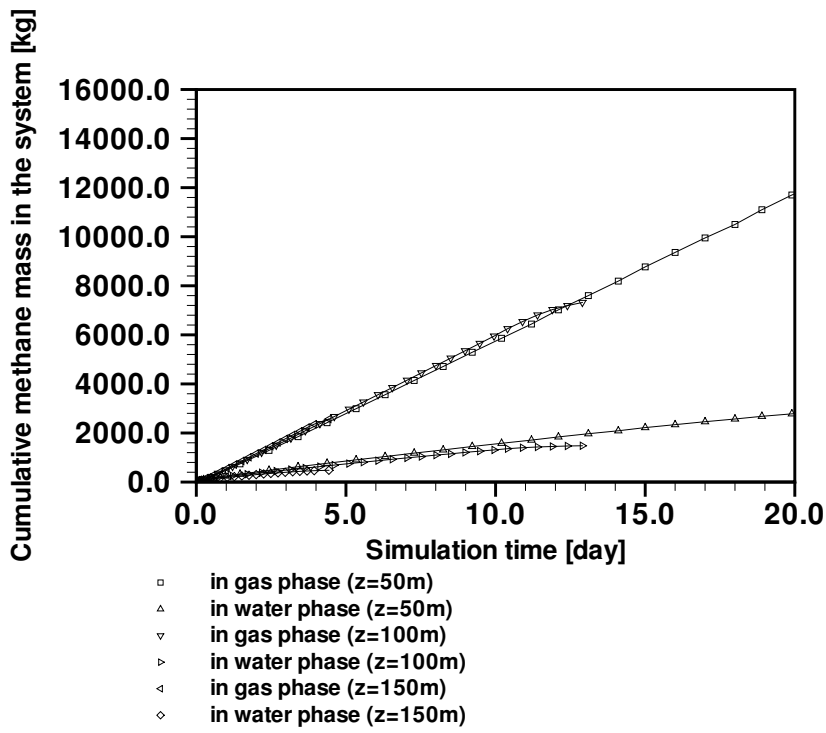

Figure 4.7: The cumulative mass of the methane in each phase

4.2 Gas-Water Processes in Three-Dimensional Porous Media

4.2.1 Example 3

System Set-Up

Almost the same procedures are taken in this section as in the previous section, except that a three-dimensional domain is used to study the 3D effects on the methane-migration behavior. The entire computational domain and the inner meshes on the plane of $x = 100m$ and $z = 50m$ are shown on the left- and right-hand side of Figure 4.8 respectively. The domain is a cube of $200m \times 200m \times 200m$ and is discretized spatially by 4096 elements and 4913 nodes. The initial and boundary conditions are exactly the same as in the two-dimensional case except that the methane sources are located on a line of $30m \leq x \leq 170m$, $y = 100m$ over the three-horizontal planes of $z = 50m$, $100m$, or $150m$.

Simulation Results

The results of the simulations when the line source is located on the $z = 50m$ plane are shown in Figure 4.9. The two figures in the upper row are the simulation results after ca. 10.0 days, while those in the lower row are after 20.0 days. The left hand side figures show the iso-surfaces of the gas saturation ($S_g = 0.12$), while the right-hand-side figures show the distribution of the gas saturation on the plane $x = 100m$ and $z = 50m$. We can clearly observe from these figures that the migration of the gas phase in the y-direction is not of a great extent, although it does exist especially around the middle area between $z = 50m$ and the top. This is easily inferred because the density difference of the two phases is the main driving force of the methane movement in this example, and this generally produces an upward, not a lateral migration. On the left-hand side of Figure 4.11, the ratios of the methane mass in each phase to the total mass are shown with regard to the aforementioned three-different levels. On the right-hand side, the comparison between the $3D$ case and the corresponding $2D$ case, where the methane source is located at $z = 50m$, is shown. One characteristic difference is that the ultimate ratio in the gas phase is larger in the $2D$ case than in the $3D$ case. This is most probably because of methane migration in the y-direction, even if it is small extent. In other words, the methane migrating in the y-direction dissolves in the water phase in the $3D$ case, which as a result yields a higher ratio in the water phase, especially after some time when the methane reaches around the middle area as mentioned. In Figure 4.12, the simulation results after ca. 10 days are shown for the $3D$ case on the cross-section of $y = 100m$ plane (left), and for the $2D$ case (right).

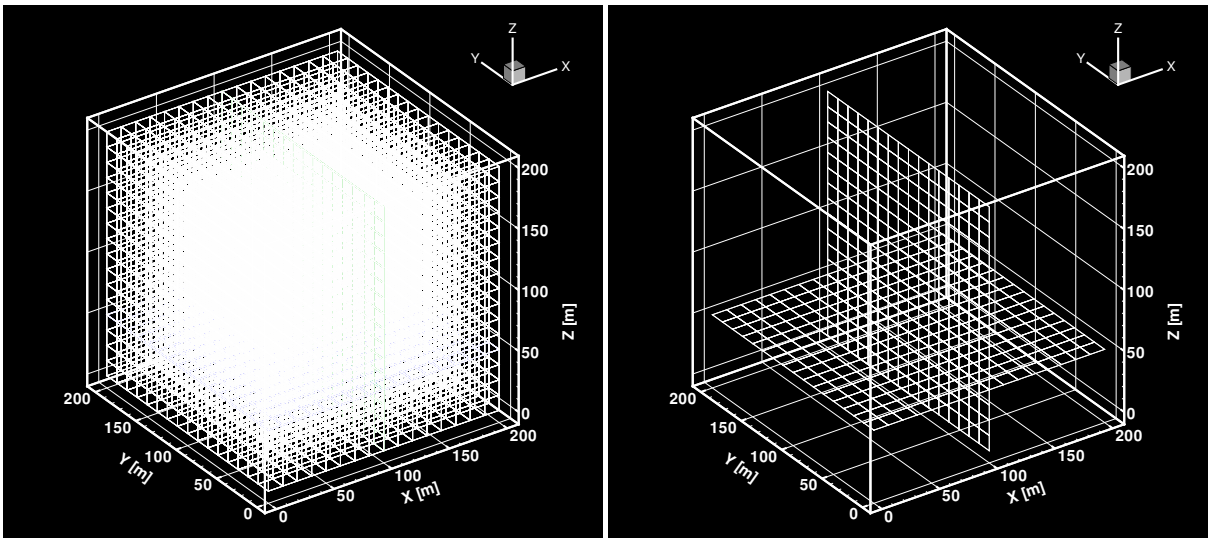

Figure 4.8: Three-dimensional computational domain (left) and the inner meshes on $x = 100m$ and $z = 50m$ planes (right)

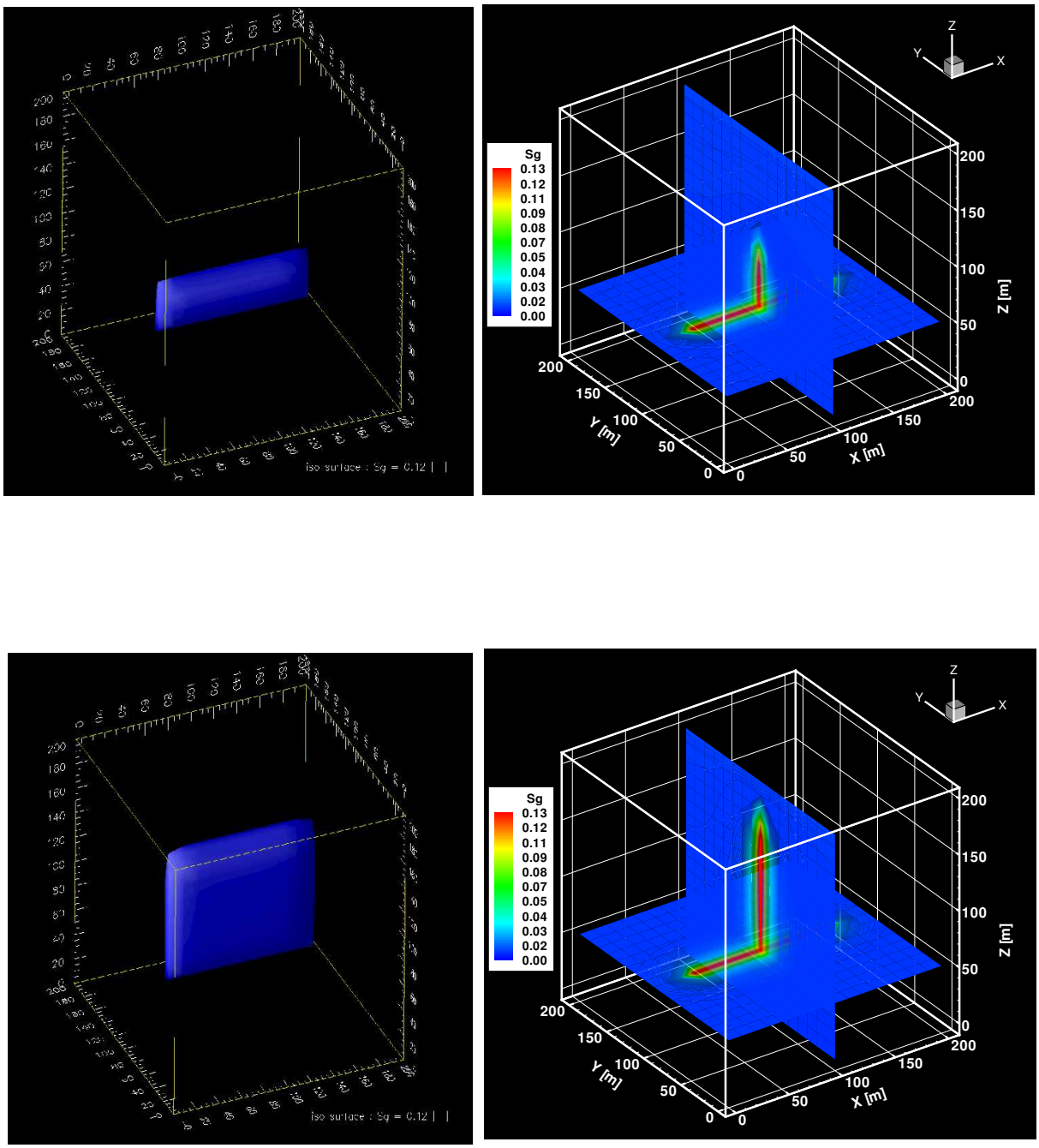

Figure 4.9: Iso-surface of the gas saturation ($S_g = 0.12$) after ca. 10 days (upper left), distribution of the gas saturation at $x = 100m$ and $z = 50m$ planes after ca. 10 days (upper right); iso-surface of the gas saturation ($S_g = 0.12$) after ca. 20 days (lower left); distribution of the gas saturation at $x = 100m$ and $z = 50m$ after ca. 20 days (lower right).

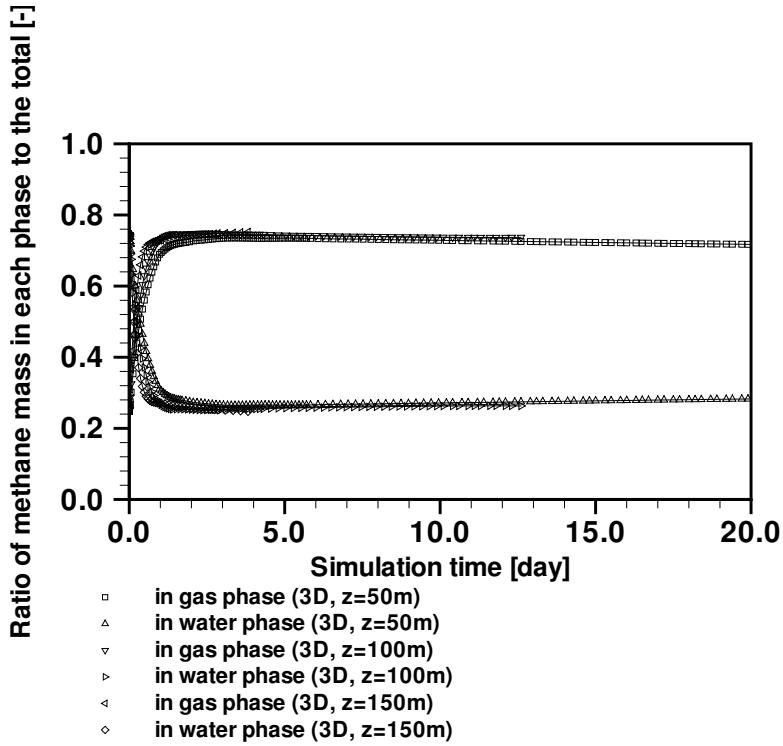

Figure 4.10: Ratio of methane mass in each phase to the total for the $3D$ case

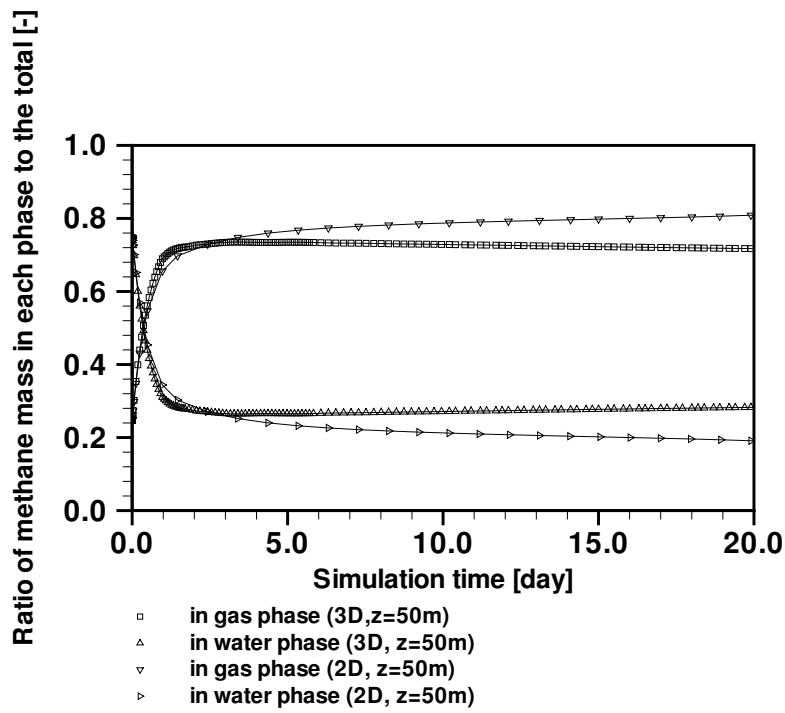

Figure 4.11: Comparison of the mass ratios between the $2D$ and $3D$ case, when the methane source is located at $z = 50m$.

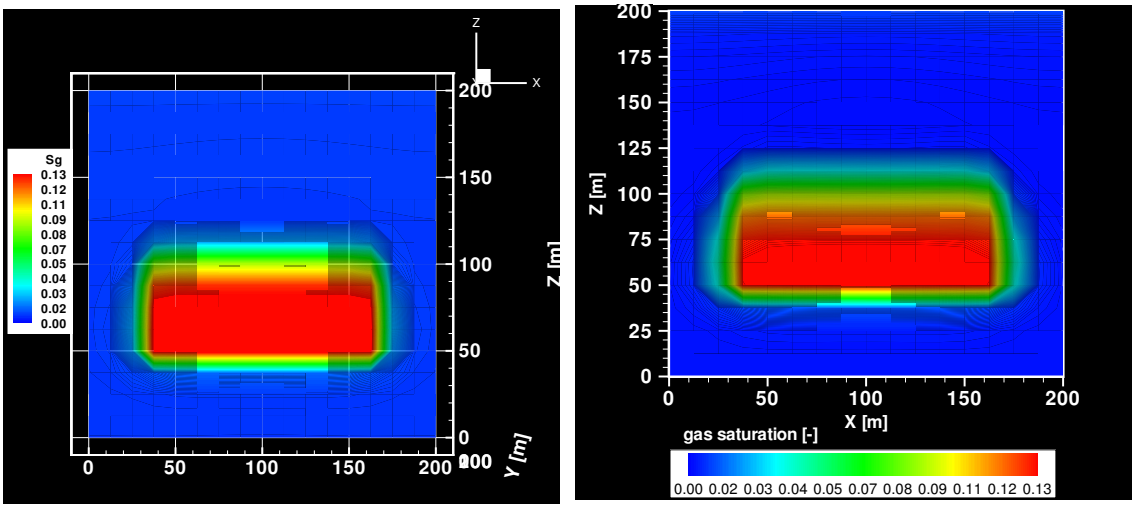

Figure 4.12: Simulation results after ca. 10 days for the $3D$ case on $y = 100m$ cross-section in $3D$ domain (left) and the $2D$ case (right)

Conclusion

From these comparative studies, it is clear that we often cannot neglect the amount of methane dissolved in the water phase. This dissolution process often causes problems such that:

- the speed of the upward migration of the methane gas front can be overestimated if we apply the two-phase, instead of the two-phase/ three-component model;
- in the extraction process of the methane, we also have to consider how to deal with the amount of methane dissolved in the water phase,

Thus, applying the two-phase/ three-component model is recommended, although the two-phase model could be a good alternative, especially in that the CPU time is shorter and the handling of the model is easier than the two-phase/ three-component model. As the next step, the validation of the model by experimental data is necessarily, although it seems to be rather difficult to obtain sets of accurate and extensive data.

Chapter 5

Application of MUFTE-SA

5.1 An Abandoned Coal Mine in Ruhrgebiet

In this chapter, the aforementioned simulation-optimization model MUFTE-SA (see Sections 2.3 and 2.4) is applied to a site in Dortmund, Germany where there used to be a coal mine below ground, and at present a furniture company is opening its store on the surface. This site was selected following discussions with Deutsche Montan Technologie Gmbh (DMT), a German company which provided us with the data set.

The location of the site is shown in Figure 5.1. The site is in Dortmund, a part of the so-called Ruhrgebiet. This area is indicated by a red circle on the upper left-hand side. The right-hand side shows a larger scale of the map of the area around the site. A 3D view of the site is shown in the upper part of Figure 5.2. The red color in the figure shows a former coal road at the level $z = -40$ m (the origin of the z-coordinate is the surface), while the grey color is at the level $z = -60$ m. Coal seams are not shown in this figure. Two vertical shafts (dark green) used to be utilized as access to the coal workings underneath, although they are now filled up. The photo in the bottom half of the figure shows one of the vertical shafts after sealing.

Figure 5.3 shows a plan of the site. The six small dots in the figure show where so-called passive extraction wells are installed, see also Figure 5.4. Passive means that no artifical energy is imposed for the use; instead, the gas underneath is sucked up only by the pressure difference between the atomosphere (ca. 1 *bar*) and the pressure undergroud (ca. 1 *bar* + 10 to 100 *Pa*). On the other hand, active extraction wells for which energy is supplied to extract the methane are used also sometimes. As a reference, an active extraction well is shown in Figure 5.5. This is a mobile type and can produce energy from the extracted methane. The release points of the passive extraction wells have protecture caps and must, by law, be located 3 m above ground level in order to prevent any danger caused by the methane production. This is why all the wells are fairly tall. Similar to the 3D view, the orange color in the plan represents the upper level of the coal working at a depth of 40 m from the surface, the blue color the lower level at 60 m.

At present, we have almost no information on the conditions of these coal workings. A breakdown of the surrounding strata in the roadways may have taken place, resulting in a filling up of the roadways; however this is not known. Methane absorbed in coal seams is continuously desorbed; thus, we want to extract the methane from this abondoned coal mine by installing passive

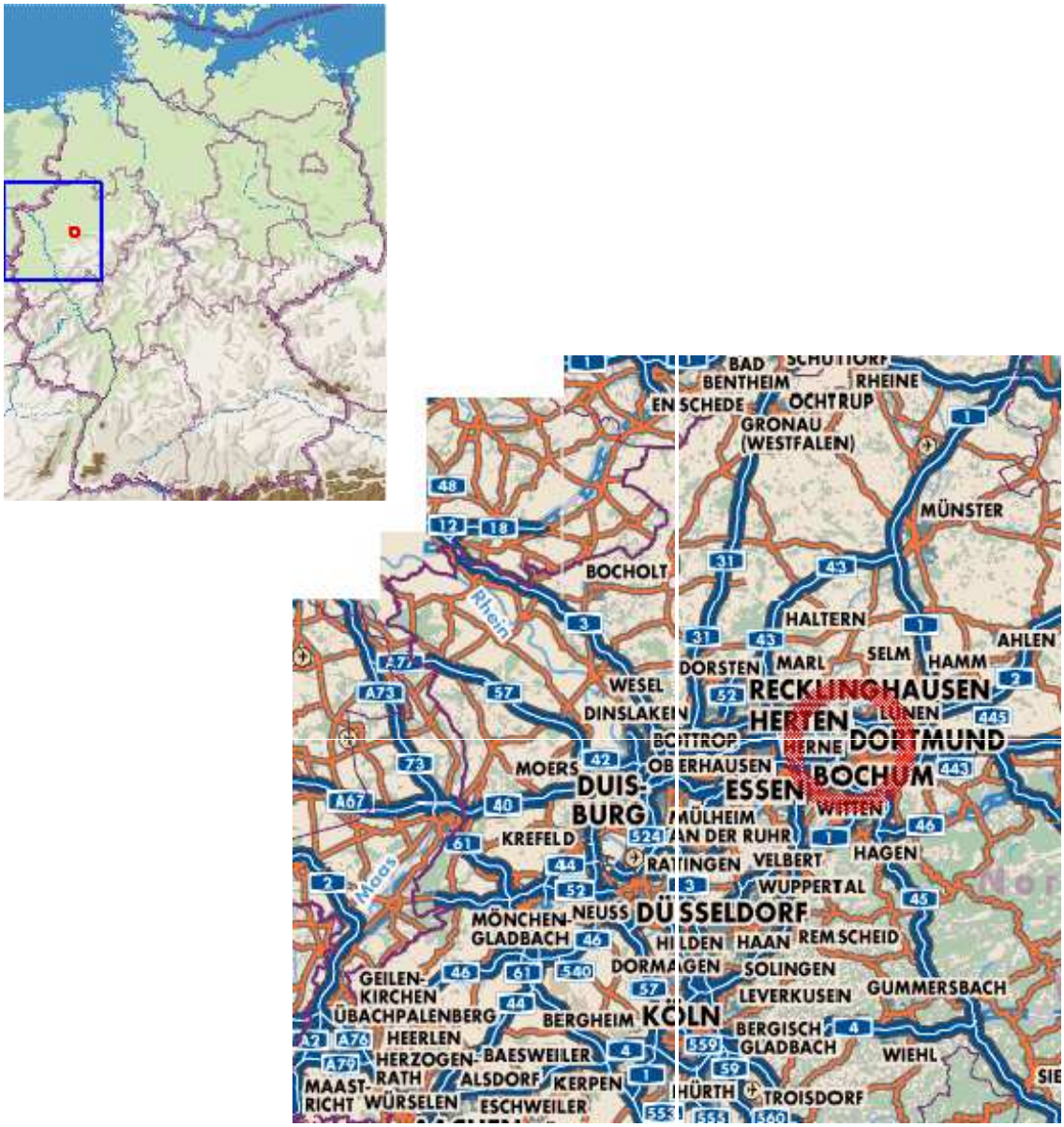

Figure 5.1: The location of site (This map was downloaded from Stadtplandienst website http://www.stadplandienst.de and reconstructed).

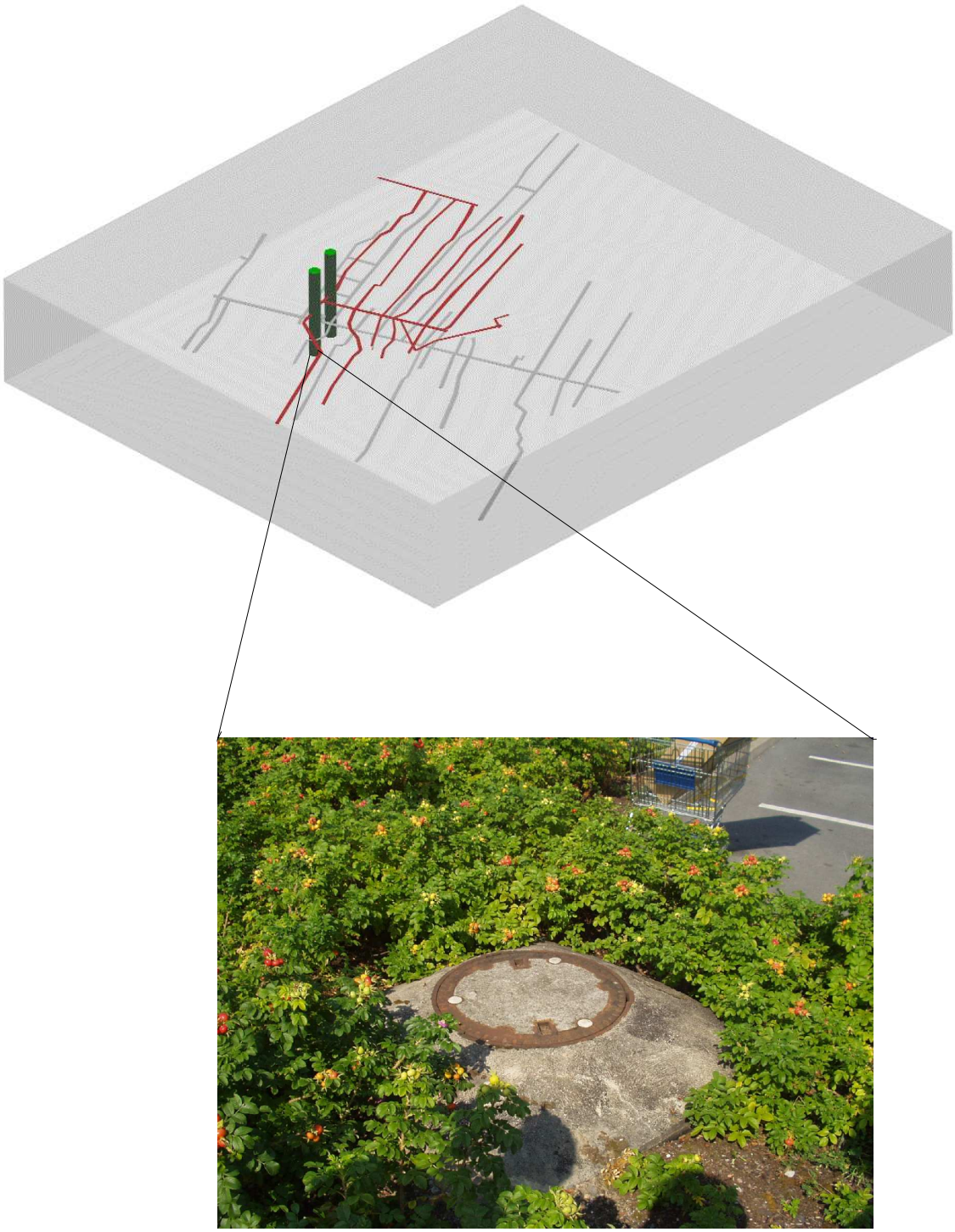

Figure 5.2: A 3D view of the abandoned coal mine in Dortmund, Germany (top). The red color shows the coal roads at the level $z = -40\ m$ (the origin is the surface); the grey color at the level $z = -60\ m$. Coal seams are not shown in this figure. The photo below shows one of the vertical shafts after sealing.

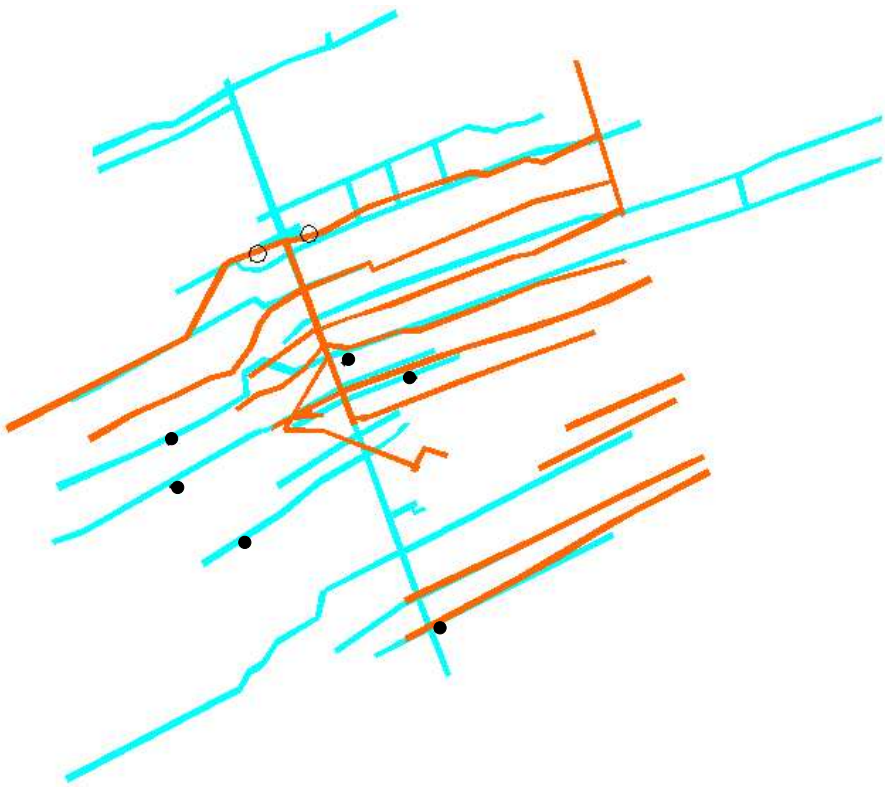

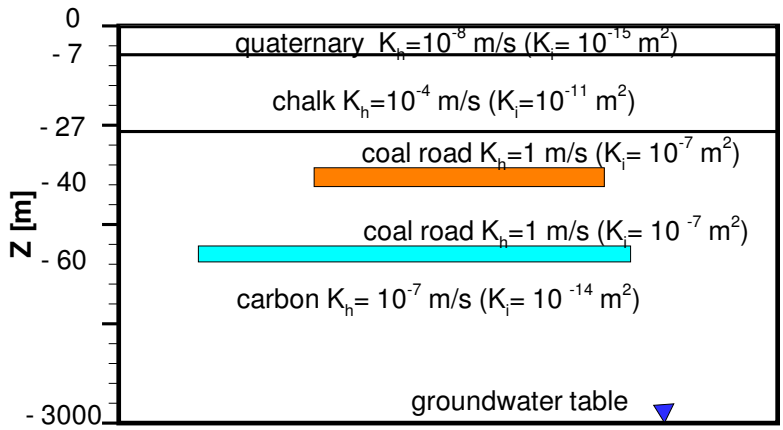

Figure 5.3: A plan (top) and a schematic diagram of the geological structure (bottom) of the site in Dortmund, Germany. The orange color in the figures shows the coal roads at a depth of 40 m, the light blue color at a depth of 60 m. K_h and K_i in the lower figure stand for the hydraulic and intrinsic permeability. Those valuse are rough estimates.

Figure 5.4: Each photo shows a passive extraction well installed on the site. The release point with a protective cap has to be located 3m above ground level.

Figure 5.5: An active extraction well in Dortmund, Germany.

extraction wells. There are already six passive extraction wells installed in this site, although these installation are done mainly by intuition without reasonable strategy obtained by fluid-mechanics study. One main goal of this work is to investigate how these passive extraction wells can be optimally positioned within the range of available data and whether or not we could obtain the same effect of extraction by installing less wells in these optimized location.

5.2 Objective Function

I, now, want to study how passive extraction wells can be installed effectively, i.e. how can optimal installation be realized. Of course, first of all, I have to define what kind of condition can be defined as optimal; in other words, the objective function itself has to be defined. Generally, we want to minimize the objective (cost) function, for example as follows:

$$Obj = \sum_{i}^{num} \left\{ f_1(p_i) + f_2(\mathbf{x}_i) + f_3(Q_{g,i}(p_i, \mathbf{x}_i)) + ... \right\} + f_k(Q^{top}) + ... \tag{5.1}$$

where i is the i-th well, num the number of wells, p_i the pressure at the extraction well i, $\mathbf{x}_i = (x_i, y_i, z_i)$ the coordinates of the the well i, $Q_{g,i}$ the amount of the gas containing methane extracted at the well i, Q^{top} the amount of the gas containing methane which reaches the top. Each function is explained as follows: $f_1(p_i)$ the operational cost (positive) required for active suction (in the case of passive suction, it is zero), $f_2(\mathbf{x}_i)$ the cost (positive) required for the well installation (This installation cost changes according to the location of the well, i.e. because of the geology and topology of the field), $f_3(Q_{g,i})$ the profit (negative) obtained from the energy production by the extracted gas containing methane and $f_k(Q^{top})$ the cost (or risk, positive) due to the gas containing methane which reaches the surface. Of course, there are more factors which influence the cost function.

However, I encountered difficulties during the formulation of this objective function. The problems are:

- the unavailability of accurate-well installation costs with regard to the depth, of information on the income obtained from the energy production, of the costs equivalent to the risks due to the methane reaching to the surface which should be avoided etc. and
- the lack of information for the source term, especially the spatial and temporal distributions (e.g. where exactly the source is located, how much exactly methane is produced, when the methane disappears).

For these reasons, for the time being, the following simplified objective function is used instead:

$$Obj \quad = \sum_{i}^{num} \left\{ f(Q_{g,i}(p_{atm}, \mathbf{x}_i)) \right\} \tag{5.2}$$

where p_{atm} is the atomospheric pressure which indicates the installation of the passive extraction wells. This function (5.2) indicates that the problem is reduced to maximize the sum of the gas extractions from the passive extraction wells.

One remark is that this simplification does not violate the applicability of MUFTE-SA in principle, because the objective function is already nonlinear. In other words, MUFTE-SA can be applied for any simulation-optimization problem with the original form like objective functions only if the information is available, although the number of iteration steps until the optimization algorithm reaches the global extremum will increase.

5.3 Simulation–Optimization

5.3.1 Conditions and Assumptions for Simulations

Now, the abandoned coal mine has to be modelled by MUFTE-UG. However, to start from the 3D modelling of the entire working is quite complex, or could be too expensive in terms of computational time (or could not be!) for the optimization purpose. Thus, I decided to begin by modelling only the coal working at the level $z = -40\ m$ in a 2D cut with the two-phase/ three-component model (Section 3.2.5). The coal working is in the unsaturated zone, so that the two-phase (gas-water)/ three-component (air, water and methane) model is not necessarily required; however, the model is used intentionally, bearing the later cases in mind when the groundwater rebound and/or recharge takes place.

First of all, I made the following assumptions:

- the methane source is uniformly distributed in the domain and
- the extraction wells can be represented as rectangular holes with edges 0.3 m long.

Then the first attempt to model the entire working, i.e. not only the roadways but also the surrounding matrix, in a consistent manner was made as shown in Figure 5.6.

However, other difficulties emerged at this point:

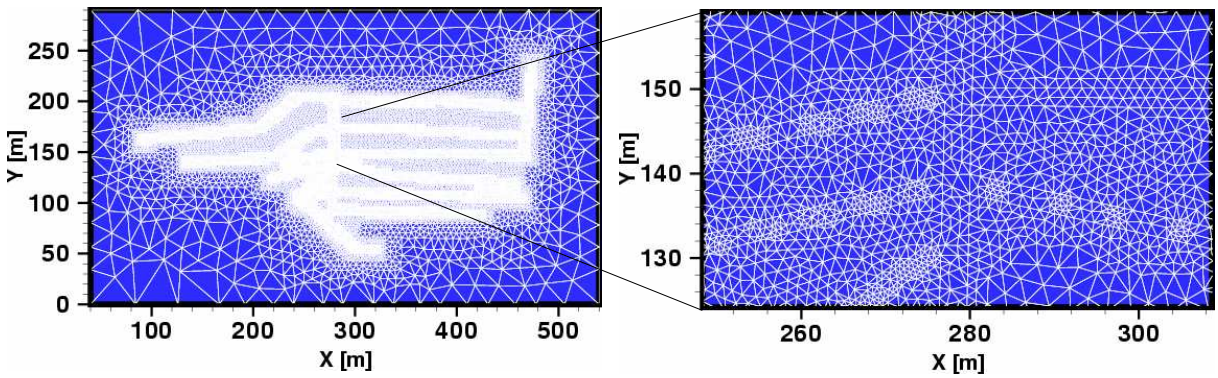

Figure 5.6: Computational mesh for the entire coal working (left) and the enlarged view of the center of the computational domain (right).

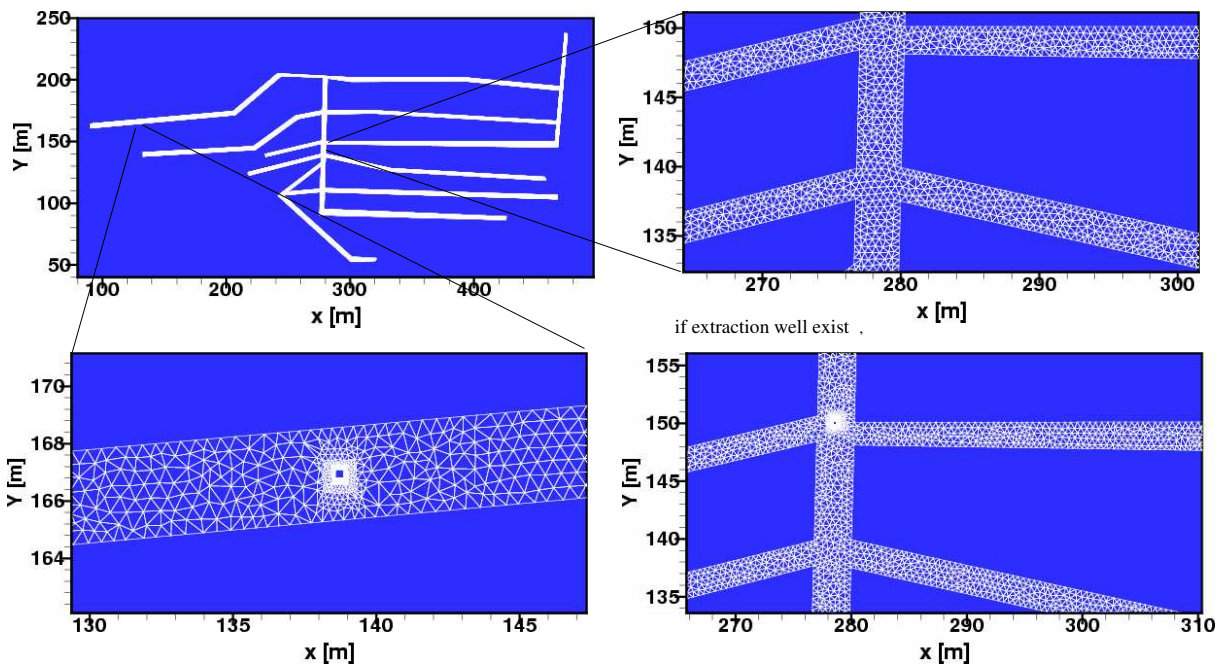

Figure 5.7: Computational mesh for the roadways and the enlarged views.

- dealing with the interaction between the roadways and the surrounding matrix is difficult, especially because the difference in the system properties between the two is quite large (e.g. the absolute permeabiliy of the roadway:10^{-7} m^2, of the matrix:10^{-14} m^2 as in Figure 5.3) and
- obtaining a high mesh resolution in the roadway, especially around the extraction wells, is difficult since the width of the roadways is 2 to 3 m and the well diameter is treated as ca. 0.3 m, while the entire working is around 500 $m \times 200$ m.

Thus, after discussions with DMT, I decided not to model the coal seams for the time being as shown in Figure 5.7. In this case, the methane desorption is represend by the source term in the model flowing from the boundaries of the roads. The advantages and disadvantages of this approach are as follows.

Advantages:

- The methane source is injected along the boundary of the roadways, i.e. the end of the coal seams. In this way, the 2D effects of the flow field can be simulated which would not be possible if I used a 1D-pipe flow network model,
- the composition of the gas phase can be calculated by the two-phase/ three-component model, which is again not possible with a single-phase pipe-flow network model,
- later extensions and improvements to the model concept are possible (e.g. the inclusion of the surrounding matrix in the simulation, the coupling of a (multiphase) pipe flow model with a porous-media multiphase-flow model etc.). The basics for the latter coupling are not yet well established for multiphase-flow models but concerning a simple groundwater model and a single phase pipe model, see for example, Adams and Younger (2001)[1] and
- it is possible to obtain enough mesh resolution. The number of elements is then about 25000, while 100000 elements are needed if I want to obtain the same level of resolution including the surrounding matrix.

Disadvantages:

- The porosity is set to almost 1 for this roadway because the roadway is, in principle, a void space, although the surrounding matrix might have collapsed (in this case, the roadway must be filled with the surrounding carbon). Thus, the validity of the porous media model is, without the inclusion of the surrounding matrix, is anyway a first step and thus
- the Reynolds number for Darcy's law is partially violated, at least around the extraction wells because of the strong pressure gradient there, although it is satified in most of the domain.

Nevertheless, these disadvantages are accepted for the time being because of the limitations.

The initial and boundary conditions and simulation parameters necessary for the two-phase/ three-component model are described in the following tables. A schematic diagram for these boundary

and initial conditions is shown in Figure 5.8. Note that the Henry coefficients and viscosity for the liquid phase are not of great significance since there is almost no liquid phase. However, these things are kept, as they are in the further extention of the model.

Initial and Boundary Conditions:

Neumann:	$q_g^m = 0.8 \cdot q^{tot}$	$q_g^a = 0.19 \cdot q^{tot}$	$q_g^w = 0.01 \cdot q^{tot}$
Dirichlet:	$p_g = 100000\,[Pa]$	$x_g^m = 0.8[-]$	$S_w = 0.01[-]$
Initial:	$p_g = 100000\,[Pa]$	$x_g^m = 0.6[-]$	$S_w = 0.01[-]$

where $q^{tot} = 6.59 \times 10^{-4}\ mol/ms$ which equivalents to $2.506\ mol/s$ totally.

Simulation Parameters:

Henry coeff (air) :	$H_w^a = 1.34 \times 10^{-10} Pa^{-1}$
Henry coeff (methane) :	$H_w^m = 2.08 \times 10^{-10} Pa^{-1}$
dynamic viscosity (gas) :	$\mu = 1.72 \times 10^{-5} Pa\,s$
dynamic viscosity (liquid) :	$\mu = 1.0 \times 10^{-3} Pa\,s$
relative permeabilty :	Brooks-Corey ($S_g \approx 1.0$)
capillary pressure :	Brooks-Corey ($S_g \approx 1.0$)
entry pressure :	$p_d = 0$
form parameter :	$\lambda = 2$

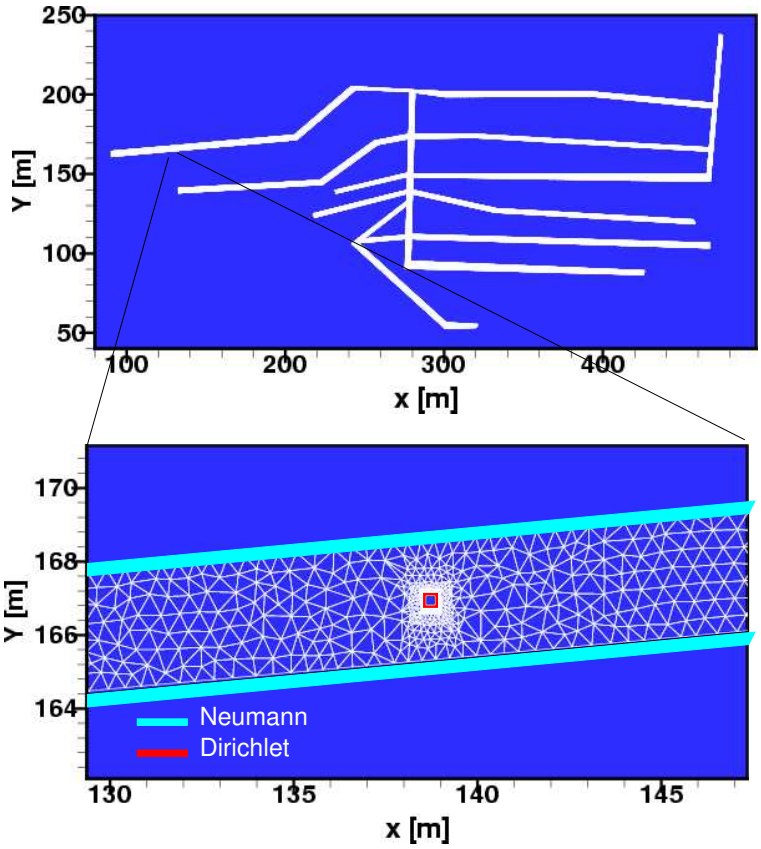

Figure 5.8: System set-up and boundary conditions for the simulation.

5.3.2 Parameters for Simulated Annealing

Parameters for Simulated Annealing, i.e. the standard deviation for the search space, the Boltzmann constant for the acceptance of a deteriorated solution and the temperature for the cooling schedule in the applications are the same as those in Figures 2.3 to Figure 2.5. This initial temperature is determined experimentally and is rather low, although this seems to be appropriate for this specific problem. This is mainly because the amounts of gas extracted from the wells is rather similar, yielding the Boltzmann probability large enough to escape from local maxima, even if the temperature is small.

5.3.3 Parallerization Design for the Problem

A more general description for the pseudo-parallel design of optimization models is given in Section 2.4. Here, the design is specifically tailored for this application by means of a domain decomposition. As mentioned in Section 2.4, the total time was expected to be around $\frac{7\,hrs \times 1000\,iterations}{24\,hrs} \approx 292\,days$ (for one well case), so the use of a parallel computer was inevitable. Thus, I decided to decompose the entire roadway into n segments (here $n = 23$). Then, k extraction wells are installed in k of the n segments according to reasonable assumptions from the engineering point of view. Each MUFTE-SA procedure is then carried out on a node of the parallel computer. After this, the results from each node are summarized and, if the summarized result reach the stopping criterion, the entire procedure stops, otherwise it iterates the same procedures. By doing this, the total time for one well case was expected to be reduced; for example with 23 nodes to $292\,day/23 \approx 12.7day$. The chart of this procedure is shown in Figure 5.9.

One thing we should note is that the simulation itself by MUFTE-UG is carried out in the whole domain, although the optimization is carried out in the subdomains. The result of the simulation-optimization should not change by carring out the optimization in this way in principle. The key to obtain the better solution depends on the number of total iterations steps, thus the solution is expected to be more or less the same if the sum of the sub iterations in eash sub domain corrsponded to the number of iterations if we had carried out the optimization without using the parallel computer.

The procedure for deciding the initial and subsequent decision vector for this particular case is described in Equations (5.3) to (5.7). A schematic diagram explaining this procedure is shown at the bottom right of Figure 5.9. The values at both side boundaries of the roadway are denoted by the subscripts L and R, while U and D indicate whether the coordinates exist upside or the downside (read XRD in the figure as x_{RD}).

$$x_{up} = 0.5(x_{RU} + x_{LU}), \quad y_{up} = 0.5(y_{RU} + y_{LU}), \tag{5.3}$$

$$x_{down} = 0.5(x_{RD} + x_{LD}), \quad y_{down} = 0.5(y_{RU} + y_{LU}), \tag{5.4}$$

$$x_{init} = 0.5(x_{up} + x_{down}), \quad y_{init} = \frac{(y_{up} - y_{down})}{(x_{up} - x_{down})}(x_{init} - x_{down}) + y_{down}, \tag{5.5}$$

$$x_{new} = (\Delta x \cdot f(\sigma, \mu) + x_{old}), \quad (x_{down} \leq x_{new} \leq x_{up}, \Delta x = 2(x_{up} - x_{down})/5), \tag{5.6}$$

$$y_{new} = \frac{(y_{up} - y_{down})}{(x_{up} - x_{down})}(x_{new} - x_{down}) + y_{down}, \tag{5.7}$$

where $f(\sigma, \mu)$ is a psuedo-random number from a Gaussian distribution with the aformentioned mean μ and the standard deviation σ.

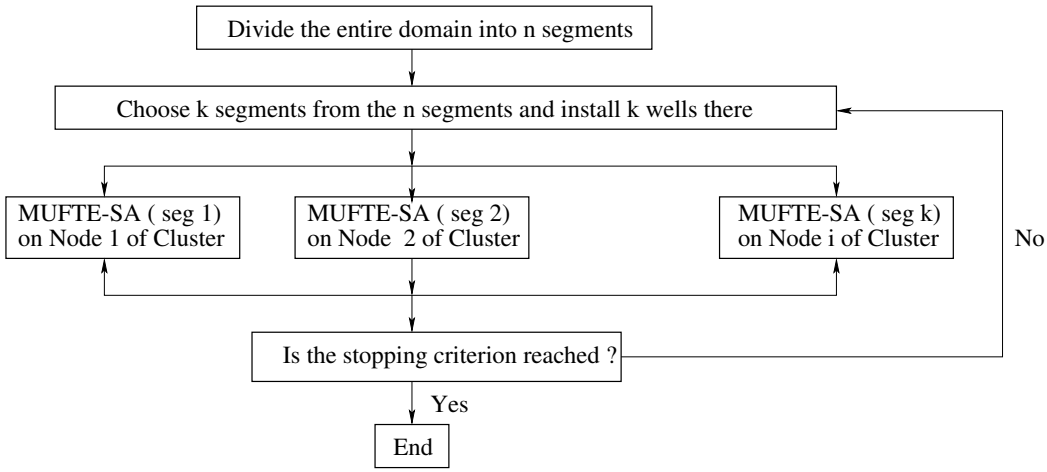

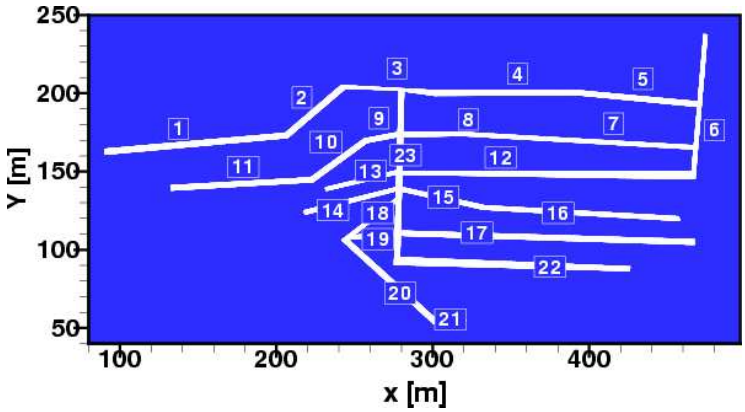

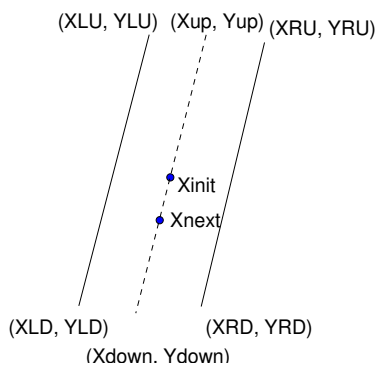

Figure 5.9: Parallelization strategy by means of a domain decomposition (above). Decomposed roadways (below left). A schematic diagram for the next coordinate decision (below right).

5.3.4 Preliminary Test Cases

Before this simulation-optimization model is applied to the coal mining site, MUFTE-SA is applied as a preliminary step to examples with simpler domains where one to three extraction wells are installed. This step is necessary to understand the basic system behavior.

5.3.4.1 One Well in a Straight Road

System Description
First of all, a simple rectangular domain with one extraction well is used. The schematic diagram of the system set-up, the computational mesh and the boundary conditions when the extraction well is located in the center of the domain are shown in Figure 5.10. In this figure, the length in the y-direction of the domain is exaggerated for a better visualization; thus, the proportionality between the x- and y-directions is not accurate. The system is 500 m long and 3 m wide. The extraction well is represented as a rectangle hole as mentioned and has edges of 0.3 m. The fluxes of the components are given as Neumann conditions from the outer boundary of the system. This amount is equivalent to 2.506 mol/s (80 % methane, 19 % air and 1 % water). A Dirichlet condition is given around the extraction well. These conditions are the same as those for the mine site already mentioned.

Steady State
Two different types of steady state should be distinguished. The first is the steady state of the phase flux calculated by the velocity field, while the second is the steady state of the mole fractions in the phase. First of all, let us consider the steady state for the first type, i.e. the mass flux of the gas phase (accordingly the gas extraction at the extraction well). Figure 5.11, left shows the gas extraction against simulation time at the well which is installed in the center of the domain. In this example, the gas extraction attains a quasi-steady state at around 280 sec simulation time. At this steady state, the global mass balance between the influx from the surrounding boundaries and outflux to the extraction well is almost satisfied with regard to the gas phase total although the composition of the gas phase is not identical at the outer and inner boundaries. Unfortunatelly, the perfect mass balance is not satified because; the mass injected partially goes into the water phase, the mass flux at the extraction wells is the approximated value based on a midpoint rule, some numerical problems might have happened, nevertheless these shortcomings are considered to be of minor importance and accepted.

Then, four points are selected for the steady-state study with regard to the composition as shown in the left hand side of Figure 5.12. Ideally speaking, this steady-state condition should be investigated at the boundary of the extraction well, but this was not done since the so-called free-flow boundary condition has not yet been correctly developed. This aspect will be addressed later on in more detail. The steady state for the mole fraction of the methane at those points is shown in the right hand side of Figure 5.12. The mole fraction attains the quasi-steady state after 1.3 $days$. In reality, it is assumed that these compositions become ultimately the same more or less in the whole domain, although the simulation exhibits very slight differences in the composition from place to place. This aspect will probably be improved if the mole fraction of the methane in the gas phase at the extraction well can develop freely according to the system changes. However, the value x_g^m is fixed to 0.8, thus the whole system reaches quasi-steady state after some time with

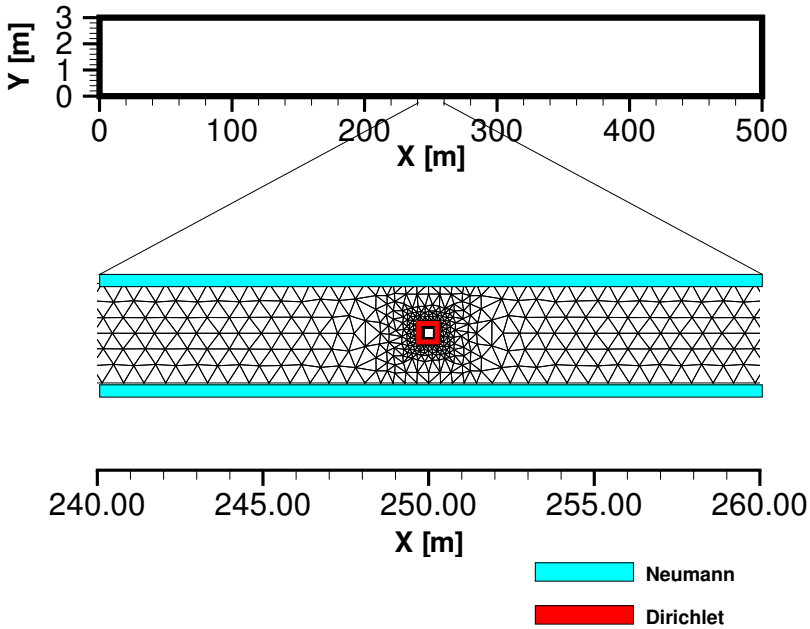

Figure 5.10: Compuational domain (above) and the mesh and boundary conditions (below). Note that the length in the y-direction is exaggerated for visualization's sake.

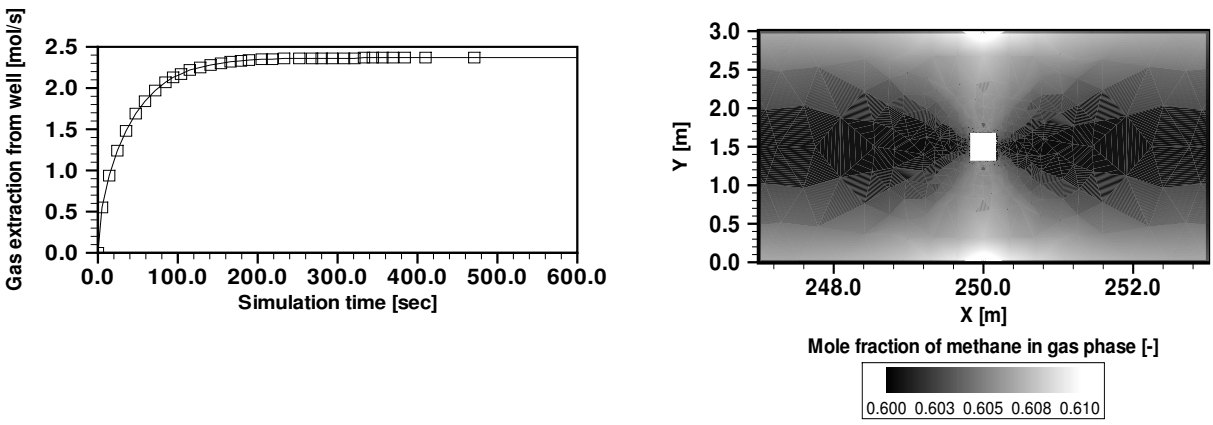

Figure 5.11: Steady state for the gas flux at the extraction well when the well is installed in the center of the domain (left). Distribution of the mole fraction of the methane in the gas phase after 280 *sec* simulation time when an extraction well is installed in the center of the domain. Note that the proportionality between the x- and y-direction is distorted for the sake of a better visualization (right).

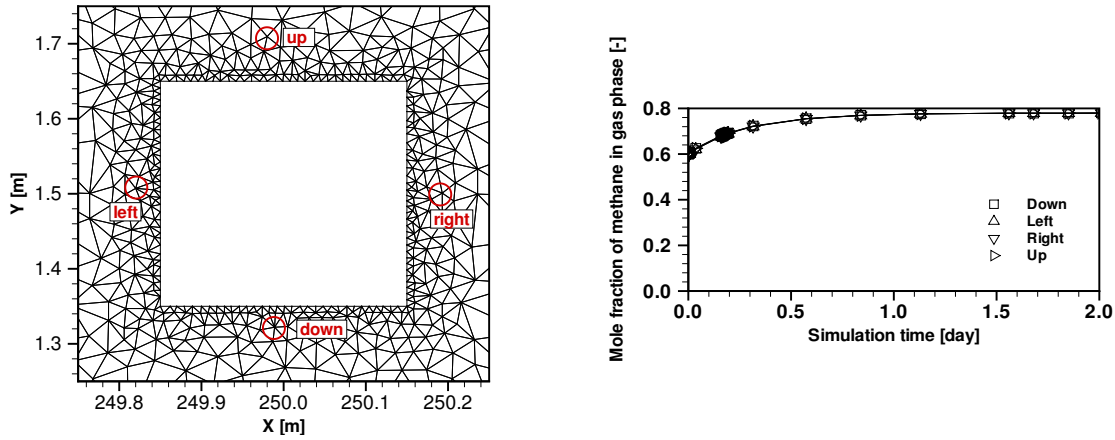

Figure 5.12: Four points chosen for steady-state study (left). Steady state for the mole fraction of the methane in the gas phase when the well is installed in the center of the domain (right).

regard to the composition, although the composition cannot be completely the same in the whole domain. Figure 5.11, right shows the distribution of the mole fraction of the methane in the gas phase after 280 *sec* simulation time. As shown, methane from the surrounding boundaries moves toward the extraction well.

One possible solution to this problem is, as mentioned, to develop the so-called free-flow boundary condition which, allows the increase and decrease of the methane composition on the inner boundary to the value interpolated from those surrounding values. However, this development is not easy and was not possible within the framework of this thesis. Thus, only the mass balance of the gas phase is considered in the following applications. Additionally, the computational time required until the system attains steady state with regard to the composition is too long (ca. 3 *days* for this simplest domain!). Thus, there is almost no chance at present to conduct the simulation-optimization for the second steady state (However, additionally speaking, this simplification is proved to be of minor importance later in Section 5.3.4.5).

When the appropriate free-flow boundary condition has been implemented and the problem of the computational time has been solved in future, it will be better to reformulate the objective function (5.2) as:

$$Obj \quad = \sum_{i}^{num} \{f(Q_{m,i}(p_{atm}, \mathbf{x}_i))\} = \sum_{i}^{num} \left\{f(x_{g,i}^{m} Q_{g,i}(p_{atm}, \mathbf{x}_i))\right\} \tag{5.8}$$

where $x_{g,i}^{m}$ is the mole fraction of the methane in the gas phase and $Q_{m,i}$ the extracted methane in mol/s. This objective function means that the optimal condition is to maximize the amount of the methane component in the gas phase (not the gas phase itself!) from the wells. This objective function may exhibit stronger nonlinearity than the function (5.2) does because the location where the mole fraction of the methane in the gas phase reaches the maximum may not always correspond to the place where the gas extraction reaches the maximum (this aspect will be addressed in Section 5.3.4.2). At any rate, the objective function to be optimized from now on is the function (5.2).

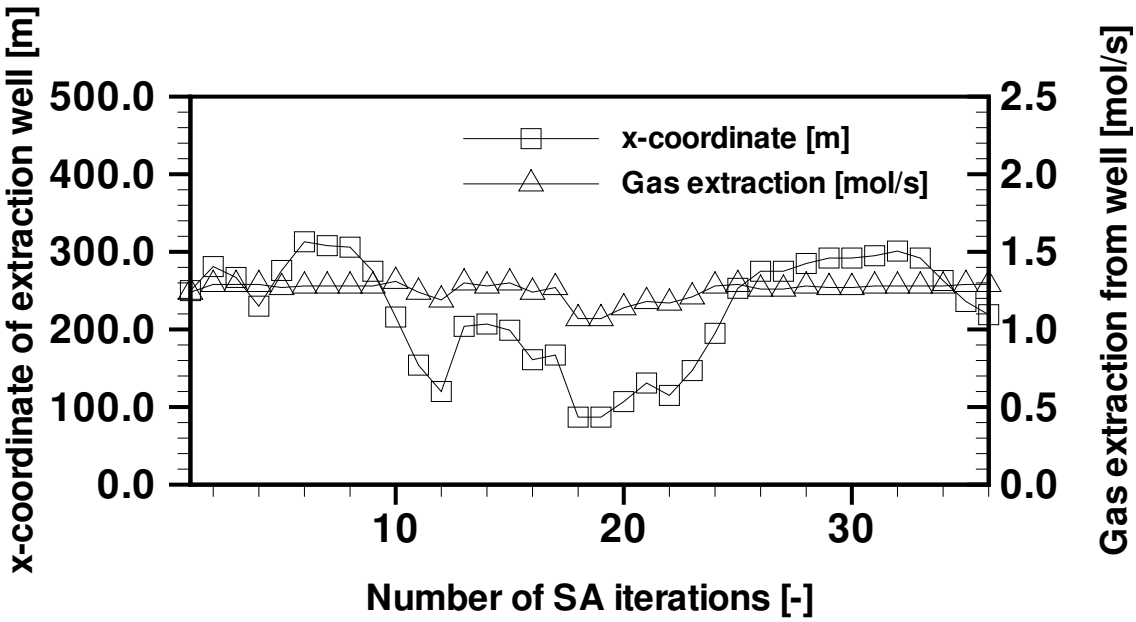

Figure 5.13: The well location and the amount of gas extracted from the well after 27 *sec* in simulation time against the number of SA iterations. The simulations are terminated after the wells attain around 50 % of the extraction of the inflow.

Results

The simulations in this case are terminated after the well extracts around 50 % of the 2.506 mol/s of gas inflow since the computational time is large (around 3 to 4 hours). The overall tendency does not change even if we run the simulation until the well extracts almost 100 % of the gas inflow.

Figure 5.13 shows the result of the simulation-optimization. As can easily be imagined, the amount of gas extraction from each well is mostly the same, irrespective of the well locations because there are almost no heterogeneities in the system set-up. It is inferred that the slight difference in the amount comes mainly from the fact that the distance between the extraction well and the side boundaries of the roadway changes; thus, the flow often cannot develop enough after some time, especially when the well is near the side boundary and/or a small numerical oscillation (e.g. cross diffusion) occurs due to the difference of the mesh. The former reason probably causes the relatively high difference of the extraction amount as can be seen in the difference between the initial simulation where the extraction well is installed in the center of the domain and the simulation where the extraction well is located at $x = 87.0\,m$, near the left boundary. The pressure fields for these cases are shown in the left and right hand side of Figure 5.14. These pressures increase up to 100050 to 100100 Pa due to the injection. The velocity due to the resultant flow field is around the order of $10^{-3}\ m/s$, thus the Reynolds number is $\Re = \frac{vd_{50}}{\nu} = \frac{10^{-3}d_{50}}{10^{-6}} = 10^3 d_{50}$, where d_{50} can be the particle size, although there is no way so far to determine the porosity and sand type in the roadway. In any casey, Darcy's law may be violated around the extraction well.

When I look at the aspect of the SA functioning, the final value is not the global maximum. The reason lies simply in the fact that the total number of SA iterations is low (ca. 40 to 50 iterations) and the difference in the extraction amount is quite small. Nevertheless, this shortcoming has to

be accepted because of the enormous computational time (this becomes more problematic in the case of the coal-mining site). Therefore, if the final value is not the global maximum, the best value among all the values within the SA iterations is always chosen a-posteriori.

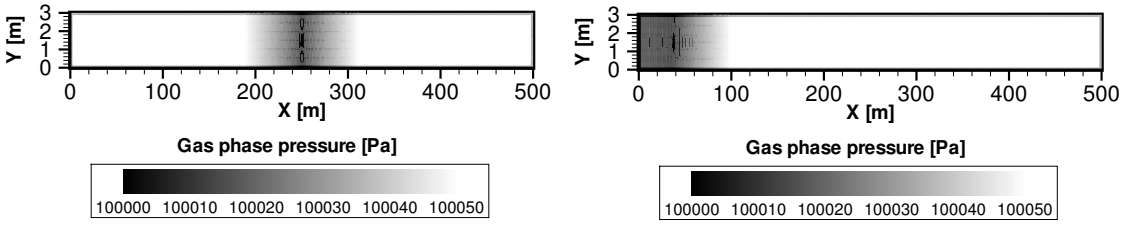

Figure 5.14: Pressure field after 27 *sec* simulation time when an extraction well is installed in the center of the domain (left) and at $x = 87.0\ m$ (right). Note that the length of the domain in the y-direction is exaggerated for the sake of a better visualization.

5.3.4.2 One Well at a Crossroads

As a second step, a crossroads at which one well is installed is chosen as shown in Figure 5.15. The initial and boundary conditions as well as the parameters used in this case are exactly the same as for the mine site. The simulation is terminated again after the well extracts around 50 % of the gas inflow.

The result of the simulation-optimization is shown in Figure 5.16. As can be imagined, the extraction when the well is installed close to the crossing of these two-roads shows the maximum, while it decreases when the well moves away from the center. The movement of the well by SA is limited to the area near the crossing point because the initial coordinate is the best point. The best value attained is 1.30 mol/s (51.3 %) after 27 *sec*, while the worst is 0.783 mol/s (31.2 %). Figure 5.17 show the gas-pressure field after 27 *sec* when the gas extraction wells are installed at the best (left) or worst (right) locations.

The simulations using these best and worst sytem-set ups were then reconducted until firstly the velocity field and secondly the mole fraction of the methane in the gas phase attain steady state. The amount of gas extracted at the extraction well against the simulation time for the best and worst case until the steady state with regard to the gas extraction (i.e the velocity field) is attained is shown in Figure 5.18. As shown, the best case attains steady-state after around 380 *sec*, the worst at around 1800 *sec*. Thus, the time difference is a factor of 4.8. Concerninig the mole fractions, four points are chosen both for the best and worst cases since the values at the extraction wells are fixed (see Figure 5.19) and the mole fractions at those points are plotted against the simulation time in Figure 5.20.

As is apparent, both the best and worst cases attain steady-state after around 4 *days* and the difference between these cases is mostly negligible. This is probably because the two distances between the surrounding boundaries and one of the extraction wells is not so very different. Thus, the times when the methane from the surrounding boundaries reaches the extraction well are not so different either. This fact implies that the location of maximum gas extraction realizes also

that of maximum methane extraction as well under these conditions. This implication is very important in that it may be true for the following mine-site application.

As a reference, a distribution of the mole fraction of the methane in the gas phase is shown in Figure 5.21 after 300 *sec* simulation time when an extraction well is installed at the crossing point of those two roads.

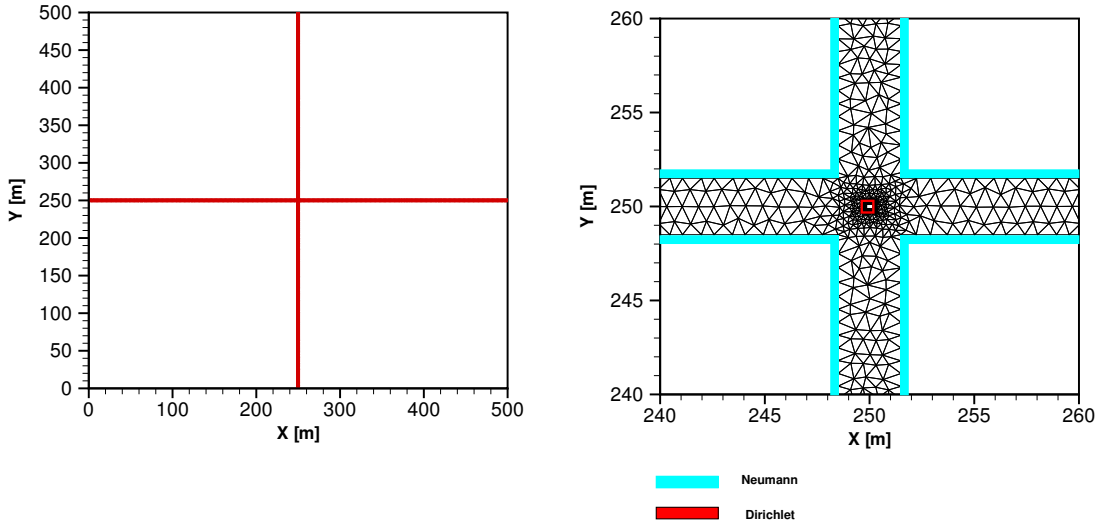

Figure 5.15: Compuational domain (left) and the mesh and boundary conditions (right).

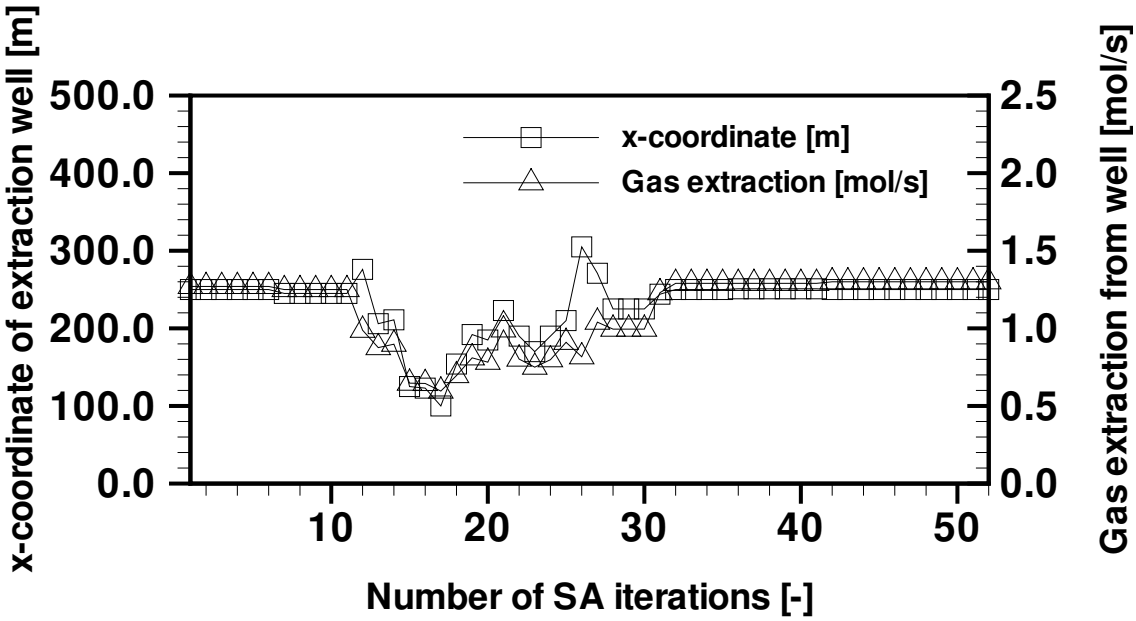

Figure 5.16: The well location and the amount of gas extracted from the well after 27 *sec* simulation time against the number of SA iterations. The simulations are terminated after the wells attain around 50 % extraction of the inflow.

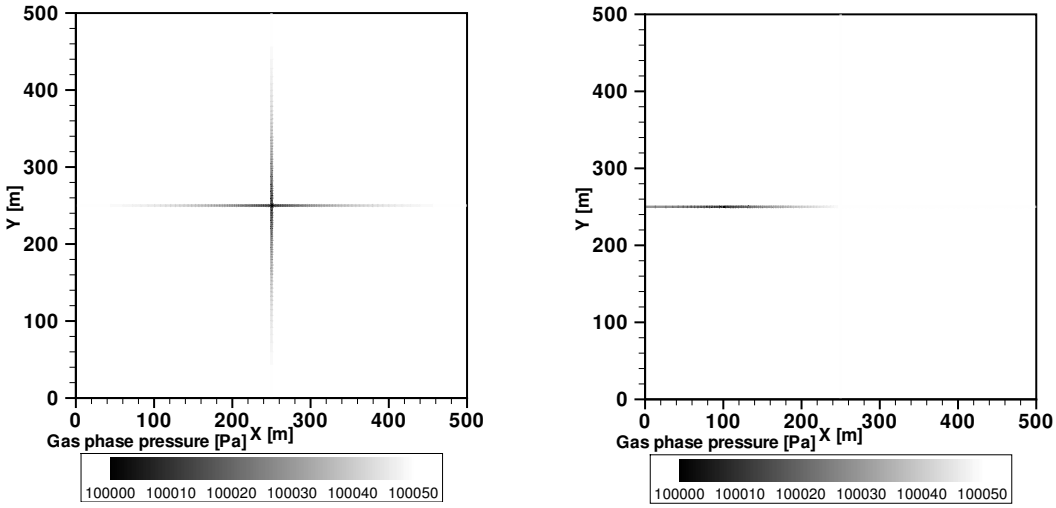

Figure 5.17: Pressure field after 27 *sec* when an extraction well is installed in the center of the domain as the best case (left) and at $x = 100.443$ m as the worst case (right).

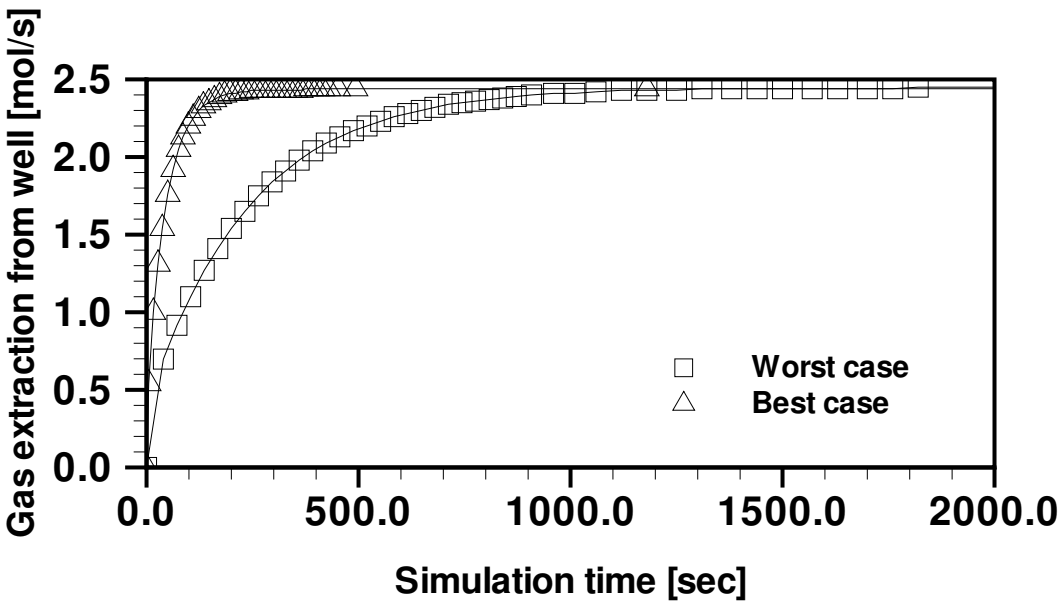

Figure 5.18: Steady states with regard to the gas extraction at the extraction wells for the best and worst cases.

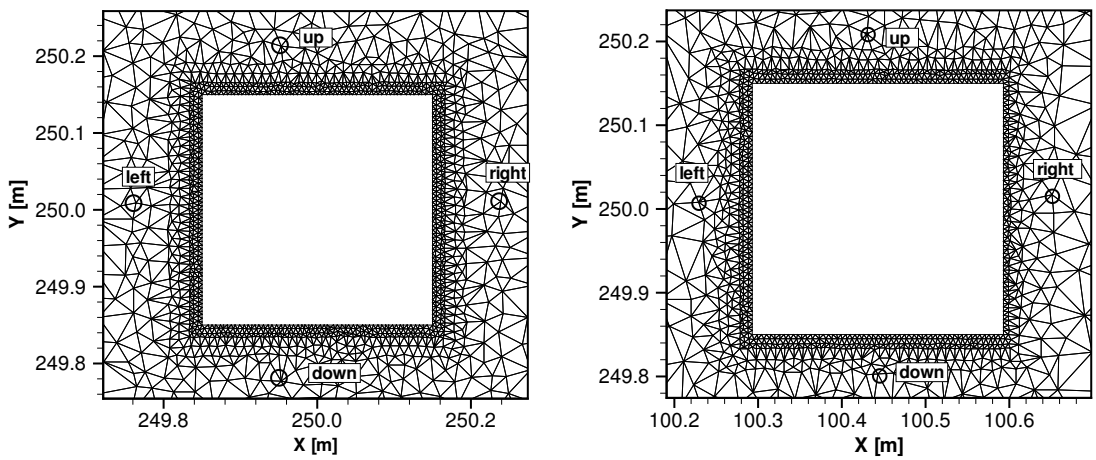

Figure 5.19: Four points chosen for steady-state study for the best case (left) and the worst case (right).

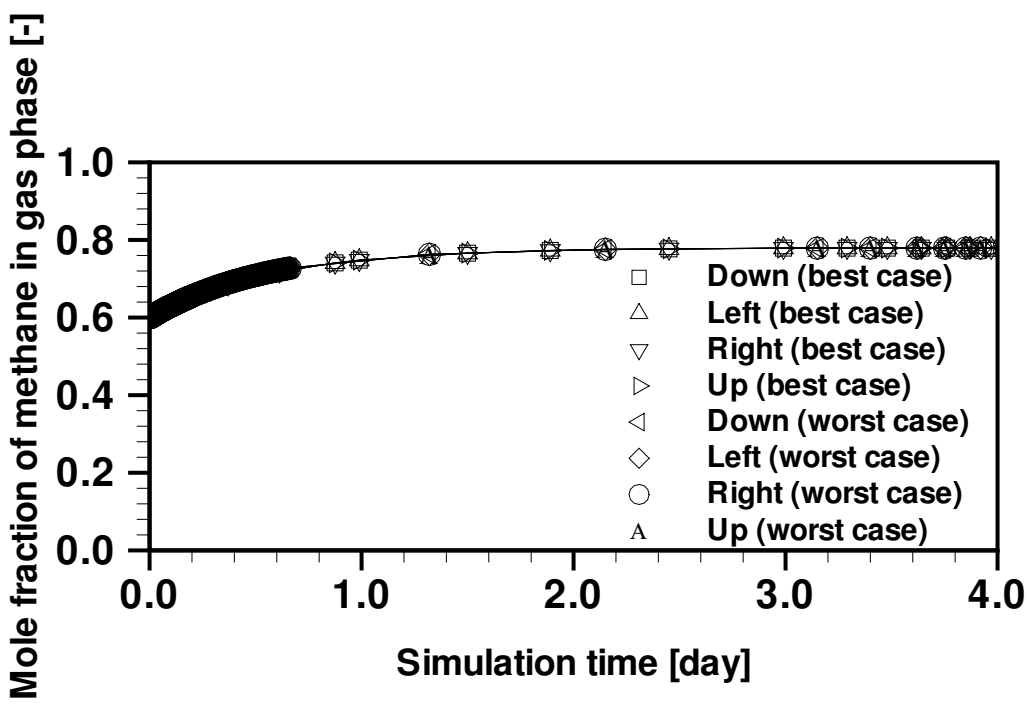

Figure 5.20: Steady states with regard to the mole fraction at the four points for the best or worst cases.

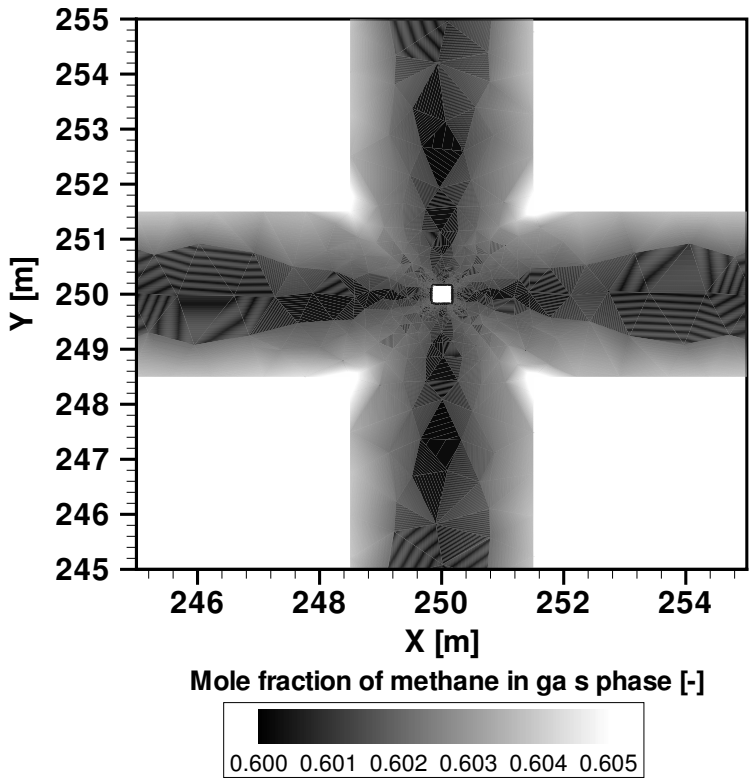

Figure 5.21: Distribution of the mole fraction of the methane in the gas phase after 300 *sec* simulation time when an extraction well is installed at the crossing point of two roads.

5.3.4.3 Two Wells in a Straight Road

The number of extraction wells is then increased from one to two in the straight roadway. The simulation conditions are exactly the same. Initially, two wells are located at $x = 150$ m and $x = 350$ m. Here, simulation-optimization is carried out twice, first after these two extraction wells suck up around 50 % of the gas inflow, mainly for comparison with the former two cases, and second after around 90 % extraction. An advantage of multiple wells is that the velocity field attains the quasi-steady state faster in terms of computational time because the forces driving the system change are stronger.

The results for 50 % extraction are shown in the left columm of Figure 5.22, while those for 90 % are presented in the right columm of Figure 5.22. Top left and right of Figure 5.22 show the x-coordinates of the two wells and the total amount of gas extracted from them after 7.7 *sec* and 38.0 *sec* simuation time against the number of SA iterations respectively. Middle left and right of Figure 5.22 show the amount of gas extracted from each well and its total after 7.7 *sec* and 38.0 *sec* simuation time against the number of SA iterations. Bottom left and right of Figure 5.22 show the distance between the coordinates of the two wells and the total amount of gas extraction against the number of SA iterations. The last two figures especially make it clear that the gas extraction becomes small when two wells are located very close or far beyond a certain value.

Top left and right of Figure 5.23 show the pressure fields for the best combinations, while the middle left and right as well as the bottom left and right illustrate some of the bad cases within the SA iterations. Now let us begin by looking at the bad cases. The amounts of gas extraction

always become lower when the positions of the wells are too close to each other as shown in the middle and bottom row of the figure. This is most probably because of interactions between two wells. In other words, the gas in the area between these two wells is sucked equally and strongly by the wells on both sides. As a result, the gas extraction becomes smaller.

On the other hand, the extraction becomes also worse when the two wells are moved away from each other. However, the reason for this tendency probably does not come from the interactions of the wells, but from the effects of the side boundaries (i.e the flow field cannot develop well enough (at least at this stage in time) due to the limitaions of the boundaries). Thus, the optimal locations of the wells is between these two extreme cases. For example, the coordinates of the well locations in the best cases are $x = 96.042$ m and $x = 389.056$ m and $x = 93.695$ m and $x = 380.016$ m respectively. Thus, the distance between the x-coordinates is 293.014 m and 286.321 m respectively. Since these two coordinates are close, we can infer that the coordinates yielding maximal gas extraction are located around these positions at least for this system set-up. However, if the system is infinitely long laterally, many combinations of coordinates producing global maxima exist since it is inferred that the key is not the coordinates themselves but the distance between the coordinates.

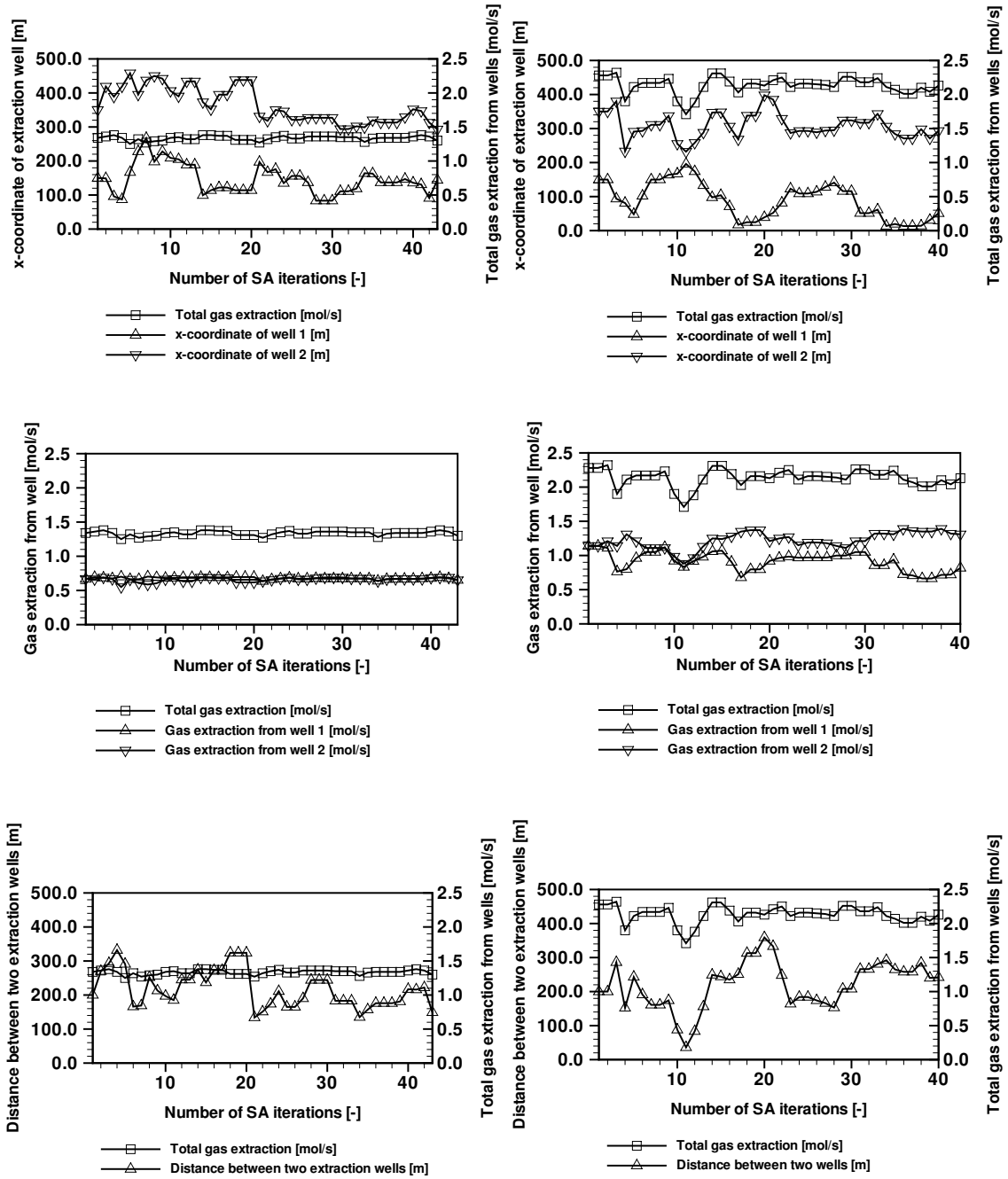

Figure 5.22: x-coordinates of two wells and the total amount of gas extracted from them after 7.7 *sec* (top left) and after 38.0 *sec* (top right) simulation time against the number of SA iterations. Amount of gas extracted from each well and its total after 7.7 *sec* (middle left) and 38.0 *sec* (middle right) simulation time against the number of SA iterations. Distance between the coordinates of two wells and the total amount of gas extracted from those wells after 7.7 *sec* (bottom left) and 38.0 *sec* (bottom right) simulation time against the number of SA iterations.

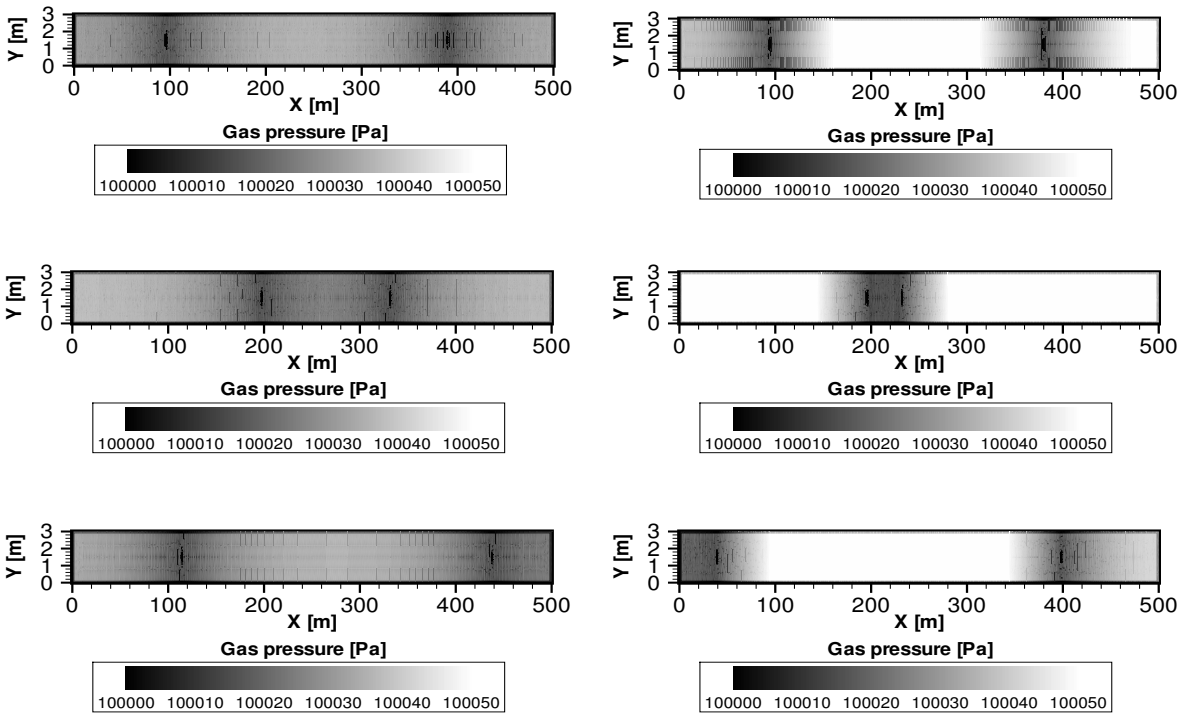

Figure 5.23: Pressure field of the best case after 7.7 *sec* simulation time when two extraction wells are located at $x_1 = 96.042\ m$, $x_2 = 389.056\ m$, $\Delta x = 293.014\ m$ (top left); at $x_1 = 93.695\ m$, $x_2 = 380.016\ m$, $\Delta x = 286.321\ m$ (top right); at $x_1 = 197.418\ m$, $x_2 = 331.424\ m$, $\Delta x = 34.006\ m$ (center left); at $x_1 = 195.901\ m$, $x_2 = 231.913\ m$, $\Delta x = 36.012\ m$. (center right); at $x_1 = 114.123\ m$, $x_2 = 437.907\ m$, $\Delta x = 323.784\ m$ (bottom left); at $x_1 = 38.991\ m$, $x_2 = 398.274$, $\Delta x = 359.283\ m$ (bottom right), where $\Delta x = x_2 - x_1$.

5.3.4.4 Three Wells in a Straight Road

As in the previous preliminary test case, three wells are installed in the straight road initially at $x = 150\ m$, $x = 250\ m$ and $x = 350\ m$. Then, exactly the same procedure is carried out. The results are shown in Figure 5.24. Top left and right of Figure 5.24 show the amount of gas extracted from each well and its total after around 50 % and 90 % extraction. From these figures, it is clear that, although SA has not attained the global maximum yet, the total gas extraction is slightly improved compared with the initial configuration.

For the detailed study of better system configurations, the locations of three wells against the number of SA iterations are plotted in the middle left for around 50 % extraction and in the middle right for around 90 % extraction. Additionally, the differences between the two intervals between the three wells, i.e. $(x_{max} - x_{mid}) - (x_{mid} - x_{min})$ where x_1, x_2 and x_3 could be either x_{max}, x_{mid} or x_{min} according to the locations is plotted in the bottom left and right. As shown in these figures, the extraction is not always best when the two intervals are equidistant (i.e. $(x_{max} - x_{mid}) - (x_{mid} - x_{min}) = 0$). Rather, the maximal value is observed when the well in the middle is located slightly towards one of the side wells. The reason is probably that the best distance between the middle well and one of the side wells yields a better extraction than two equidistant wells. Although the extraction may be slightly smaller for the combination of the third well and the middle well than for the equidistant case, as a sum, this configuration (the best positions between two wells plus slightly bad position for the third well) can yield a better value than the equidistant cases. This might be different when the system is laterally long enough so that the three wells can have great enough intervals between them and the flow fields can develop fast and freely.

Top left and right of Figure 5.25 show the pressure field for the best locations, while the bottom left and right show some of the bad locations. As mentioned, the middle well is located slightly towards one of the side wells; then the total extraction is best, as shown in the top left and right of the figure. On the other hand, the bad cases are always when the flow field developed by (two or three) wells interact too much because the wells are too close one another.

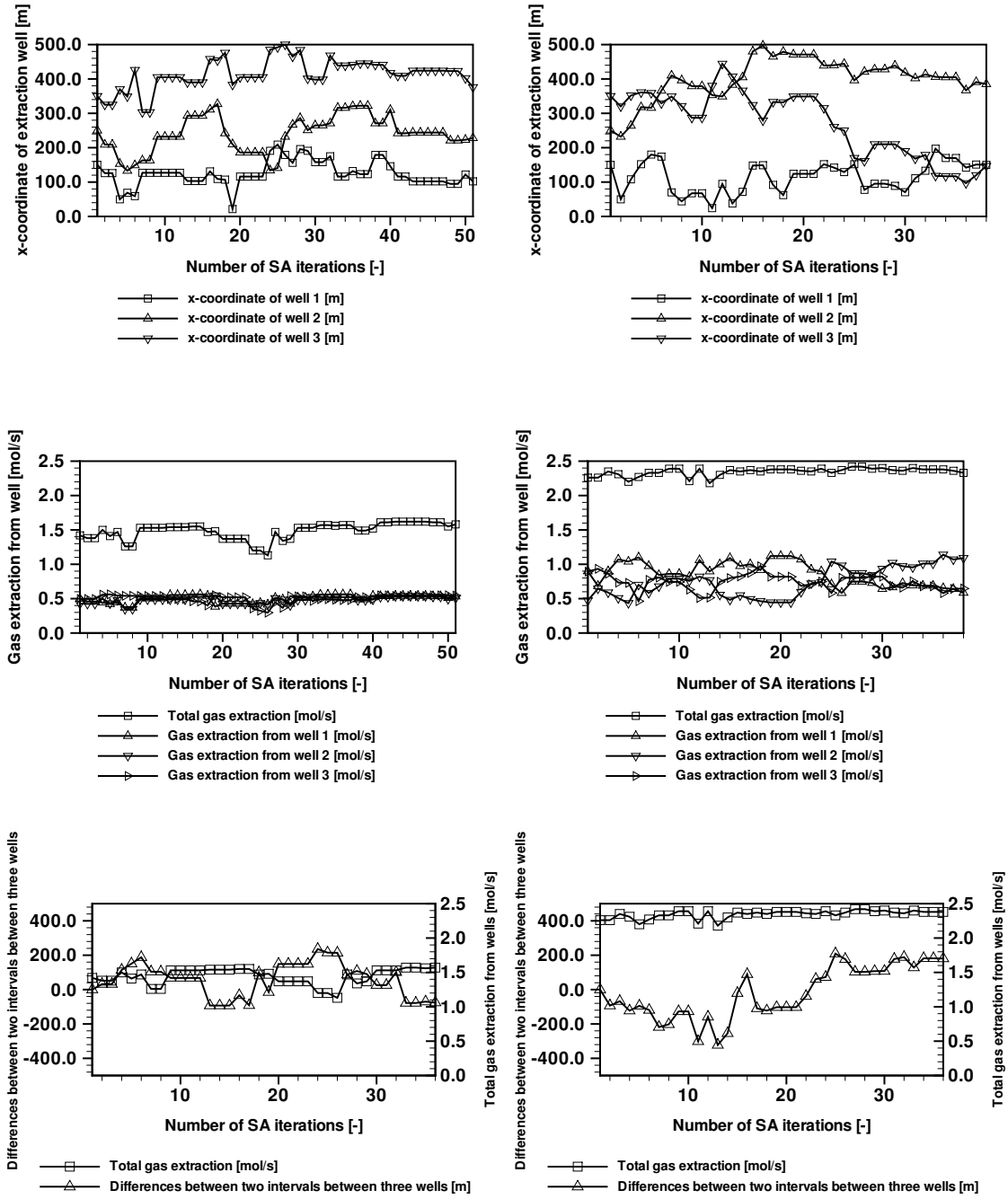

Figure 5.24: x-coordinates of three wells against the number of SA iterations after 5.1 *sec* (top left) and 38.0 *sec* (top left) simulation time. Amount of gas extracted from each well and its total after 5.1 *sec* (middle left) and 38.0 *sec* (middle right) simulation time against the number of SA iterations. Differences between two intervals between three wells against the number of SA iterations after 5.1 *sec* (bottom left) and 38.0 *sec* (bottom right) simulation time.

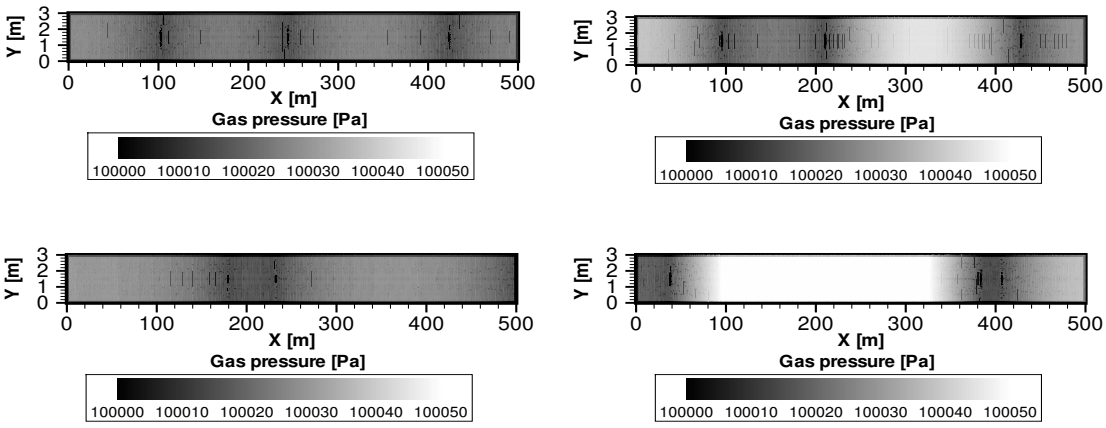

Figure 5.25: Pressure field of the best case after 5.1 *sec* simulation time when three extraction wells are located at $x_1 = 102.382\ m$, $x_2 = 243.913\ m$, $x_3 = 423.605\ m$, $|\Delta x_1 - \Delta x_2| = 38.161\ m$ (top left); at $x_1 = 95.243\ m$, $x_2 = 428.09\ m$, $x_3 = 210.08\ m$, $|\Delta x_1 - \Delta x_2| = 84.343\ m$ (top right); at $x_1 = 178.997\ m$, $x_2 = 232.23\ m$, $x_3 = 499.777\ m$, $|\Delta x_1 - \Delta x_2| = 214.314\ m$ (bottom left); at $x_1 = 37.864\ m$, $x_2 = 383.48\ m$, $x_3 = 406.73\ m$, $|\Delta x_1 - \Delta x_2| = 322.366\ m$ (bottom right). Here $\Delta x_1 = x_{max} - x_{mid}$, $\Delta x_2 = x_{mid} - x_{min}$.

5.3.4.5 Short Summary of the Preliminary Tests

The following intermediate summary is derived from these preliminary test cases:

- In general, after a certain time, the gas extraction tends to be large when the well is installed at the place where several roads meet (i.e. at the crossing point). On the other hand, the gas extraction tends to be small when the well is installed near the roadway boundaries, or when the wells are too close to one another.
- If we have several extraction wells and the distances between the surrounding boundaries and one of the extraction wells are not so very different, the times when the methane from the surrounding boundaries reaches the extraction well are not so different either. This fact implies that the location of maximum gas extraction realizes also that of maximum methane extraction as well under these conditions. This implication is very important in that it may be true for the following mine-site application.

In the following, the validity of these conclusions is finally studied using the mine example.

5.3.5 Coal-Mine-Case

5.3.5.1 One Well in the Mine Site

As has already been mentioned, the whole domain is divided into 23 segments for the parallerization design. Thus, the following explanations are carried out by focusing on each segment. The simulations are terminated after the wells expected to be best have extracted around 50 % of the gas influx. Firstly, the pressure fields of the gas phase after 40 *sec* simulation time when the well is installed where maximal extraction is obtained within each segment are shown in Figures 5.26 to 5.28. The extraction well is installed around the center of the blue region, which indicates the range of the atomospheric pressure. As shown in these figures, the optimal locations are always at the crossing of two or three roads. Such crossings are to be found in Segments $3, 5, 6, 8, 9, 12, 13, 14, 15, 17, 18, 19, 20, 22, 23$, although the case in Segment 7 (probably Segment 12 as well) seems to be trapped by a local maximum.

The combined results of the 23 sub-simulation-optimizations are shown in Figures 5.29 and 5.30. Figure 5.29 shows the gas extraction after 40 *sec* simulation time against a set of 23 SA iterations ordered from Segment 1 to Segment 23. Figure 5.30 shows the percentages of the best extraction from each segment and averaged extraction over each segment to the total inflow 2.506 mol/s. As can be seen in Figure 5.30, the wells in the best locations (e.g. Segments 14, 23) can already extract around 50 % of the gas influx at this stage, while the worst cases only do around 12.5 % (e.g. Segments 1, 21). When we look at the percentages for the averaged values, the segments which have a connection with the central Segment 23 always tend to yield better results (e.g. Segments $3, 8, 9, 13, 14, 15, 17, 18, 19, 22$). The value for Segment 12 is smaller although this segment has a connection with Segment 23. This must be, as already mentioned, because the well is trapped by the local maximum at the opposite side boundary of the segment. The two best locations for this single-well case are shown in Figure 5.31 and 5.32.

The following summary can be derived from these results:

- the optimal locations of the extraction wells are generally at the crossing point of the roads and
- the averaged extraction becomes relatively high when the segment has a connection with the central Segment 23.

On the basis of these results, we move on to the two-well case.

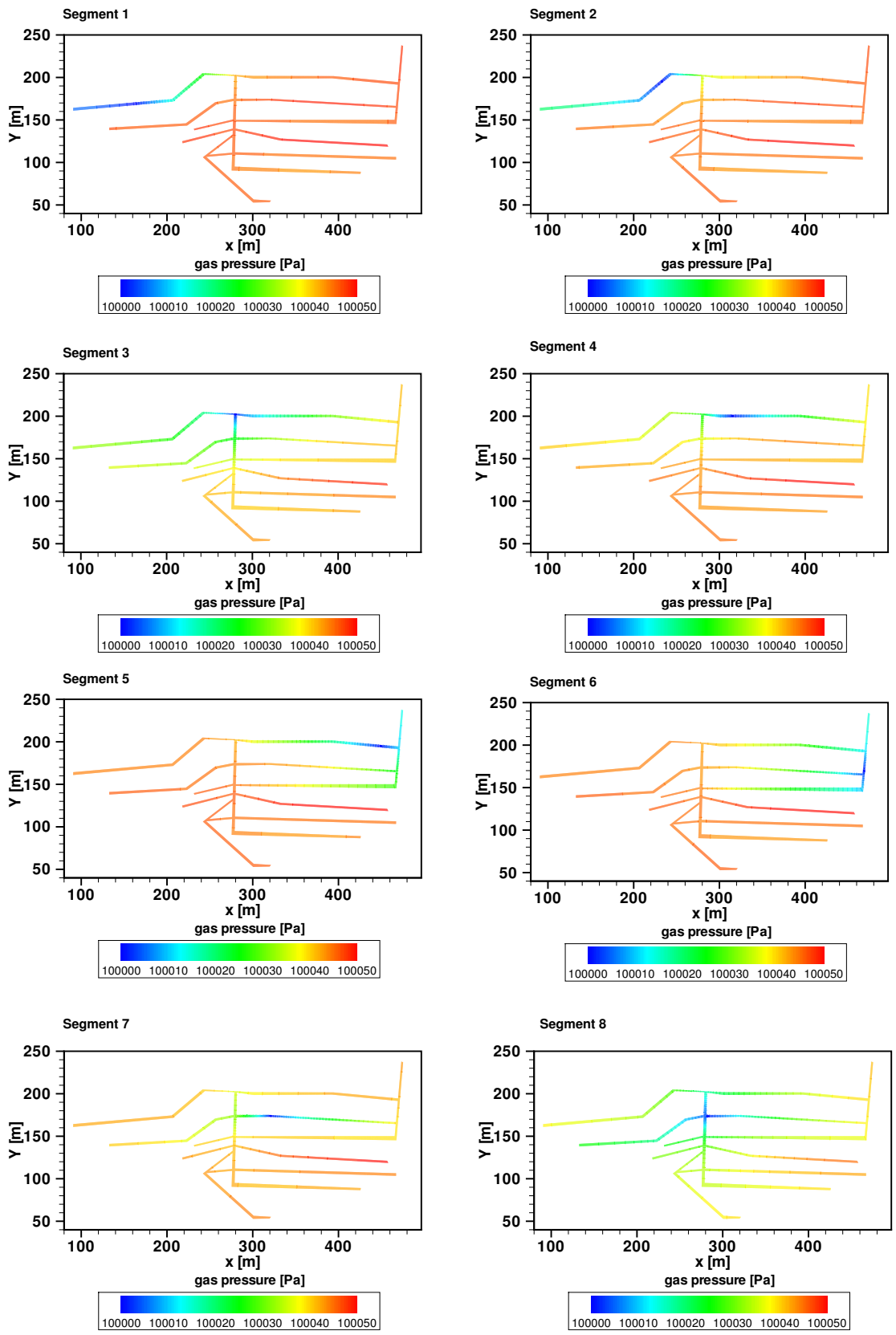

Figure 5.26: Pressure fields of the gas phase after 40 *sec* simulation time, simultaneously indicating the optimized locations of the extraction wells (blue region) in Segments 1 to 8.

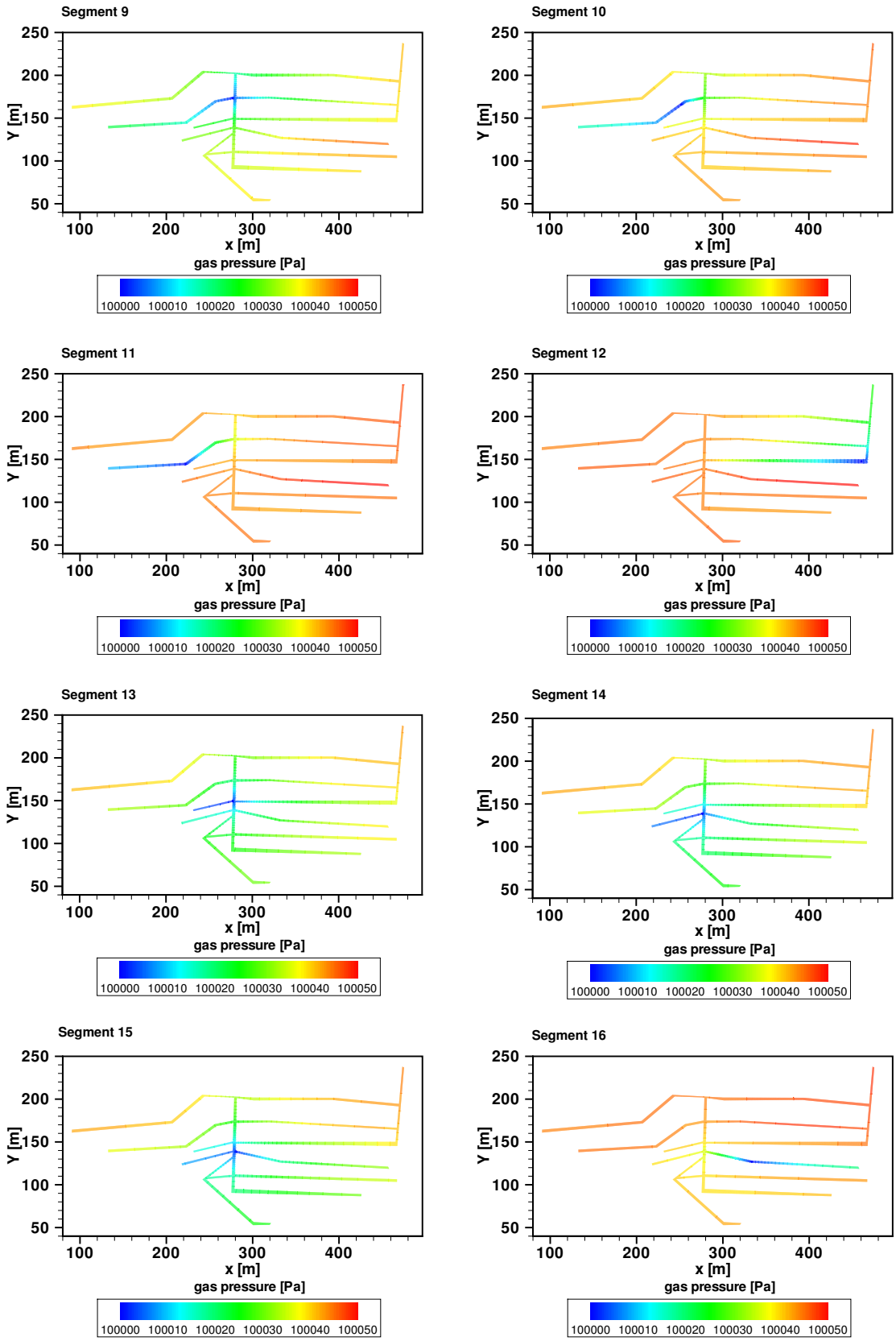

Figure 5.27: Pressure fields of the gas phase after 40 *sec* simulation time, simultaneously indicating the optimized locations of the extraction wells (blue region) in Segments 9 to 16.

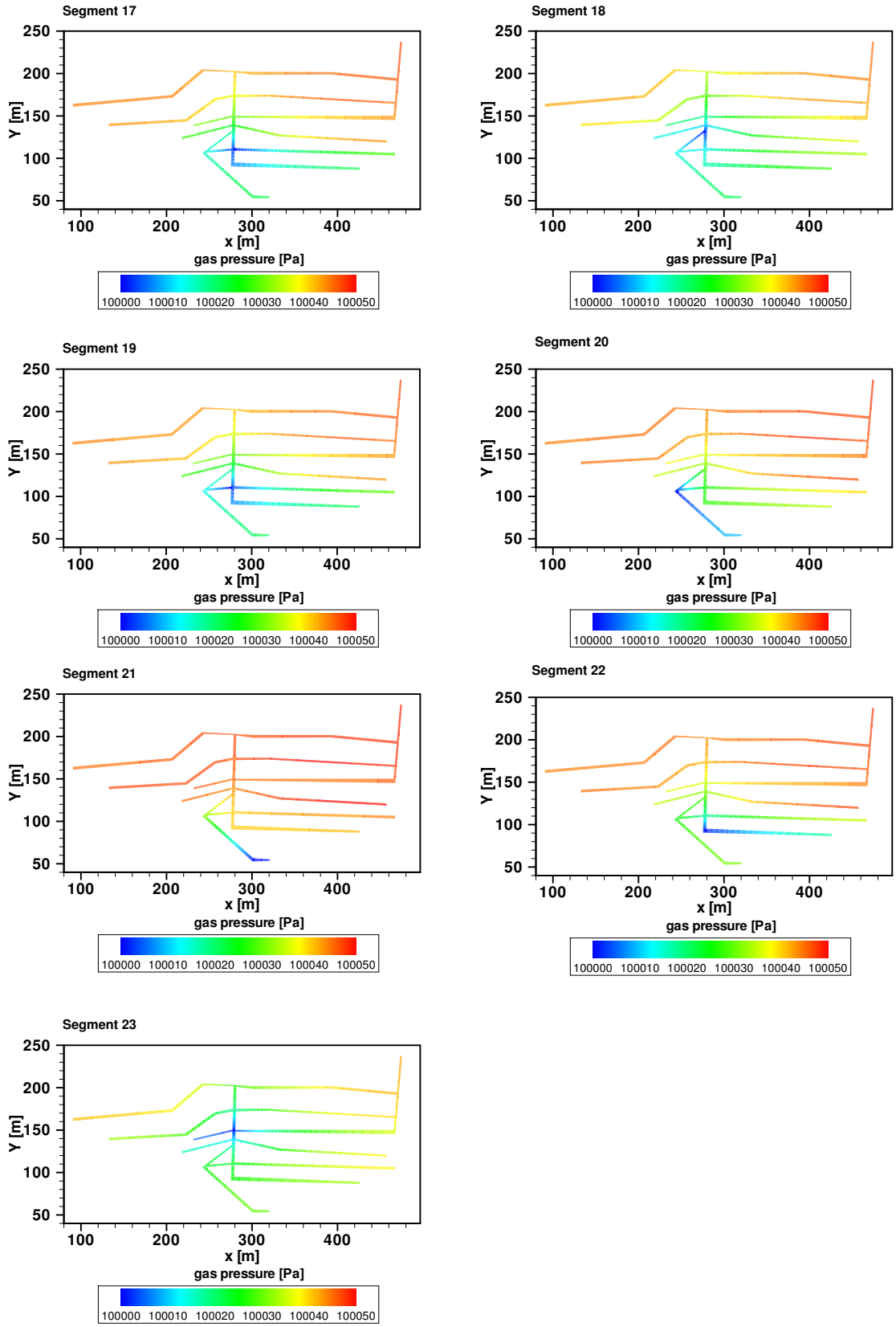

Figure 5.28: Pressure fields of the gas phase after 40 *sec* simulation time, simultaneously indicating the optimized locations of the extraction wells (blue region) in Segments 17 to 23.

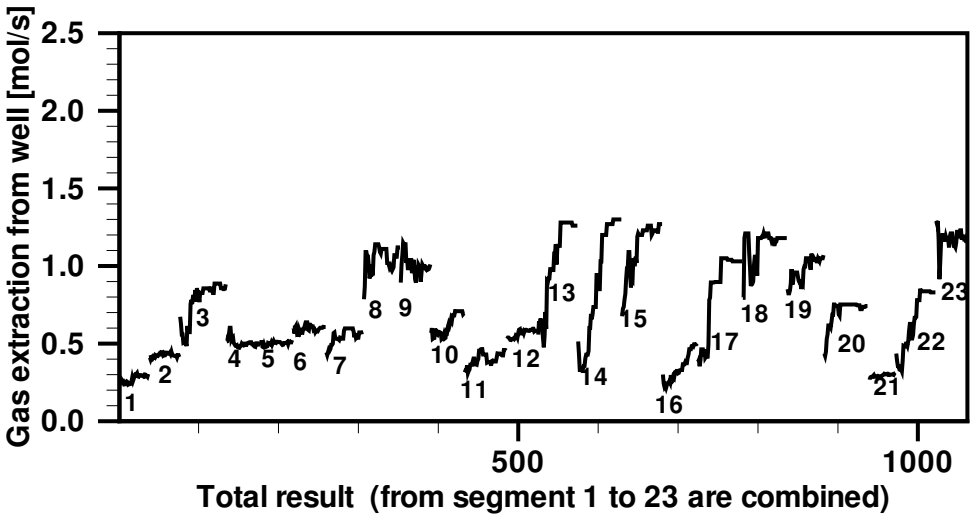

Figure 5.29: Gas extractions after 40 *sec* simulation time against the set of 23 sub-SA iterations from Segments 1 to 23.

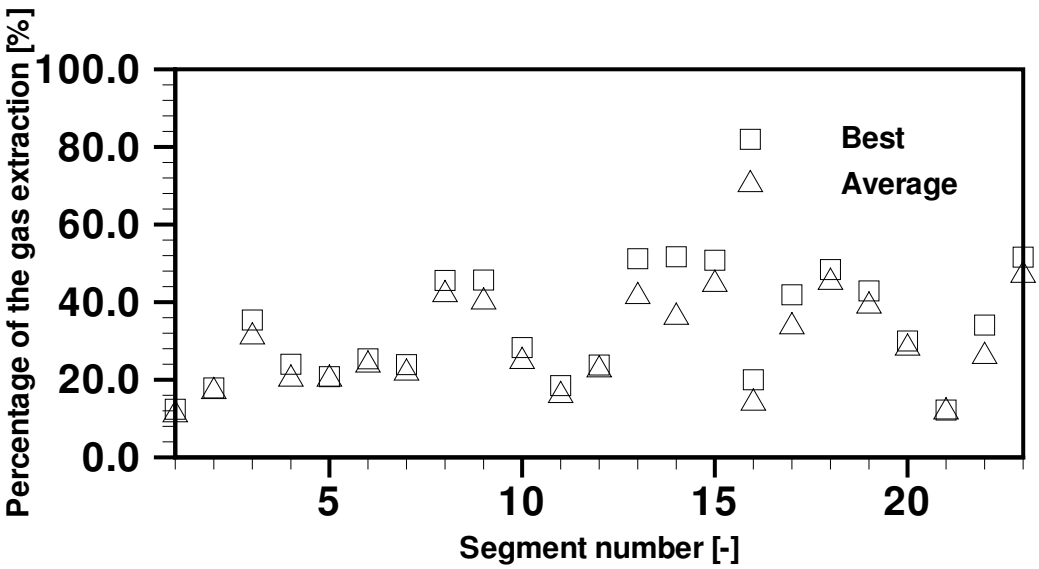

Figure 5.30: Percentages of the best and averaged gas extractions to the total inflow 2.506 mol/s for the single-well case.

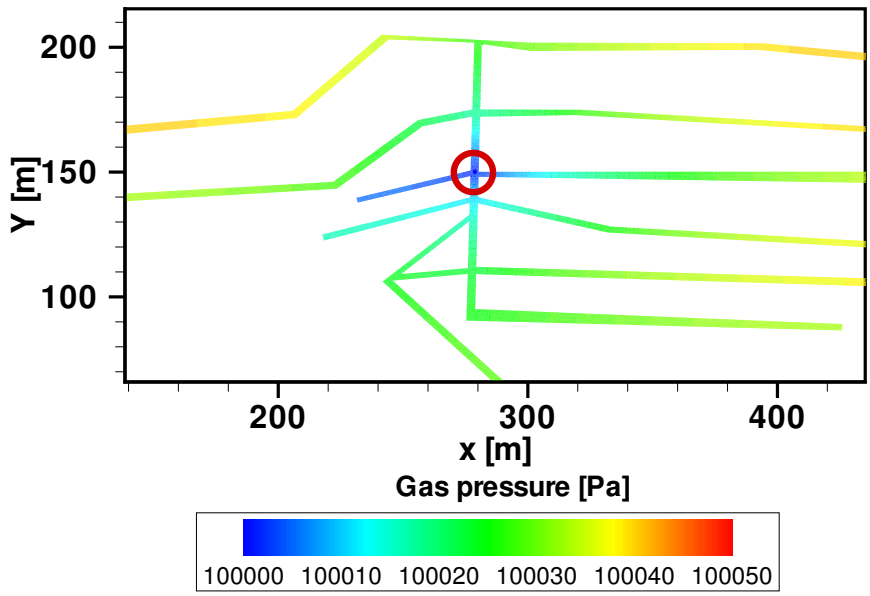

Figure 5.31: One of the two best locations for the single-well case. The well is installed in Segment 23.

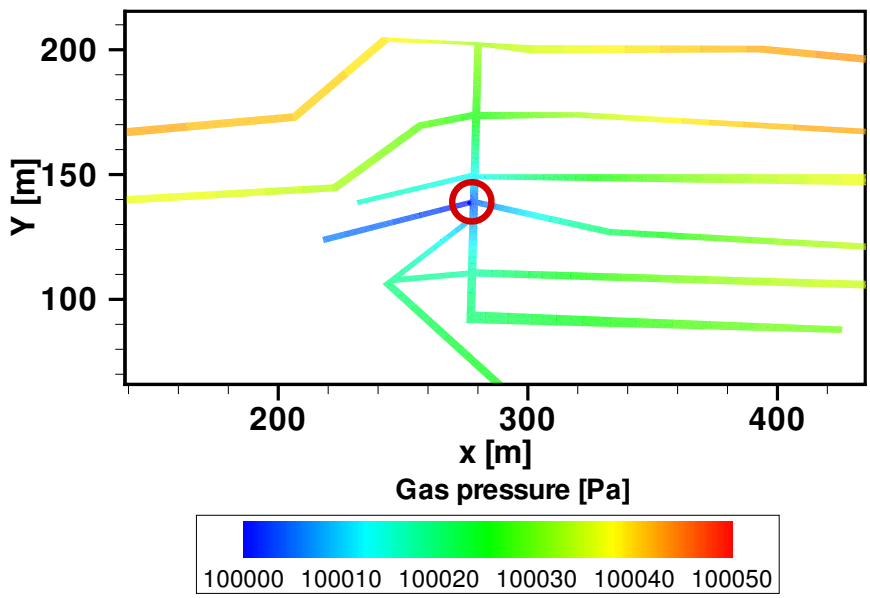

Figure 5.32: One of the two best locations for the single-well case. The well is installed in Segment 14.

5.3.5.2 Two Wells in the Mine Site

The number of extraction wells is increased to two from one as usual. Since the previous case has clearly shown that the averaged and best gas extraction is always largest when the well is located in the central Segment 23, I decided to limit the location of one of the wells to within Segment 23. Those two wells are called well 1 and well 2, well 1 is installed somewhere in Segment i ($i = 1$ to 23), while well 2 is always in Segment 23. This is a necessary and probably reasonable constraint since otherwise, simulating all possible combinations would mean $22 \times 23/2 = 253$ combinations and the total computational time, even using all 56 nodes of the parallel computer, would be $253 \times 292\,days/56\,nodes \approx 1319\,days$, i.e. not feasible. If we introduce the constraint, the total time should be almost as same as the case with one well. In the following, each simulation is again terminated after the combination of two wells expected to be the best have extracted totally around 50 % of the gas influx from surrounding boundaries.

The pressure fields after 33 *sec* simulation time for the case where the two wells in Segment i ($i = 1$ to 23) and 23 obtained the best extraction are shown in Figures 5.33 to 5.35. Figure 5.36 shows the combined results of the 23 sub-simulation-optimizations, while Figure 5.37 presents the percentages of the best and averaged gas extractions for each combination $i-23$ ($i = 0$ to 23) to the total inflow 2.506 mol/s. Suprisingly, Figure 5.37 shows that the best and averaged gas extractions in combination $6-23$ are as high as those in combination $23-23$.

In order to clarify why this happens, the amount of gas extraction from well 1 in Segment i ($i = 0$ to 23), well 2 in Segment 23 and its total are shown in Figures 5.38 to 5.40. In most cases, the extraction from well 2 in Segment 23 is larger than that from well 1 in Segment i. Some exceptions, i.e. the extraction from well 1 becomes larger than that from well 2, are observed when well 1 is located as in Segments $8, 14, 15, 18$. The pressure fields for two cases among the exceptions are shown in Figures 5.41 and 5.42. As is apparent from these figures, these phenomena occur when well 1 is installed near the crossing with Segment 23, while well 2 is inside the narrow roadway in Segment 23. This is easily understandable from the previous test cases and the single-well case.

Now let us focus on combinations $6-23$ and $23-23$. The two best locations for this two-well case are shown in Figures 5.43 and 5.44. Figure 5.45 plots the gas extractions for both combinations $6-23$ and $23-23$ against the number of SA iterations. Apparently, the gas extraction from one of the wells in the combination $23-23$ is on average lower than that from well 2 in combination $6-23$. This tells us that the interaction between these two wells in combination $23-23$ restrains the extraction from each well, while the interaction between wells in combination $6-23$ seems to be quite low because the distance between the wells is the greatest of all $i-23$ combinations. In other words, well 1 in Segment 6 can extract the surrounding gas independently of well 2.

We can infer that the well in the segment which has no direct connection with the central Segment 23, such as Segments $1, 2, 4, 5, 6, 7, 10, 11, 16, 20, 21$, should have a similar extraction tendency. Thus, first of all, the percentages of the averaged extraction for these segments from the previous single-well case are replotted as in Figure 5.46. This figure shows that the best value is obtained in Segment 20, then Segment 10 and Segment 6. However, when well 1 is installed in Segments 20 or 10, the total extraction is less than in Segment 6, as shown in Figure 5.45. Thus, the well in either Segment 20 or 10 is probably subject to less influence from well 2 in Segment 23 than the well in the segments with a direct connection with the central Segment 23. However, the distance from well 2 in Segment 23 is not far enough compared with the case when well 1 is installed

in Segment 6, so the extraction is still restrained due to the mutual influence. As can be seen, Segment 6 is located furthest from Segment 23. Thus, the combination $6-23$ yields one of the best averaged extractions. On the other hand, segments such as $1, 11, 16$ and 21 may be as far from Segment 23 as 6 is but, as the previous single-well case shows, the well in these segments can extract only less gas after a certain time than the well in Segment 6; thus the total extractions are lower.

The following summary can be made on the basis of these results:

- the total (best and averaged) gas extraction is large when two wells are installed either in Segments 6 and 23 or in 23 and 23. The combination $6-23$ yields (surprisingly) a very good extraction. This is most probably because the distance between these wells is great enough, decreasing the interaction and resulting in a higher extraction from each well, while the second combination $23-23$ yields a better extraction, as can be imagined, probably because both wells are installed in the central main roadway where the surrounding gas can be accumulated most easily and quickly. Moreover, the quasi-best total gas extraction is always observed when these two wells are again at the crossing of two roads.

We now proceed to the three-well case.

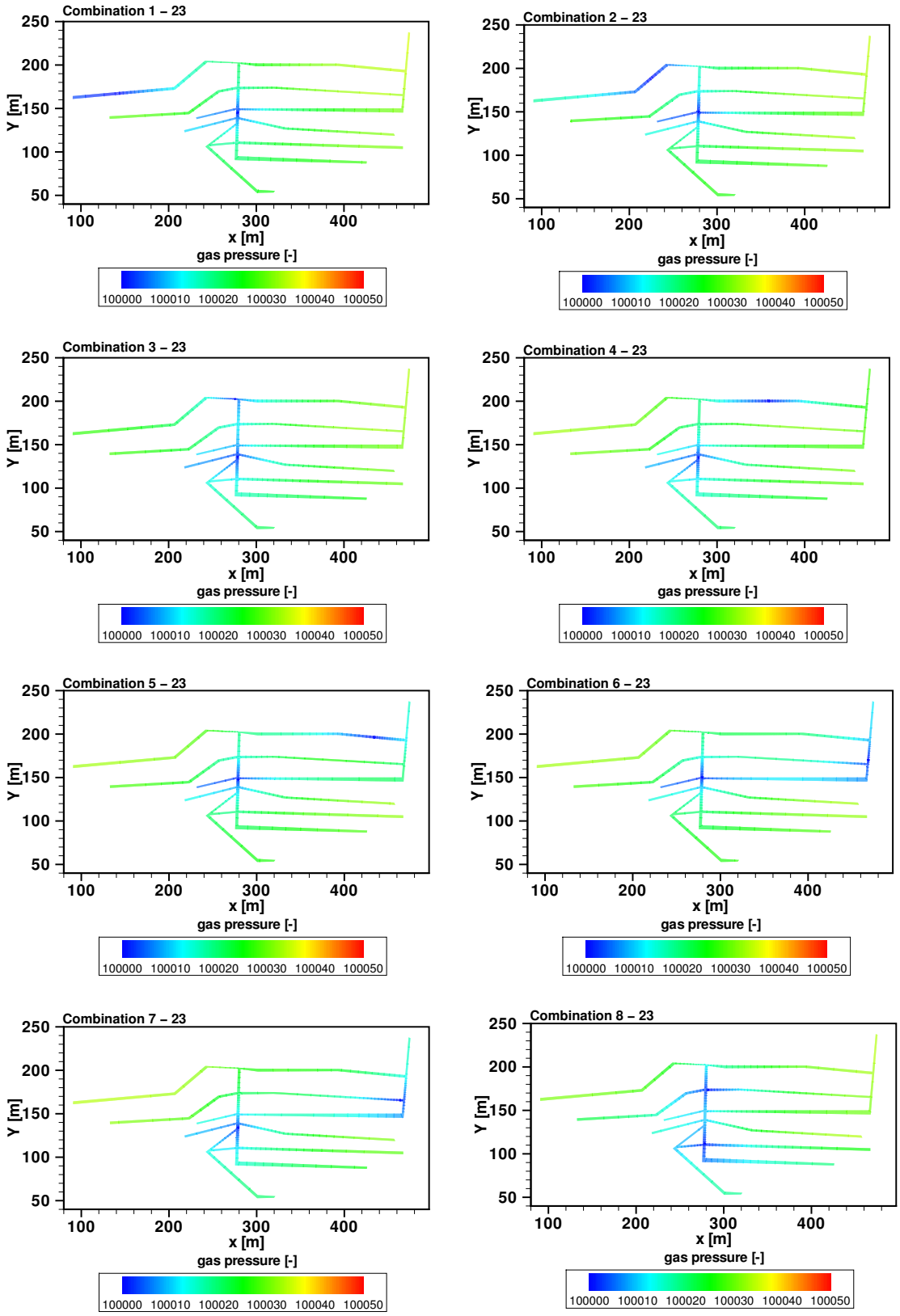

Figure 5.33: Pressure fields of the gas phase, simultaneously indicating the optimized locations of the extraction wells for combinations 1− to 8 − 23.

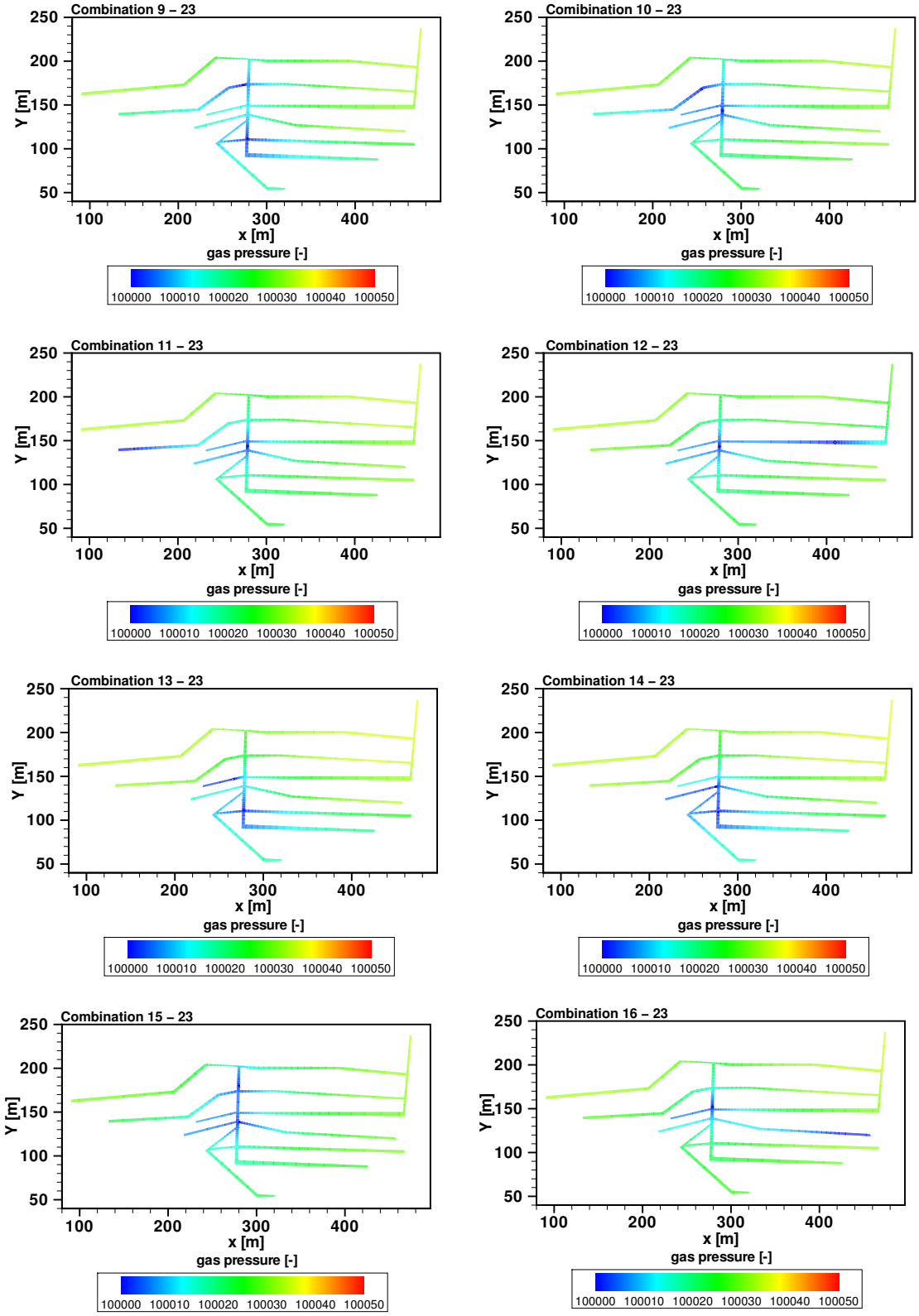

Figure 5.34: Pressure fields of the gas phase, simultaneously indicating the optimized locations of the extraction wells for combinations 9− to 16 − 23.

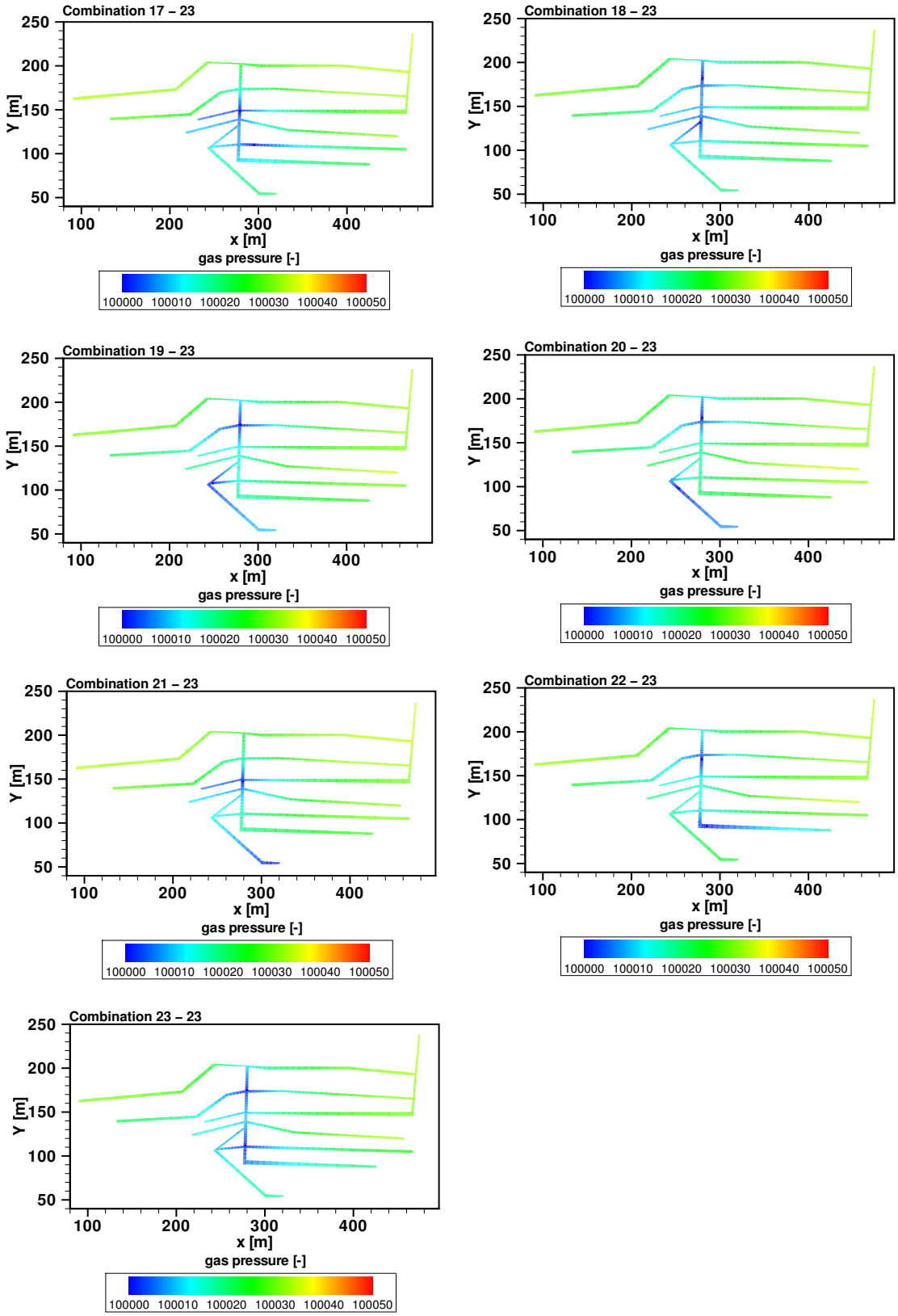

Figure 5.35: Pressure fields of the gas phase, simultaneously indicating the optimized locations of the extraction wells for combinations 17− to 23 − 23.

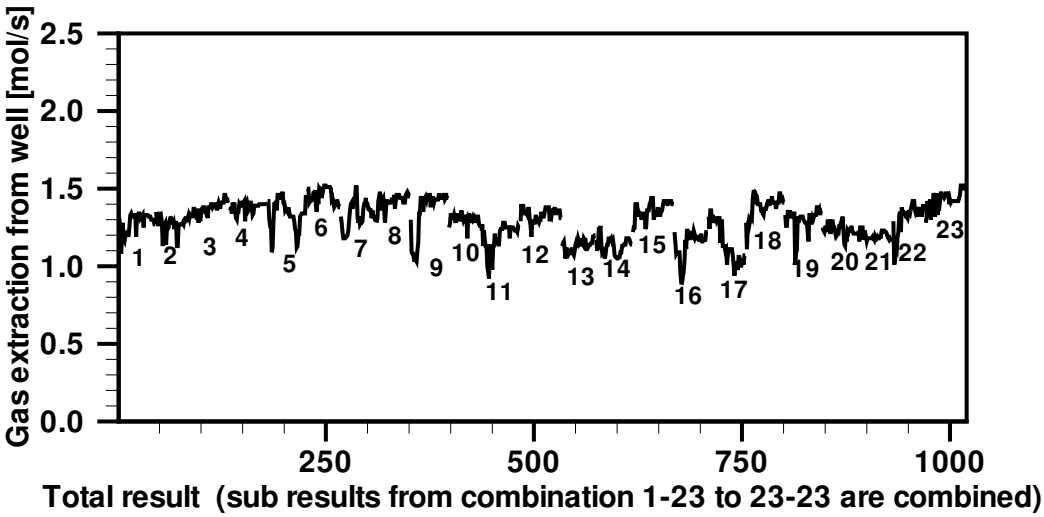

Figure 5.36: Gas extractions after 32 *sec* simulation time against the set of 23 sub SA iterations from combinations $1-23$ to $23-23$.

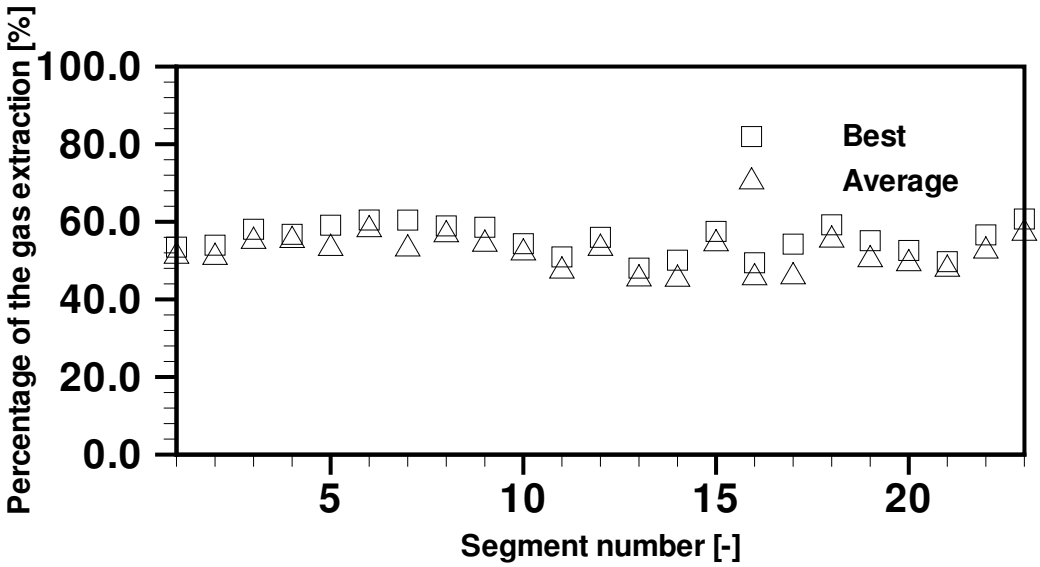

Figure 5.37: Percentages of the best and averged extracted gas to the total inflow 2.506 mol/s for combinations $1-23$ to $23-23$.

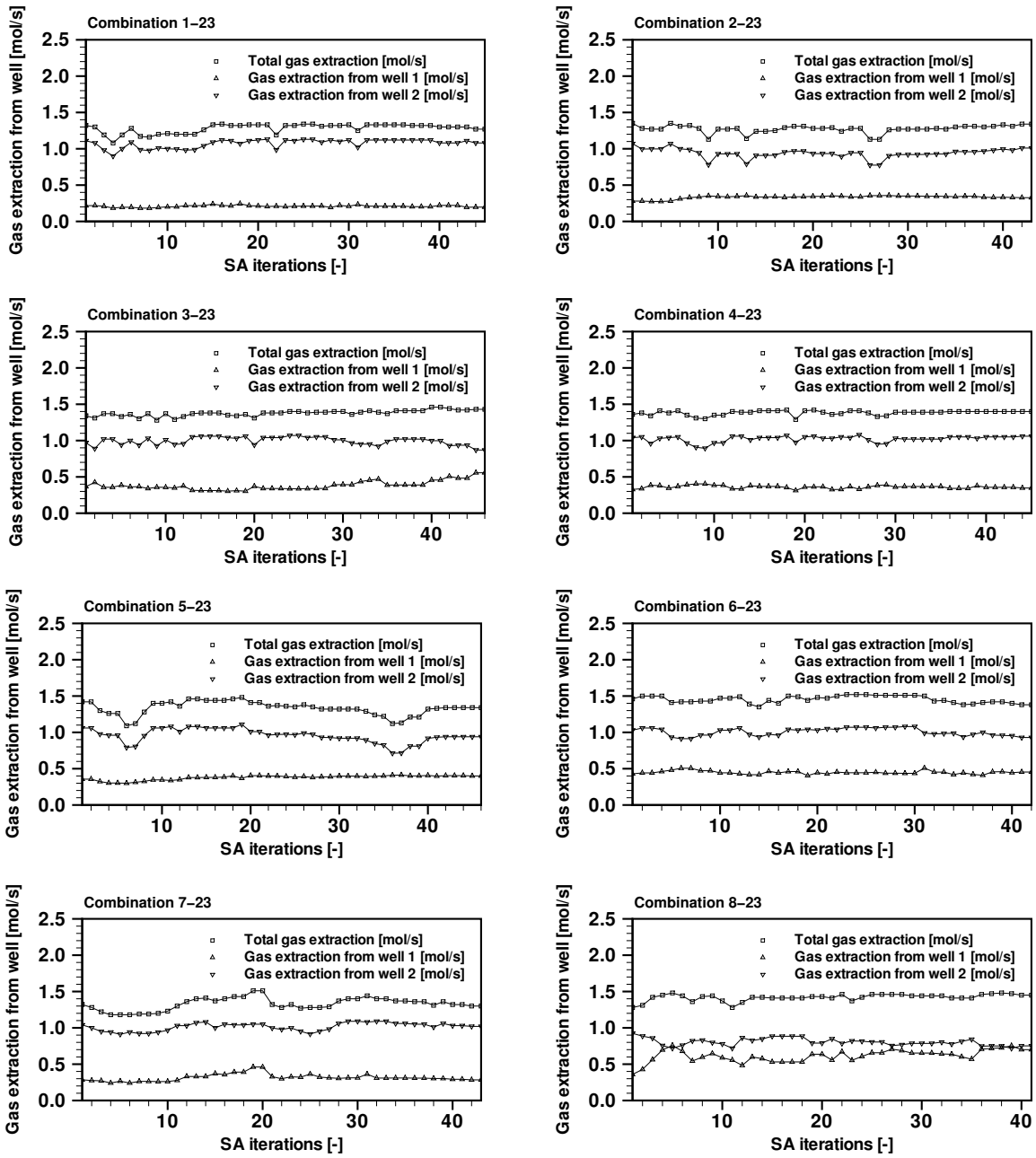

Figure 5.38: Gas extraction from well 1 in Segment i ($i = 0$ to 23), well 2 in Segment 23 and its total for combinations $1-23$ to $8-23$.

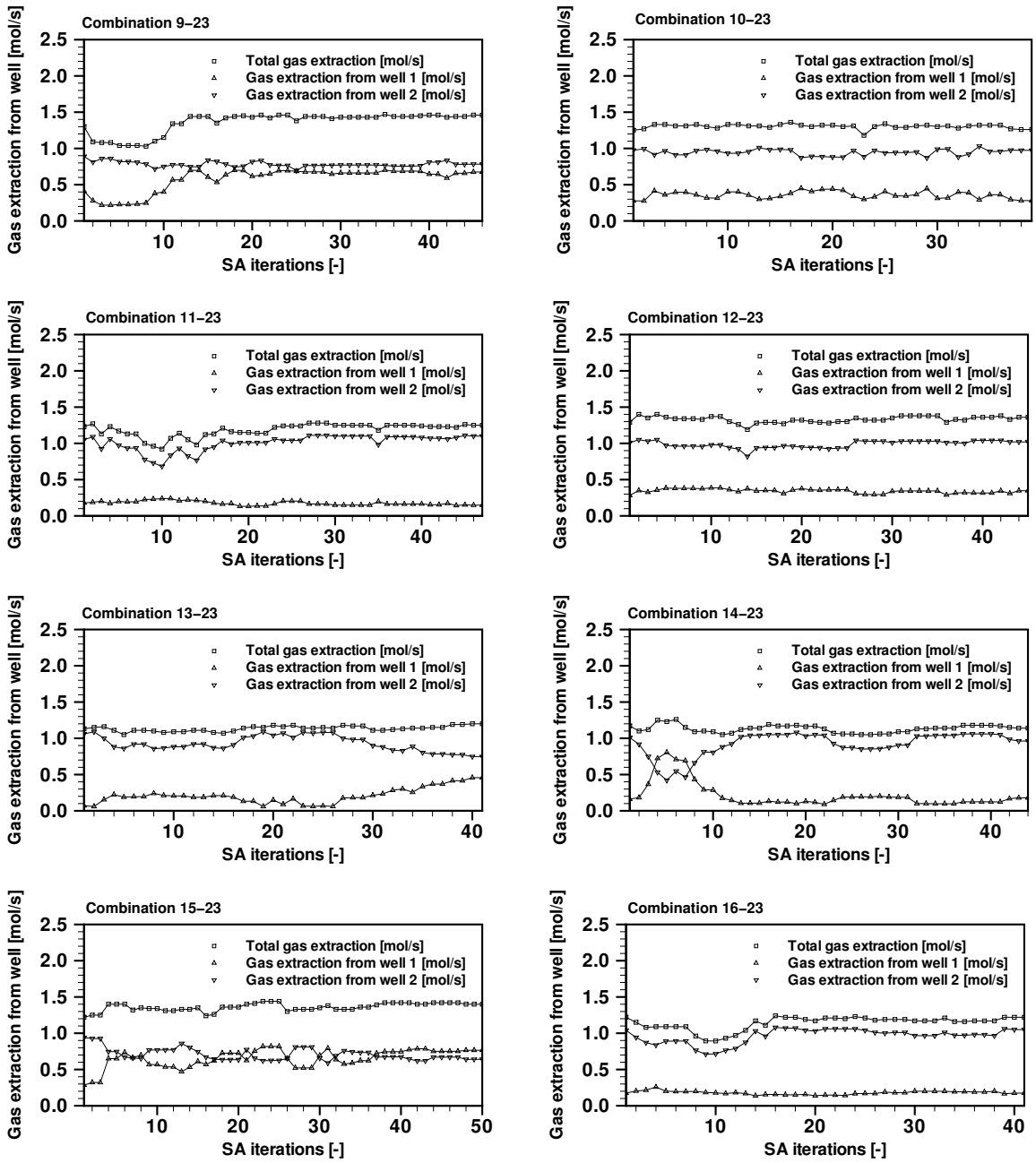

Figure 5.39: Gas extraction from well 1 in Segment i ($i = 0$ to 23), well 2 in Segment 23 and its total for combinations $9-23$ to $16-23$.

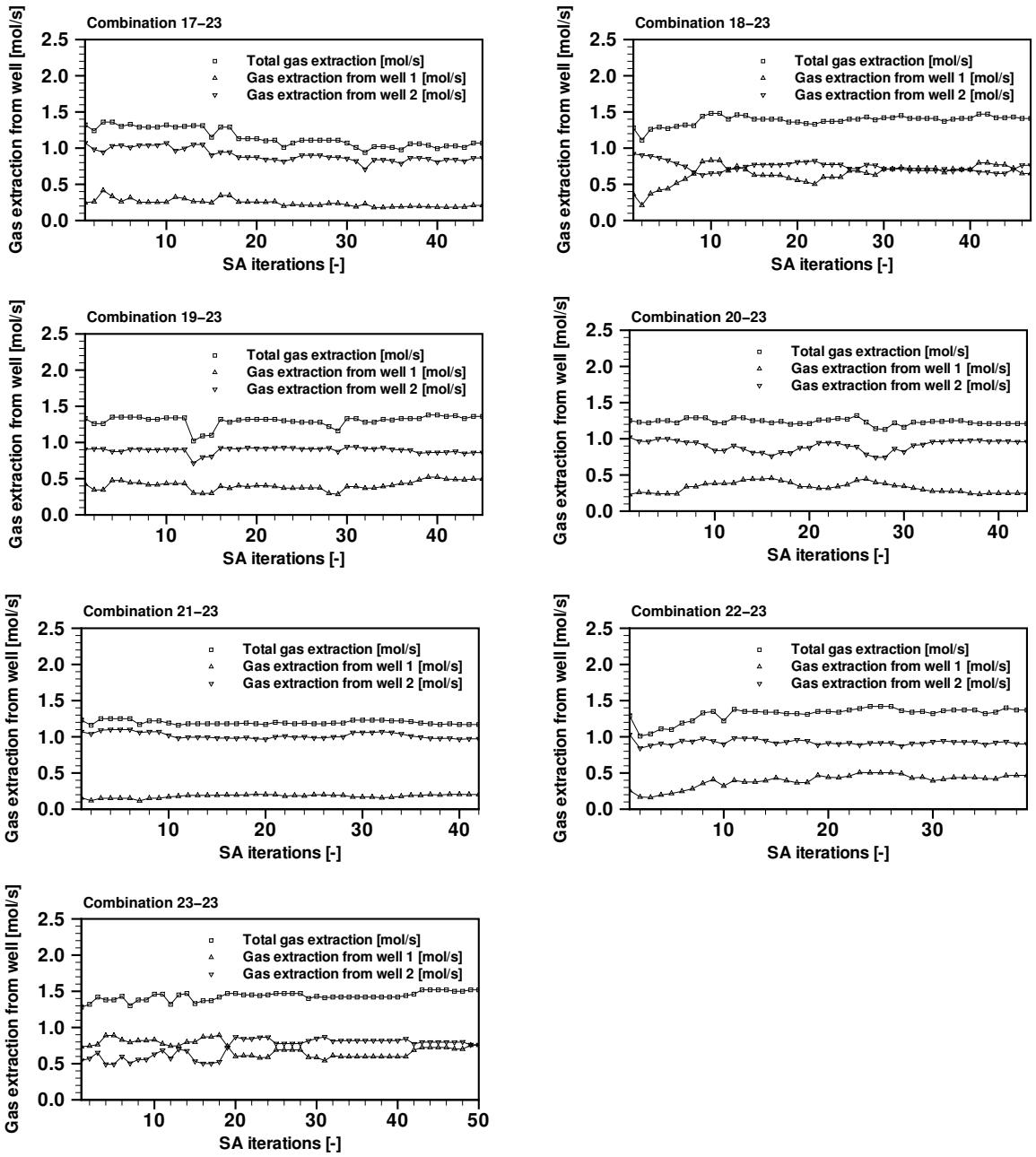

Figure 5.40: Gas extraction from well 1 in Segment i ($i = 0$ to 23), well 2 in Segment 23 and its total for combinations $17-23$ to $23-23$.

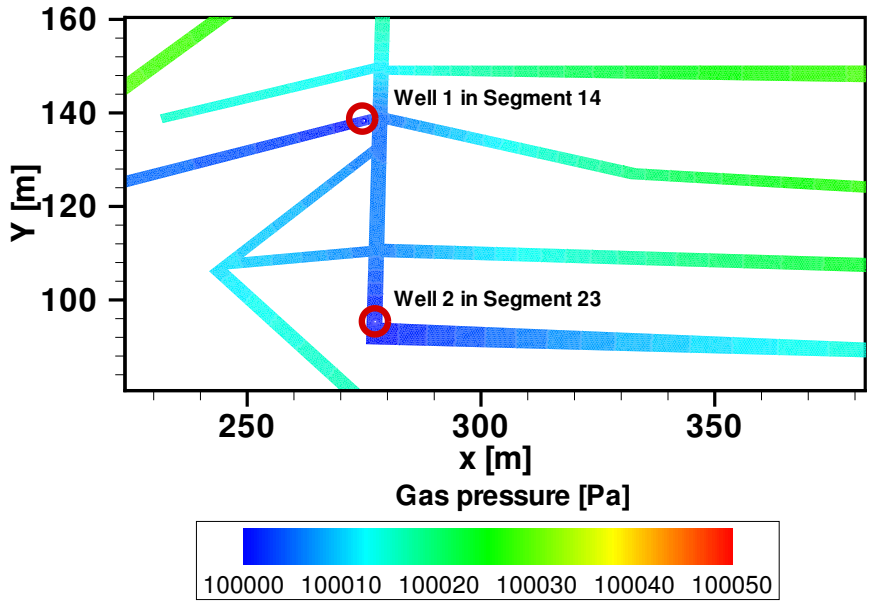

Figure 5.41: Pressure field of the gas phase when the extraction from well 1 is larger than that from well 2. In this case, well 1 is installed in Segment 14 and well 2 in Segment 23.

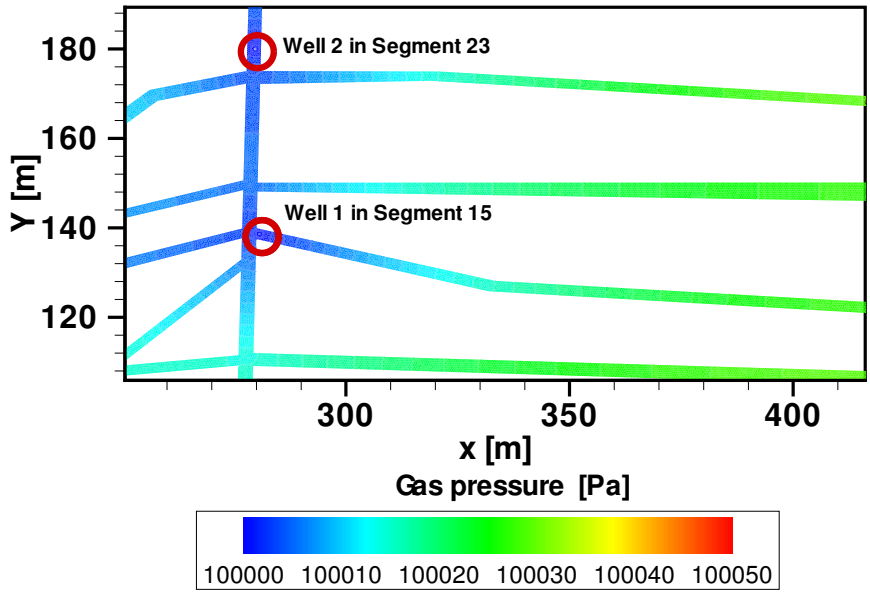

Figure 5.42: Pressure field of the gas phase when the extraction from well 1 is larger than that from well 2. In this case, well 1 is installed in Segment 15 and well 2 in Segment 23.

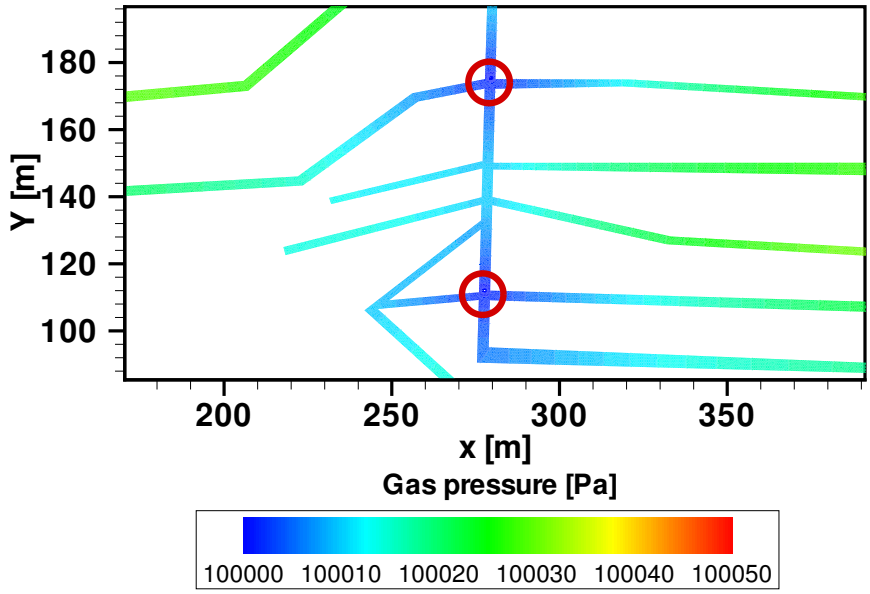

Figure 5.43: One of the two best locations for the two-well case. The well is installed in the combination 23 – 23.

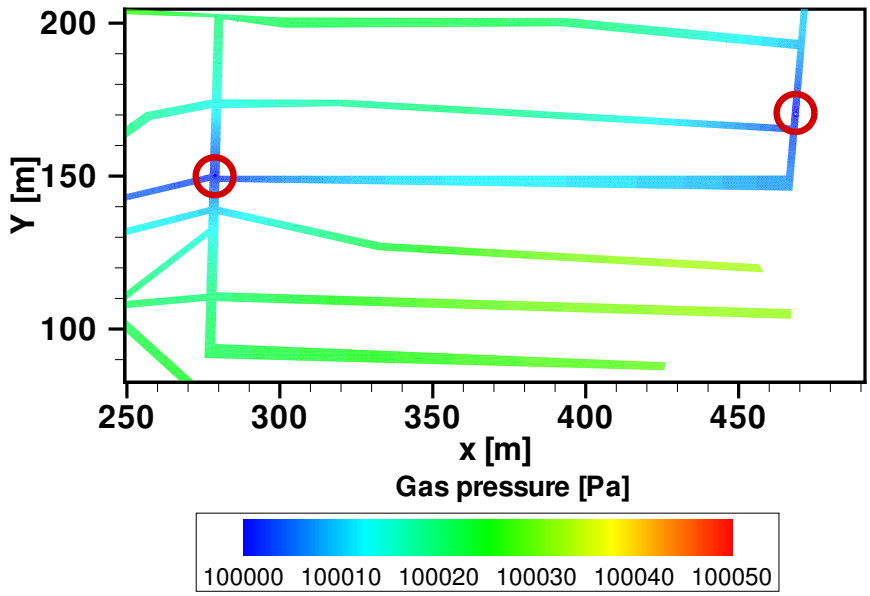

Figure 5.44: One of the two best locations for the two-well case. The well is installed in combination 6 – 23.

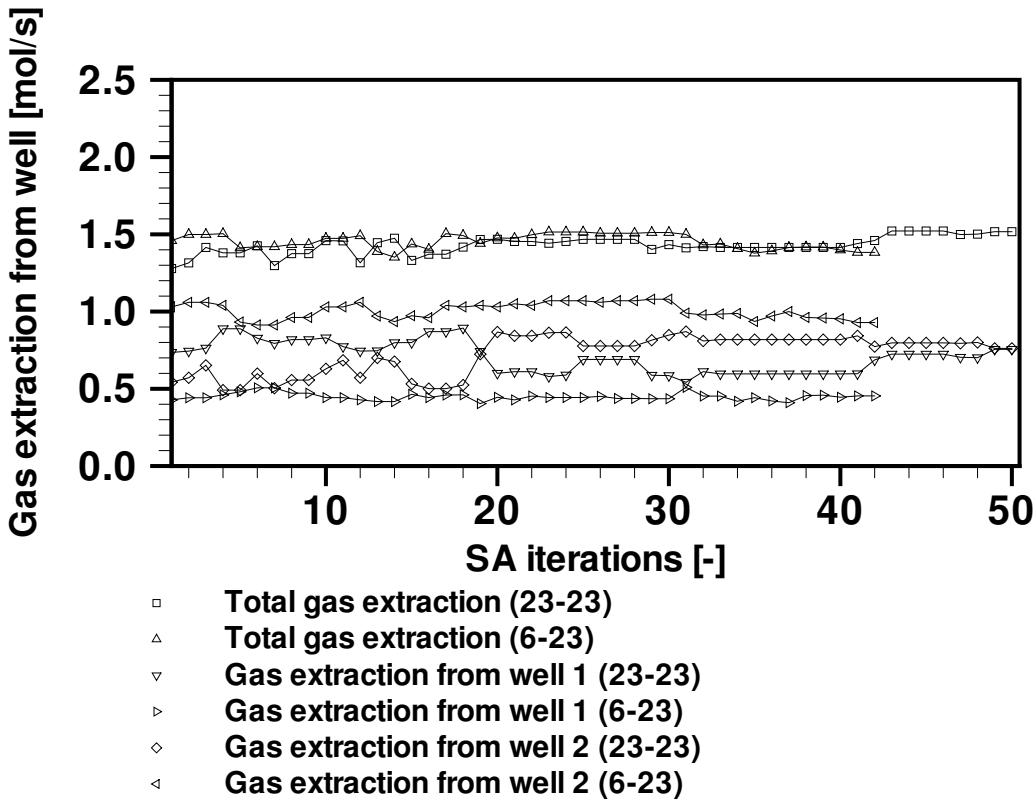

Figure 5.45: Gas extractions for combinations $6-23$ and $23-23$ against the number of SA iterations.

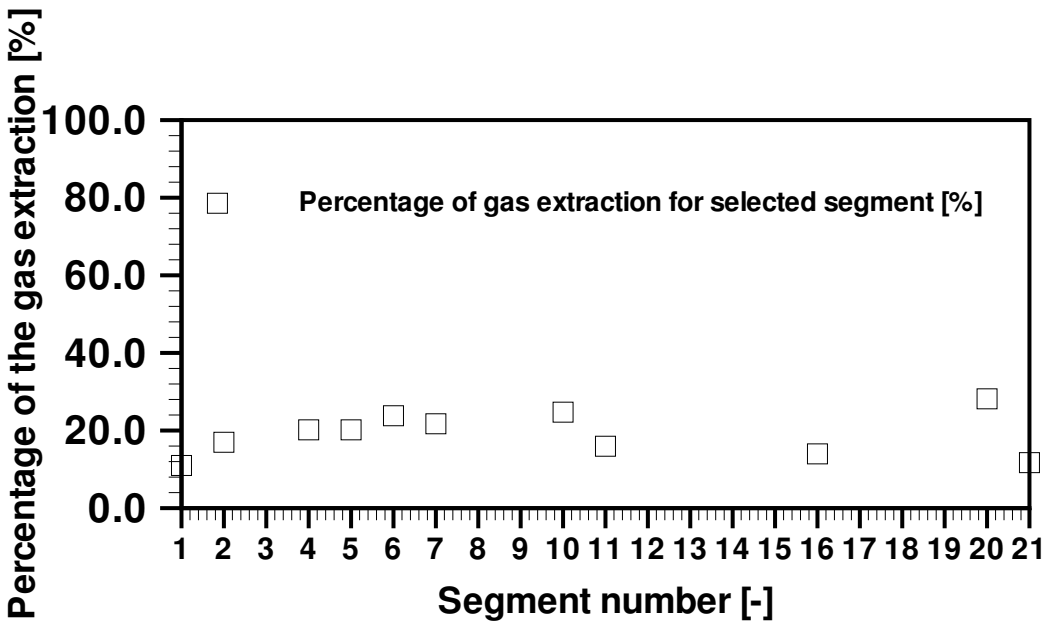

Figure 5.46: Percentages of the extracted amount to the total inflow 2.506 mol/s.

5.3.5.3 Three Wells in the Mine Site

As a final step in this thesis, the number of extraction wells is increased to three. Since the computational time is again expected to be enormous if we take all combinations of three-segments where the extraction wells are installed into consideration, two of the three wells are located only in the central Segment 23. The third well is installed in Segment i ($i = 0, ..23$). In the following, the well in Segment i is called well 1, while two wells in Segment 23 are called well 2 and well 3.

The pressure fields after 20.5 *sec* simulation time for the case where these three wells obtained the best extraction are shown in Figures 5.47 to 5.49. Figures 5.50 and 5.51 show the combined results of the 23 sub-simulation-optimizations and the percentages of the best and averaged gas extraction for each combination $i-23-23$ ($i = 0$ to 23) to the total inflow 2.506 mol/s respectively. This time, as can be imagined from the previous example, the best and averaged gas extractions are observed in combination $6-23-23$ (see e.g. Figure 5.52), while combination $23-23-23$ yields relatively low gas extraction (see e.g. Figure 5.51). The amount of gas extraction from well 1 in Segment i ($i = 0$ to 23), well 2 and 3 in Segment 23 and its total are shown in Figures 5.54 to 5.56. Generally, the extraction from well 1 is always lowest except in the combinations $3-23-23$, $14-23-23$, $18-23-23$ and $23-23-23$. The reason for this seem to be the same as for the two well case. One example of this case is shown in Figure 5.57 when well 1 is installed in Segment 18. As shown, wells 2 and 3 in Segment 23 are trapped in the narrow roadway, while well 1 is close to the crossing with Segment 23.

Figures 5.58 and 5.59 show the combined results of combinations $6-23-23$ and $23-23-23$. In Figure 5.58, only the gas extractions from wells 2 and 3 are shown to illustrate how the third well restrains the extraction of these two wells. This figure shows that the extractions from wells 2 and 3 are higher in combination $6-23-23$ than in $23-23-23$. On the other hand, the extraction from well 1 is generally higher in combination $23-23-23$ than in $6-23-23$, as shown in Figure 5.59. As a result, the sum of the two better extractions from wells 2 and 3 in combination $6-23-23$ plus the lower extraction from well 1 yields in total better extractions than the combination $23-23-23$, which restrains the extractions on average. The best locations of the extraction wells within the SA iterations for combinations $6-23-23$ and $23-23-23$ are shown in Figures 5.52 and 5.53 respectively.

Thus, we can summarize as follows:

- when three wells are installed in Segment 23, where the gas can generally be extracted most easily, the interaction between these wells is too strong because two intervals among three wells within Segment 23 are too short. Thus, two extraction wells can be effectively installed in Segment 23 but not more. The gas extraction is good when well 1 is installed in Segment 6, as is easily imaginable from the two-well case where combination $6-23$ yielded quite good extraction.

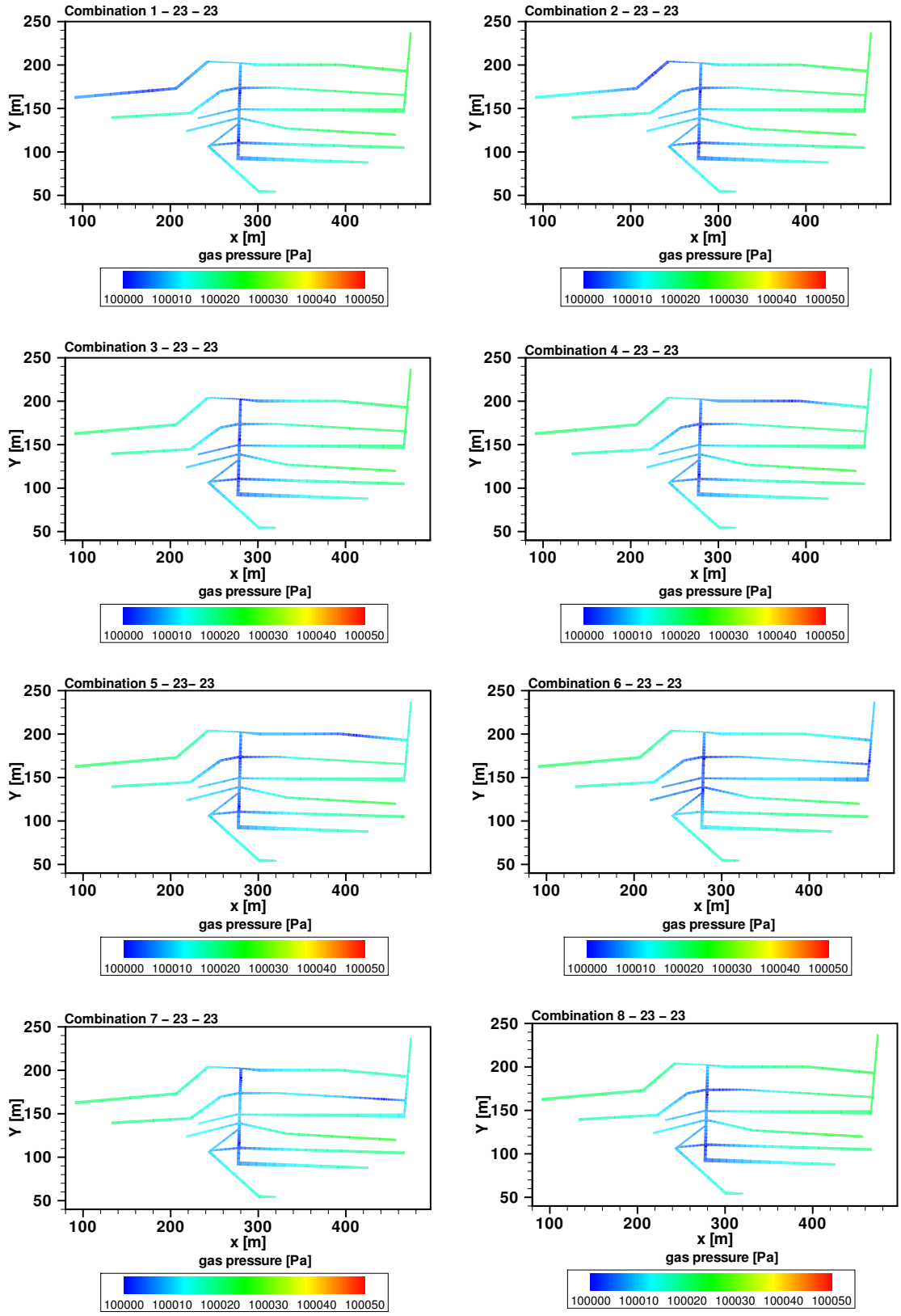

Figure 5.47: Pressure fields of the gas phase, simultaneously indicating the optimized locations of the extraction wells for combinations 1 – 23 – 23 to 8 – 23 – 23.

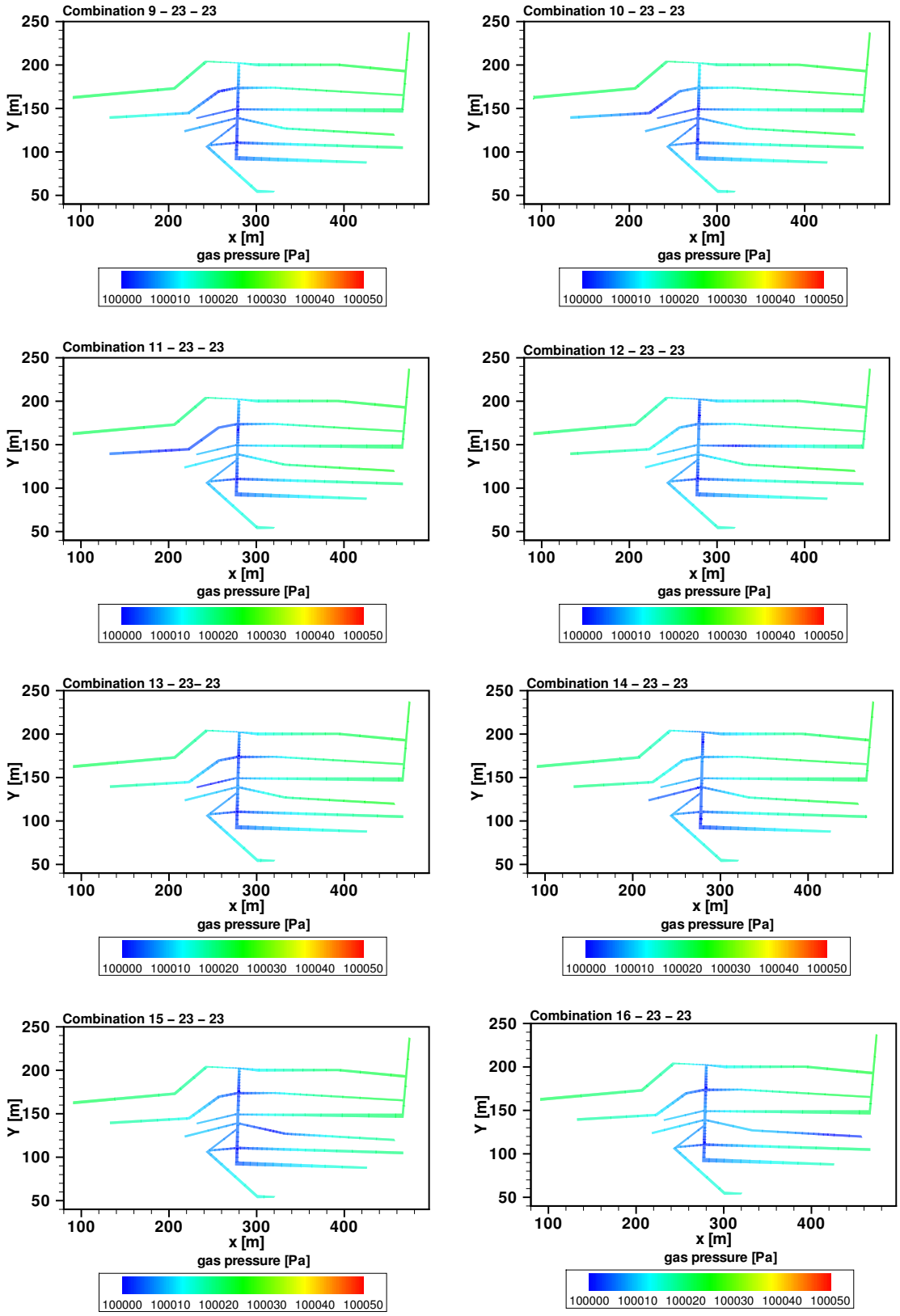

Figure 5.48: Pressure fields of the gas phase, simultaneously indicating the optimized locations of the extraction wells for combinations $9-23-23$ to $16-23-23$.

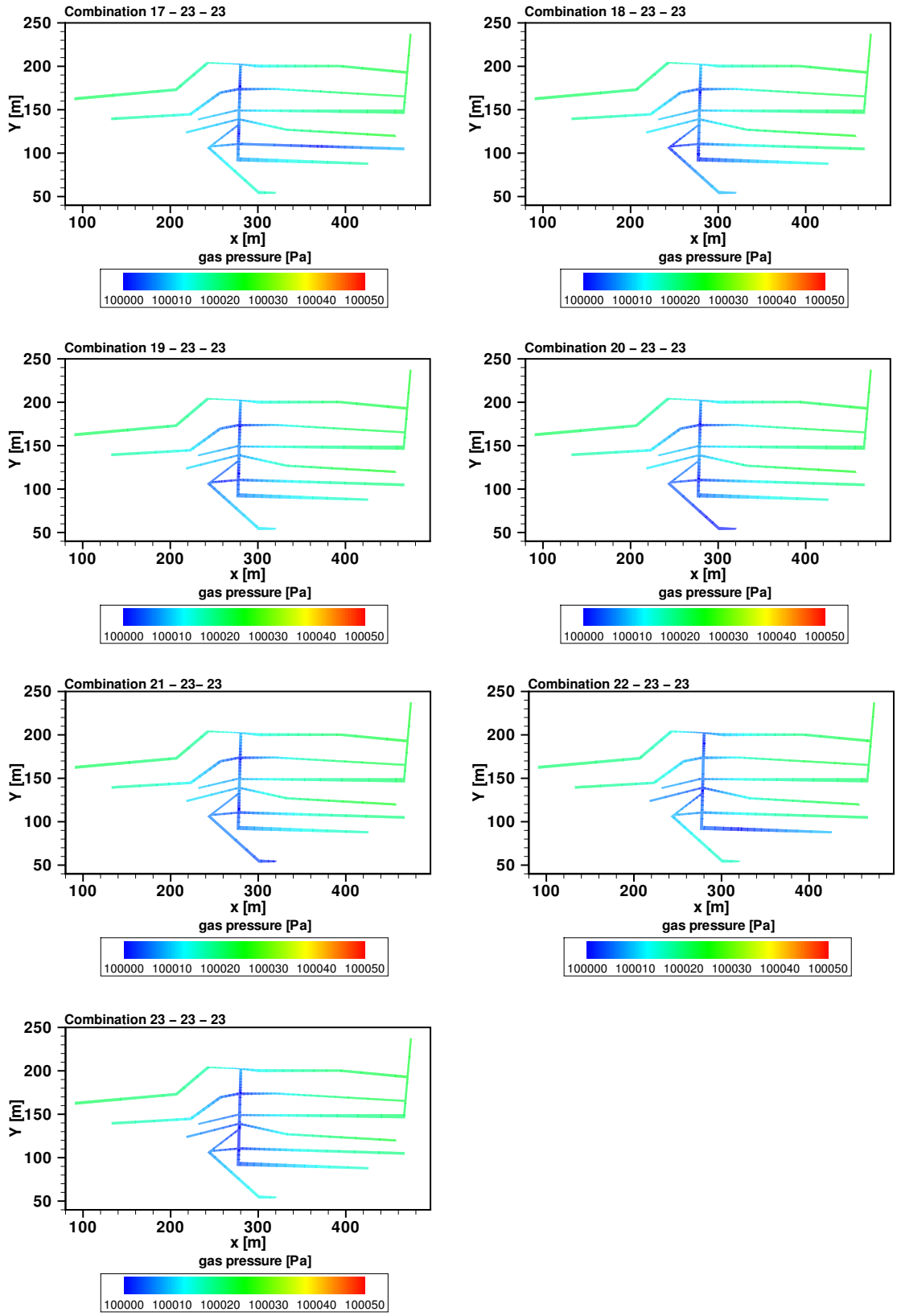

Figure 5.49: Pressure fields of the gas phase, simultaneously indicating the optimized locations of the extraction wells for combinations 17 – 23 – 23 to 23 – 23 – 23.

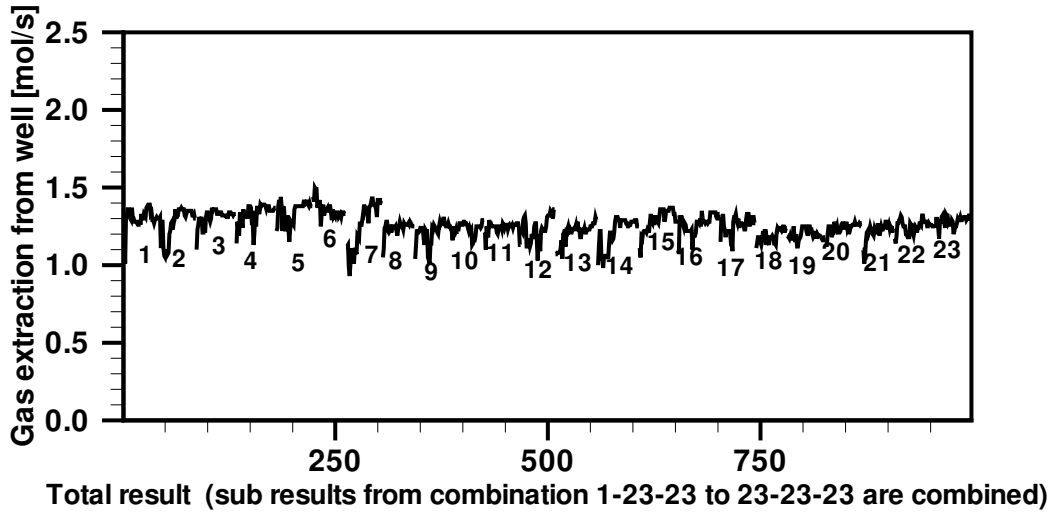

Figure 5.50: Gas extractions after 20.5 *sec* simulation time against the set of 23 sub-SA iterations from combinations $1-23-23$ to $23-23-23$.

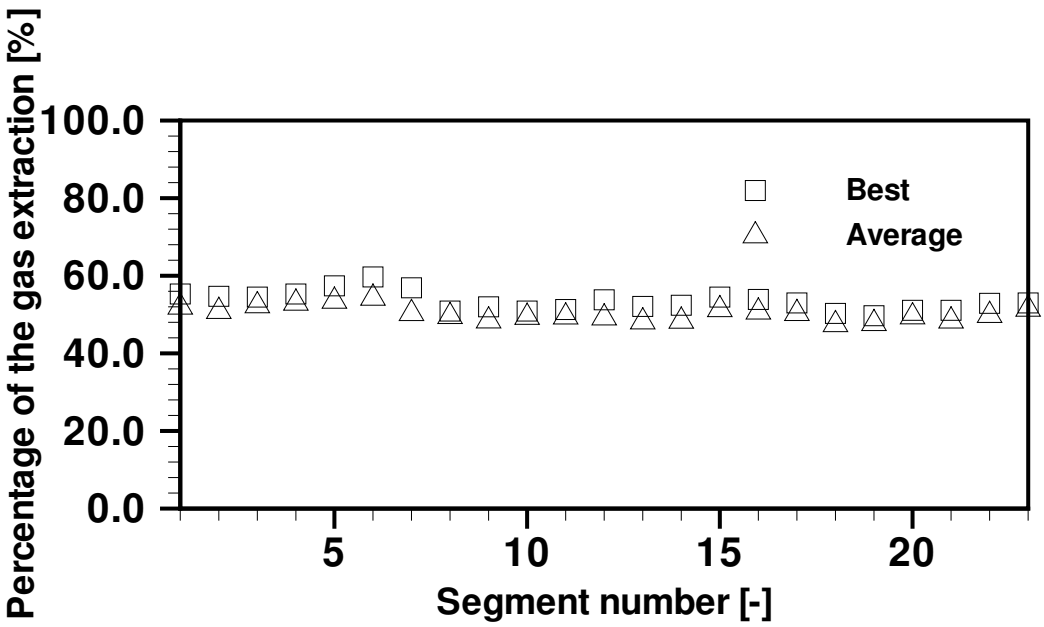

Figure 5.51: Percentages of the best and averged extracted gas to the total inflow 2.506 mol/s for combinations $1-23-23$ to $23-23-23$.

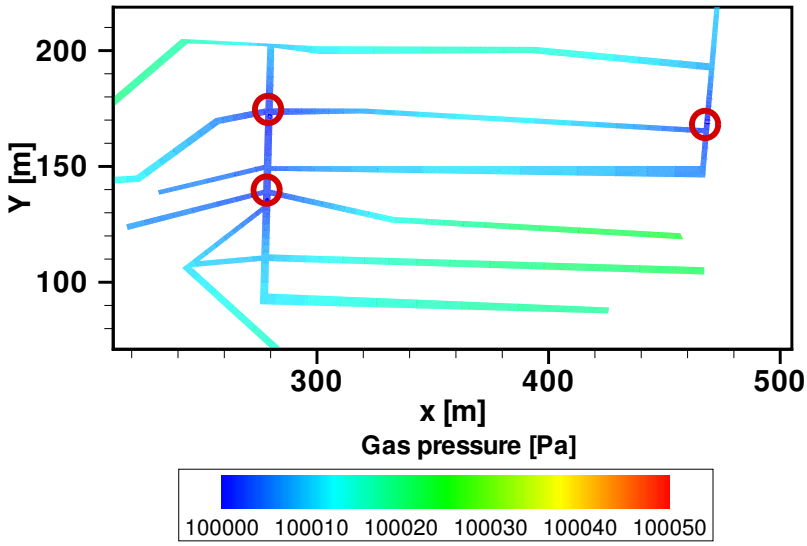

Figure 5.52: A global best location within the SA iterations, here for the three-well case observed in combination $6-23-23$.

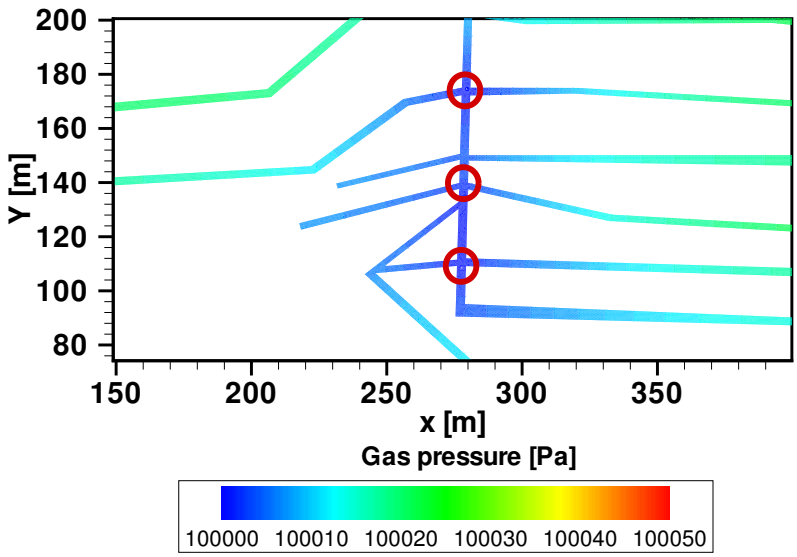

Figure 5.53: A local best location within the SA iterations, here for the three-well case in combination $23-23-23$.

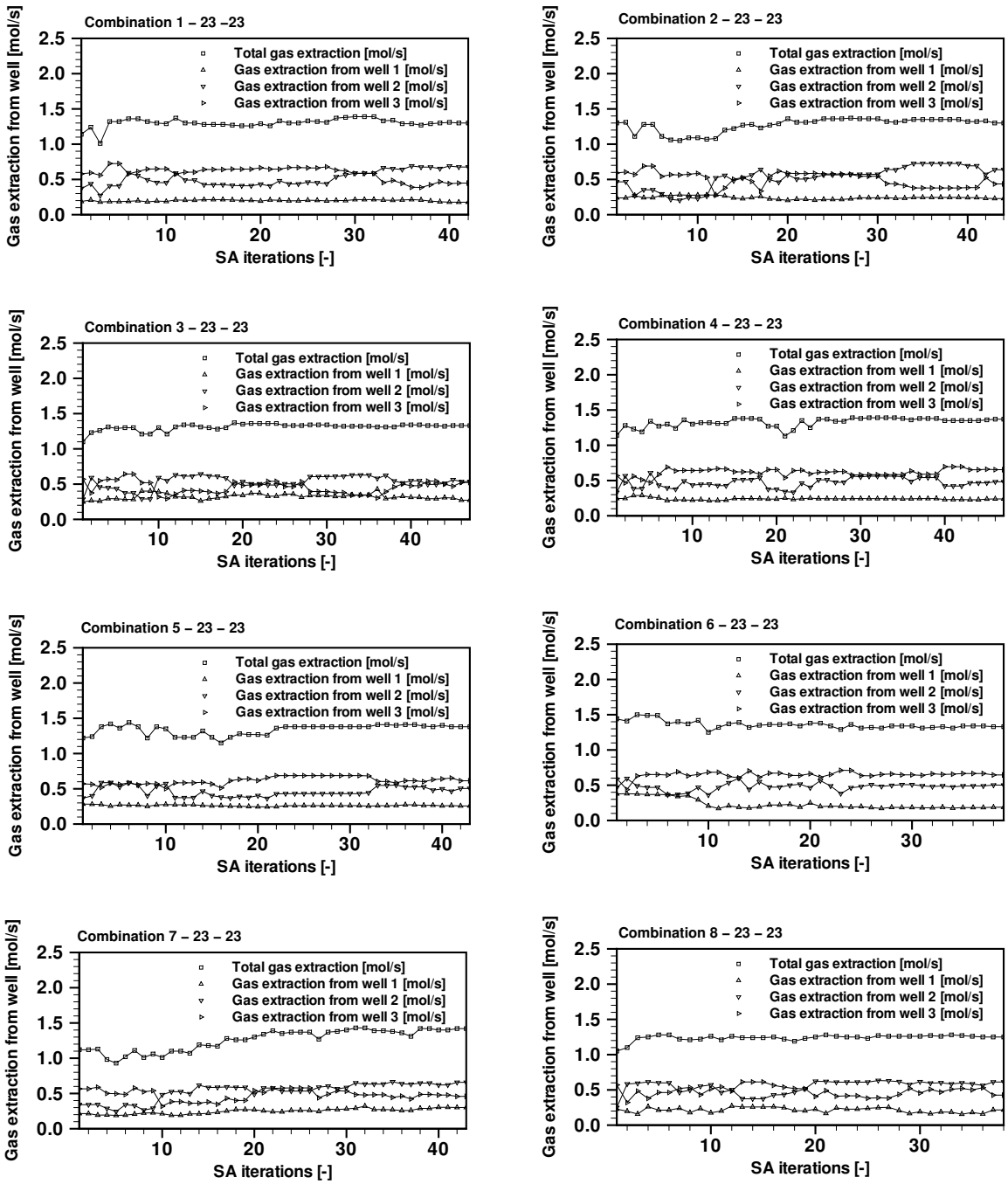

Figure 5.54: Gas extraction from well 1 in Segment i ($i = 0$ to 23), well 2 in Segment 23, well 3 in Segment 23 and its total for combinations $1-23-23$ to $8-23-23$.

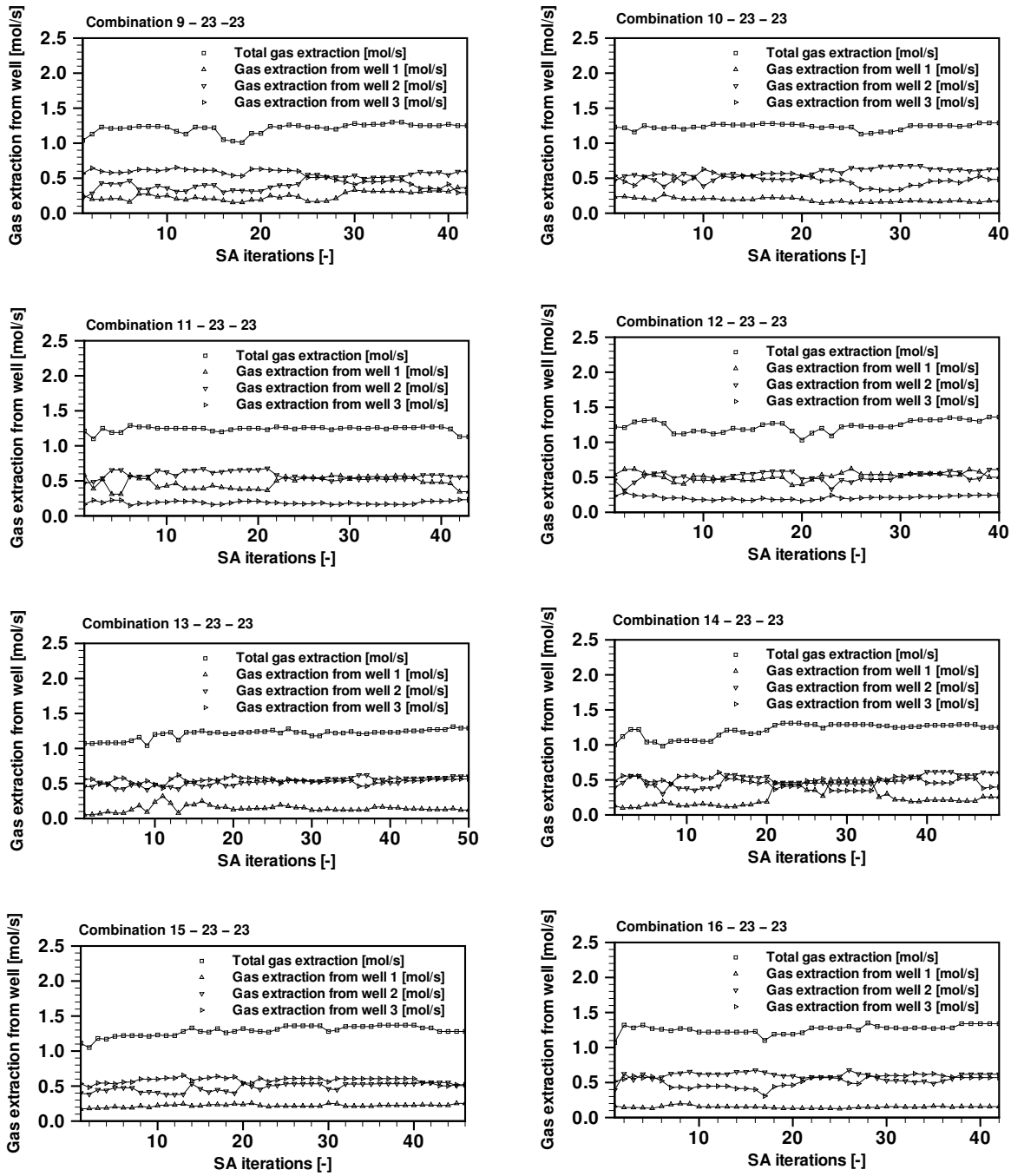

Figure 5.55: Gas extraction from well 1 in Segment i ($i = 0$ to 23), well 2 in Segment 23, well 3 in Segment 23 and its total for combinations $9-23-23$ to $16-23-23$.

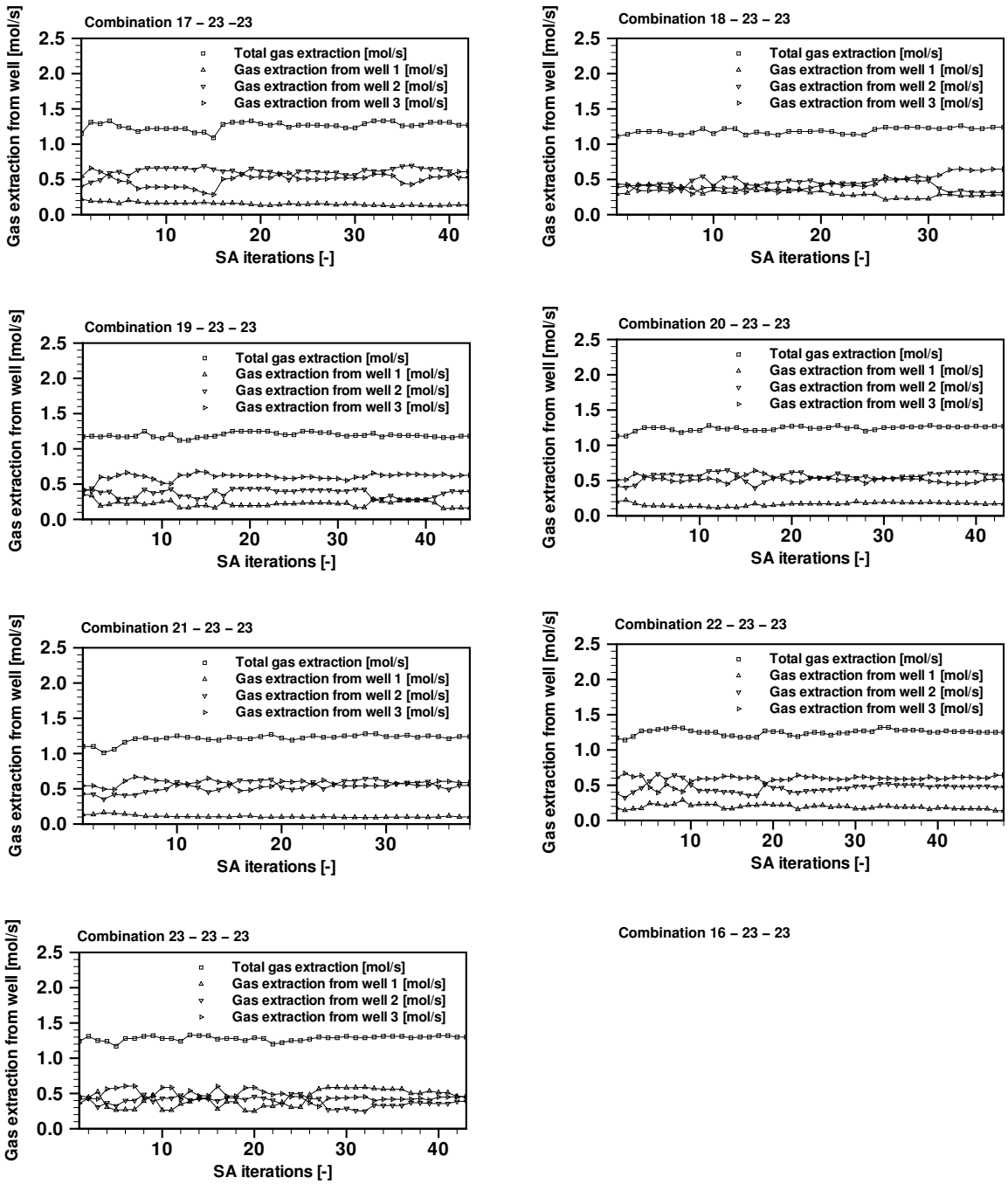

Figure 5.56: Gas extraction from well 1 in Segment i ($i = 0$ to 23), well 2 in Segment 23, well 3 in Segment 23 and its total for combinations $17-23-23$ to $23-23-23$.

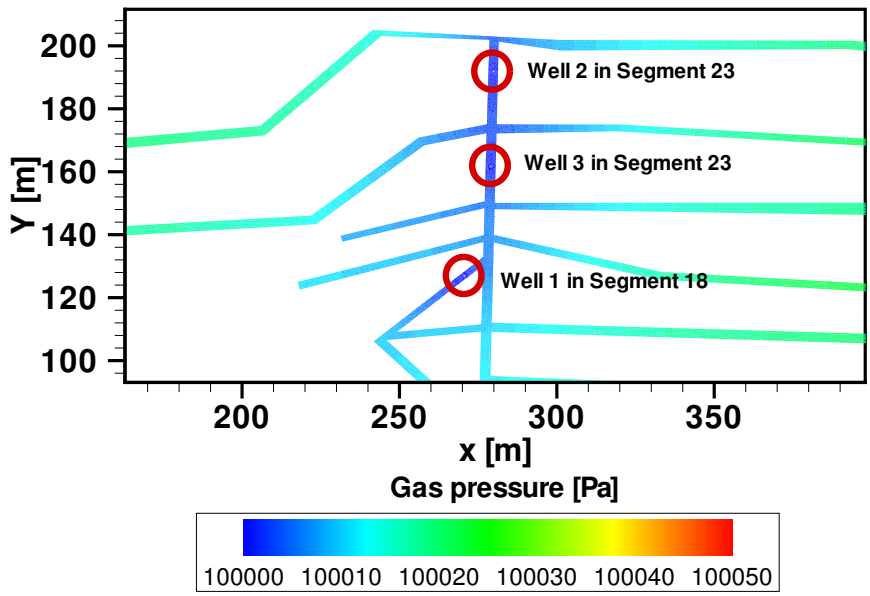

Figure 5.57: Pressure field of the gas phase when the extraction from well 1 is larger than that of well 2 and 3. In this case, well 1 is installed in Segment 18 and wells 2 and 3 in Segment 23.

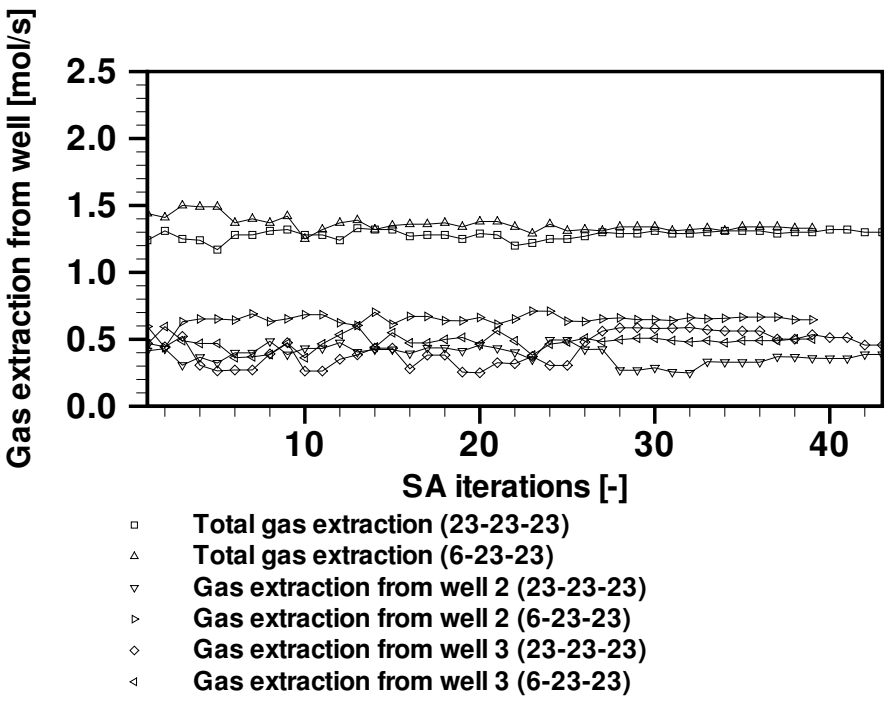

Figure 5.58: Combined result showing the gas extraction from wells 2, 3 and its total in combinations $6-23-23$ and $23-23-23$.

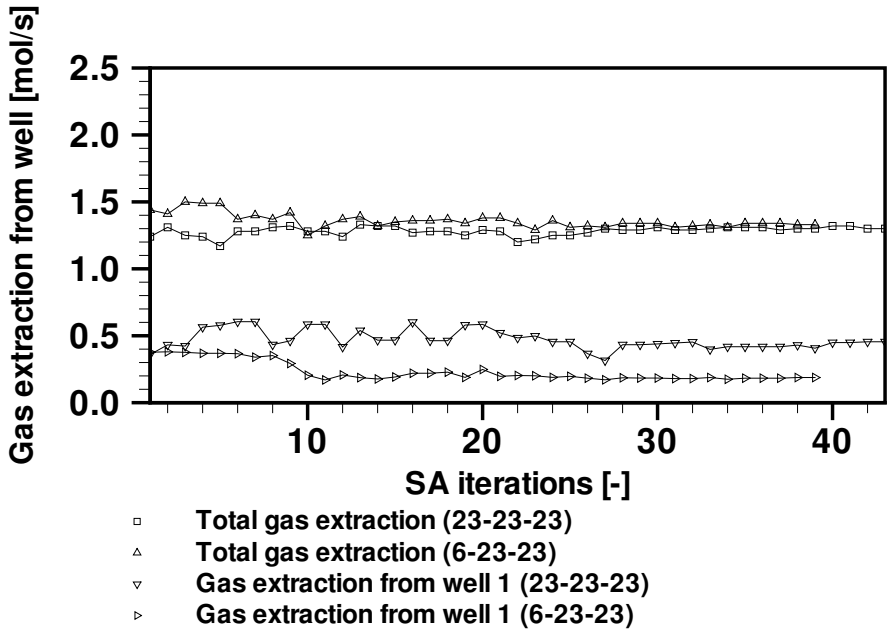

Figure 5.59: Combined result showing the gas extraction from well 1 and its total in combination $6-23-23$ and $23-23-23$.

5.3.5.4 Comparison of the results from the single-well to the three-well installation

As a final step in this chapter, the results when one, two and three wells are installed at the optimized locations in the mine site are compared. The intention of this section is to make a small suggestion on whether installing only one well is enough, or whether we need more wells to prevent gas migration to the surface. Three simulations using three optimized set-ups are reconducted until those simulations reach steady-states with regard to gas extraction (i.e. the velocity field). The total amounts of gas extraction against the simulation time for the single-, the two- and the three-well case are shown in Figure 5.60. Figure 5.60 also shows the partial extractions from each well for the two- and the three-well case. Unfortunately, perfect mass balance is not satisfied because the mass injected goes partially into the water phase, the mass flux at the extraction wells is the approximated value based on a midpoint rule and some numerical problems might have occured. Nevertheless, these shortcomings are considered to be of minor importance and acceptable.

As is apparent, the times required until steady-state is attained do not differ much. This implies that one well is enough to realize the same amount of gas extraction within mostly the same time range for the system up in this chapter. Additionally, as is shown in the crossroads example, if we have several extraction wells and the distances between the surrounding boundaries and one of the extraction wells do not differ much, the times when the methane from the surrounding boundaries reach the extraction well do not differ either. Thus, the location of maximum gas extraction realize that of maximum methane extraction as well under these conditions. The mole fraction of the methane in the gas phase against the simulation time for these cases is shown in Figure 5.61. Note in this figure that, first, a point under each well is chosen to trace the mole fractions, although these points are not located at exactly the same relative location from the well and these values should thus be regarded as a reference, and, secondly, that since these simulations run quite slowly, the simulation is terminated after 2 hours simulation time; the computational time is around 10 *days*. From this figure, the above assumption is expected to be satisfied. Thus, the overall tendency is expected to be similar whether gas extraction or methane extraction is considered.

However, unfortunately, this horizontal example cannot guarantee whether upward methane migration takes place and reaches the surface or not. On the other hand, this horizontal example could show that the pressure can increase up to, at most, around 100100 Pa, i.e. it is rather low. Additionally, the absolute permeability surrounding the workings is also rather low ($10^{-14}\ m^2$). Moreover, the principal flow direction of the gas phase is determined by the pressure differences between the atmospheric pressure and the pressure inside the workings. If extraction wells are installed, the principal direction is most probably towards the extraction well, unless the influences due to the pressure changes from the subsurface are huge. In other words, most methane is transported by convection towards the extraction wells, and, thus, upward migration of methane is mainly due to diffusion, i.e. not so large. As a conclusion, a single well installation may produce the same effects as several wells, although this has to be guaranteed by a three-dimensional simulation (see Figure 5.62) and will be different if we have connected fracture systems reaching from the working to the surface and open side walls or an horizontally ”unlimited” system.

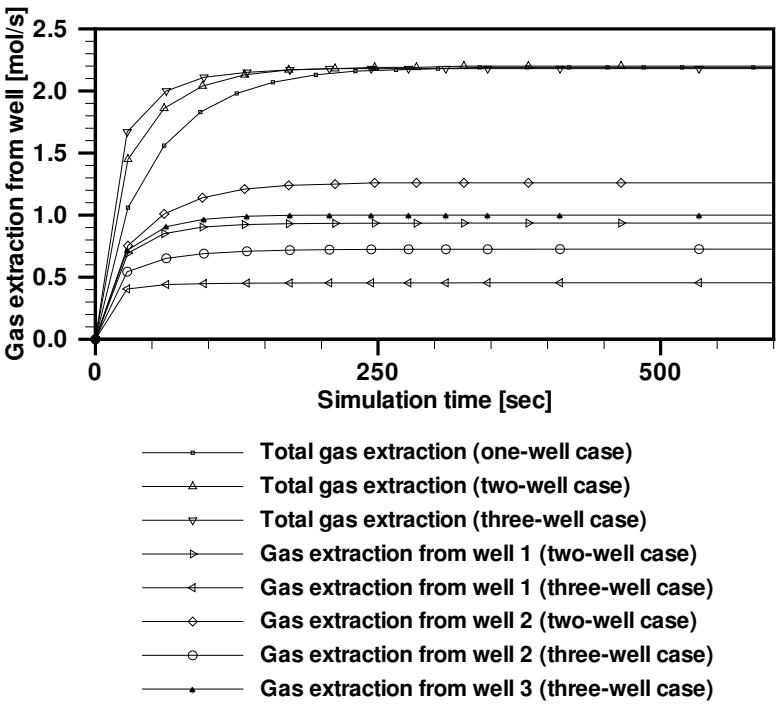

Figure 5.60: The total amounts of gas extraction against the simulation time for the best single-, two- and three-well cases.

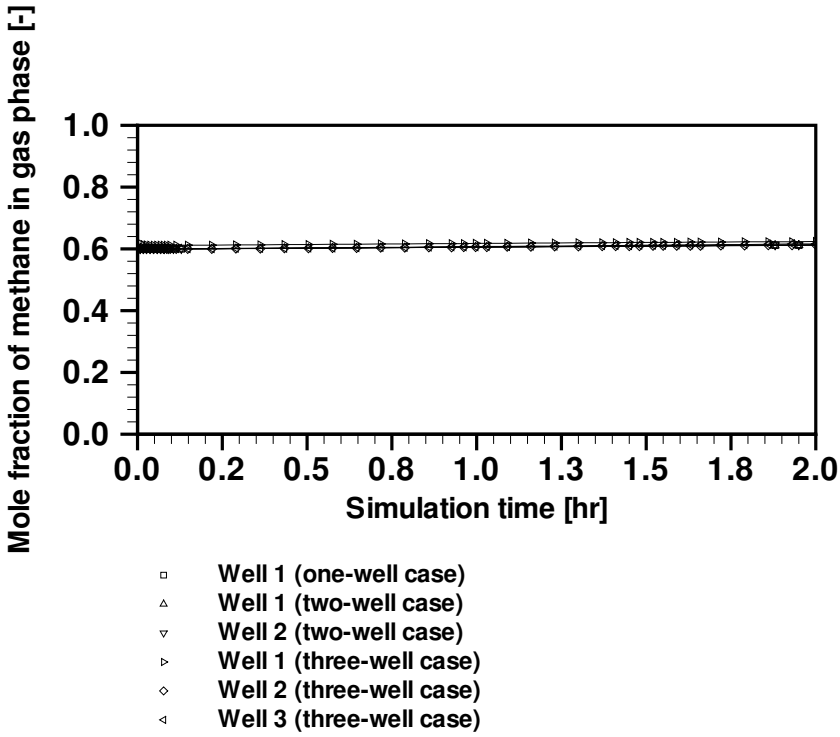

Figure 5.61: Mole fraction of the methane in the gas phase against the simulation time for the best single-, two- and three-well cases.

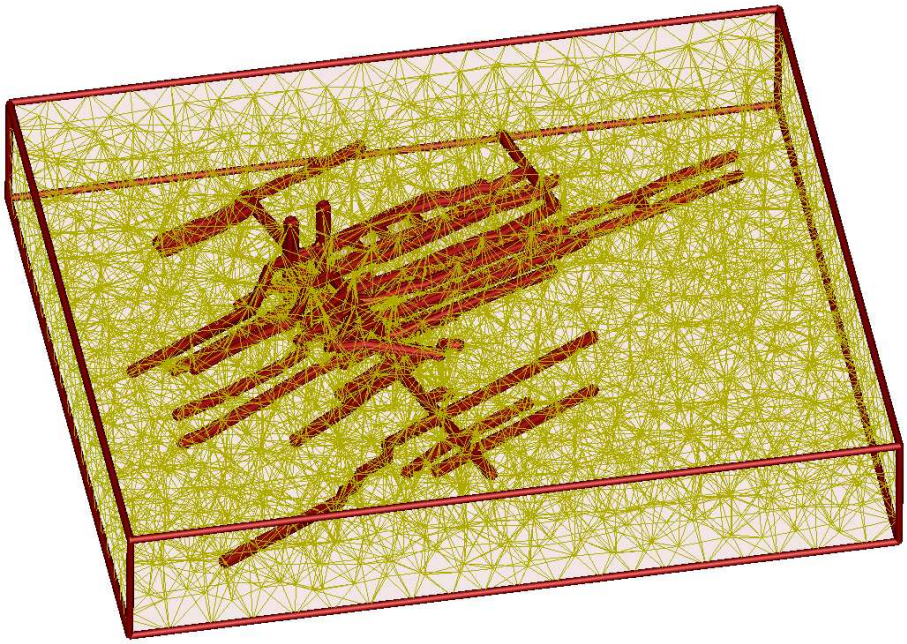

Figure 5.62: Computaional domain and mesh in 3D for the mining site.

Chapter 6

Conclusions and Outlook

6.1 Conclusions

First of all, as the main task in this thesis, a simulation-optimization model (MUFTE-SA) is developed and applied to an abandoned coal mine in the Ruhrgebiet, Germany, in order to develope a better methane-extraction strategy. What can be pointed out as the prominent feature is its application to a real site, which is generally not an easy task because of the enormous computational time required for iterations of real-world simulations. As a countermeasure to solve this huge computational time problem, a parallel computer was used. Additionally, the comparisons of different model concepts, i.e a two-phase (gas-liquid) and a two-phase (gas-liquid)/ three-component (air, methane and water) model are carried out. The two-phase/ three-compoment model can estimate the amount of methane dissolved in the liquid phase. Thus, the effects due to the dissolution can be investigated by comparing these two models.

The main conclusions and contributions of this thesis can be summarized as follows.

New developments in this thesis
A couple of new functions are added and/ or developed in the course of this research work.

- A two-phase (gas-liquid)/ three-component (air, methane and water) model is further developed. This model concept allows us to estimate the degassing/ dissolution from/ in the liquid phase.
- A Simulated Annealing algorithm is newly coded, tailored to the study of a better gas-extraction strategy from the abandoned coal mine in a complex coal-working system. The feature especially tailored is the movement of extraction wells along the coal working.
- The coupling of the aforementioned two-phase (gas-liquid)/ three-component (air, methane and water) model with the Simulated Annealing algorithm, i.e. MUFTE-SA, was carried out. MUFTE-SA can be utilized in principle for any natural processes that can be modelled by multiphase/ multicomponent models in porous and fractured-porous media.
- Optimization procedures in MUFTE-SA are parallerized. A pseudo-parallelization design is proposed for this purpose. This design enabled us to reduce the total time by

a factor of 23. The total computational time would have been $7hr \times 1000\,iterations \times 3\,times/(24hrs/day) = 875\,days$, if we had used only one processesor.

Insights obtained by comparing different model concepts
From the gas (methane) injection into artificially designed aquifers in Chapter 4, we gain the following insights:

- The methane injected into the saturated aquifer is first dissolved in the water phase until the amount of dissolution is beyond the capacity expressed by Henry's law, and then the gas saturation (i.e. the mass of methane in the gas phase) starts to increase. The ultimate ratio of the methane mass in the water phase for this artificially designed example reaches around 20% although this value itself changes widely according to the simulation conditions. Thus, it is clear that we often cannot neglect the amount of methane dissolved in the water phase. In other words, we need the two-phase/ three-component model in some conditions.
- As a possible outcome of the model difference, the speed of the upward migration of the methane gas front can be overestimated if we apply the two-phase model instead of the two-phase/ three-component model.
- To counteract methane problems (e.g. to extract methane), we also have to consider how to deal with the amount of the methane dissolved in the water phase.

Insights obtained from the MUFTE-SA application
Applying MUFTE-SA to the real abandoned coal mine in the Ruhrgebiet, Germany, in Chapter 5 provided the following insights:

General:

- The closer the well is to the side boundary of the roadways, or the closer two wells are to each other, the less gas can be extracted.
- Gas extraction is large when the well is installed at a place where several roads meet (i.e. at the crossing point).
- If we have several extraction wells and the distances between the surrounding boundaries and one of the extraction wells do not differ much, the times when the methane from the surrounding boundaries reaches the extraction well do not differ either. This fact implies that the location of maximum gas extraction realizes that of maximum methane extraction as well under these conditions.

Specific to the problem :

- The averaged gas extraction obtained by averaging all the values over each segment is generally large when the well is installed in the central segment where the gas in the surroundings can accumulate most easily and quickly. This tendency also holds for the segments which have a connection with the central segment. This is important in that, even though the assumptions made in this thesis are not hold in reality (e.g. the source is not uniformly distributed), there is still greater possibility that we could realize the better gas extraction by installing the wells in those segments.

- The best gas extraction for one- and two-well cases are found at the crossing points of several roadways in the central segment. But this is not true for the three-well case. In other words, when the third well is installed as well in the central segment, the extraction becomes lower than the other combinations when the third well is installed in one of the most remote segments due to the interaction of the wells. For the three-well case, the combination of two wells in the central segment and one in the segment farest from the central segment achieve the best extraction. This is because the distance between the wells is great enough, reducing the interaction and resulting in a higher extraction from each well.
- The installation of a single well could be enough since the time until the velocity field attains steady state does not differ much whether we use one, two or three wells. However, we must be able to guarantee that the methane does not escape from the mine. Unfortunately, however this can not be confirmed by this horizontal example alone.

6.2 Outlook

This thesis contained quite a lot of challenges and some shortcomings remain mainly resulting from the lack of information and enormous computational time required by iterations of real world simulations which we would not necessarily have had to take into account if we had just had to carry out a single simulation.

The shortcomings and the countermeasures of this research are as follows.

Shortcomings and countermeasures

- The simulation model has to be more sophisticated. In reality, each of the following necessary improvements is worth for further challenging research. Even then, it will still not be able to be applied for simulation-optimization purposes because the computational time will be much larger than the cases dealt with in this thesis. Nevertheless, I recommend the following improvements:
  - The so-called free flow boundary condition should be added to allow the increase/decrease of the primary variables at the extraction well. This is necessary to optimize the methane extraction instead of the gas extraction.
  - A (multiphase) pipe flow network model or (multiphase) flow model governed by Navier-Stokes equations should be applied to reproduce the natural processes in the roadways more accurately and also be coupled with this multiphase flow model for the porous media.
- Some optimization models should be added. Simulated Annealing is a non-derivative and global search method which generally requires a lot of iterations. This algorithm was applied in this thesis since we did not know the shape of the objective function. However, it was finally recognized that we could probably use other methods such as the Levenberg-Marquardt method for this example to reduce the number of iterations. A gradient type method would be useful if we used this model for parameter-identification purposes.

- The objective funtion would be more detailed if we could acquire more information. In other words, the objective function can be reformulated in such a way that it supplies additional aspects (e.g. cost, risk).
- Ideally speaking, 3D simulations should be carried out, especially in order to discover how much methane can be extracted by the wells and how much reaches the surface.

Finally, the principle in this thesis can be extended widely to many contexts for simulation-optimization and parameter identification. For instance, reseach into parameter identification which will utilize the know-how obtained in this thesis has already started.

Bibliography

[1] Adams, R. and Younger, P. L. A strategy for modeling ground water rebound in abandoned deep mine systems. *Ground Water*, 39(2):249 – 261, 2001.

[2] Aly, A. H. and Peralta, R. C. Comparison of genetic algorithm and mathematical programing to the design of groundwater cleanup systems. *Water Resources Research*, 35(8):2415 – 2425, 1999.

[3] Aly, A. H. and Peralta, R. C. Optimal design of aquifer cleanup systems under uncertainty using a neural network and a genetic algorithm. *Water Resources Research*, 35(8):2523 – 2532, 1999.

[4] Atkins, P. Physikalische Chemie. VCH, Weinheim, 2. Auflage, 1996.

[5] Azencott, R. (Ed.), Simulated annealing: Parallerization techniques. John Wiley and Sons Inc., USA, 1992.

[6] Barlag, C. Adaptive Methoden zur Modellierung von Stofftransport im Kluftgestein. Dissertation, Forschungsbericht 52, Institut für Strömungsmechanik und Elektron. Rechnen im Bauwesen, Universität Hannover, 1997.

[7] Bastian, P. and Helmig, R. Efficient fully-coupled solution techniques for two-phase flow in porous media, 2. Parallel multigrid solution and large scale computations. *Advances in Water Resources*, 23:199 – 216, 1997.

[8] Bastian, P. Numerical computation of multiphase flows in porous media. Habilitation, Christian-Albrechts-Universität Kiel, 1999.

[9] Battistelli, A., Calore, C., and Pruess, K. The simulator TOUGH2/EWSAG for modeling geothermal reservoirs with brines and non-condensible gas. Geothermics, Vol.26 (4), pp.437-464, 1997.

[10] Bear, J. Dynamics of fluids in porous media. Elsevier, New York, 1972.

[11] Betz, C., Färber, A., Greene, C. M., Koschitzky, H.-P., and Schmidt, R. Removing volatile and semivolatile contaminants from the unsaturated zone by injection of a steam/air mixture. Proceedings of the 6th International SZK/TNO Conference Contaminated Soil'98, Edingburgh, UK, 575-584, 1998.

[12] Björnsson, G., Hjartarson, A., Bodvarsson, G., and Steingrimsson, B. Development of a 3d geothermal reservoir model for the greater hengill volcano in sw-iceland. In: Finsterle, S., G.J. Moridis, C.M. Oldenburg, and Y. -S. Wu (Eds.), Proceedings of the TOUGH symposium 2003, Berkeley, California, May 12-14, LBNL-52494, Lawrence Berkeley National Laboratory, Berkeley, California, 2003.

[13] Breiting, T. Modellierung und Analyse von Mehrphasenprozessen zur Simulation von Methanausgasung im Untergrund. Project report, Institut für ComputerAnwendungen im Bauingenieurwesen, Technische Universität Brauschweig, 2000.

[14] Breiting, T., Hinkelmann, R., and Helmig, R. Modeling of hydrosystems with MUFTE-UG: Multiphase flow and transport processes in the subsurface. Proceedings of the 4th International Conference on Hydroinformatics, Iowa, USA, 2000.

[15] Brooks, R. and Corey, A. Hydraulic properties of porous media. Fort Collins, 1964. Hydrol. Pap. 3, Colorado State University.

[16] Chow, V., Maidment, D., and Mays, L. Applied hydrology. McGraw-Hill, International editions, 1988.

[17] Class, H. and Helmig, R. Numerical simulation of non-isothermal multiphase multicomponent prcesses in porous media. 2. Applications for the injection of steam and air. *Advances in Water Resources*, 25:551 – 564, 2002.

[18] Class, H. and Helmig, R. Numerical simulation of non-isothermal multiphase multicomponent processes in porous media. 1. An efficient solution technique. *Advances in Water Resources*, 25:533 – 550, 2002.

[19] Class, H. Theorie und numerische Modellierung nichtisothermer Mehrphasenprozesse in NAPL-kontaminierten porösen Medien. Dissertation, Universität Stuttgart, Institut für Wasserbau, 2001.

[20] Delshad, M., Pope, G., and Sepehrnoori, J. H. A compositional simulator for modeling surfactant enhanced aquifer remediation. 1. Formulation. *Journal of Contaminant Hydrology*, 23:303–328, 1996.

[21] Doherty, J. Groundwater model calibration using pilot points and regularisation. *Ground Water*, 41(2):170 – 177, 2002.

[22] Doherty, J. and Johnston, M. Methodologies for calibration and predictive analysis of a watershed model. *Journal of American Water Resources Association*, 39(2):251 – 265, 2003.

[23] Durner, W., Schultze, B., and Zurmühl, T. State of the art in inverse modeling of inflow/outflow experiments. In: van Genuchten, M. Th., F.J. Leij., and L. Wu (Eds.), Proceedings of the International Workshop on Characterization and Measurement of the Hydraulic Properties of Unsaturated Porous Media, Riverside, California, Oct. 22-24, 1997. University of California, Riverside, 661-681.

[24] Engelhardt, I., Finstelre, S., and Hofstee, C. Experimental and numerical investigation of flow phenomena in nonisothermal, variably saturated bentonite/crushed rock mixtures. *Vadose Zone Jounal*, 2:239 – 246, 2003.

[25] Ewing, R. and Lin, T. A class of parameter estimation techniques for fluid flow in porous media. *Advances in Water Resources*, 14:89 – 97, 1991.

[26] Falta, R., Pruess, K., Finsterle, S., and Battistelli, A. T2VOC user's guide. Lawrence Berkeley Laboratory Report, LBL-36400, 1995.

[27] Falta, R., Pruess, K., Javandel, I., and Witherspoon, P. Numerical modelling of steam injection for the removal of nonaqueous phase liquids from the subsurface. 2. Code validation and application. *Water Resources Research*, 28:451 – 65, 1992.

[28] Finsterle, S. iTOUGH2 user's guide. Project Report 34581, Lawrence Berkeley National Laboratory, University of California, Berkeley, 1993.

[29] Finsterle, S. Demonstration of optimization techniques for groundwater plume remediation. Project Report 46746, Lawrence Berkeley National Laboratory, University of California, Berkeley, 2000.

[30] Finsterle, S. Multiphase inverse modeling: Review and iTOUGH2 applications. *Vadose Zone Journal*, 2004.

[31] Finsterle, S. and Najiita, J. Robust estimation of hydrogeologic model parameters. *Water Resources Research*, 34:2939 – 2947, 1998.

[32] Finsterle, S., Pruess, K., Björnsson, G., and Battistelli, A. Evaluation of geothermal well behavior using inverse modelling. In: B.Faybishenko (Ed.), Dynamics of Fluids in Fractured Rocks Geophysical Monograph 122, American Geophysical Union, Washington DC, 377-387, 2000.

[33] Finsterle, S. and Pruss, K. Solving the estimation-identification problem in two-phase flow modelling. *Water Resources Research*, 31:913 – 924, 1995.

[34] Forsyth, P. and Shao, B. Numerical simulation of gas venting for NAPL site remediation. *Advances in Water Resources*, 16:354–367, 1991.

[35] Fuchs, A. Optimierte Delaunay-Triangulierungen zur Vernetzung getrimmter NURBs-Körper. Dissertation, Universität Stuttgart, Mathematisches Institut A, Shaker-Verlag, 1999.

[36] Gray, W. G. General conservation equations for multiphase systems. 4. Constitutive theory including phase change. *Advances in Water Resources*, 6:130 – 140, 1983.

[37] Greening, D. Parallel simulated annealing techniques. Physica D., Vol.,2, pp.293 - 306, 1990.

[38] Hassanizadeh, M. and Gray, W. G. General conservation equations for multiphase systems. 3. Constitutive theory for porous media flow. *Advances in Water Resources*, 3:25 – 40, 1980.

[39] Hassanizadeh, M. and Gray, W. G. Deriviation of basic equations for multiphase systems. 2. Generalized Darcy's and Fick's laws. *Advances in Water Resources*, 9:207 – 222, 1986.

[40] Helmig, R. Theorie und Numerik der Mehrphasenströmungen in geklüftet-porösen Medien. Universität Hannover, Institut für Strömungsmechanik und Elektron. Rechnen im Bauwesen, 1993.

[41] Helmig, R. Multiphase flow and transport processes in the subsurface. Springer - Verlag, Heidelberg, 1997.

[42] Helmig, R. and Bastian, P. Fully-coupled solution of two-phase flow in porous media, 1. Comparison and verification. Preprint 97/30, Sonderforschungsbereich 404, 1997.

[43] Helmig, R., Bastian, P., Hartmut, J., and Reichenberger, V. Multiphase multicomponent processes in fractured porous media. Final report 10/1997 - 12/2000, Institut für Computer-Anwendungen im Bauingenieurwesen, Technische Universität Braunschweig, 2000.

[44] Helmig, R., Braun, C., and Emmert, M. MUFTE - a numerical model for the simulation of multiphase flow processes in porous and fractured- porous media - nonisothermal twophase-twocomponent module. Institut für Wasserbau, Universität Stuttgart, Programmdokumentation, 1996.

[45] Helmig, R., Class, H., Huber, R., Sheta, H., Ewing, J., and Bastian, P. Architecture of the modular program system MUFTE-UG for simulating multiphase flow and transport processes in heterogeneous porous media. *Mathematische Geologie*, 2, 123-131, 1998.

[46] Helmig, R. and Huber, R. Comparison of Galerkin-type discretization techniques for two-phase flow in heterogeneous porous media. *Advances in Water Resources*, 21(8):697 – 711, 1998.

[47] Helmig, R., Jakobs, H., Bastian, P., and Reichenberger, V. Multiphase multicomponent processes in fractured porous media. Project Report 6, Technische Universität Carolo Wilhelmina zu Braunschweig, Institut für ComputerAnwendungen im Bauingenieurewesen, 2000.

[48] Hill, M. Methods and guidelines for effective model calibration. Project report, US. Geological Survey Water-Resources Investigation Reports 98-4005, 1998.

[49] Hinkelmann, R. Efficient numerical methods and information-processing techniques in environment water. Habilitation, Universität Stuttgart, 2002.

[50] Hopmans, J. and Simunek, J. Review of inverse estimation of soil hydraulic properties. In: van Genuchten, M. Th., F.J. Leij., and L. Wu (Eds.), Proceedings of the International Workshop on Characterization and Measurement of the Hydraulic Properties of Unsaturated Porous Media, Riverside, California, Oct. 22-24, 1997. University of California, Riverside, 634-659.

[51] Huber, R. Compositional multiphase flow and transport in heterogeneous porous media. Dissertation, Technische Universität Brauschweig, Institut für Computeranwendungen im Bauingenieurwesen, 1999.

[52] Huber, R. and Helmig, R. Investigation and simulation of three-phase flow in porous media. Technical Report 97/2, Inst. f. Angew. Mechanik, Fachgeb. f. Num. Methoden und Informationsverarb., TU Braunschweig, 1997.

[53] Huber, R. and Helmig, R. Node-centered finite volume discretizations for the numerical simulation of multiphase flow in heterogeneous porous media. Project report, Technische Universität Braunschweig, Inst. f. ComputerAnwendungen, Preprint, 1998.

[54] Huber, R. and Helmig, R. Multiphase flow in heterogeneous porous media: A classical finite element method versus an implicit pressure - explicit saturation-based mixed finite element - finite volume approach. *International Journal for Numerical Methods in Fluids*, 29:899 – 920, 1999.

[55] Jakobs, H. Simulation nicht-isothermer Gas-Wasser-Prozesse in komplexen Kluft-Matrix-Systemen. Dissertation, Institut für Wasserbau, Universität Stuttgart, 2003.

[56] Jakobs, H., Helmig, R., Miller, T., Class, H., Hilpert, M., and Kees, C. Modeling of DNAPL flow in saturated heterogeneous porous media. Preprint for SFB404, 2003.

[57] Kinzelbach, W. Numerische Methoden zur Modellierung des Transports von Schadstoffen im Grundwasser, 2.Auflage. R. Oldenburg Verlag, München, Wien, 1992.

[58] Kirkpatrick, S., Gelatt Jr, C., and Vecchi, M. Optimization by simulated annealing. *Science*, 220:671 – 680, 1983.

[59] Kobayashi, K., Hinkelmann, R., and Helmig, R. Comparison of different model concepts for gas-water processes in the subsurface. XXX IAHR Congress 24-29 August 2003 (CD-ROM), Thessaloniki, Greece, 2003.

[60] Kobus, H. and de Haar, U. Perspektiven der Wasserforschung. Deutsche Forschungsgemeinshaft, 1995.

[61] Kool, J., Parker, J., and van Genuchten, M. Parameter estimation for unsaturated flow and transport models - a review. *Journal of Hydrology*, 91:255–293, 1987.

[62] Lacroix, S., Vassilevski, Y., and Wheeler, M. F. Iterative solvers of the implicit parallel accurate reservoir simulator (IPARS). *Numerical Linear Algebra with Applications*, 4:537–549, 2001.

[63] Lang, C. Zur Schwebstoffdynamik von Trübungszonen in Ästuarien. Dissertation, Institut für Ströngsmechanik und Elektr. Rechnen im Bauwesen, Universität Hannover, Bericht Nr. 26, 1990.

[64] Lenhard, R. and Parker, J. A model for hysteric constitutive relations governing multiphase flow. 3. Refinements and numerical simulations. *Water Resources Research*, 24:373 – 380, 1980.

[65] McDonald, M. and Harbaugh, A. A modular three-dimensional finite-difference groundwater flow model. U.S. Geological Survey Water-Resources Investigations, Book 6, Chap. A1, 586 p., 1988.

[66] Metropolis, N., Rosenbluth, A., Teller, A., and Teller, E. Equation of state calculations by fast computing machines. *J. Chem. Phys.*, 21:1087 – 1092, 1953.

[67] Moridis, G. and Pruess, K. Flow and transport simulations using T2CG1, a package of conjugated gradient solvers for the TOUGH2 family of codes. Project Report 36235, Lawrence Berkeley National Laboratory, University of California, Berkeley, 1995.

[68] Neumann, S. Calibration of distributed parameter groundwater models viewed as a multi-objective decision process under uncertainty. *Water Resources Research*, 9:1006 – 1021, 1973.

[69] Oldenburg, C. and Pruess, K. Higher-order differencing for geothermal reservoir simulation. Proceedings of the Twenty-Second Workshop on Geothermal Reservoir Engineering, Stanford University, Stanford, CA, 1997.

[70] Oldenburg, C., Pruess, K., and Lippmann, M. Heat and mass transfer in hypersaline geothermal systems. Proceedings of the World Geothermal Congress, 1995, pp. 1647-1652, International Geothermal Association, 1995.

[71] Paul, M. Simulation of two-phase flow processes in heterogeneous porous media with adaptive methods. Dissertation, Institut für Wasserbau, Universität Stuttgart, 2003.

[72] Paul, M., Stauffer, F., Hinkelmann, R., and Helmig, R. Calibration of a water-gas flow model for dike systems. In: Bentley, L.R. and Sykes, J.F. and Brebbia, C.A. and Gray, W.C. and Pinder G.F. (Eds.), Proceedings of XIII. Conference on Computational Methods in Water Resources, 25. - 29. June, A.A. Balkema - Rotterdam, Brookfield, Calgary, Canada, 2000.

[73] Poeter, E. and Hill, M. Documentation of UCODE, a computer code for universal inverse modeling. Project report, US. Geological Survey Water-Resources Investigation Reports 98-4080, 1998.

[74] Press, W., Teukolsky, S., Vetterling, W., and Flannery, B. Numerical recipes in C, the art of scientific computing. Second edition. Cambridge University Press, Cambridge, 1995.

[75] Pruess, K., Finsterle, S., Moridis, G., Oldenburg, C., and Wu, Y.-S. General purpose reservoir simulators: the TOUGH2 family. Project report, Lawrence Berkeley National Laboratory Report LBL-40140, 1997.

[76] Reid, R., Praismotz, J., and Poling, B. The properties of gases and liquids. McGraw-Hill, 1987.

[77] Sait, M. and Youssef, H. Iterative computer algorithms with applications in engineering – solving combinatorial optimization problems. IEEE Computer Society -Wiley, 1999.

[78] Sanchez, S. H. and Frausto-Solis, J. A methodology to parallel the temperature cycle in simulated annealing. In: O.Cairo, L.E.Sucar and F.J.Cantu (Eds.), MICAI 2000, LNAI 1793, Springer-Verlag, Germany, pp.63 -74, 2000.

[79] Sanchez, S. H. and Frausto-Solis, J. MPSA: a methodology to parallelize simulated annealing and its application to travelling salesman problem. Lectures notes on computer science, Springer Verlag, 2002.

[80] Schultze, B., Ippisch, B., Huwe, B., and Durner, W. Dynamic nonequilibrium during unsaturated water flow. In: van Genuchten, M. Th., F.J. Leij., and L. Wu (Eds.), Proceedings of the International Workshop on Characterization and Measurement of the Hydraulic Properties of Unsaturated Porous Media, Riverside, California, Oct. 22-24, 1997. University of California, Riverside, 877-892.

[81] Senger, R., Lanyon, P., Marschall, S., Vomvoris, S., and Ando, K. TOUGH2/iTOUGH2 modeling in support of the gas migration test (GMT) at the Grimsel test site (Switzerland). In: Finsterle, S., Moridis, G.J., Oldenburg, C.M., and Wu, Y.-S. (Eds.), Proceedings of the TOUGH Symposium 2003, Berkeley, California, May. 12-14, LBNL-52494, Lawrence Berkeley National Laboratory, University of California, Berkeley, 2003.

[82] Sheta, H., Hinkelmann, R., and Helmig, R. Two-phase flow problems in porous media for sharp interface problems. International Symposium on Computer Methods for Engineering in Porous Media, Flow and Transport, Giens, France, 1998.

[83] Tran, T., Wen, X.-H., and Behrens, R. Efficient conditioning of 3d fine-scale reservoir model to multiphase production data using streamline-based coarse scale inversion and geostatistical downscaling. Paper SPE56518, presented at 1999 SPE Annual Techical Conference and Exhibition. Houston, Texas. October 3-6, 1999.

[84] Van Genuchten, M. A closed form equation for predicting the hydraulic conductivity of unsaturated soils. *Soil Sci Soc Am J*, 44:892 – 8, 1980.

[85] Vasco, D. W. and Datta-Gupta, A. Integrating multiphase production history in stochastic reservoir characterization. *SPEFE*, 9:149 – 156, 1997.

[86] Vega, L., Rojas, D., and Datta-Gupta, A. Scalability of the deterministic and Bayesian approaches to production data integration into field-scale reservoir models. Paper SPE 79666, presented at the SPR Reservoir Simulation Symposium. Houston, Texas. February 3-5, 2003.

[87] Versteeg, H. and Malalasekera, W. An introduction to computational fluid dynamics, the finite volume method. Longman Scientific and Technical, 1995.

[88] Vogel, H. RöFo. Fortschritte auf dem Gebiet der Röntgenstrahlen und der bildgebenden Verfahren. *Title Page*, 169, 1998.

[89] Whitaker, S. Flow in porous media. 1: A theoretical derivation of Darcy´s law. *Transport in Porous Media*, 1:3 – 25, 1986.

[90] Whitaker, S. Flow in porous media. 2: The governing equations for immiscible, two-phase flow. *Transport in Porous Media*, 1:105 – 125, 1986.

[91] White, M. and Oostrom, M. STOMP subsurface transport over multiple phases: User's guide. Project report, PNNL-11218, UC-814, Pacific Northwest National Laboratory, Richland, Washington, 1996.

[92] White, S., Creighton, P., Bixley, P., and Kissling, W. Modelling the dewatering and depressurisation of the Lihir open-pit gold mine. In: Finsterle, S., Moridis, G.J., Oldenburg, C.M., and Wu, Y.-S. (Eds.), Proceedings of the TOUGH symposium 2003, Berkeley, California, May. 12-14, LBNL-52494, Lawrence Berkeley National Laboratory, University of California, Berkeley, 2003.

[93] Wu, Z., Teynolds, A., and Oliver, D. Conditioning geostatistical models to two-phase production data. *SPEJ*, 4:140 – 155, 1999.

[94] Yeh, W. W.-G. Review of parameter identification procedures in groundwater hydrology: The inverse problem. *Water Resources Research*, 22:95 – 108, 1986.

[95] Zheng, C. and Wang, P. P. An integrated global and local optimization approach for remediation system design. *Water Resources Research*, 35(1):137 – 146, 1999.

[96] Zheng, C. and Wang, P. Optimal remediation policy selection under general condition. *Ground Water*, 35(5):215 – 224, 1996.

[97] Zheng, C. and Wang, P. Parameter structure identification using tabu search and simulate annealing. *Advances in Water Resources*, 19(4):215 – 224, 1996.

[98] Zheng.C. MT3D, a modular three-dimensional transport model for simulation of advection, dispersion and chemical reactions of contaminants in groundwater systems. Report to the U.S. Environmental Protection Agency, 170 pp., 1990.

[99] Zimmerman, D., de Marsily, F., Gotway, C., Marietta, M., Axness, C., Beauheim, R., Bras, R., Carrera, J., Dagan, G., Davies, P., Gallegos, D., Galli, A., Gomez-Hernandez, J., Grindrod, P., Gutjahr, A., Kitadinis, P., Lavenue, A., McLaughlin, D., Neuman, S., Rama-Rao, B., Ravenne, C., and Rubin, Y. A comparison of seven geostatistical based inverse approaches to estimate transmissivities for modeling advective transport groundwater flow. *Water Resources Research*, 34:1373 – 1413, 1998.

Zusammenfassung

Einleitung

Innerhalb der letzten Jahrzehnte spielte der Bergbausektor eine große Rolle bei der Energieproduktion auf der ganzen Welt. Die wichtige Bedeutung des Kohlebergbaus kann an der Tatsache abgelesen werden, dass 1951 die Europäische Kohle- und Stahlgemeinschaft (European Coal and Steel Community, ECSC) eingerichtet wurde, die den Ursprung der heutigen Europäischen Union bildet.

Da Erdöl die Kohle im Laufe der letzten Zeit als Hauptenergiequelle ablöste, veränderte sich gezwungenermaßen die Rolle des Bergbaus. Dieser Umschwung führte zu einem Schließen der Kohlebergwerke in den industrialisierten Ländern.

Aus den Schließungen ergeben sich einige negative Aspekte. Zum Beispiel werden nach dem Abwerfen einer Kohlegrube in der Regel die Bewetterung und die Wasserhaltung eingestellt. In den Kohlebergwerken wurde normalerweise Methangas innerhalb der Kohleflöze adsorbiert. Methan ist ein Treibhausgas, dessen Einfluss sehr viel größer als der von Kohlenstoffdioxid ist.

Die Methanemissionen rufen kaum Probleme hervor, wenn die Bergwerke in Betrieb sind, da hier die Emission über die Ventilation der Anlage kontrolliert wird. Das Einstellen der Belüftung und damit das Schließen von Gaskontrolleinrichtungen, hat jedoch zu einer unkontrollierten Methangasmigration an die Erdoberfläche geführt, die über Schächte, durchlässige Schichten, Verwerfungen und durch den Bergbau hervorgerufene Klüfte stattfindet.

Methangasaustritte in bewohnten Gebieten sind gefährlich, da Methan explosiv ist und die Ansammlung von Methan in Häusern eine Gesundheitsgefährdung der Bewohner darstellt. Wenn jedoch der Gasstrom groß genug ist und ein kontrolliertes Fördern möglich ist, kann Methan auch als Energiequelle genutzt werden (z.B. Abandoned Mine Methane (AMM), Methanhydrat, etc.).

Um eine Förderung ermöglichen zu können, wird von vielen Institutionen eine große Anzahl von Untersuchungen durchgeführt. Die vorliegende Arbeit konzentriert sich hauptsächlich auf zwei Aspekte:

Der erste Schwerpunkt ist die Entwicklung eines sogenannten Simulations-Optimierungs-Modells. Der Autor hat ein Optimierungsmodell eingesetzt, welches mit einem Mehrphasen-Mehrkomponenten-Modell gekoppelt ist. In der vorliegenden Arbeit wird dieses Modell daraufhin zugeschnitten, bessere (optimale) Methanextraktionsmaßnahmen aus Kohlebergwerken zu finden.

Die Frage, wie das Methan aus den Bergwerken extrahiert werden kann, ist immer von großer Bedeutung für die Betreiber. Deshalb wird versucht, ein numerisches Tool zur Verfügung zu

stellen, um die Entscheidungsfindungen unterstützen zu können. Die Möglichkeiten der Modellierung von realen Lagerstätten haben innerhalb der letzten Jahrzehnte stark zugenommen, da leitungsfähige numerische Methoden und Rechner (Parallelrechner) entwickelt worden sind.

Heutzutage wird die Entwicklung von sogenannten 'decision support systems' (Entscheidungshilfesystemen), die auch die Fähigkeiten der Modellierung in sich vereinigen, immer häufiger in Erwägung gezogen. Das hier vorgestellte Simulations-Optimierungs-Modell ist in diese Richtung ausgelegt. Obwohl der Einsatz des Simulations-Optimierungs-Modells in dieser Arbeit auf die Anwendung beschränkt ist, geeignete Methanextraktionsmodelle zu untersuchen, kann das Modell an sich in analoger Weise für viele Problemstellungen verwendet werden, deren abstrahierte Prozesse mit Mehrphasen-Mehrkomponenten-Modellen berechnet werden können.

Der zweite Schwerpunkt dieser Arbeit liegt darin, Vergleichsstudien für die Simulation der Methanmigration und Methan-Wasser-Interaktion in wassergesättigten Kohlebergwerken mit unterschiedlichen Modellkonzepten durchzuführen. Diese Arbeit beinhaltet eine Weiterentwicklung eines Zweiphasen-Dreikomponenten-Modells (Phasen: Wasser, Gas; Komponenten: Wasser, Luft, Methan), um die Massentransferprozesse zwischen den Phasen mit einbeziehen zu können. Das neu entwickelte Modell wurde mit einem bereits vorhandene Zweiphasen-Modell für einen Beispielfall in der gesättigten Zone verglichen.

Diese Vorgehensweise ist notwendig, um ein geeignetes Modellkonzept wählen zu können, das für die gesamte Forschungsarbeit angewendet werden kann. Eine Berücksichtigung der Massentransferprozesse zwischen den Phasen kann sehr wichtig werden, besonders wenn die Kohlebergwerke nach dem Wiederanstieg des Grundwassers modelliert werden. Hierbei kann die Lösung des Methans in der flüssigen Phase unter bestimmten Bedingungen große Ausmaße annehmen.

Mehrphasen-Mehrkomponenten-Modell

Zwei Modelle werden in dieser Arbeit verwendet. Dies ist zum einen ein Zweiphasen-Modell (Wasser, Gas) und zum anderen ein Zweiphasen-Dreikomponenten-Modell (Phasen: Wasser, Gas; Komponenten: Wasser, Methan, Luft). Der größte Unterschied zwischen diesen beiden Modellen besteht darin, dass der Massentransfer zwischen den Phasen vom Zweiphasen-Dreikomponenten-Modell mit berücksichtigt werden kann und der Transport der Komponenten in den Phasen.

Zweiphasen-Modell

Eine schematische Darstellung des Zweiphasen-Modellkonzepts wird links in Abb. 1 gezeigt. Es gibt zwei nicht-mischbare Phasen: eine flüssige Phase und eine Gasphase. In diesem Modellkonzept werden die Massenübergänge zwischen den Phasen nicht berücksichtigt. Die Massenerhaltungsgleichungen für dieses Zweiphasen-Modell werden für jede einzelne Phase hergeleitet, so dass sich zwei Gleichungen für die Primärvariabeln ergeben. Dieses Gleichungssystem wird mit Nebenbedingungen und konstitutiven Beziehungen geschlossen.

Zweiphasen-Dreikomponenten-Modell

Eine weitere schematische Darstellung des Zweiphasen-Dreikomponenten-Modellkonzepts wird rechts in Abb. 1 dargestellt. Hier gibt es wiederum zwei nicht-mischbare Phasen, eine flüssige Phase und eine Gasphase, wobei beide aus den drei Komponenten Wasser, Methan und Luft bestehen. Dieses Modell kann die Massenübergangsprozesse (z.B. Lösung, Ausgasung), die durch das Henry-Gesetz beschrieben werden, berücksichtigen. Die Massenerhaltungsgleichungen werden für dieses Modell in Bezug auf die einzelnen Komponenten hergeleitet. Somit liegen hier drei Gleichungen vor.

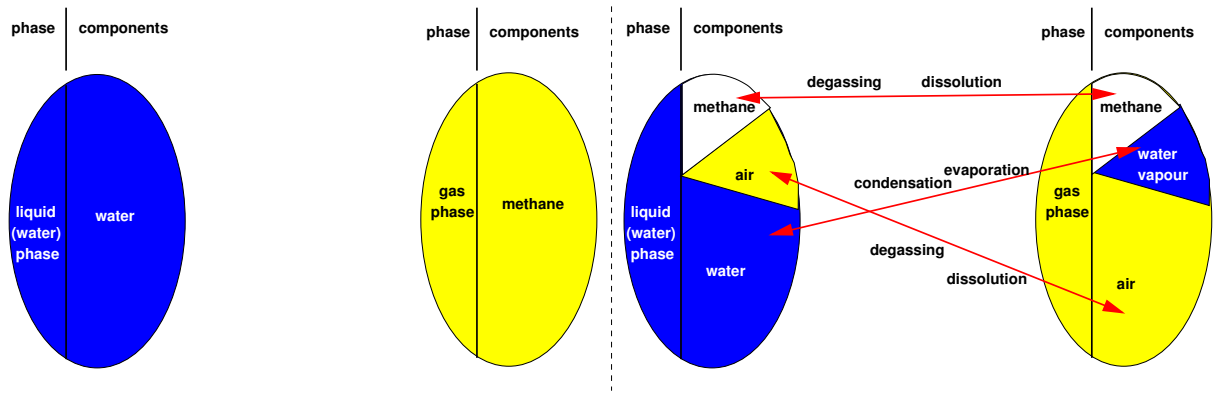

Abb. 1: Konzeptionelle Darstellung für das Zweiphasen-Modell (links) und das Zweiphasen-Dreikomponenten-Modell (rechts)

Vergleichende Untersuchung

Mit den beiden vorhergenannten Modellen wird eine vergleichende Untersuchung durchgeführt, um ein besseres Modellkonzept für die Simulation von Methanmigrationen wählen zu können. Hierzu wurde ein einfaches Beispiel innerhalb der gesättigten Zone gewählt.

Bedingungen der Simulation

Die Parameter, die für die beiden Modelle benötigt werden, sind teilweise unterschiedlich. Dies bedeutet, dass es sehr schwer ist, genau das selbe Beispiel berechnen zu können, solange keine Transformationen zwischen den entsprechenden Parametern gegeben sind. Dennoch werden die Beispiele so aufgestellt, dass sie einander so ähnlich wie möglich sind. Der Einfachheit halber wird ein System betrachtet, das aus einer homogenen Schicht besteht in dem eine linienförmige Methanquelle liegt (s. Abb. 2). Die schematische Darstellung, das Berechnungsgitter und das Feld der absoluten Permeabilität sind jeweils auf der linken, mittleren und rechten Seite gezeigt. Das System soll ein wassergesättigtes Kohlenbergwerk repräsentieren nachdem der Grundwassereintritt stattgefunden hat. Das System ist 200 m lang und 200 m hoch, das Gebiet ist mit 256 rechteckigen Elementen und 289 Knoten diskretisiert. Die Linienquelle des Methans befindet sich bei 30 m $\leq x \leq$ 170 m, z = 50m (150 m unter der Oberfläche). Die absolute Permeabilität beträgt $1.0 \times 10^{-12}\ m^2$. Die weiteren Parameter sind in Kapitel 4 im Hauptteil der Arbeit genannt.

Mit Hilfe der beiden Modelle wird nun für diese Bedingungen das aufwärtsgerichtete Migrieren des Methans simuliert. Die Ergebnisse sind in Abb. 3 gezeigt. Die Verteilung der Methansättigung ist für den Zeitpunkt t = 10 Tage für das Zweiphasen-Dreikomponenten-Modell oben links und für das Zweiphasen-Modell oben in der Mitte dargestellt. Man kann deutlich sehen, dass das Methan bei der Anwendung des Zweiphasen-Modells schneller nach oben migriert. Um untersuchen zu können wo dieser Unterschied entsteht, wird für jeden Zeitschritt die Masse des Methans in jeder Phase an jedem Knoten berechnet ($\rho_\alpha^{mass} S_\alpha X_\alpha^m \phi$ $(\alpha = w, g)$ $[kg/m^3 s]$). Die Verteilungen in der Gasphase (oben rechts) und in der Wasserphase (unten links) zum Zeitpunkt t = 10 Tage sind in Abb. 3 gezeigt. Zusätzlich wird die gesamte Masse des Methans basierend auf den Knotenwerten berechnet und das Verhältnis der Methanmasse in jeder Phase zur gesamten Masse wird für die ersten 20 Tage ausgewertet. Das Ergebnis ist unten rechts in Abb. 3 dargestellt.

Das Methan, das in das System eingebracht wird, löst sich zunächst in der Wasserphase bis die Menge der Lösung die Kapazität erreicht, die durch das Henry-Gesetzt festgelegt wird. Dann

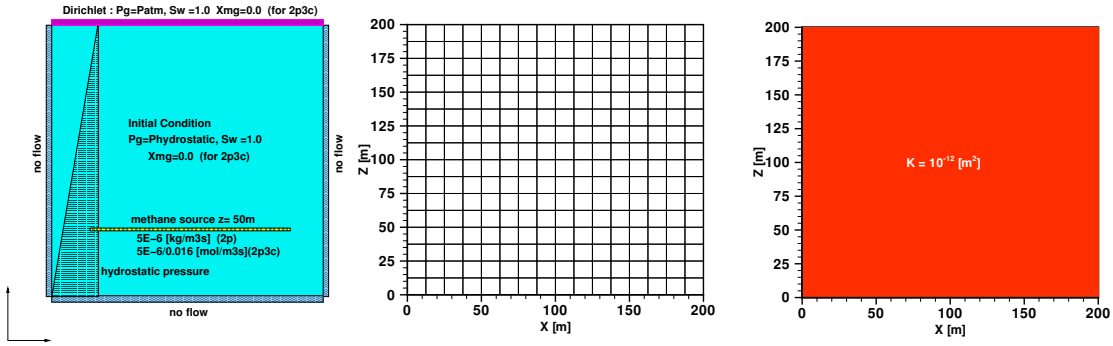

Abb. 2: Schematische Darstellung des Systems (links), des Berechnungsgitters (Mitte) und des Feldes der absoluten Permeabilität $[m^2]$ (rechts)

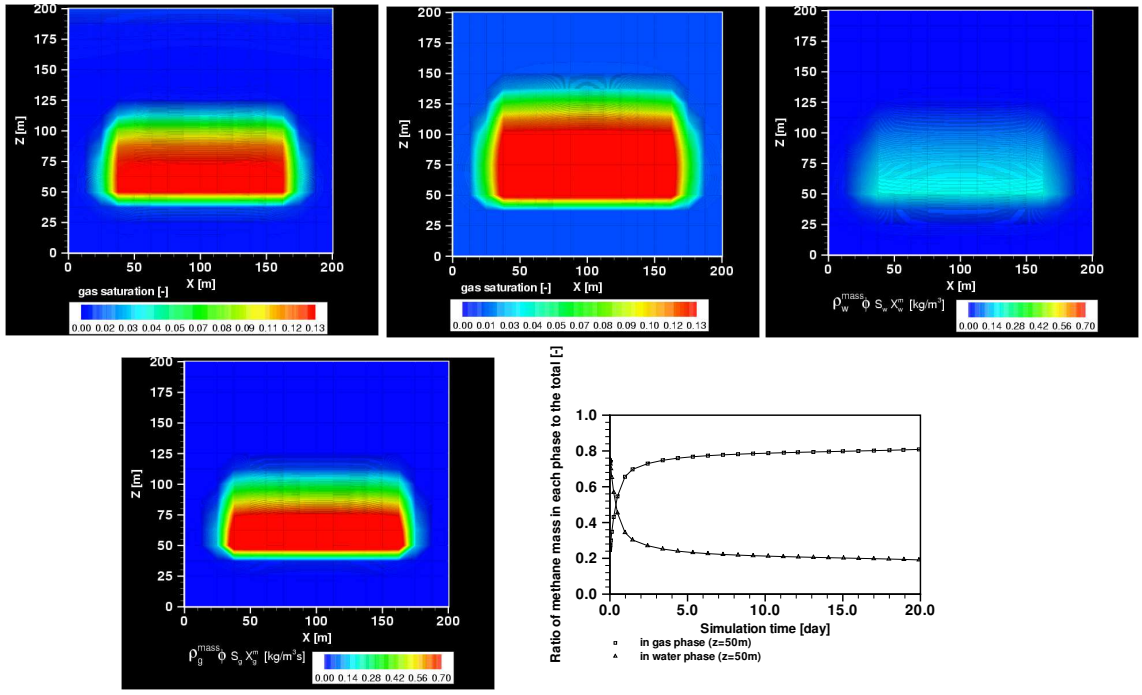

Abb. 3: Verteilung der Gassättigung nach 10 Tagen. Simulation mit Zweiphasen-Dreikomponenten-Modell (oben links) und Zweiphasen-Modell (oben Mitte). Verteilung der Methanmasse in jedem Knoten in der Gasphase (oben rechts) und in der Wasserphase (unten links). Das Verhältnis der Methanmasse in jeder Phase zur gesamten Masse bis zum Tag 20 (unten rechts).

kann kein weiteres Methan mehr von der Wasserphase aufgenommen werden ,und die Masse des Methans in der Gasphase beginnt zu steigen. Der Anteil in der Gasphase nimmt im Laufe der Simulation weiter zu. Am Ende der Simulation wird eine endgültige Verteilung der Methanmasse in Wasser und Gas erreicht. Das Verhältnis der Methanmasse in der Wasserphase zur Gesamtmasse beträgt in dem hier dargestellten Fall ca. 20%, wobei dieser Wert selbst stark schwankt in Abhängigkeit von den Simulationsbedingungen. Hiermit ist folgende Erkenntnis verdeutlicht:Die Ursache für eine langsamere aufwärtsgerichtete Methanmigration im Falle des Zweiphasen-Dreikomponenten-Modells wird durch das Lösen des Methans in der Wasserphase hervorgerufen. D.h. die Masse, die in die Gasphase übergeht ist kleiner, was höchstwahrscheinlich zu einer langsameren Migration der Methanfront führt.

Mit diesen und den weiteren Ergebnissen aus Kapitel 4 können wir die folgenden Schlüsse ziehen.

- Das Methan, welches in den gesättigten Aquifer eingebracht wird, wird zunächst in der Wasserphase gelöst. Anschließend beginnt die Masse des Methans in der Gasphase zu steigen. Das endgültige Verhältnis der Methanmasse in der Wasserphase zur Gesamtmasse für dieses künstlich erzeugte Beispiel betragt in etwa 20%.
- Die durchgeführten Vergleiche zeigen, dass aufgrund der Modellunterschiede die Geschwindigkeit der nach oben migrierenden Methangasfront überschätzt werden kann, wenn das Zweiphasen-Modell anstatt des Zweiphasen-Dreikomponenten-Modells angewendet wird.
- Wenn man sich in der ungesättigten Zone befindet, ist es möglich, das Methan durch Gasextraktion zu fördern. In der ungesättigten Zone muss jedoch berücksichtigt werden, dass sich das Methan auch als Komponente in der Wasserphase befindet.

Optimierungsmodell

Nachdem durch die durchgeführten Vergleichsrechnungen ein geeignetes Modellkonzept ausgewählt wurde, war das Ziel, ein Optimierungsmodell zu entwickeln und dieses für das Auffinden der optimalen Lage von Extraktionsbrunnen einzusetzen. Hierzu wurde ein geschlossenes Kohleabbaugebiet in der ungesättigten Zone simuliert, indem die Lage von ein bis drei Brunnen festgelegt werden sollte.

Simulated Annealing
Die Wahl eines geeigneten Optimierungsmodells hängt im Wesentlichen von den Eigenschaften der Zielfunktion ab. Die Eigenschaften, die für die Zielfunktion der folgenden Anwendungen angenommen werden, lauten:

- Die exakte Form der Zielfunktion ist unbekannt. Es ist jedoch sicher, dass es mehrere lokale Extrema gibt.
- Es ist nicht sicher, ob die Zielfunktion ohne Schwierigkeiten ableitbar ist.

Deshalb wurde in dieser Arbeit ein Simulated Annealing (SA) Algorithmus gewählt, da hier keine Ableitungen berechnet werden müssen und der Algorithmus relativ robust ist, unabhängig von der Form der Zielfunktion. Eine typische Eigenschaft des Simulated Annealing ist, dass es neben

Lösungen mit einer verbesserten Zielfunktion auch - in einem gewissen Maße - Lösungen mit einer verschlechterten Zielfunktion akzeptiert

Nach Abschluss der Untersuchungen wurde deutlich, dass unter Umständen auch andere Methoden, inklusive Verfahren mit Berechnung der Ableitung, verwendet werden könnten. Diese Erkenntnis war jedoch erst nach Untersuchungen mit dem Simulated-Annealing-Algorithmus möglich.

Die Kopplung in MUFTE-SA
Um Simulations-Optimierungs-Probleme lösen zu können, muss ein Optimierungsmodell mit einem Simulationsmodell gekoppelt werden. Die Kopplung eines Mehrphasen-Mehrkomponenten-Modells (MUltiphase/multicomponent, Flow, Transport and Energy model - Unstructured Grid (MUFTE-UG)) mit dem Simulated-Annealing-Algorithmus ist in Abbildung 4 gezeigt. Das Gesamtmodell wird im Folgenden als MUFTE-SA bezeichnet.

Zuerst müssen die für MUFTE-SA notwendigen Anfangsparameter gesetzt werden. Diese sind unter anderem, der anfängliche Entscheidungsvektor für Simulated Annealing und die Anfangs- und Randbedingungen für MUFTE. Dann wird das Anfangsnetz mit Hilfe der Eingangsinformationen vom Netzgenerator ART generiert. Die Anfangs- und Randbedingungen werden anschließend gemäß den Regeln des Simulationsprogramms MUFTE-UG dem Netz zugewiesen und die erste Simulation wird gestartet.

Der Wert ist nichts anderes als die Antwort auf diese Simulation. Somit erhalten wir diesen Wert, der mit dem anfänglichen Entscheidungsvektoqr berechnet worden ist. Der nächste Entscheidungsvektor ergibt sich aus dem Simulated Annealing basierend auf dem SA-Algorithmus, ART generiert ein neues Netz und MUFTE-UG berechnet die Zielfunktion für den nächsten Vektor.

Anschließend wird die aktuelle Zielfunktion mit der vorherigen Zielfunktion verglichen ,und die Akzeptanz für die neue Lösung wird nach der Regel der Boltzmann-Wahrscheinlichkeit bestimmt. Nachdem diese Prozedur wiederholt wird, endet die Optimierung wenn das Abbruch-Kriterium erreicht ist.

Parallelisierung von MUFTE-SA
SA wurde mit Hilfe der Gebietszerlegungsmethode parallelisiert, da ein Zyklus der SA-Prozedur (z.B. von der Generierung des nächsten Zustandes bis zur Überprüfung des Abbruch-Kriteriums in Abb. 4) ca. 7 - 8 Stunden für die vorliegende Anwendung dauert (ein Iterationsschritt). Im Allgemeinen benötigt jedoch SA Hunderte von Iterationen. Als ein Beispiel können wir die gesamte Zeit für einen Extremfall mit einer einfachen Berechnung abschätzen: 7 Stunden $\times$ 1000 Iterationen / 24 Stunden = 292 Tage, was als Berechnungsdauer nicht akzeptabel ist. Aus diesem Grund war eine Parallelisierung notwendig.

Die verwendete Parallelisierungsstrategie ist in Abb. 5 gezeigt. Für die Parallelisierung werden die Strecken im Abbaugebiet in n Segmente unterteilt (hier: n = 23). Dann werden k Extraktionsbrunnen in k von den n Segmenten eingerichtet. Die Verteilung erfolgt nach einer Pertubationsregel oder nach ingenieurmäßiger Abschätzung. Jede MUFTE-SA-Prozedur wird dann auf einem Knoten des Parallelrechners ausgeführt. Anschließend werden die Ergebnisse der einzelnen Knoten zusammengeführt.Die Rechnung wird beendet, wenn das Gesamtergebnis das Abbruch-Kriterium erfüllt. Andernfalls wird eine neue Iteration gestartet. Hierdurch wird die Gesamtzeit reduziert. Bei 23 Knoten ergibt sich zum Beispiel eine Rechenzeit von 292 Tagen / 23 $\approx$ 12,7 Tage.

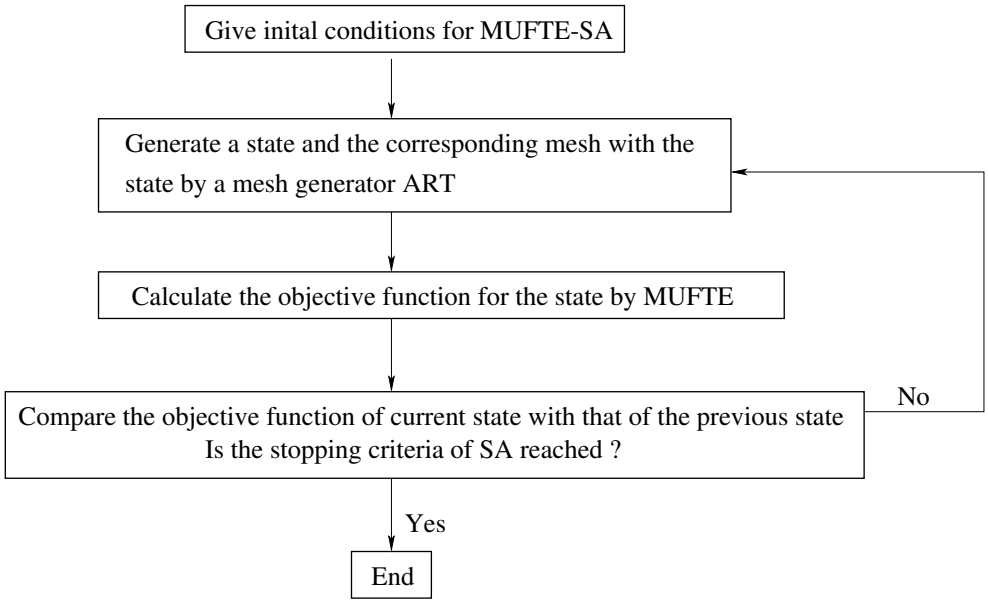

Abb. 4: Kopplung von MUFTE mit SA (MUFTE-SA) und dem Netzgenerator ART

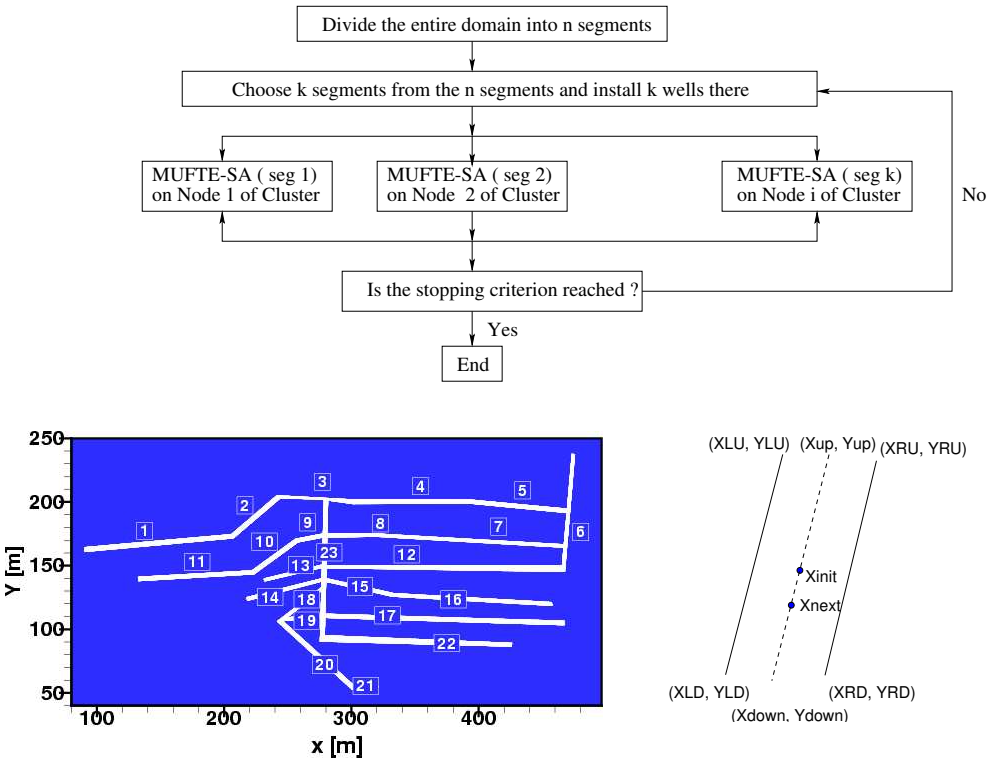

Abb. 5: Parallelisierung durch Gebietszerlegung (oben). Beispielgebiet für die Gebietszerlegung (unten).

Anwendung von MUFTE-SA

Als die Hauptaufgabe in dieser Arbeit wird das Simulations-Optimierungs-Modell MUFTE-SA am Standort Dortmund, Deutschland angewendet. Hier existierte eine stillgelegte Kohlengrube untertage, und zur Zeit befindet sich über dieser Stelle ein Möbelgeschäft. Der Standort wurde durch Diskussion mit der Deutschen Montan Technologie GmbH (DMT) gewählt, die uns die Daten zur Verfügung gestellt hat.

Stillgelegte Kohlengrube im Ruhrgebiet

Die Lage des Standorts ist in Abb. 6 gezeigt. In der linken oberen Karte wird Dortmund durch einen Kreis markiert. Die Karte auf der rechten Seite stellt die Umgebung im Ruhrgebiet dar. Eine schematische 3D-Ansicht der Kohlengrube ist Abb. 7 links gezeigt. Die dunklen Linien im Bild zeigen Strecken in einem ehemaligen Kohleabbau, die einem Höhenniveau von z = - 40 m (der Ursprung der z-Koordinate ist an der Erdoberfläche) entsprechen. Die hellen Linien zeigen das Höhenniveau bei z = - 60 m. Zwei vertikale Schächte wurden als Einstieg zu den Kohlearbeiten untertage benutzt. Die Schächte sind jetzt verfüllt, das Foto rechts in Abb. 7zeigt eine Schachtöffnung nach der Versiegelung.

Es gibt zur Zeit kaum Informationen, wie der Zustand in dem ehemaligen Bergwerk ist. In anderen Worten: Das Zusammenbrechen umliegender Schichten könnte zu einem Verfüllen der Strecken geführt haben. Dies wird jedoch im Weiteren nicht berücksichtigt. Methan, das in den nicht abgebauten Kohleflözen in der Mine noch adsorbiert ist, wird kontinuierlich desorbiert. Dieses soll aus den abgeworfenen Anlagen mit Hilfe von passiven Entgasungsbrunnen extrahiert werden.

Die Lage der Extraktionsbrunnen soll optimiert werden. Für diesen Fall kann die Zielfunktion folgendermaßen ausgedrückt werden:

$$Obj \quad = \sum_{i}^{num} \left\{ f(Q_{g,i}(p_{atm}, \mathbf{x}_i)) \right\} \tag{1}$$

Hierbei ist p_{atm} der atmosphärische Druck, der das Einrichten einer passiven Extraktionsanlage anzeigt. $\mathbf{x}_i$ =(x_i, y_i, z_i) sind die Koordinaten des Extraktionsbrunnens. $Q_{g,i}$ ist die geförderte Methanmenge pro Brunnen i.

Es zeigte sich, dass die Simulierung des gesamten Abbaugebietes mit einem 3D-Modell zu komplex ist, und dass es zu viel Berechnungszeit für die Optimierung in Anspruch nehmen würde. Deshalb wurde entschieden, nur das Abbaugebiet, welches sich auf einem Level von z = - 40 m befindet, mit dem Zweiphasen-Dreikomponenten-Modell zu modellieren. Der Kohleabbau befindet sich in der ungesättigten Zone, so dass das Zweiphasen-Dreikomponenten-Modell nicht unbedingt notwendig ist. Dieses Modell wird jedoch mit dem Hintergrund verwendet, dass auch spätere Fälle, in denen das Grundwasser wieder in das System eingetreten wird, berechnet werden können. Der Entscheidungsvektor $\mathbf{x}_i$ entspricht der x-Koordinate des Extraktionsbrunnens, die entlang der Mittellinie eines der 23 Segmente verläuft in die das Gebiet aufgeteilt wurde (siehe Abb. 5). Da zu erwarten war, dass die Rechenzeit sehr groß sein wird wenn alle möglichen Kombinationen von zwei oder drei Segmenten berücksichtigt werden, in denen der Extraktionsbrunnen liegen kann, wurde folgende ingenieurmäßige Vereinfachung gewählt: Ein Brunnen von zwei (für den Zwei-Brunnen-Fall) oder zwei Brunnen von drei (für den Drei-Brunnen-Fall) dürfen sich nur im zentralen Segment 23 bewegen. Der zweite bzw. dritte Brunnen wird dann im Segment i ($i = 0, ..23$) eingerichtet.

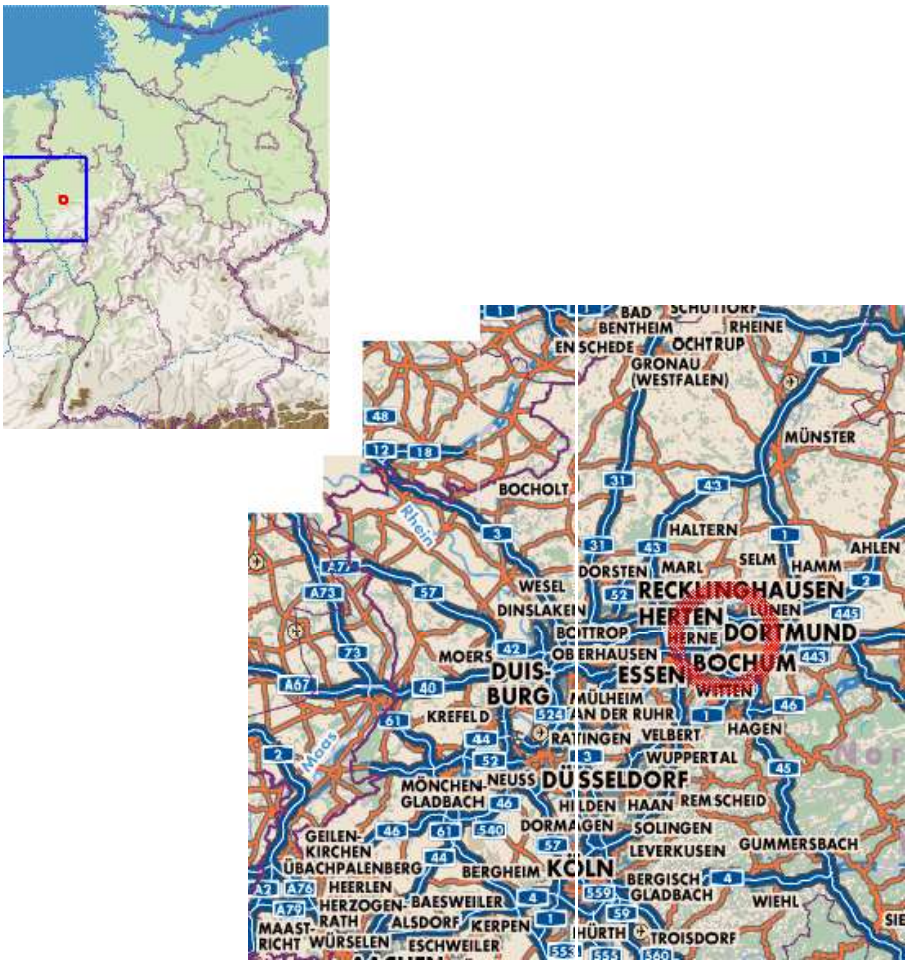

Abb. 6: Lage des Standorts (Diese Karte wurde vom Stadtplandienst http://www.stadplandienst.de heruntergeladen und nachbearbeitet.)

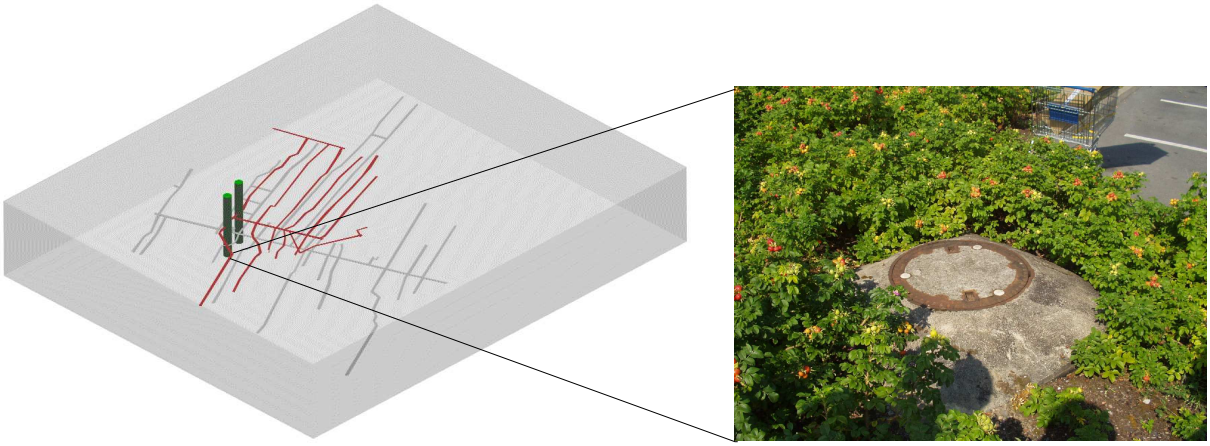

Abb. 7: Eine 3D-Ansicht der abgeworfenen Schachtanlage in Dortmund (links). Die dunkle Farbe zeigt den Abbau auf Level z = - 40 m, die helle Farbe auf Level z = - 60 m. Das Foto auf der rechten Seite zeigt einen versiegelten Schachteingang.

Ein bis drei Brunnen im Grubengebiet
In Abb. 8 werden Druckfelder gezeigt, die Beispiele für ein bis drei Brunnen veranschaulichen, an deren Stellen Extraktionsraten in optimaler Weise erhalten wurden. Weitere Einzelheiten sind in Kapitel 5 im Hauptteil der Arbeit erläutert.

Durch diese und vorausgehende Anwendungen konnten die folgenden Aussagen getroffen werden:

- Je dichter ein Brunnen an einem Ende der Strecken liegt oder je enger zwei Brunnen beieinander liegen, desto geringer wird die erhaltene Gasmenge.
- Die größte durchschnittliche Gasmenge in einem Segment ergibt sich, wenn der Brunnen im zentralen Segment 23 eingerichtet wird, wo das Gas der Umgebung am einfachsten und schnellsten gesammelt werden kann. Diese Tendenz lässt sich auch für Segmente beobachten, die mit dem zentralen Segment 23 verbunden sind.
- Die beste Gasextraktionsrate kann in der Regel in den Kreuzungspunkten erreicht werden, wo mehrere Strecken Segment 23 schneiden. Dies ist jedoch nur gültig für bis zu zwei Brunnen. Sobald ein dritter Brunnen in Segment 23 errichtet wird, verringert sich die Extraktionsrate aufgrund von Interaktionen zwischen den Brunnen. Die Kombination $23-23$ für den Zwei-Brunnen-Fall oder $6-23-23$ für den Drei-Brunnen-Fall erzielt sehr gute Resultate. Hier ist der Abstand zwischen den Brunnen groß genug, so dass kaum eine gegenseitige Beeinflussung stattfinden kann.
- Die Einrichtung von nur einem Brunnen könnte ausreichen, da sich die Zeitspanne, die das Geschwindigkeitsfeld benötigt, um einen stationären Zustand zu erreichen, für den hier betrachteten Fall und das hier betrachtete System nur sehr wenig unterscheidet, wenn ein, zwei oder drei Brunnen eingerichtet werden. Wenn jedoch ein anderer Systemaufbau gewählt wird, in dem das Gas auch durch die seitlichen Begrenzungsflächen der Strecken entweichen kann, muss weiterhin sichergestellt werden, dass der Großteil des Methans extrahiert werden kann. Eine Aussage hierüber ist jedoch mit dem vorliegenden Modell grundsätzlich möglich, wurde aber nicht untersucht.

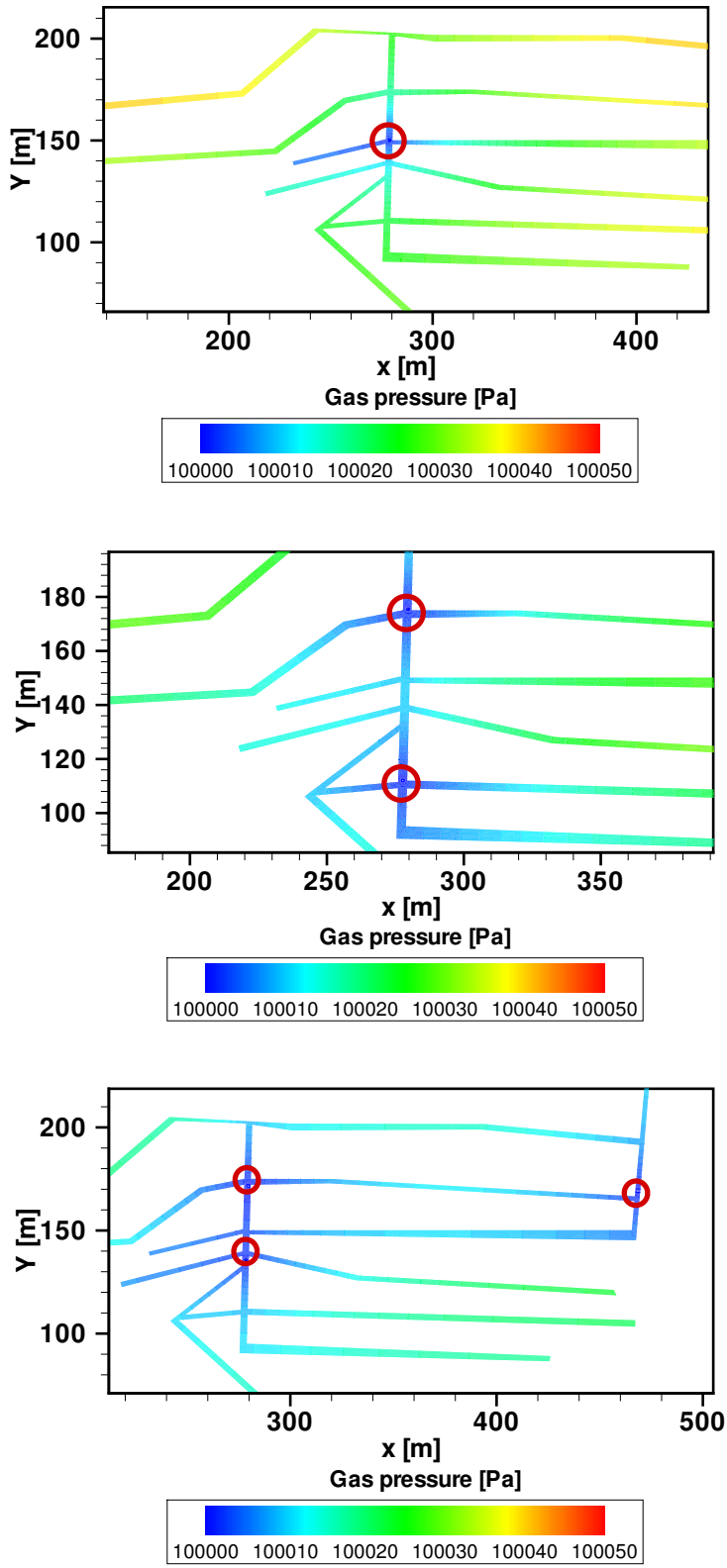

Abb. 8: Optimaler Standort für einen (oben), zwei (Mitte) oder drei (unten) Brunnen. Die Kreise zeigen an, wo die Brunnen eingerichtet sind.

Zusammenfassung

Die Hauptaufgabe dieser Arbeit war, eine Kopplung eines Simulations- mit einem Optimierungsmodell durchzuführen. Dieses Modell wurde auf eine abgeworfene Kohlengrube im Ruhrgebiet angewendet, um eine bessere Methanextraktionsstrategie entwerfen zu können. Hierbei kann besonders hervorgehoben werden, dass es sich um eine Anwendung für ein reales System handelt, was im Allgemeinen keine einfache Aufgabe ist aufgrund der enormen Berechnungszeiten, die für eine 'Real-World'-Simulation und für die Iterationen für den Optimierungsprozess notwendig sind. Um dieses Problem der sehr großen Rechenzeiten lösen zu können, wurde ein Parallelrechner eingesetzt.

Weiterhin wurden verschiedene Modellkonzepte, z.B. ein Zweiphasen-Modell (Flüssigkeit, Gas) und ein Zweiphasen-Dreikomponenten-Modell (Phasen: Flüssigkeit, Gas; Komponenten: Wasser, Methan, Luft) miteinander verglichen, um den Effekt untersuchen zu können, dass sich das Methan in der Flüssigphase löst.

Die Hauptergebnisse sind:

- Ein Zweiphasen-Dreikomponenten-Modell wurde weiter entwickelt. Dieses Modell erlaubt es, den Lösungsprozess in und den Ausgasungsprozess aus der flüssigen Phase abzuschätzen.
- Der Simulated Annealing Algorithmus wurde neu programmiert und dabei besonders auf eine Untersuchung von Gasextraktionsraten in abgeworfenen Kohlegruben in komplexen Abbaugebieten zugeschnitten. Hierbei wurde ins Besondere die Bewegung der Extraktionsbrunnen entlang der Abbaustrecken angepasst.
- Eine Kopplung des Zweiphasen-Dreikomponenten-Modells mit dem Simulated Annealing Algorithmus wurde realisiert (MUFTE-SA). MUFTE-SA kann generell für alle Fälle angewendet werden, die mit einem Mehrphasen-Mehrkomponenten-Modell simuliert werden können.
- Die Prozeduren der Optimierung wurden parallelisiert. Hiermit konnte eine deutliche Verringerung der Gesamtzeit erreicht werden.

Die grundlegenden Methoden und Prozeduren, die im Rahmen dieser Arbeit entwickelt wurden, können in vielen Bereichen für die Simulations-Optimierung und die Parameter-Identifizierung erweitert werden. Zum Beispiel hat bereits eine Arbeit zur Parameter-Identifizierung begonnen, die das in der vorliegenden Arbeit erarbeitete Know-How einsetzen wird.

Institut für Wasserbau
Universität Stuttgart

Pfaffenwaldring 61
70569 Stuttgart (Vaihingen)
Telefon (0711) 685 - 4717/41/52 o. - 4679
Telefax (0711) 685 - 7020 o. 4746 o. 4681
email: iws@iws.uni-stuttgart.de
http://www.iws.uni-stuttgart.de

Verzeichnis der Mitteilungshefte

1 Röhnisch, Arthur: *Die Bemühungen um eine Wasserbauliche Versuchsanstalt an der Technischen Hochschule Stuttgart*, und
Fattah Abouleid, Abdel: *Beitrag zur Berechnung einer in lockeren Sand gerammten, zweifach verankerten Spundwand*, 1963

2 Marotz, Günter: *Beitrag zur Frage der Standfestigkeit von dichten Asphaltbelägen im Großwasserbau*, 1964

3 Gurr, Siegfried: *Beitrag zur Berechnung zusammengesetzter ebener Flächentragwerke unter besonderer Berücksichtigung ebener Stauwände, mit Hilfe von Randwert- und Lastwertmatrizen*, 1965

4 Plica, Peter: *Ein Beitrag zur Anwendung von Schalenkonstruktionen im Stahlwasserbau*, und Petrikat, Kurt: *Möglichkeiten und Grenzen des wasserbaulichen Versuchswesens*, 1966

5 Plate, Erich: *Beitrag zur Bestimmung der Windgeschwindigkeitsverteilung in der durch eine Wand gestörten bodennahen Luftschicht*, und
Röhnisch, Arthur; Marotz, Günter: *Neue Baustoffe und Bauausführungen für den Schutz der Böschungen und der Sohle von Kanälen, Flüssen und Häfen; Gestehungskosten und jeweilige Vorteile*, sowie Unny, T.E.: *Schwingungsuntersuchungen am Kegelstrahlschieber*, 1967

6 Seiler, Erich: *Die Ermittlung des Anlagenwertes der bundeseigenen Binnenschiffahrtsstraßen und Talsperren und des Anteils der Binnenschiffahrt an diesem Wert*, 1967

7 *Sonderheft anläßlich des 65. Geburtstages von Prof. Arthur Röhnisch mit Beiträgen von* Benk, Dieter; Breitling, J.; Gurr, Siegfried; Haberhauer, Robert; Honekamp, Hermann; Kuz, Klaus Dieter; Marotz, Günter; Mayer-Vorfelder, Hans-Jörg; Miller, Rudolf; Plate, Erich J.; Radomski, Helge; Schwarz, Helmut; Vollmer, Ernst; Wildenhahn, Eberhard; 1967

8 Jumikis, Alfred: *Beitrag zur experimentellen Untersuchung des Wassernachschubs in einem gefrierenden Boden und die Beurteilung der Ergebnisse*, 1968

9 Marotz, Günter: *Technische Grundlagen einer Wasserspeicherung im natürlichen Untergrund*, 1968

10 Radomski, Helge: *Untersuchungen über den Einfluß der Querschnittsform wellenförmiger Spundwände auf die statischen und rammtechnischen Eigenschaften*, 1968

11 Schwarz, Helmut: *Die Grenztragfähigkeit des Baugrundes bei Einwirkung vertikal gezogener Ankerplatten als zweidimensionales Bruchproblem*, 1969

12 Erbel, Klaus: *Ein Beitrag zur Untersuchung der Metamorphose von Mittelgebirgsschneedecken unter besonderer Berücksichtigung eines Verfahrens zur Bestimmung der thermischen Schneequalität*, 1969

13 Westhaus, Karl-Heinz: *Der Strukturwandel in der Binnenschiffahrt und sein Einfluß auf den Ausbau der Binnenschiffskanäle*, 1969

14 Mayer-Vorfelder, Hans-Jörg: *Ein Beitrag zur Berechnung des Erdwiderstandes unter Ansatz der logarithmischen Spirale als Gleitflächenfunktion*, 1970

15 Schulz, Manfred: *Berechnung des räumlichen Erddruckes auf die Wandung kreiszylindrischer Körper*, 1970

16 Mobasseri, Manoutschehr: *Die Rippenstützmauer. Konstruktion und Grenzen ihrer Standsicherheit*, 1970

17 Benk, Dieter: *Ein Beitrag zum Betrieb und zur Bemessung von Hochwasserrückhaltebecken*, 1970

18 Gàl, Attila: *Bestimmung der mitschwingenden Wassermasse bei überströmten Fischbauchklappen mit kreiszylindrischem Staublech*, 1971, vergriffen

19 Kuz, Klaus Dieter: *Ein Beitrag zur Frage des Einsetzens von Kavitationserscheinungen in einer Düsenströmung bei Berücksichtigung der im Wasser gelösten Gase*, 1971, vergriffen

20 Schaak, Hartmut: *Verteilleitungen von Wasserkraftanlagen*, 1971

21 *Sonderheft zur Eröffnung der neuen Versuchsanstalt des Instituts für Wasserbau der Universität Stuttgart mit Beiträgen von*
Brombach, Hansjörg; Dirksen, Wolfram; Gàl, Attila; Gerlach, Reinhard; Giesecke, Jürgen; Holthoff, Franz-Josef; Kuz, Klaus Dieter; Marotz, Günter; Minor, Hans-Erwin; Petrikat, Kurt; Röhnisch, Arthur; Rueff, Helge; Schwarz, Helmut; Vollmer, Ernst; Wildenhahn, Eberhard; 1972

22 Wang, Chung-su: *Ein Beitrag zur Berechnung der Schwingungen an Kegelstrahlschiebern*, 1972

23 Mayer-Vorfelder, Hans-Jörg: *Erdwiderstandsbeiwerte nach dem Ohde-Variationsverfahren*, 1972

24 Minor, Hans-Erwin: *Beitrag zur Bestimmung der Schwingungsanfachungsfunktionen überströmter Stauklappen*, 1972, vergriffen

25 Brombach, Hansjörg: *Untersuchung strömungsmechanischer Elemente (Fluidik) und die Möglichkeit der Anwendung von Wirbelkammerelementen im Wasserbau*, 1972, vergriffen

26 Wildenhahn, Eberhard: *Beitrag zur Berechnung von Horizontalfilterbrunnen*, 1972

27 Steinlein, Helmut: *Die Eliminierung der Schwebstoffe aus Flußwasser zum Zweck der unterirdischen Wasserspeicherung, gezeigt am Beispiel der Iller*, 1972

28 Holthoff, Franz Josef: *Die Überwindung großer Hubhöhen in der Binnenschiffahrt durch Schwimmerhebewerke*, 1973

29 Röder, Karl: *Einwirkungen aus Baugrundbewegungen auf trog- und kastenförmige Konstruktionen des Wasser- und Tunnelbaues*, 1973

30 Kretschmer, Heinz: *Die Bemessung von Bogenstaumauern in Abhängigkeit von der Talform*, 1973

31 Honekamp, Hermann: *Beitrag zur Berechnung der Montage von Unterwasserpipelines*, 1973

32 Giesecke, Jürgen: *Die Wirbelkammertriode als neuartiges Steuerorgan im Wasserbau*, und
Brombach, Hansjörg: *Entwicklung, Bauformen, Wirkungsweise und Steuereigenschaften von Wirbelkammerverstärkern*, 1974

33 Rueff, Helge: *Untersuchung der schwingungserregenden Kräfte an zwei hintereinander angeordneten Tiefschützen unter besonderer Berücksichtigung von Kavitation*, 1974

34 Röhnisch, Arthur: *Einpreßversuche mit Zementmörtel für Spannbeton - Vergleich der Ergebnisse von Modellversuchen mit Ausführungen in Hüllwellrohren*, 1975

35 *Sonderheft anläßlich des 65. Geburtstages von Prof. Dr.-Ing. Kurt Petrikat mit Beiträgen von*: Brombach, Hansjörg; Erbel, Klaus; Flinspach, Dieter; Fischer jr., Richard; Gàl, Attila; Gerlach, Reinhard; Giesecke, Jürgen; Haberhauer, Robert; Hafner Edzard; Hausenblas, Bernhard; Horlacher, Hans-Burkhard; Hutarew, Andreas; Knoll, Manfred; Krummet, Ralph; Marotz, Günter; Merkle, Theodor; Miller, Christoph; Minor, Hans-Erwin; Neumayer, Hans; Rao, Syamala; Rath, Paul; Rueff, Helge; Ruppert, Jürgen; Schwarz, Wolfgang; Topal-Gökceli, Mehmet; Vollmer, Ernst; Wang, Chung-su; Weber, Hans-Georg; 1975

36 Berger, Jochum: *Beitrag zur Berechnung des Spannungszustandes in rotationssymmetrisch belasteten Kugelschalen veränderlicher Wandstärke unter Gas- und Flüssigkeitsdruck durch Integration schwach singulärer Differentialgleichungen*, 1975

37 Dirksen, Wolfram: *Berechnung instationärer Abflußvorgänge in gestauten Gerinnen mittels Differenzenverfahren und die Anwendung auf Hochwasserrückhaltebecken*, 1976

38 Horlacher, Hans-Burkhard: *Berechnung instationärer Temperatur- und Wärmespannungsfelder in langen mehrschichtigen Hohlzylindern*, 1976

39 Hafner, Edzard: *Untersuchung der hydrodynamischen Kräfte auf Baukörper im Tiefwasserbereich des Meeres*, 1977, ISBN 3-921694-39-6

40 Ruppert, Jürgen: *Über den Axialwirbelkammerverstärker für den Einsatz im Wasserbau*, 1977, ISBN 3-921694-40-X

41 Hutarew, Andreas: *Beitrag zur Beeinflußbarkeit des Sauerstoffgehalts in Fließgewässern an Abstürzen und Wehren*, 1977, ISBN 3-921694-41-8, vergriffen

42 Miller, Christoph: *Ein Beitrag zur Bestimmung der schwingungserregenden Kräfte an unterströmten Wehren*, 1977, ISBN 3-921694-42-6

43 Schwarz, Wolfgang: *Druckstoßberechnung unter Berücksichtigung der Radial- und Längsverschiebungen der Rohrwandung*, 1978, ISBN 3-921694-43-4

44 Kinzelbach, Wolfgang: *Numerische Untersuchungen über den optimalen Einsatz variabler Kühlsysteme einer Kraftwerkskette am Beispiel Oberrhein*, 1978, ISBN 3-921694-44-2

45 Barczewski, Baldur: *Neue Meßmethoden für Wasser-Luftgemische und deren Anwendung auf zweiphasige Auftriebsstrahlen*, 1979, ISBN 3-921694-45-0

46 Neumayer, Hans: *Untersuchung der Strömungsvorgänge in radialen Wirbelkammerverstärkern*, 1979, ISBN 3-921694-46-9

47 Elalfy, Youssef-Elhassan: *Untersuchung der Strömungsvorgänge in Wirbelkammerdioden und -drosseln*, 1979, ISBN 3-921694-47-7

48 Brombach, Hansjörg: *Automatisierung der Bewirtschaftung von Wasserspeichern*, 1981, ISBN 3-921694-48-5

49 Geldner, Peter: *Deterministische und stochastische Methoden zur Bestimmung der Selbstdichtung von Gewässern*, 1981, ISBN 3-921694-49-3, vergriffen

50 Mehlhorn, Hans: *Temperaturveränderungen im Grundwasser durch Brauchwassereinleitungen*, 1982, ISBN 3-921694-50-7, vergriffen

51 Hafner, Edzard: *Rohrleitungen und Behälter im Meer*, 1983, ISBN 3-921694-51-5

52 Rinnert, Bernd: *Hydrodynamische Dispersion in porösen Medien: Einfluß von Dichteunterschieden auf die Vertikalvermischung in horizontaler Strömung*, 1983, ISBN 3-921694-52-3, vergriffen

53 Lindner, Wulf: *Steuerung von Grundwasserentnahmen unter Einhaltung ökologischer Kriterien*, 1983, ISBN 3-921694-53-1, vergriffen

54 Herr, Michael; Herzer, Jörg; Kinzelbach, Wolfgang; Kobus, Helmut; Rinnert, Bernd: *Methoden zur rechnerischen Erfassung und hydraulischen Sanierung von Grundwasserkontaminationen*, 1983, ISBN 3-921694-54-X

55 Schmitt, Paul: *Wege zur Automatisierung der Niederschlagsermittlung*, 1984, ISBN 3-921694-55-8, vergriffen

56 Müller, Peter: *Transport und selektive Sedimentation von Schwebstoffen bei gestau tem Abfluß*, 1985, ISBN 3-921694-56-6

57 El-Qawasmeh, Fuad: *Möglichkeiten und Grenzen der Tropfbewässerung unter besonderer Berücksichtigung der Verstopfungsanfälligkeit der Tropfelemente*, 1985, ISBN 3-921694-57-4, vergriffen

58 Kirchenbaur, Klaus: *Mikroprozessorgesteuerte Erfassung instationärer Druckfelder am Beispiel seegangsbelasteter Baukörper*, 1985, ISBN 3-921694-58-2

59 Kobus, Helmut (Hrsg.): *Modellierung des großräumigen Wärme- und Schadstofftransports im Grundwasser*, Tätigkeitsbericht 1984/85 (DFG-Forschergruppe an den Universitäten Hohenheim, Karlsruhe und Stuttgart), 1985, ISBN 3-921694-59-0, vergriffen

60 Spitz, Karlheinz: *Dispersion in porösen Medien: Einfluß von Inhomogenitäten und Dichteunterschieden*, 1985, ISBN 3-921694-60-4, vergriffen

61 Kobus, Helmut: *An Introduction to Air-Water Flows in Hydraulics*, 1985, ISBN 3-921694-61-2

62 Kaleris, Vassilios: *Erfassung des Austausches von Oberflächen- und Grundwasser in horizontalebenen Grundwassermodellen*, 1986, ISBN 3-921694-62-0

63 Herr, Michael: *Grundlagen der hydraulischen Sanierung verunreinigter Porengrundwasserleiter*, 1987, ISBN 3-921694-63-9

64 Marx, Walter: *Berechnung von Temperatur und Spannung in Massenbeton infolge Hydratation*, 1987, ISBN 3-921694-64-7

65 Koschitzky, Hans-Peter: *Dimensionierungskonzept für Sohlbelüfter in Schußrinnen zur Vermeidung von Kavitationsschäden*, 1987, ISBN 3-921694-65-5

66 Kobus, Helmut (Hrsg.): *Modellierung des großräumigen Wärme- und Schadstofftransports im Grundwasser*, Tätigkeitsbericht 1986/87 (DFG-Forschergruppe an den Universitäten Hohenheim, Karlsruhe und Stuttgart) 1987, ISBN 3-921694-66-3

67 Söll, Thomas: *Berechnungsverfahren zur Abschätzung anthropogener Temperaturanomalien im Grundwasser*, 1988, ISBN 3-921694-67-1

68 Dittrich, Andreas; Westrich, Bernd: *Bodenseeufererosion, Bestandsaufnahme und Bewertung*, 1988, ISBN 3-921694-68-X, vergriffen

69 Huwe, Bernd; van der Ploeg, Rienk R.: *Modelle zur Simulation des Stickstoffhaushaltes von Standorten mit unterschiedlicher landwirtschaftlicher Nutzung*, 1988, ISBN 3-921694-69-8, vergriffen

70 Stephan, Karl: *Integration elliptischer Funktionen*, 1988, ISBN 3-921694-70-1

71 Kobus, Helmut; Zilliox, Lothaire (Hrsg.): *Nitratbelastung des Grundwassers, Auswirkungen der Landwirtschaft auf die Grundwasser- und Rohwasserbeschaffenheit und Maßnahmen zum Schutz des Grundwassers*. Vorträge des deutsch-französischen Kolloquiums am 6. Oktober 1988, Universitäten Stuttgart und Louis Pasteur Strasbourg (Vorträge in deutsch oder französisch, Kurzfassungen zweisprachig), 1988, ISBN 3-921694-71-X

72 Soyeaux, Renald: *Unterströmung von Stauanlagen auf klüftigem Untergrund unter Berücksichtigung laminarer und turbulenter Fließzustände*,1991,ISBN 3-921694-72-8

73 Kohane, Roberto: *Berechnungsmethoden für Hochwasserabfluß in Fließgewässern mit überströmten Vorländern*, 1991, ISBN 3-921694-73-6

74 Hassinger, Reinhard: *Beitrag zur Hydraulik und Bemessung von Blocksteinrampen in flexibler Bauweise*, 1991, ISBN 3-921694-74-4, vergriffen

75 Schäfer, Gerhard: *Einfluß von Schichtenstrukturen und lokalen Einlagerungen auf die Längsdispersion in Porengrundwasserleitern*, 1991, ISBN 3-921694-75-2

76 Giesecke, Jürgen: *Vorträge, Wasserwirtschaft in stark besiedelten Regionen; Umweltforschung mit Schwerpunkt Wasserwirtschaft*, 1991, ISBN 3-921694-76-0

77 Huwe, Bernd: *Deterministische und stochastische Ansätze zur Modellierung des Stickstoffhaushalts landwirtschaftlich genutzter Flächen auf unterschiedlichem Skalenniveau*, 1992, ISBN 3-921694-77-9, vergriffen

78 Rommel, Michael: *Verwendung von Kluftdaten zur realitätsnahen Generierung von Kluftnetzen mit anschließender laminar-turbulenter Strömungsberechnung*, 1993, ISBN 3-92 1694-78-7

79 Marschall, Paul: *Die Ermittlung lokaler Stofffrachten im Grundwasser mit Hilfe von Einbohrloch-Meßverfahren*, 1993, ISBN 3-921694-79-5, vergriffen

80 Ptak, Thomas: *Stofftransport in heterogenen Porenaquiferen: Felduntersuchungen und stochastische Modellierung*, 1993, ISBN 3-921694-80-9, vergriffen

81 Haakh, Frieder: *Transientes Strömungsverhalten in Wirbelkammern,* 1993, ISBN 3-921694-81-7

82 Kobus, Helmut; Cirpka, Olaf; Barczewski, Baldur; Koschitzky, Hans-Peter: *Versuchseinrichtung zur Grundwasser und Altlastensanierung VEGAS, Konzeption und Programmrahmen*, 1993, ISBN 3-921694-82-5

83 Zang, Weidong: *Optimaler Echtzeit-Betrieb eines Speichers mit aktueller Abflußregenerierung*, 1994, ISBN 3-921694-83-3, vergriffen

84 Franke, Hans-Jörg: *Stochastische Modellierung eines flächenhaften Stoffeintrages und Transports in Grundwasser am Beispiel der Pflanzenschutzmittelproblematik*, 1995, ISBN 3-921694-84-1

85 Lang, Ulrich: *Simulation regionaler Strömungs- und Transportvorgänge in Karstaquiferen mit Hilfe des Doppelkontinuum-Ansatzes: Methodenentwicklung und Parameteridentifikation*, 1995, ISBN 3-921694-85-X, vergriffen

86 Helmig, Rainer: *Einführung in die Numerischen Methoden der Hydromechanik*, 1996, ISBN 3-921694-86-8, vergriffen

87 Cirpka, Olaf: *CONTRACT: A Numerical Tool for Contaminant Transport and Chemical Transformations - Theory and Program Documentation -*, 1996, ISBN 3-921694-87-6

88 Haberlandt, Uwe: *Stochastische Synthese und Regionalisierung des Niederschlages für Schmutzfrachtberechnungen*, 1996, ISBN 3-921694-88-4

89 Croisé, Jean: *Extraktion von flüchtigen Chemikalien aus natürlichen Lockergesteinen mittels erzwungener Luftströmung*, 1996, ISBN 3-921694-89-2

90 Jorde, Klaus: *Ökologisch begründete, dynamische Mindestwasserregelungen bei Ausleitungskraftwerken*, 1997, ISBN 3-921694-90-6

91 Helmig, Rainer: *Gekoppelte Strömungs- und Transportprozesse im Untergrund - Ein Beitrag zur Hydrosystemmodellierung-*, 1998, ISBN 3-921694-91-4

92 Emmert, Martin: *Numerische Modellierung nichtisothermer Gas-Wasser Systeme in porösen Medien*, 1997, ISBN 3-921694-92-2

93 Kern, Ulrich: *Transport von Schweb- und Schadstoffen in staugeregelten Fließgewässern am Beispiel des Neckars*, 1997, ISBN 3-921694-93-0

94 Förster, Georg: *Druckstoßdämpfung durch große Luftblasen in Hochpunkten von Rohrleitungen 1997*, ISBN 3-921694-94-9

95 Cirpka, Olaf: *Numerische Methoden zur Simulation des reaktiven Mehrkomponententransports im Grundwasser*, 1997, ISBN 3-921694-95-7

96 Färber, Arne: *Wärmetransport in der ungesättigten Bodenzone: Entwicklung einer thermischen In-situ-Sanierungstechnologie*, 1997, ISBN 3-921694-96-5

97 Betz, Christoph: *Wasserdampfdestillation von Schadstoffen im porösen Medium: Entwicklung einer thermischen In-situ-Sanierungstechnologie*, 1998, ISBN 3-921694-97-3

98 Xu, Yichun: *Numerical Modeling of Suspended Sediment Transport in Rivers*, 1998, ISBN 3-921694-98-1, vergriffen

99 Wüst, Wolfgang: *Geochemische Untersuchungen zur Sanierung CKW-kontaminierter Aquifere mit Fe(0)-Reaktionswänden,* 2000, ISBN 3-933761-02-2

100 Sheta, Hussam: *Simulation von Mehrphasenvorgängen in porösen Medien unter Einbeziehung von Hysterese-Effekten*, 2000, ISBN 3-933761-03-4

101 Ayros, Edwin: *Regionalisierung extremer Abflüsse auf der Grundlage statistischer Verfahren*, 2000, ISBN 3-933761-04-2, vergriffen

102 Huber, Ralf: *Compositional Multiphase Flow and Transport in Heterogeneous Porous Media*, 2000, ISBN 3-933761-05-0

103 Braun, Christopherus: *Ein Upscaling-Verfahren für Mehrphasenströmungen in porösen Medien*, 2000, ISBN 3-933761-06-9

104 Hofmann, Bernd: *Entwicklung eines rechnergestützten Managementsystems zur Beurteilung von Grundwasserschadensfällen*, 2000, ISBN 3-933761-07-7

105 Class, Holger: *Theorie und numerische Modellierung nichtisothermer Mehrphasenprozesse in NAPL-kontaminierten porösen Medien,* 2001, ISBN 3-933761-08-5

106 Schmidt, Reinhard: *Wasserdampf- und Heißluftinjektion zur thermischen Sanierung kontaminierter Standorte*, 2001, ISBN 3-933761-09-3

107 Reinhold Josef:, *Schadstoffextraktion mit hydraulischen Sanierungsverfahren unter Anwendung von grenzflächenaktiven Stoffen*, 2001, ISBN 3-933761-10-7

108 Schneider, Matthias: *Habitat- und Abflussmodellierung für Fließgewässer mit unscharfen Berechnungsansätzen*, 2001, ISBN 3-933761-11-5

109 Rathgeb, Andreas: *Hydrodynamische Bemessungsgrundlagen für Lockerdeckwerke an überströmbaren Erddämmen*, 2001, ISBN 3-933761-12-3

110 Lang, Stefan: *Parallele numerische Simulation instätionärer Probleme mit adaptiven Methoden auf unstrukturierten Gittern*, 2001, ISBN 3-933761-13-1

111 Appt, Jochen; Stumpp Simone: *Die Bodensee-Messkampagne 2001, IWS/CWR Lake Constance Measurement Program 2001*, 2002, ISBN 3-933761-14-X

112 Heimerl, Stephan: *Systematische Beurteilung von Wasserkraftprojekten,* 2002, ISBN 3-933761-15-8

113 Iqbal, Amin: *On the Management and Salinity Control of Drip Irrigation,* 2002, ISBN 3-933761-16-6

114 Silberhorn-Hemminger, Annette: *Modellierung von Kluftaquifersystemen: Geostatistische Analyse und deterministisch-stochastische Kluftgenerierung,* 2002, ISBN 3-933761-17-4

115 Winkler, Angela: *Prozesse des Wärme- und Stofftransports bei der In-situ-Sanierung mit festen Wärmequellen,* 2003, ISBN 3-933761-18-2

116 Marx, Walter: *Wasserkraft, Bewässerung, Umwelt - Planungs- und Bewertungsschwerpunkte der Wasserbewirtschaftung,* 2003, ISBN 3-933761-19-0

117 Hinkelmann, Reinhard: *Efficient Numerical Methods and Information-Processing Techniques in Environment Water,* 2003, ISBN 3-933761-20-4

118 Samaniego-Eguiguren, Luis Eduardo: *Hydrological Consequences of Land Use / Land Cover and Climatic Changes in Mesoscale Catchments*, 2003, ISBN 3-933761-21-2

119 Neunhäuserer, Lina: *Diskretisierungsansätze zur Modellierung von Strömungs- und Transportprozessen in geklüftet-porösen Medien*, 2003, ISBN 3-933761-22-0

120 Paul, Maren: *Simulation of Two-Phase Flow in Heterogeneous Poros Media with Adaptive Methods*, 2003, ISBN 3-933761-23-9

121 Ehret, Uwe: *Rainfall and Flood Nowcasting in Small Catchments using Weather Radar*, 2003, ISBN 3-933761-24-7

122 Haag, Ingo: *Der Sauerstoffhaushalt staugeregelter Flüsse am Beispiel des Neckars - Analysen, Experimente, Simulationen -,* 2003, ISBN 3-933761-25-5

123 Appt, Jochen: *Analysis of Basin-Scale Internal Waves in Upper Lake Constance,* 2003, ISBN 3-933761-26-3

124 Hrsg.: Schrenk, Volker; Batereau, Katrin; Barczewski, Baldur; Weber, Karolin und Koschitzky, Hans-Peter: *Symposium Ressource Fläche und VEGAS - Statuskolloquium 2003, 30. September und 1. Oktober 2003,* 2003, ISBN 3-933761-27-1

125 Omar Khalil Ouda: *Optimisation of Agricultural Water Use: A Decision Support System for the Gaza Strip,* 2003, ISBN 3-933761-28-0

126 Batereau, Katrin: *Sensorbasierte Bodenluftmessung zur Vor-Ort-Erkundung von Schadensherden im Untergrund*, 2004, ISBN 3-933761-29-8

127 Witt, Oliver: *Erosionsstabilität von Gewässersedimenten mit Auswirkung auf den Stofftransport bei Hochwasser am Beispiel ausgewählter Stauhaltungen des Oberrheins*, 2004, ISBN 3-933761-30-1

128 Jakobs, Hartmut: *Simulation nicht-isothermer Gas-Wasser-Prozesse in komplexen Kluft-Matrix-Systemen*, 2004, ISBN 3-933761-31-X

129 Li, Chen-Chien: *Deterministisch stochastisches Berechnungskonzept zur Beurteilung der Auswirkungen erosiver Hochwasserereignisse in Flussstauhaltungen,* 2004, ISBN 3-933761-32-8

130 Reichenberger, Volker; Helmig, Rainer; Jakobs, Hartmut; Bastian, Peter; Niessner, Jennifer: *Complex Gas-Water Processes in Discrete Fracture-Matrix Systems Upscaling, Mass-Conservative Discretization and Efficient Multilevel Solution,* 2004, ISBN 3-933761-33-6

131 Hrsg.: Barczewski, Baldur; Koschitzky, Hans-Peter; Weber, Karolin; Wege, Ralf: *VEGAS - Statuskolloquium 2004,* 5. Oktober 2004, 2004, ISBN 3-933761-34-4

132 Asie, Kemal Jabir: *Finite Volume Models for Multiphase Multicomponent Flow through Porous Media*. 2005, ISBN 3-933761-35-2

133 Jacoub, George: *Development of a 2-D Numerical Module for Particulate Contaminant Transport in Flood Retention Reservoirs and Impounded Rivers,* 2004, ISBN 3-933761-36-0

134 Nowak, Wolfgang: *Geostatistical Methods for the Identification of Flow and Transport Parameters in the Subsurface,* 2005, ISBN 3-933761-37-9

135 Süß, Mia: *Analysis of the influence of structures and boundaries on flow and transport processes in fractured porous media*, 2005, ISBN 3-933761-38-7

136 Jose, Surabhin Chackiath: *Experimental Investigations on Longitudinal Dispersive Mixing in Heterogeneous Aquifers,* 2005, ISBN: 3-933761-39-5

137 Filiz, Fulya: *Linking Large-Scale Meteorological Conditions to Floods in Mesoscale Catchments,* 2005, ISBN 3-933761-40-9

138 Qin, Minghao: *Wirklichkeitsnahe und recheneffiziente Ermittlung von Temperatur und Spannungen bei großen RCC-Staumauern*, 2005, ISBN 3-933761-41-7

139 Kobayashi, Kenichiro: *Optimization Methods for Multiphase Systems in the Subsurface - Application to Methane Migration in Coal Mining Areas*, 2005, ISBN 3-933761-42-5